Exploring extracellular vesicles for siRNA delivery and Raman-based diagnostics

Stephan Stremersch

Pharmacist

Master of Science in Drug Development

2016

Thesis submitted to obtain the degree of

Doctor in Pharmaceutical Sciences

Proefschrift voorgedragen tot het bekomen van de graad van

Doctor in de Farmaceutische Wetenschappen

Dean

Prof.dr.apr. Jan Van Bocxlaer

Promotor

Prof.dr.apr. Stefaan De Smedt

Promotor

Dr.apr. Koen Raemdonck

Promotor

Prof.dr. Kevin Braeckmans

Members of the Exam Committee:

Prof.dr.apr. **Serge Van Calenbergh** (chairman)	Ghent University
Prof.dr.apr. **Filip Van Nieuwerburgh** (secretary)	Ghent University
Prof.dr.apr. **Olivier De Wever**	University Hospital Ghent
Prof.dr. **Raymond Schiffelers**	University Medical Center Utrecht
Prof.dr. **Roos Vandenbroucke**	VIB-Ghent University

The author and the promotors give the authorization to consult and to copy parts of this thesis for personal use only. Any other use is limited by the Laws of Copyright, especially the obligation to refer to the source whenever results from this thesis are cited.

De auteur en de promotoren geven de toelating dit proefschrift voor consultering beschikbaar te stellen en delen ervan te kopiëren voor persoonlijk gebruik. Elk ander gebruik valt onder de beperkingen van het auteursrecht, in het bijzonder met betrekking tot de verplichting uitdrukkelijk de bron te vermelden bij het aanhalen van resultaten uit dit proefschrift.

Ghent, June 24th 2016

The promotors:

Prof.dr.apr. Stefaan De Smedt

Dr.apr. Koen Raemdonck

Prof.dr. Kevin Braeckmans

The author:

Apr. Stephan Stremersch

Table of Contents

List of abbreviations

AAV	adeno-associated virus
ADSC	adipose-derived stem cells
AgNP	silver nanoparticles
AGO2	argonaute 2
APC	antigen presenting cell
API	active pharmaceutical ingredient
AUC	area under the curve
AuNP	gold nanoparticles
BALF	bronchoalveolar lavage fluid
BBB	blood brain barrier
BSA	bovine serum albumin
CARS	coherent anti-stokes Raman spectroscopy
(c)CCM	(concentrated) conditioned cell medium
CD	cluster of differentiation
CEA	carcinoembryonic antigen
CHEMS	3β-hydroxy-5-cholestene 3-hemisuccinate
chol-siRNA	cholesterol-conjugated siRNA
DC	dendritic cell
DLS	dynamic light scattering
DMAP	4-dimethylaminopyridine
DMEM	dulbecco's modified eagle medium
DNA	deoxyribonucleic acid
DOPE	1,2-dioleoyl-*sn*-glycero-3-phosphoethanolamine
dsRNA	double stranded RNA
EBV	epstein-bar virus
EDTA	ethylenediaminetetraacetic acid
eGFP	enhanced green fluorescent protein
EGFR	epidermal growth factor receptor
EGTA	ethylene-bis(oxyethylenenitrilo)tetraacetic acid
ELV(s)	exosome-like vesicle(s)
EP	electroporation
EPCAM	epithelial cell adhesion molecule
EPR	enhanced permeability and retention
EV(s)	extracellular vesicle(s)
FBS	fetal bovine serum
FDA	food and drug administration

FFS	fluorescence fluctuation spectroscopy
FITC	fluorescein isothiocyanate
gag	group specific antigen
GM-CSF	granulocyte macrophage colony stimulating factor
GP100	glycoprotein 100
HDL	high density lipoprotein
HEPES	4-(2-hydroxyethyl)-1-piperazineethanesulfonic acid
HER2	human epidermal growth factor receptor 2
HRP	horseradish peroxidase
Hsp	heat shock protein
ILV	intraluminal vesicle
iNKT	invariant natural killer T cell
IP	intraperitoneal
ISEV	international society of extracellular vesicles
IV	intravenous
L1CAM	L1 cellular adhesion molecule
LBPA	lysobisphosphatidic acid
LDL	low density lipoprotein
MCR-ALS	multivariate curve resolution alternating least squares
MFI	mean fluorescence intensity
MHC	major histocompatibility complex
miRNA	microRNA
MPS	mononuclear phagocyte system
mRNA	messenger RNA
MSC	mesenchymal stem cell
MVB	multivesicular body
NK-cells	natural killer cells
NSCLC	non-small-cell lung carcinoma
nt	nucleotides
OMV	outer membrane vesicle
ORF	open reading frame
PAGE	polyacrylamide gel electrophoresis
PBS	phosphate buffered saline
PCR	polymerase chain reaction
pDNA	plasmid DNA
PEG	polyethylene glycol
PK	pharmacokinetics
PLS-DA	partial least square discriminative analysis
pre-miRNA	precursor-miRNA

pri-miRNA	primary-miRNA
PS	phosphatidylserine
PSA	prostate specific antigen
PSMA	prostate-specific membrane antigen
PVDF	polyvinylidene difluoride
PVP	polyvinylpyrrolidone
RBC	red blood cell
RISC	RNA-induced silencing complex
RNA	ribonucleic acid
RNAi	RNA interference
RNase	ribonuclease
RT-PCR	reverse transcription polymerase chain reaction
SC	subcutaneous
SD	standard deviation
SDS	sodium dodecyl sulfate
SEC	size exclusion chromatography
SEM	standard error of the mean
SERS	surface enhanced Raman spectroscopy
siCD45	siRNA targeted against CD45
siCTRL	siRNA control sequence
siGFP	siRNA targeted against eGFP
siRNA	small interfering RNA
SPR	surface plasmon resonance
SPT	single particle tracking
TAA	tumor associated antigen
TEM	transmission electron microscopy
TERS	tip-enhanced Raman spectroscopy
TLR	toll-like receptor
Tris	tris(hydroxymethyl)aminomethane
TRL	technology readiness level
TYRP2	tyrosinase-related protein 2
UC	ultracentrifugation
UF	ultrafiltration
UTR	untranslated region
VSV	vesicular stomatitis virus

AIM AND OUTLINE OF THIS THESIS

The first observation of vesicular structures outside of the cell dates back to the 1960s. Initially, these vesicles were believed to be mainly involved in extracellular processes like blood clotting and in maintaining the cellular homeostasis by acting as waste removal entities. However, during the last decade these extracellular vesicles (EVs) are increasingly regarded as important mediators of intercellular communication. It was this novel insight that sparked the mounting interest in these nanosized vesicles from both the therapeutic and diagnostic field, which is accompanied by numerous new applications exploiting EVs in different pharmaceutical domains.

Because of their natural function as transporters of macromolecular components, it is hypothesized that EVs are endowed with unique features that rationalize their exploitation as a drug carrier system. Macromolecular therapeutics with an intracellular target, including nucleic acids and pharmaceutical proteins, require formulation into nanoparticles (i.e. so-called nanomedicines) to guide them across the many extra- and intracellular barriers. Unfortunately, many synthetic nanomedicines fail to merge drug delivery efficiency with acceptable biocompatibility. In light of these shortcomings, the first aim of this thesis is to explore EVs as bio-inspired carriers for small interfering RNA (siRNA) delivery. Indeed, the field of RNA interference (RNAi) is still struggling to translate its wide potential into a clinical applicable technology due to a lack of targeted and functional delivery.

Chapter 1 provides a general introduction to EVs with a focus on their therapeutic and diagnostic applications. An overview of the main historical findings that shaped the further development of the field is followed by a more in depth discussion of the different EV types and their respective biogenesis pathways. Next, different methods to purify EVs are listed and discussed for their potential in a clinical setting. Finally, a comprehensive overview of the different fields of application for which EVs have been explored is given. Here, the main emphasis is put on exploiting EVs as a drug delivery vehicle with an outline of the most important strategic choices to be considered. In parallel, we aimed to pinpoint some of the major hurdles that need to be overcome to accelerate the development of this application.

One of the first critical steps in harnessing EVs as a therapeutic carrier is developing robust methods to load these nanosized membranous vesicles with the therapeutic cargo of interest. In **chapter 2** we thoroughly investigated the value of electroporation to load isolated EVs with siRNA and provide details on the emergence of electroporation artifacts that substantially overestimate the EV loading efficiency.

Furthermore, it is important to bear in mind that EVs are typically present in complex media (i.e. cell medium, serum, *etc*.). The strategies to isolate EVs are continuously evolving, though the field has not yet reached consensus on a gold standard protocol. In **chapter 3** we provide a comparative analysis of different EV purification strategies, discuss the purity of the final isolate, both for endogenous as well as exogenous contaminants, and indicate some misinterpretations that impurities can entail in downstream experimental readouts.

In light of the results obtained in the previous chapters, a new strategy to associate small RNAs to EVs is described in **chapter 4**. Here, cholesterol-conjugated siRNA (chol-siRNA) was used to anchor the siRNA duplex in the EV membrane. This feat allowed us to provide a direct comparison between purified EVs and a lipid-based synthetic carrier for their ability to functionally deliver siRNA over the cellular barriers. In addition, in this chapter we evaluated the functional delivery of endogenous miRNA by EVs.

Besides drug delivery, there is increasing interest in exploiting EVs for diagnostic applications. As EVs can be regarded as miniature windows on the composition and status of the parent cell, they are considered as an interesting biomarker source in liquid biopsies to detect and monitor a plethora of diseases. However, techniques that combine a broad molecular fingerprint with single vesicle sensitivity and high speed are currently lacking. Hence, a second aim in this thesis is to advance the field of EV characterization for diagnostics. In **chapter 5** we describe a new nanotechnology platform based on surface enhanced Raman spectroscopy (SERS), which allows us to characterize and discriminate between EVs from different cellular origin in a mixture.

Finally, in **chapter 6** we aim to put both fields of application for EVs, as described in this thesis, in a broader perspective. Our own findings are positioned within these two frameworks by discussing the contributions of our studies to the respective fields. Furthermore, we pinpoint the predominant hurdles and suggest new approaches to accelerate future progress of both applications. Finally, the current status and future perspectives of all EV application fields are discussed in a pharmaceutical context.

1

Therapeutic and diagnostic applications of extracellular vesicles

A manuscript of this chapter is published as:

Stephan Stremersch[1], Stefaan C. De Smedt[1], Koen Raemdonck[1]. Therapeutic and diagnostic applications of extracellular vesicles. *J. Control. Release* (2016) *In press* doi: 10.1016/j.jconrel.2016.07.054.

[1]Laboratory of General Biochemistry and Physical Pharmacy, Ghent University, Ghent, Belgium

Chapter 1: ToC

Abstract

During the past two decades, extracellular vesicles (EVs) have been identified as important mediators of intercellular communication, enabling the functional transfer of bioactive molecules from one cell to another. Consequently, it is becoming increasingly clear that these vesicles are involved in many (patho)physiological processes, providing opportunities for therapeutic application. Moreover, it is known that the molecular composition of EVs reflects the physiological status of the producing cell and tissue, rationalizing their exploitation as biomarker for various diseases. In this chapter the composition, biogenesis and diversity of EVs is discussed in a therapeutic and diagnostic context. We describe emerging therapeutic applications, including the use of EVs as drug delivery vehicles and as cell-free vaccines, and reflect on future challenges for clinical translation. Finally, we discuss the use of EVs as a biomarker source and highlight recent studies and clinical successes.

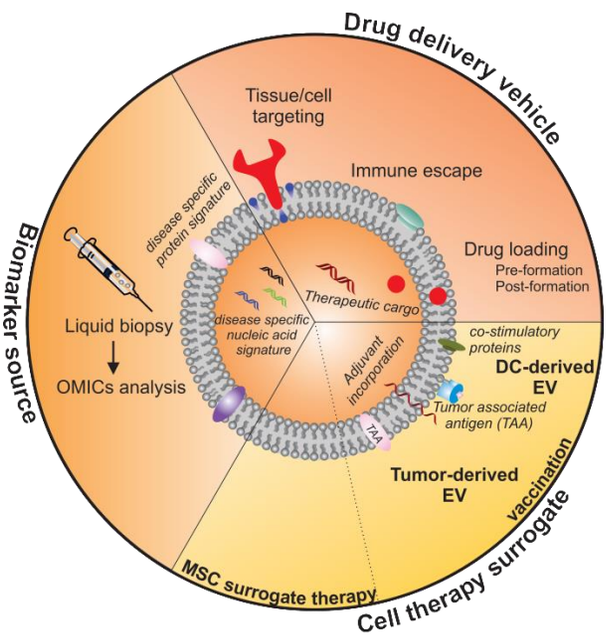

1. A general introduction to EVs

1.1. A brief historical overview

Cells release, in addition to single molecules (i.e. small molecules, peptides and proteins), macromolecular complexes (e.g. Argonaute2 (AGO2)-RNA complex) and lipoproteins, also membrane-enclosed vesicles in the extracellular medium. The first reports on such extracellular vesicles (EVs) date back to the late 1960s when it was observed that platelet free plasma contains vesicular material that could be pelleted down by ultracentrifugation (UC). These vesicles were mainly composed of phospholipids and appeared to promote blood clothing [1] and cartilage calcification [2]. In the years that followed, using electron microscopy imaging, vesicular structures could be visualized in duodenal fluid [3] and the first observations were made on tumor cell-derived membrane vesicles [4, 5]. Initially it was assumed that the observed vesicles were solely released by outward budding of the cell membrane. Several years later, Johnstone and colleagues reported on the formation of intraluminal vesicles (ILVs) in late endosomes by inward budding of the endosomal limiting membrane. Following the fusion of these so-called multivesicular bodies (MVBs) with the cell's plasma membrane, the ILVs are released in the surrounding medium [6, 7]. This discovery was made based on the observation that reticulocytes release their transferrin receptor, as part of the maturation into erythrocytes, associated to vesicles. As this mechanism was also observed in other species and appeared to be selective for certain membrane-associated proteins [8], these EVs were initially presented as a conserved and regulated waste removal pathway [9]. A seminal paper by Raposo *et al.* in 1996, reporting on the immune-modulating activity of B cell-derived EVs, inspired many others to evaluate the biological implications of these vesicles [10]. Two years later, Zitvogel *et al.* used EVs derived from tumor peptide-pulsed dendritic cells (DCs) as a cell-free anti-cancer vaccine providing the first therapeutic application of EVs [11]. Among others, these reports introduced the notion that EVs cannot solely be considered as a waste disposal mechanism but also as important mediators of intercellular communication. Owing to the work of many, it was becoming increasingly clear that EVs likely play a fundamental role in many (patho)physiological processes. Besides deciphering the biological function of EVs, their potential as biomarker source [12, 13] was recognized and the first clinical trials using EVs as an anti-cancer vaccine were initiated [14]. In addition, around a decade ago different groups identified the presence of miRNA, mRNA and proteins in EVs and, more importantly, the ability to functionally shuttle their cargo into recipient cells, reinforcing the belief that EVs facilitate communication between cells [15, 16] and fuelling the idea of exploiting these vesicles for drug delivery applications.

1.2. Biogenesis, cargo loading and composition

EVs are generally categorized in three subtypes (i.e. exosomes, ectosomes and apoptotic bodies), based on distinct biogenesis pathways [17]. Apoptotic bodies are formed when a cell is dying *via* apoptosis, leading to blebbing and finally disintegration of the cellular plasma membrane with partitioning of the cellular content in different membrane-enclosed vesicles. Apoptotic bodies typically are larger particles (~0.5 - 4 μm) containing cytoplasmic organelles and fragmented nuclei [18]. Although some studies have reported a communication and biological function for these vesicles [19, 20], in this thesis we will focus on the smaller sized exosomes and ectosomes. Hence, apoptotic bodies are not considered when referring to EVs throughout this dissertation. Exosomes (50 – 150 nm) and ectosomes (50 – 1000 nm) do not only show a partly overlapping size distribution but also their biogenesis pathways are very similar (**figure 1A**). In both cases their formation is preceded by the assembly of membrane micro-domains composed of specific lipids (with an important role for ceramide) [21] and proteins, followed by budding and subsequent fission or pinching off. The main difference between both formation pathways is the location of the initial budding process. Indeed, ectosomes (also termed shedding vesicles or microvesicles) are released directly from the cell's plasma membrane. Exosomes on the other hand, originate from the inward budding of early and late endosomes forming MVBs containing ILVs [22, 23]. Subsequently, the MVBs are transported to and fuse with the plasma membrane, requiring a dynamic interplay between members of the Rab and SNARE protein family, concurrently releasing the ILVs in the extracellular space [24-28]. Partly because both biogenesis pathways are analogous, to date there is no defined panel of markers to distinguish between both vesicle subtypes in a vesicular isolate. Nevertheless, a panel of generic markers (e.g. CD9, CD81, CD63, TSG101, *etc.*) was defined by the International Society of Extracellular Vesicles (ISEV) to indicate the presence of EVs in a sample [29].

Numerous papers report that the relative molecular composition of EVs differs from the producer cell. Lipidomic analysis showed an accumulation of cholesterol, sphingomyelin, glycerophospholipids and phosphatidylserine (PS) in EVs [30]. Certain membrane-associated proteins, for example many tetraspanins (e.g. CD9, CD81), appear enriched on the EV surface [31]. Finally, an array of reports show that specific mRNAs, miRNAs and other non-coding RNAs (e.g. t-RNA, Y-RNA, vault RNA, *etc*.) are enriched or underrepresented in EVs compared to their respective parent cells [32-37]. Based on these observations it is generally accepted that the composition of EVs is, at least partially, actively regulated by the parent cell [38], albeit that the mechanisms and associated key players regulating this cargo sorting remain largely elusive to date [34, 39-42].

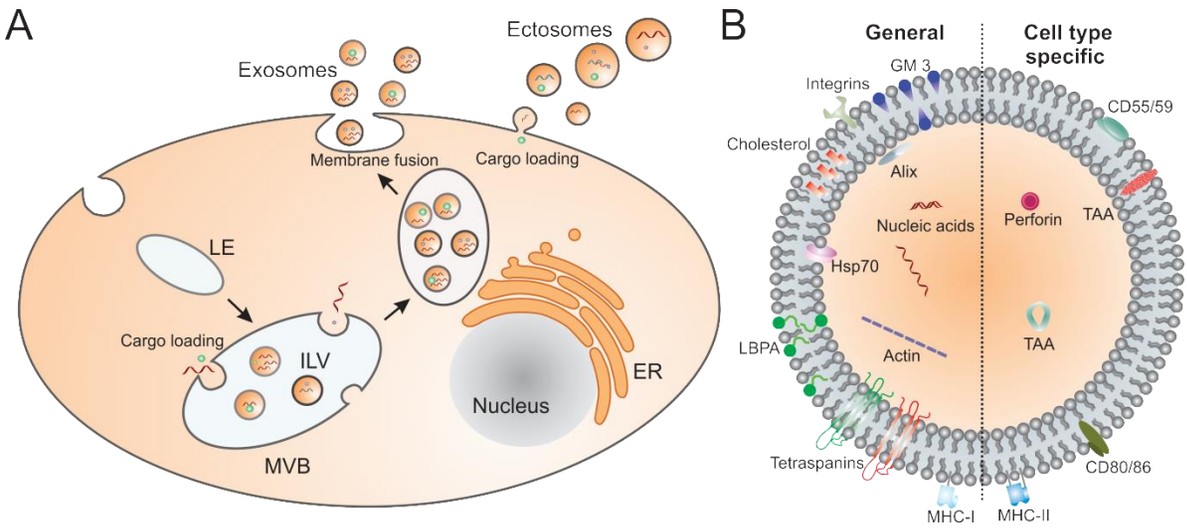

Figure 1. Schematic representation of the EV biogenesis and architecture. [A] The biogenesis pathways of exosomes and ectosomes (or shedding vesicles). Exosomes are formed by inward budding of the limiting membrane of early or late endosomes (LE) forming multivesicular bodies (MVBs) containing so-called intra-luminal vesicles (ILVs). Upon fusion of the MVBs with the cell membrane, the ILVs are released as exosomes in the extracellular medium. In contrast, ectosomes are released by direct budding from the plasma membrane. [B] The molecular architecture of extracellular vesicles with some key general and cell-type specific molecular components. General: Tetraspanins (e.g. CD63, CD81), Alix, Heat shock proteins (e.g. Hsp70), major histocompatibility complex (MHC)-I, structural proteins (e.g. actin), nucleic acids (e.g. miRNA, mRNA), integrins (type of integrin can be cell-type specific), lysobisphosphatidic acid (LBPA), cholesterol, ganglioside GM3 [43, 44]. Specific: MHC-II, CD80, CD86 and complement shielding proteins CD55/59 (in DC) [45], tumor-associated antigens (TAA; e.g. GP100 in melanoma cells) [46], perforin (in natural killer T cells) [47].

The overall EV configuration (i.e. a lipoprotein shell encapsulating an aqueous core containing soluble proteins and nucleic acids) and part of the molecular composition (i.e. proteins and lipids required in the EV biogenesis) are common among EVs isolated from different cells [43]. However, some EV-associated molecules are unique for the producing cell type (**figure 1B**). For example, MHC II is found on EVs secreted by antigen presenting cells (APC) [31, 48]. As another example, CD2, CD8 and CD56 were found in EVs derived from natural killer (NK) T cells and not in EVs derived from platelets, where the opposite holds true for CD41b, CD42a and CD61 [49].

Furthermore, it appears that the culture conditions not only influence the cellular phenotype but also the number and/or composition of the secreted EVs. For instance, hypoxia triggers cancer cells to release more CD63-positive vesicles [50] with a modified molecular composition and distinct effect on recipient cells [51]. Comparable observations were made for an altered extracellular pH [52] and the presence of stress-inducing molecules (e.g. lipopolysaccharide, H_2O_2, *etc.*) in general [53]. Besides the cellular microenvironment also the status of the cell influences the EV composition and

downstream activity. Where mature DCs release pro-inflammatory EVs enriched in MHC II and ICAM-1 [54], EVs derived from DCs cultured in the presence of IL10, an anti-inflammatory cytokine, suppress the onset of inflammation in a mouse arthritis model [55]. The fact that phenotypic alterations in the parent cells are mirrored by the composition of the secreted EVs, can be exploited for diagnostic purposes (**section 3.2**).

The influence of the surrounding medium on the EV composition may have relevant clinical implications. For instance, Li *et al*. compared EVs derived from N2A neuroblastoma cells cultured both in serum containing cell medium or under starvation conditions, showing marked alterations in the protein composition [56]. Besides the changes in the composition of the EV itself, the presence or absence of serum proteins will likely also influence the protein corona surrounding the EVs [57]. It is well documented that this corona strongly influences the extra- and intracellular (transfection) behavior of synthetic nanoparticles, including liposomes [58, 59]. Given the analogy between EVs and liposomes [60], it is conceivable that a protein corona will also impact the EV interactome and thus biological function. However, to date the influence of these parameters on the EV functionality has not been thoroughly investigated.

1.3. EV heterogeneity

Evidence is mounting that within the exosome and ectosome population more distinct vesicle subtypes exist. When a specific exosome release pathway (i.e. *via* Rab27a inhibition) was silenced, the secretion of only a specific set of exosome-related molecules (i.e. CD63, Tsg101, Alix and Hsc70) decreased, whereas others (CD9 and Mfge8) were not affected [61]. This could indicate that different exosome subtypes exist of which the release is regulated by slightly different pathways. Additionally, Van Niel *et al.* showed a clear discrepancy in protein profile between EVs released from the apical or basolateral side of polarized epithelial cells [62]. Another report showed that vesicles isolated from conditioned cell medium and plasma by UC could be divided in two distinct populations by bottom-up density gradient UC. Both populations showed a different protein and nucleic acid composition, which correlated with a distinct biological effect on recipient cells [63]. To address this heterogeneity in more detail, more sensitive techniques have to be developed allowing single vesicle analysis. In this respect, a recent study by Smith and coworkers used Raman microspectroscopy to obtain a Raman spectrum, which can be regarded as a molecular fingerprint, on the single vesicle level. Following principal component analysis of the obtained spectra, these authors concluded that at least four types of vesicles with a clearly distinct molecular composition are released by a single cell type [64]. Conceivably, this is still an underestimation of the factual heterogeneity among EVs. Yet to date, it is impossible to physically separate

these specific EV subtypes, as reliable markers are lacking. This implies that the composition and functions, currently attributed to EVs, are likely the combined effect of multiple subtypes of vesicles. This notion further complicates the adoption of EVs in a pharmaceutical context as it is well possible that only a specific sub-fraction of vesicles induces a desired effect while others might entail off-target or even opposing effects.

1.4. EV purification protocols

EVs represent only a fraction of the cell's secretome. Parallel to the growing research interest in EVs, different methods to isolate and purify EVs from conditioned cell medium or biological fluids have been developed. The most common approaches are listed in **table 1** and discussed further with a focus on their applicability in a pharmaceutical context. The predominant technique in the literature relies on differential centrifugation followed by UC, which is based on a difference in size and density between EVs and other components present in the respective medium [65]. It is important to note that many potential contaminants are co-purified using UC (e.g. lipoprotein particles, protein(-RNA) aggregates, *etc.*) [66] and that the yield is relatively low (i.e. 10 – 20 %) and dependent on the medium viscosity [67, 68]. Additionally, the impact of the high shear forces on the vesicle integrity are under debate. While some studies indicate no changes in the integrity of the EVs after UC [69, 70], others show subtle EV aggregation influencing the EV biodistribution [71, 72].

To safeguard EV stability and increase both the vesicle yield as well as purity of the isolate, density gradient UC (iodixanol or sucrose) can be used [66, 73]. To underscore the superior separation resolution, it was shown that viral particles could be physically separated from EVs by using an iodixanol-based density gradient [74]. The major disadvantage of this technique is the long processing time.

Another method, which was originally developed to concentrate viral particles [75], employs hydrophilic polymers (e.g. poly(ethylene glycol); PEG) and (high) salt concentrations to precipitate EVs. Although this method provides a high yield, which makes it interesting for small amounts of starting material or as a preparative concentrating step, it lacks specificity as many contaminants (e.g. protein aggregates) are co-isolated [66]. Hence, interpreting downstream analysis of precipitated EV isolates, should be done with caution. Additionally, the PEG polymer is also present in the final isolate, potentially shielding the EV surface and interfering with their functionality or downstream analysis [76].

Table 1. EV purification strategies.

Method	Principle of separation	Purity	Integrity	Disadvantages	Advantages
Ultracentrifugation (UC)	Size and density	Medium	High shear forces might affect the EV integrity/functionality	Relatively long procedure (~4 - 5 hours) The yield is drastically reduced when the viscosity of the samples is high (plasma > serum > cell medium > PBS) [68]	Most used technique throughout the literature
Density gradient UC / sucrose cushion UC	Buoyant density	High	Mild forces	Long procedure (~18 hours)	Previously used in clinical settings [14, 77-79]
Precipitation	Salting out EVs using a PEG/salt solution	Low	Mild forces	Low purity The PEG chain might envelope the EVs, possibly interfering with their functionality	Applicable for large volumes Experience from the viral field Previously used in a clinical setting (as an EV concentration step prior to UC) [80]
Affinity capture	Binding of EV surface components	High	Mild forces	Expensive (if antibody based) EV elution might damage surface proteins and functionality	This method has the highest potential to physically separate different EV (sub)populations. However, due to the lack of specific markers for EV subtypes to date, this method is most frequently applied in the diagnostic field
Size exclusion chromatography (SEC)	Size	Medium to high	Mild forces	The final EV isolate is diluted	Increasingly used and promoted by the ISEV community Chromatographic methods (e.g. SEC and IEC) are often used in clinical settings (e.g. to purify monoclonal antibodies)
Sequential filtration	Size	Unknown	Risk of modifying the original EV architecture due to extrusion	Sticking of EVs to the filter membrane lowers the yield	Useful as a pre-process concentration step. Previously used for this purpose in clinical settings [14, 79]

Affinity-based capture of EVs has the potential to yield subpopulations with high purity. The best-known affinity-based approach exploits EV-surface protein recognition *via* antibodies (e.g. associated to beads, a polymer surface in a chip or a chromatography column) [81, 82]. Of note, this method requires knowledge of specific EV markers, which are however difficult to identify. To circumvent the lack of specific markers, a more general approach was recently presented in which antibodies are substituted by heparin as it appears to have a general affinity for EVs. However, the cross-reactivity with other components present in the respective media is a possible concern [83]. Overall, affinity-based capture of EVs might be very useful in an on-chip diagnostic set-up using small sample sizes [84, 85]. Yet from a pharmaceutical point of view, when contemplating to use EVs as medicinal products, larger volumes will have to be processed, thus augmenting manufacturing costs.

Finally, several separation methods are being developed for EVs that exploit differences in size, including size-exclusion chromatography (SEC) and filtration [86]. SEC enables fast sample processing. However, sample dilution is inherent to the technique as well as co-purification of large protein aggregates and larger lipoproteins. The main advantage of SEC is the mild conditions in combination with acceptable purity [71, 86, 87]. Alternatively, sequential filtration steps can first eliminate larger contaminants and subsequently concentrate EVs and eliminate smaller contaminants. Yet a major disadvantage compared to SEC are the often high forces used (*via* air pressure or centrifugal forces) possibly compromising the EV integrity. Moreover, sticking of EVs to the membrane filters might limit the yield [87]. In most cases filtration is used as a preparative step prior to one of the techniques mentioned above.

Combining different purification methods based on complementary principles will be imperative to process very complex samples (e.g. plasma). The sequential combination of techniques is already commercially available, e.g. with the exo-spin^{TM} system (CELL guidance systems). This approach merges an initial concentrating step using the precipitation method with subsequent SEC to enhance the sample purity. It is of note that the diversity of purification techniques used throughout the literature hampers unambiguous comparison of different studies. Until now, the importance of EV purity is most emphasized in the field of biomarker discovery as it is clearly shown that different isolation methods might greatly alter the obtained RNA/protein profiles [66]. In **chapter 3** of this thesis we will experimentally compare different purification strategies and discuss the importance of EV purity outside the field of biomarker discovery.

2. Therapeutic applications of EVs

2.1. Harnessing the intrinsic biological effect of EVs

As discussed above, EVs are composed of numerous potentially bioactive molecules (i.e. lipids, proteins, nucleic acids and carbohydrates) of which the relative composition is regulated by the producer cell. In this respect, it is no surprise that EVs have an intrinsic biological effect that modulates the recipient cell's phenotype [88], which can be exploited in a therapeutic context. These phenotypical alterations can be elicited by a receptor-ligand interaction at the cellular surface [89, 90] or at the luminal side of the (late) endosomes, thus triggering a downstream signaling pathway [91, 92]. Alternatively, it is believed that EVs can fuse with cellular membranes (plasma membrane and/or endosomal membrane) and release their content in the cytoplasm [93] (**figure 2**).

As mentioned earlier, Raposo *et al*. showed that EVs derived from activated APCs could stimulate the immune system by presenting functional antigen-MHC complexes to T cells [10]. This observation was followed by many pre-clinical and clinical studies using antigen pulsed, DC-derived EVs as a cell-free alternative for cancer vaccination [94]. This application will be further discussed in **section 2.3**.

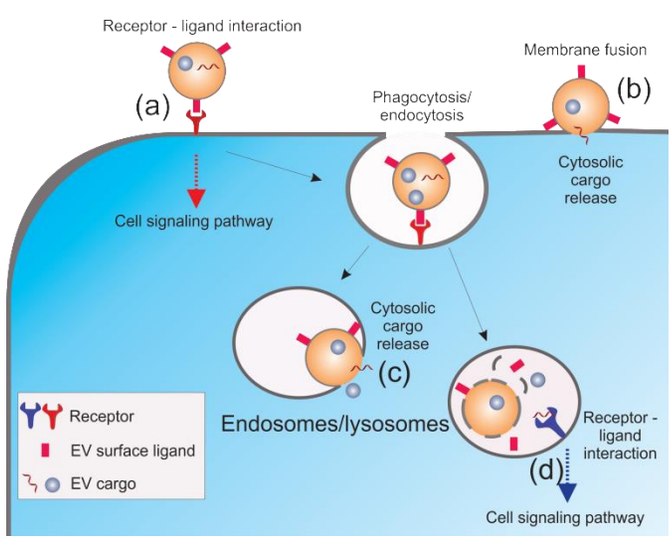

Figure 2. Mechanisms behind EV-mediated phenotypical changes in recipient cells. (a) The EV surface proteins/lipids can interact with receptors on the recipient cell's surface, eliciting an intracellular signaling pathway or triggering receptor mediated endocytosis. Alternatively, (b) the EV cargo (e.g. proteins and nucleic acids) can be released in the cell's cytoplasm *via* membrane fusion with the limiting cell membrane or (c) with the endosomal membrane after initial internalization *via* phagocytosis/endocytosis. Finally, it is also possible that (d) EVs release their content (after partial degradation) in the endolysosomes where it can trigger endosomal receptors (e.g. toll-like receptors).

Another example of the use of EVs as a cell surrogate therapy are mesenchymal stem cell (MSC)-derived vesicles. MSC are stromal cells with multipotent differentiation capacity and have been intensively investigated for their potential regenerative and immunosuppressive effects in many animal models and clinical trials. Although originally believed to be the result of MSC homing to and engraftment at injured tissues, it is now becoming increasingly clear that the biological effect of these cells is mainly to be attributed to their secretome, including EVs [95, 96]. In this respect, MSC-derived EVs have been studied in dedicated mouse models for their tissue-protective effects following acute kidney failure [95], myocardial infarct [97], liver injury [98] and neural injury after middle cerebrate artery occlusion [99]. Considering their immunosuppressive nature, MSC EVs are also under investigation for a multitude of inflammatory conditions. For instance, in the field of auto-immune diseases, EVs shed by MSC have shown to limit the pro-inflammatory response and induce a shift towards a beneficial regulatory T cell profile in type I diabetes [100], which is currently being investigated in a clinical setting (NCT02138331). As another example, MSC EVs are also successfully investigated in refractory graft-*versus*-host disease [80]. The exact mechanism behind the therapeutic effect of MSC-derived EVs remains largely obscure and is a topic of intensive investigation [101]. It is however known that stem cell EVs are enriched in signaling proteins, including cytokines, chemokines, interleukins and growth factors [102]. The use of EVs as a surrogate for cell based therapies is intensively studied as it might entail some benefits. EVs are more resistant to freeze-thaw processes, are genetically stable making them a safer alternative to whole cells and they are likely less immunogenic allowing allogeneic therapy. Multiple comprehensive reviews have been published giving a more detailed overview of published data on this topic [103, 104].

Next to their exploitation as surrogates for cell therapy, EVs from specific cell types have shown interesting features that can be exploited in a therapeutic context. For example, NK-cell derived EVs were shown to contain killer proteins (e.g. perforins) which are taken up by tumor cells and induce tumor cell death [47]. Adipose-derived stem cells (ADSC) release EVs containing Neprilysin (i.e. an Aβ-degrading enzyme), which lowered the Aβ-level secreted by N2A cells and thus might be a valuable therapy to investigate further in Alzheimer's disease [105].

It is of note that these reports have to be interpreted with careful consideration of the used EV purification protocol. Dependent on the selected method, non-EV contaminants can be co-isolated, possibly leading to observations being incorrectly attributed to EVs [29]. Moreover, many reports focus on a specific component of EVs, e.g. small non-coding RNA such as miRNAs, often neglecting the true complexity of the EV composition in which lipids and proteins likely also play a key role [106]. As a result of this

complexity, EVs can simultaneously interfere with different signaling pathways, leading to pleiotropic effects. For example, it was observed that EVs derived from immortalized cardiomyocytes (HL-1 cells) significantly altered the expression of 161 genes in fibroblasts (NIH/3T3 cells) after co-culture [107]. This complexity implies that the observed effects are likely very difficult to mimic by synthetic, single-API (active pharmaceutical ingredient) drug therapies. On the other hand, care should be taken that this intrinsic complexity does not impede the translatability of EVs into a viable pharmaceutical product [108].

2.2. Harnessing EVs as a drug delivery vehicle

2.2.1. Beneficial features of EVs as nanocarriers

As outlined above, EVs are involved in the communication between cells due to their ability to deliver biomolecules from one cell type to another, thereby crossing both extra- and intracellular barriers. Based on this particular feature, EVs are also envisioned as biological nanocarriers for the delivery of exogenous therapeutic (macro)molecules. The encapsulation of drugs in nanoparticles (creating so-called nanomedicines) is a well-established approach to (1) modify the pharmacokinetics (PK) and biodistribution of the therapeutic cargo, (2) solubilize hydrophobic drugs, (3) protect the drug from the extracellular environment and (4) guide the therapeutic cargo across existing extra- and intracellular barriers. Both low molecular weight chemotherapeutics, but especially membrane-impermeable macromolecular drugs (e.g. nucleic acids and proteins) require nanocarriers to enhance their delivery across biological membranes. Unfortunately, many synthetic nanoparticles, including lipid and polymer-based nanoparticles, demonstrate insufficient *in vivo* targeting to extrahepatic tissues and fail to merge (intracellular) drug delivery efficacy with biocompatibility [109]. Since the identification of EVs as nature's own intercellular communication tools, it is hypothesized that their Darwinian optimization could outperform conventional synthetic nanomedicines [110]. Indeed, EVs are believed to encompass many interesting features for drug delivery: (1) a proteo-lipid architecture that protects the encapsulated cargo, (2) their specific composition minimizes recognition by the mononuclear phagocyte system (MPS) [111], (3) their possibility to be patient self-derived nature mitigates activation of the adaptive immune system, (4) they contain specific lipids that help stabilize the vesicles in the blood circulation (e.g. GM3, sphingomyelin and cholesterol) and stimulate membrane fusion [52, 112] as well as surface proteins that have likewise been linked to membrane fusion in cell-cell and virus-cell interactions (e.g. CD9, CD81) [113, 114] and finally (5) EVs seem to possess intrinsic cell and tissue targeting properties [115].

2.2.2. Extracellular behavior of EVs

One of the main motivations to incorporate drugs into nanocarriers is to modulate their biodistribution and tissue targeting. Free drugs are often rapidly cleared from the body and show poor tissue selectivity, which can in part be remedied by their formulation into nanomedicines. Unfortunately, without appropriate surface modification (e.g. PEGylation), they are easily recognized by the MPS and rapidly cleared from the blood circulation, leading to predominant sequestration by liver and spleen and limiting extravasation in other tissues of interest. As EVs are abundantly present and stable in the blood circulation, it was speculated that EVs could have longer circulation times and mediate drug targeting to extrahepatic and non-lymphoid tissues. However, reports studying the PK of IV injected EVs observed short half-lives (~2 minutes [116, 117] and ~20 minutes [118]) with predominant uptake by liver, lung, kidney and spleen, thus closely resembling the biodistribution of synthetic liposomes [71, 119, 120]. The elimination after IV injection occurs *via* hepatic and renal routes [118] in which MPS-associated macrophages seem to play a key role [119]. It is conceivable that this recognition is in part mediated by the exposure of PS at the external side of EV (subtypes) [121, 122]. It is of note that in these studies tumor- or HEK 293T-derived EVs have been used. For immature DC-derived EVs it was reported that they carry surface proteins (i.e. CD55 and CD59) that inhibit complement-mediated clearance [123]. On the other hand, Whitehead *et al.* showed that EVs derived from malignant cells were far more prone to complement activation compared to non-malignant cells, which might help to explain some of the reported PK data [124]. Furthermore, also the selected purification protocol or the transfer of allogeneic EVs can potentially influence the EV's PK profile [71].

Despite the intrinsic targeting to APC and limited circulation time often reported for EVs, it appears that a certain fraction is still able to home to alternative organs and tissues. For instance, it was shown by Hoshino *et al.* that the integrins present on the surface of tumor-derived EVs determined the organs/cell types that are preferentially targeted [115]. Such observations rationalize the engineering of EVs with specific targeting moieties to enhance tissue or cell specific homing. One of the first engineered EVs was reported by Alvarez-Erviti *et al.* who equipped EVs from immature DCs with a Lamp2b-RVG targeting peptide, *via* genetic engineering of the producer cell with the respective plasmid construct, to enable delivery of siRNA across the blood brain barrier (BBB) [125]. The same targeting ligand was also used to shuttle liposomes over the BBB for the delivery of siRNA [126]. The BBB targeting enhancement was later quantified by Wiklander *et al.* to be around two-fold [120]. Nonetheless, the majority of the vesicles is still present in MPS-associated tissues (i.e. liver, spleen and lung) [120]. The fact that targeting ligands are providing modest benefits is likely the result of the short circulation

time. On the other hand, the partial degradation of the RVG targeting peptide during EV formation might also contribute to this observation. Indeed, Hung *et al.* showed that when fusing a targeting peptide to the Lamp2b protein (a protein inherently present on the EV surface), it should be equipped with glycosylation sites to protect it against protease degradation by the producing cell. The unprotected Lamp2b-RVG targeting construct showed only marginally improved internalization by N2A cells bearing the nicotinic acetylcholine receptor (i.e. the RVG target) compared to non-targeted EVs due to peptide degradation [127]. In analogy with reports on synthetic liposomes, efforts to simultaneously enhance the circulation time and confer specific targeting properties have also been explored for EVs. For instance, hydrophilic PEG-chains were inserted in the EV lipid bilayer carrying targeting nanobodies® at their distal end to both shield the EV surface from off-target interactions (leading to a prolonged circulation time) yet allow specific interactions with a targeted receptor [128, 129]. However, such approaches greatly alter the composition and behavior of EVs, both in the extracellular environment as well as following intracellular uptake, and the question is raised to what extent these approaches are advantageous over synthetic drug-loaded nanocarriers.

The ability to cross the BBB is an interesting and often referred to feature attributed to EVs. Although the RVG-targeting ligand associated to the EV surface in the previously mentioned studies likely plays a potentiating role [125], EVs derived for unmodified hematopoietic cells were also shown to cross the BBB. This event was reported to be rare, yet vastly increased under peripheral inflammatory conditions [130]. The mechanism behind this process remains to be elucidated. One hypothesis is based on transcytosis in which EVs are internalized by (apical) endocytosis of endothelial cells and are again released intact by exocytosis at the basolateral side [131]. A recent study compared four types of EVs derived from different brain cells (i.e. brain endothelial cells (bEND.3), glioblastoma A-172 cells, neural glyoblastoma U87 cells and neuroectodermal tumor PFSK-1 cells) for their ability to deliver cytotoxic drugs over the BBB in an embryo zebrafish model. Only the bEND.3 derived EVs were able to transfer their cargo into the brain, underscoring the existence of EV specificity [132].

Besides transferring cargo over the BBB, tumor targeting is another therapeutic application for which nanomedicines can provide a clear benefit. For this purpose, nanomedicines typically rely on the enhanced permeation and retention (EPR) effect to extravasate and accumulate in the tumor mass. Based on their small size, it is conceivable that EVs can also exploit this effect for anti-cancer treatment. However, such passive targeting of EVs to tumors gave rise to contradictory results. Smyth *et al.* IV injected EVs (60 µg) derived from the tumor itself but found very little amount in the tumor tissue (4T1 breast cancer and PC3 prostate cancer cells) compared to liver and spleen [119]. In contrast, Lai *et al.* found a marked signal of HEK293-derived EVs (100

µg) in the tumor (Gli36 glioblastoma) alongside with the liver and spleen [118]. An example of successful active tumor targeting by modified EVs was reported by Ohno *et al.* who observed a three-fold enhancement in the tumor tissue (HCC70 hepatocellular carcinoma) using EGFR-targeted (*via* the GE11 peptide) EVs [133]. Comparable results were obtained with iRGD equipped EVs that bind to $\alpha_v\beta_3$ integrins in tumor tissue. Importantly, these vesicles, when loaded with doxorubicin, strongly reduced tumor growth in a MDA-MB-231 breast cancer cell model [134]. Inspiration for targeting ligands is often obtained from viruses. For instance, HEK293-derived EVs have been modified with gp350 (i.e. a ligand for CD21 expressed on B cells and a component of the Epstein-bar virus (EBV) envelope), conferring the viral tropism to EVs for normal and leukemic B cell targeting [135].

Finally, altering the PK of EVs can also be done by changing the route of administration. Indeed, Wiklander *et al.* compared IV, SC and IP injection of HEK293T EVs showing a clear difference in biodistribution [120]. After footpad injection accumulation of EVs in the lymph nodes was reported [136, 137] and intranasal application showed an accumulation in the brain [138, 139], in which the delivered anti-inflammatory cargo (i.e. curcumin) could still be detected up to 12 hours after administration [138].

2.2.3. Intracellular trafficking of EVs

The ability of EVs to shuttle their cargo over the cellular barriers is of key importance. Especially when considering EVs for the delivery of macromolecular therapeutics, which require delivery into the cell's cytoplasm (e.g. miRNA, mRNA) or even nucleus (e.g. pDNA).

Nanoparticles can employ distinct endocytic uptake pathways to gain access to cells. Numerous studies have investigated the mechanism(s) by which EVs are associated to and subsequently internalized by cells. Many different types of surface molecules, both EV- and cell-associated, have been identified as being involved in EV-cell contact (i.e. tetraspanins, integrins, proteoglycans and lectins) as comprehensively reviewed by Mulcahy *et al.* [140]. These interactions, possible preceded by surfing onto filopodia [141], mostly lead to cell uptake *via* one of the common endocytosis pathways (i.e. clathrin- and caveolin-dependent endocytosis, lipid raft-mediated endocytosis, macropinocytosis or phagocytosis) [106, 140]. It is also interesting to note that inhibition of a given pathway is almost never able to completely abrogate the EV uptake, hinting toward the involvement of multiple uptake mechanisms and/or reflecting EV heterogeneity [140]. In this regard, it would be an interesting strategy to also link the effect of uptake inhibitors to the induced phenotypical changes in recipient cells as this would help to elucidate which specific uptake pathway(s) lead(s) to functional cellular release of the EV cargo.

As the interaction of EVs with cells likely involves multivalent ligand-receptor binding and subsequent endocytosis, it is reasonable to assume that they finally are trafficked to lysosomes for degradation [141, 142]. Hence, delivery of drugs into the cell cytoplasm will require a mechanism that allows the EV cargo to escape the endolysosomal compartment. Also for synthetic nanomedicines the endolysosomal entrapment is one of the major hurdles for efficient cellular delivery. The delivery efficiency of nanomedicines hinges on strategies to cross the endosomal barrier, such as the so-called proton sponge effect and/or lipid bilayer fusion [143]. As many of the effects mediated by EVs have been attributed to the functional delivery of miRNA and mRNA [88], this implies that (subtypes of) EVs contain built-in mechanisms to stimulate endosomal escape. The most plausible theory describes back-fusion of internalized EVs with the endosomal membrane, thus releasing their content in the cytoplasm (**figure 2**). However, few reports directly demonstrated EV fusion with plasma-and/or endosomal membranes. Some studies labeled EVs with a self-quenching dye after which they were incubated with cells. An enhancement of fluorescence was indicative of dye dequenching and hence fusion of (a fraction of) EVs with cellular membranes [52, 93]. Alternatively, luciferin containing EVs were able to evoke a luminescent signal after interaction with luciferase expressing cells, suggesting cytosolic delivery of the EV luminal cargo [93]. Whether this intracellular delivery process is linked to a particular receptor-ligand interaction or requires a specific proteolipid composition is currently unknown.

Alternative to relying on the intrinsic EV properties to obtain functional delivery, EVs have been modified with delivery-enhancing peptides. Temchura *et al.* decorated antigen-loaded EVs with a vesicular stomatitis virus G (VSV-G) protein to stimulate the cross-presentation of these antigens in recipient DCs [144]. The VSV-G protein promotes the fusion of lipid membranes at lower pH (i.e. ~6) and can thus drive destabilization of the endosomal/phagosomal membrane following internalization [145]. These authors showed that the VSV-G protein stimulated MHC I mediated antigen presentation and elicited an antigen-specific $CD8^+$ T cell response [144]. The previously mentioned RVG targeting ligand [120, 146, 147] and iRGD [134, 148] have also been reported to have membrane-destabilizing properties, possibly contributing to enhanced cytoplasmic delivery of the encapsulated cargo.

It is of note that not for all phenotypical effects EV internalization is necessary. Physiological effects attributed to EVs can be based on proteins and lipids present on the surface of EVs interacting with ligands on the target cell's surface, triggering intracellular signaling pathways (**figure 2**) [89, 149-151] or *via* enzymatic activity present inside or on the surface of EVs [152].

2.2.4. Loading EVs with a therapeutic cargo

The clinical implementation of EVs as a viable drug delivery platform will require optimized methods allowing efficient loading with the drug of choice. As already indicated above, EVs have been evaluated as a drug delivery vehicle for a vast diversity of therapeutic cargos, including both small molecules (e.g. doxorubicin, curcumin,…) and macromolecules (i.e. RNA, DNA and proteins). The strategies to incorporate these drugs into EVs can generally be divided in pre- and post-formation approaches (**figure 3**) [153]. In the former case, the therapeutic cargo is first loaded into the respective producer cell followed by its packaging into EVs during their biogenesis. For the latter approach, EVs are first purified from the producer cell's conditioned culture medium after which they are loaded with the therapeutic cargo *via* one of the methods represented in **table 2**.

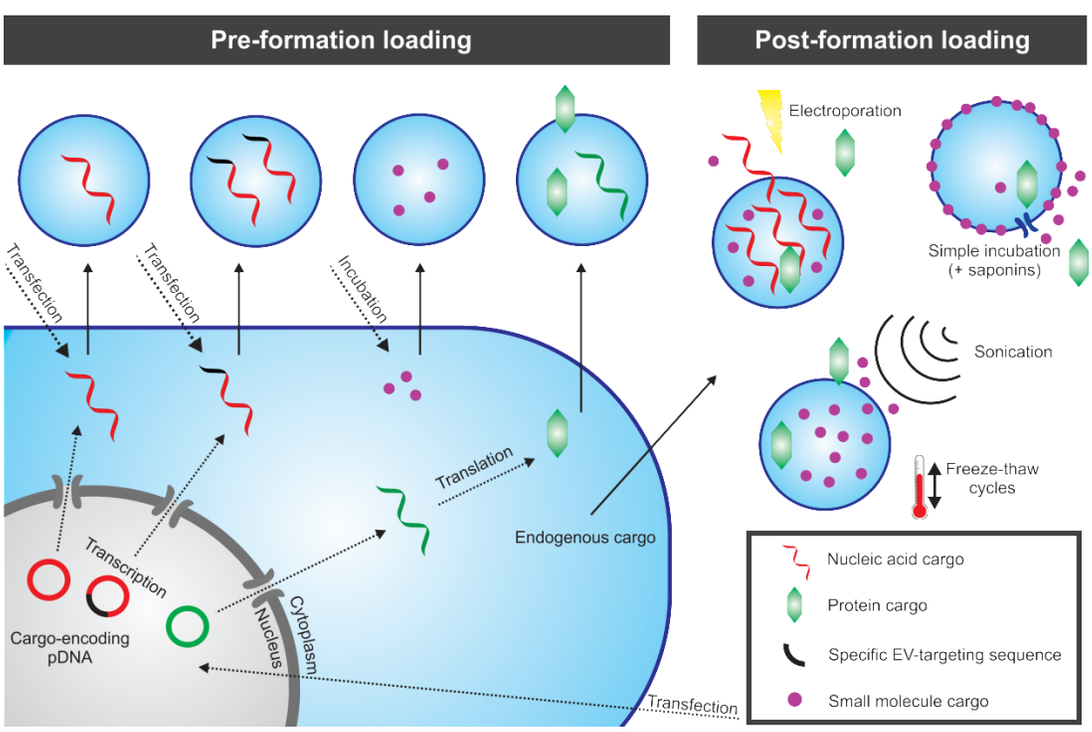

Figure 3. Schematic outline of strategies explored in the literature pertaining to the incorporation of therapeutic agents into EVs. Pre-formation strategies rely on the cell to incorporate the therapeutic cargo into EVs. This cargo can be directly transfected into the cellular cytoplasm or can be encoded for *via* the transfection of the respective pDNA, creating a more sustainable production source. Both for nucleic acids (e.g. mRNA and miRNA) and proteins, some sequences are known that can enhance the cargo's incorporation into EVs. Post-formation loading strategies start from purified EVs. Hydrophobic cargoes can be loaded into the EV membrane by incubation at ambient or enhanced temperature. Hydrophilic cargoes (e.g. enzymes, nucleic acids) are loaded by inducing transient pores *via* electroporation, sonication, freeze-thaw cycles or saponins in the EV membrane enabling the cargo to passively migrate into the EV lumen.

Table 2. Post-formation loading strategies for EVs

Method	Cargo	Efficiency	Remarks	Ref.
EP: • M^+ electrodes (400 V; 125 µF) • Buffer: Optiprep™; neutral pH	siRNA	25 % of the total siRNA	EVs are equipped with a RVG targeting peptide and show functional transfer of siRNA over the BBB	[125]
EP: • M^+ electrodes (150 V; 100 µF) • Buffer: Cytomix buffer	siRNA	90 % of the total number of beads carrying EVs is positive for siRNA	Delivery to monocytes and lymphocytes	[154]
EP: • N.R.	miRNA	No significant encapsulation reported	Switched to pre-formation loading (see table 3)	[133]
EP: • M^+ electrodes (0.75 kV/cm) • Buffer: Trehalose containing buffer	5 nm superparamagnetic iron oxide nanoparticles	0.40 - 0.45 µg iron/µg EV		[155]
EP: • M^+ electrodes • Buffer: PBS	70 kDa Dextran /Saporin	0.4 % and 0.5 % of the total dextran and saporin, respectively.	Required Lipofectamine LTX and GALA fusogenic peptide for functional, *in vitro* delivery	[156]
EP: • M^+ electrodes (350 V; 150 µF) • Buffer: non-specified electroporation buffer	Doxorubicin	20 % of the added doxorubicin	EVs equipped with a targeting ligand (i.e. iRGD associated to LAMP2) – non targeted EVs were not functional	[134]
Co-incubation (T=37°C)	miRNA (miR-150)	N.R.	Indirect proof of successful delivery is provided *via* restoration of the effect when using miR-150 knockout EVs	[157]
Co-incubation + 0.01 % saponins, *freeze/thaw, *sonication, *extrusion	Catalase (240 kDa)	~15 – 25 % of the added catalase	* indicated techniques show significant alteration of the EV structure	[139]
Co-incubation (+ 0.01 % saponins), hypotonic dialysis	Porphyrins	Up to ~2.5 x 10^{15} molecules/EV	Allowed to induce phototoxicity in tumor cells	[158]
Co-incubation (T=22°C – 5 minutes)	Curcumin	2.9 µg/µg EVs	IP injection	[159]
Co-incubation (T=22°C – 5 minutes)	Cucumin / JSI-124	N.R.	Intranasal administration	[138]
Co-incubation (T=37°C – 2 h)	Doxorubicin / paclitaxel	132 ng/µg and 7.3 ng/µg, respectively		[132]
EV-liposome mixing followed by freeze-thaw cycles	Lipids (-PEG)	N.A.	Alteration of the EV membrane composition	[129]

Method	Cargo	Efficiency	Remarks	Ref.
EV-micelle mixing followed by elevation of temperature (40°C)	Lipids (-PEG) (-nanobody®)	N.A.	Incorporation of targeting nanobodies + PEGylation for an enhanced circulation time *in vivo*	[128]

EP electroporation; M^+ metal; PBS phosphate buffered saline; N.R. not reported; N.A. not applicable; GALA: a pH-sensitive fusogenic peptide; IP intraperitoneal; PEG poly(ethylene glycol).

In a pre-formation loading approach the endogenous sorting machinery of the cell is used to load the cargo into the EVs (**table 3**). Loading of specific nucleic acids (siRNAs, miRNAs, mRNAs) into EVs can be accomplished by transfection of the producer cell with the respective cargo by lipofection [53]. A comparable approach, by incubating the producer cell (i.e. MSC) with free paclitaxel, has also been evaluated. The paclitaxel-loaded EVs that were secreted by the MSCs, induced an anti-proliferative effect on *in vitro* cultured adenocarcinoma cells [160]. Alternatively, the RNA of interest can be expressed in the producer cell *via* a plasmid vector encoding for the respective therapeutic nucleic acid (e.g. miRNA [161], siRNA [162], mRNA [163]). Unfortunately, such pre-formation loading approaches typically show limited loading efficiency and should be optimized for each selected producer cell type and cargo. In addition, one needs to anticipate that the selected cargo can influence the producer cell's functionality and viability, hence impairing the loading process. Although still largely elusive, the expanding knowledge on the endogenous cargo sorting machinery can be exploited to increase the drug loading efficiency by modifying the therapeutic cargo. In this respect, proteins can be equipped with a plasma membrane anchoring and oligomerization domain to stimulate EV loading [164]. Alternatively, proteins can also be sorted into EVs by creating a fusion construct, containing the protein of interest linked to a protein that is inherently associated to EVs as has been done for EV targeting purposes (**section 2.2.2**) [146, 165] or to fluorescently label EVs (e.g. CD63-GFP) [166]. Likewise, also for nucleic acids, evidence is mounting that by altering the nucleotide sequence the sorting efficiency can be modulated. Bolukbasi *et al.* identified a specific sequence in the 3'-UTR region of mRNA strands that promotes its accumulation in glioblastoma-derived EVs. This ~25 nucleotide sequence contained a miR-1289 binding region and a CUGCC sequence. Incorporation of this so-called 'zip-sequence' in the 3'-UTR of a mRNA strand increased its packaging into EVs two-fold compared to the unmodified sequence. This enrichment could even be further enhanced when miR-1289 was overexpressed in the producing cell [35]. Regarding miRNA sorting, Koppers-lalic *et al.* discovered that 3'-uridylated miRNAs are enriched in human B cell-derived EVs [41]. Villarroya-Beltri and colleagues showed that miRNAs containing a GGAG sequence were overrepresented in primary T lymphoblast EVs. They suggest that this sequence is selectively recognized by

the RNA binding protein heterogeneous nuclear ribonucleoproteins A2/B1 (hnRNPA2B1) and subsequently drives incorporation into EVs [34]. However, these sequences could not be retrieved in miRNA accumulating in colorectal cancer-derived EVs, implying the existence of distinct sorting pathways, which possibly differ between cell types [167]. Although progress is being made, in general these sorting mechanisms remain vaguely defined.

In addition to the above mentioned loading approaches for small molecules and macromolecules, viral capsids (i.e. adeno-associated virus; AAV) have been loaded in EVs thus creating so-called vexosomes. These hybrid vesicles are composed of viral particles coated with or associated to EVs. Vexosomes aim to merge the efficient transfection capabilities of the AAV and the immune-shielding properties of EVs to produce a potentially efficient and biocompatible delivery vehicle [168-170].

On the other hand, post-formation loading approaches attempt to load drugs in isolated and purified EVs. In this regard, the most frequently reported method, especially for hydrophilic membrane-impermeable components, is electroporation (EP). EP is traditionally used to introduce nucleic acids in cells, using high-voltage electric pulses to create transient pores in the plasma membrane [171]. The group of Matthew Wood reported the first successful EP of siRNA into DC-derived EVs, allowing functional delivery across the BBB in a mouse model of Alzheimer's disease [146]. Following this pioneering report, other research groups have shown comparable results for loading siRNA and even DNA strands up to 1000 bp into EVs [154, 172-175]. Besides nucleic acids, 5 nm superparamagnetic iron oxide particles and large proteins have been loaded in purified EVs using EP (**table 2**). Despite the widespread use of this technique, no thorough investigation of the biophysical background is available. In this respect, **chapter 2** is devoted to critically evaluate EP as a loading method for siRNA. Other post-formation strategies that are being explored for hydrophilic molecules are also based on transiently destabilizing the EV membrane, including repeated freeze-thaw cycles, sonication, extrusion or saponin treatment (**table 2**). These techniques have been evaluated for both small molecules (i.e. porphyrins) [158] as well as macromolecules (i.e. the 240 kDa catalase enzyme) [139]. It is important to note that for the former methods, the integrity of the EVs can be significantly compromised [139]. One report also suggests that antibody-coated EVs derived from B1a cells can interact with and take up miRNAs from the environment by simple co-incubation and subsequently shuttle it into cells. However, the mechanism behind this post-formation miRNA loading, as well as the generality of this loading approach, remain to be elucidated [157].

For hydrophobic membrane-permeable molecules, simple co-incubation at ambient or elevated temperature are often sufficient to load EVs [132, 159]. Indeed, EVs derived

from EL4 cells incubated with curcumin at room temperature were, after intranasal delivery, able to significantly delay brain tumor growth in the GL26 mice tumor model [138]. Curcumin-loaded plant EVs for example, are currently under clinical evaluation in colon cancer (NCT01294072). An overview of other small molecules loaded *via* co-incubation is given in **table 2.** However, leakage of these therapeutics out of the vesicles in biological fluids (e.g. plasma) can limit their practicality.

As long as the fundaments of EV biogenesis and cargo sorting are not clear, pre-formation methods will suffer from limited efficiency. Indeed, when comparing both loading strategies for paclitaxel, the post-formation method yields ~21 mg/g EV [176] and ~7.3 mg/g EV [132] compared to ~2 µg/g EV [160] for the pre-formation method. Overall, loading hydrophobic small molecules in EVs is more straightforward and efficient. For post-formation loading of hydrophilic compounds, especially macromolecules, important progress still has to be made before efficient clinical application of EVs as drug delivery vehicles can be envisioned.

2.2.5. Producer cell source selection

The choice of an adequate producing cell when aiming to exploit EVs as a drug delivery vehicle, is of pivotal importance as it will define the PK behavior (i.e. the stability in the blood circulation and organotropism; **section 2.2.2**) and the intrinsic biological effect (both physiological and pathological; **section 2.1**) of the EV carrier. It has been suggested that MSCs form a sustainable source of EVs. MSCs produce high quantities of EVs and neither the EV yield nor their composition is altered by immortalizing the producer cell. Moreover, MSCs are known for their low immunogenicity making allogeneic applications possible [80, 177] (NCT02138331). However, it is also shown that MSC-derived EVs stimulate tumor vascularization and tumor growth which might induce undesirable off-target effects [178]. Besides MSCs, immature DCs have also been proposed as an interesting EV source due to their low immunogenicity, immunosuppressive effects and the ease with which autologous sources can be obtained [110, 179].

As the field is moving closer to clinical applications, the concept of high vesicle yield with minimal production costs is of increasing importance. In this respect, research groups have started to focus on alternative sources of EVs. Grapefruit- and milk-derived EVs have been investigated as drug delivery vehicles [180-182]. Additionally, the idea of creating EV mimicking vesicles is gaining interest (e.g. by means of sequential extrusion of cells through micro- and nanoporous filters [183, 184] or by mixing synthetic components attempting to reproduce the most important EV characteristics [185]). However, the latter approach is difficult to implement as long as the knowledge on which components are essential for EV functionality is lacking or incomplete.

Table 3. Pre-formation loading of EVs

Cargo	Producer cell	Method of producer cell transfection	Efficiency	Target cell/Functional delivery?	Remarks	ref
Mir-143 and mir-143BP[1]	THP-1	Lipofection: LipoTrust™ EX Oligo + miRNA	Estimation: 0.2 - 0.25 % of the stabilized miRNA present in the cell	No functional delivery reported	Differentiation of THP-1 cells into macrophages further stimulated miRNA secretion in EVs / immune-EM confirmation of miRNA presence	[186]
mRNA	HEK-293T	Lipofection: Lipofectamine 2000 + plasmid (+ 3' UTR zipcode sequence)	No absolute values reported per EV (~2 fold increase *versus* non-modified)	No functional delivery reported		[35]
mRNA (CD-UPRT [4] mRNA) / respective protein	HEK-293T	Lipofection: Lipofectamine 2000 + plasmid (equipped with a strong promoter i.e. cytomegalovirus promotor)	No absolute values	HEI-193 cells	Used as enzyme to functionalize a small molecule chemotherapeutic prodrug (5-fluorocytosine) / sucrose gradient to confirm EV association	[187]
miRNA (let7a)	HEK293	Lipofection: HiPerFect reagent + plasmid (final concentration 50 nM)	No absolute values	Breast cancer cells (HCC70)	GE11 peptide for EGFR targeting	[133]
miR-143, miR-146a, miR-155	HEK293/ COS-7	Lipofection: LipofectamineLTX + plasmid overexpressing the respective pri-miRNA	2.57 %, 15.6 %, 1.38 % (percentage extracellular *versus* intracellular)	COS-7	EV association confirmed using RNAse treatment / using the neutral sphingomyelinase inhibitor GW4869	[161]
mRNA: Cre recombinase mRNA (+ protein?)[2]	MDA-MB-231 mammary tumor cells	Lipofection: lipofectamine 2000 + plasmid	No absolute values	MCF-7 and T47D mammary tumor cells	Included delivery over long distance *in vivo*	[163]
(Cy3-tagged) miR-223	Macrophage (IL-4 activated)	Lipofection: X-tremeGENE siRNA Transfection Reagent + miRNA	No absolute values	Breast cancer cells (SKBR3)	Delivery experiment via co-culture system	[188]

Cargo	Producer cell	Method of producer cell transfection	Efficiency	Target cell/Functional delivery?	Remarks	ref
(FITC-tagged) miR-150	THP-1 cells	Lipofection: lipofectamine 2000 + pre-miRNA (400 pmol per 60 mm dish)	0.002 pmol miRNA per µg EV (protein concentration)	HMEC-1 cells	Targeting of c-myb	[53]
siRNA	L929 cells	Lipofection: lipofectamine 2000 + siRNA duplex (60 pmol per 10^5 cells)	0.001 pmol siRNA per µg EV (protein concentration)	S180 cells	0.4 pmol siRNA per mouse (400 µg EVs per mouse)	[189]
Paclitaxel	MSCs (SR4987 cells)	Incubation of producer cell with 2000 ng/ml paclitaxel for 24 h	2.03 ng paclitaxel/mg protein	CFPAC-1 (i.e. a paclitaxel sensitive adenocarcinoma cell line)	EVs loaded with paclitaxel show an anti-proliferative effect	[160]
Adeno-associated virus (AAV)	HEK 293T cells	Calcium phosphate transfection of plasmids coding for different AAV components	0.01 % - 0.2 % of the produced AAV are associated to EVs (depending on the AAV subtype)	U87 and 293T cells	EVs protect AAVs from immune recognition	[168]
TyA-GFP as model protein	Jurkat T-cells	Electroporation of the respective plasmid	>10-fold increase compared to unanchored	No functional delivery reported	Targeting proteins to EVs *via* membrane anchors[3] and the TyA-oligomerization domain	[164]
siRNA (*via* plasmid)	HEK 293T	Lipofectamine 2000 + plasmid	~0.15 pmol/µg EV	Neuro2A	RVG targeting (*via* fusion to the LAMP2 protein, which is inherently present on EVs)	[162]
Iron oxide nanoparticles	THP-1	Incubation in serum free medium		SKOV-3 cells	Magnetic targeting *in vitro*	[190]

[1]An aromatic benzene-pyridine analog was added to the 3'-overhang region of the RNA strand (higher nuclease resistance). [2]Part of Cre-LoxP system to visualize functional protein/mRNA delivery to recipient cells. [3]E.g. myristoylation tag or PIP2-binding domain. [4]Cytosine deaminase-uracyl fosforibosyltransferase.

2.3. EVs as vaccination platform

The first therapeutic application of EVs was based on the use of DC-derived EVs as a surrogate for DC-based anticancer vaccination [11]. APC-derived EVs harbor both (antigen-loaded) MHC I and II as well as the necessary co-stimulatory factors to directly trigger ($CD8^+$ and $CD4^+$) T cell activation [10, 48]. However, *in vivo,* DC-derived EVs likely interact first with endogenous DCs (*via* cell surface adhesion or intracellular processing), transferring their antigens to endogenous APCs and so augmenting T cell activation [191, 192]. The use of DC-derived EVs for cancer immunotherapy has already been evaluated in phase I clinical trials for both melanoma [14] and non-small-cell lung carcinoma (NSCLC) [78]. Although DC-derived EVs exhibited an excellent safety profile, the therapeutic effects were limited with no substantial $CD8^+$ T cell response. Nonetheless, pre-clinical studies have shown that co-delivery of adjuvants could vastly improve the evoked immune response. In this respect, Chaput *et al.* reported the combination of DC-derived EVs with CpG (a TLR3 agonist) [193], Guo and colleagues combined DC-derived EVs with another TLR3 agonist, i.e. polyinosinic-polycytidylic acid (poly(I:C)) and cyclophosphamide [194] and Gehrmann *et al.* associated α-galactosylceramide (an iNKT stimulatory factor) to antigen-loaded DC-derived EVs, which induced a potent NK, $\gamma\delta$-T cell innate immune response and enabled proliferation of antigen-specific T and B cells [195]. Currently, a phase II clinical trial in NSCLC patients (NCT01159288) is evaluating the combination of cyclophosphamide with DC-derived EVs (pulsed with a range of antigens and INF-γ) that showed an improved immune stimulatory capacity in pre-clinical studies [196].

As pointed out above (**section 1.2**), EVs derived from cancerous cells have shown to carry a panel of known (e.g. CEA, GP100, HER2, melan-A, PSMA) [46, 197] and likely to date unknown tumor antigens. This is not only of interest from a diagnostic point of view but also makes tumor-derived EVs, which have shown to outperform free antigens [195, 198] and whole tumor lysate [199, 200], an attractive candidate to evaluate as a cell-free vaccine. Building on these promising observations, a clinical trial has been conducted using EVs isolated from ascites fluid. Unfortunately, similar to the DC-derived EVs, the effect of unmodified EVs was unsatisfactory. However, when co-injecting GM-CSF as adjuvant, a more pronounced anti-tumor cytotoxic T lymphocyte response was induced [77]. Just as for DC-derived EVs, tumor-derived EVs in preclinical reports benefit from the indirect antigen presentation by endogenous APCs. This can be stimulated by combining tumor-derived EVs with synthetic adjuvants [201] or using EVs derived from (genetically) modified tumor cells to enhance the presence of adjuvant-like components (e.g. heat treatment to enhance hsp70 in tumor-derived EVs [202] or genetically engineer tumor cells to release IL18 [203] or IL12 [204] in EVs). It appears

that for both strategies of EV-mediated anticancer vaccination, vesicles have to be modified to enhance their immune stimulatory effect.

Despite the multitude of reports showing the potential of (adjuvant-modified) tumor-derived EVs as antigen delivery vehicles, caution should be taken as there is mounting evidence that tumor-derived EVs exhibit immune suppressive characteristics. Indeed, besides antigens, the presence and functional transfer of fasL [205], TGF-β [206] and NKG2D ligand [207] by tumor-derived EVs was also reported, all of which can blunt the activity of effector T cells. Moreover, some tumor-derived EVs are considered pro-metastatic *via* niche formation [115, 208], angiogenesis stimulation and extracellular matrix degradation (e.g. *via* the presence of metalloproteinases) [209]. Additionally, providing a source for tumor-derived EVs in a clinical context is not evident. The most elegant, easy accessible source is ascites fluid. However, only few tumors entail the accumulation of EVs in this biofluid [46]. Alternatively, EV mimics can be produced from cancer cell biopsies *via* sonication. Whether these vesicles have the same ability as natural EVs to evoke an anti-tumor immune response is not known [210]. To make use of tumor-antigen bearing EVs without the negative characteristics of tumor-derived EVs, a DNA vaccine (delivered *via* an adenoviral vector or EP) was developed that encodes a fusion protein comprising (the extracellular part of) a known tumor-antigen and an EV-associated protein (C1C2 domain of lactadherin or the gag protein). Expression of this fusion construct shuttles the associated antigens to the surface or lumen of secreted EVs, respectively [165, 211]. Nevertheless, this technology is limited to well-characterized antigens and would likely benefit from an additional immune modulator. Excellent dedicated reviews on the interplay between EVs and the immune system can be found in the literature [212].

Next to eukaryotic cells, also prokaryotic cells release vesicles in the extracellular environment, which are termed outer membrane vesicles (OMVs). It is interesting to note that the use of OMVs as vaccination tool against infectious diseases is currently the most advanced therapeutic application of EVs with different ongoing and completed clinical trials (up to phase IIIb; e.g. NCT01423084, NCT01478347, NCT02446743, …) and a selection of OMVs that have already reached market approval (e.g. Bexsero® and MenBvac® for serogroup B meningococcal disease). For a comprehensive discussion on the use of OMVs as vaccination technology the reader is referred to Van Der Pol *et al.* [213].

3. Diagnostic applications of EVs

3.1. An introduction to biomarkers

A biomarker can be defined as an objectively measured characteristic that indicates the medical state of the patient. Biomarkers can assist clinicians in making a reliable diagnosis and can be used as a clinical endpoint surrogate in clinical trials. For both applications it is critical that the correlation between disease and biomarker is well characterized and validated [214].

A reliable biomarker has to fulfill a number of prerequisites. First, a biomarker needs to be specific, a feature with which many known biomarkers struggle (e.g. prostate specific antigen (PSA) often gives false positives for benign prostate hypertrophy) [215]. Also, it is of critical importance that a biomarker is robust and valid meaning that under all given conditions a correlation exists between the biomarker and the disease. In this respect it is important to have a clear understanding of the role of the biomarker in the pathophysiology of the disease. Ideally, biomarkers should be predictive, indicating that the quantity of the biomarker can be (positively or negatively) correlated with the severity of the disease. Furthermore, it is of interest that the biomarker is easy accessible, thereby minimizing the burden for the patient. Finally, the sensitivity of the biomarker (or diagnostic assay to quantify the biomarker) will determine the extent to which early diagnosis is feasible [214].

Parallel with the emergence of personalized medicine, the importance of adequate biomarkers is further increasing. Personalized medicine can provide a significant benefit for diseases exhibiting a strong inter-patient pheno- and/or genotype heterogeneity, as is the case for many tumors [216]. Therapies that are tailored towards a specific phenotype (e.g. Herceptin® for HER2 positive breast cancer patients) are often developed in parallel with a biomarker assay (i.e. a companion diagnostic), which enables the clinician to select patients who are eligible for the respective therapy [217].

3.2. EVs as biomarker

EVs can be regarded as a stable and easy accessible fingerprint of the parent cell [218]. Indeed, the EV composition will depend on the type and even status of the producer cell [219, 220]. As EVs are avidly secreted by the large majority of cell types in the human body, they can be retrieved from all bodily fluid [221]. EVs have been isolated from e.g. urine [12], plasma [27], semen [26], nasal secretion [25], breast milk [222], the aqueous humor of eyes [223], cerebrospinal fluid [224], peritoneal fluid [225] and bronchoalveolar lavage (BALF) [226]. Depending on the disease for which the biomarker is being developed, an accessible biofluid should be considered in which the EVs of interest are likely the most concentrated and a liquid biopsy can be easily obtained.

Moreover, due to their liposome-like architecture, EVs protect their cargo against the harsh environment present in many of these media providing a more stable, hence reliable, biomarker source compared to naked RNA or proteins in e.g. blood.

EVs have been linked to a plethora of (patho)physiological processes. They are involved in maintaining cellular homeostasis but have also been linked to, for example cancer progression. Glioblastoma-derived EVs have shown the ability to spread oncogenic transformation by transferring the oncogenic form of the epidermal growth factor receptor (EGFRvIII) to surrounding cells [227]. These EGFRvIII expressing vesicles were also detected in the serum of 7 out of 25 glioblastoma patients and have been proposed as biomarker source [13]. Additionally, tumor-derived EVs have shown the ability to promote cancer growth by inhibiting cancer-specific immune recognition (**section 2.3**) [89, 228]. Moreover, EVs are also involved in the metastasis of tumor cells as they are believed to prepare a pre-metastatic niche at a secondary tissue or organ (the seed-and-soil hypothesis) [115, 136, 208]. The fact that EVs play such an important role in the process of tumor formation strengthens the validity and robustness of their use as biomarker in cancer detection. Besides cancer, EVs are also exploited by viral particles (e.g. HIV, EBV, hepatitis C) to mediate their spread, making EVs valuable tools to detect viral diseases as well [229]. Furthermore, EVs are associated with neurological, metabolic, cardiovascular and kidney conditions and are therefore also proposed as biomarkers for these diseases [230-232].

In the literature, many different clinical samples have been shown to contain EV-associated biomarkers with diagnostic/prognostic value or disease monitoring potential. In this respect, the EV concentration present in serum of tumor-bearing patients was shown to be increased compared to healthy controls [218, 233-236]. The EV protein abundance also has prognostic value as it was observed that patients with stage III melanoma with a high EV-associated TYRP2 protein burden, showed increased risk of disease progression [208]. Moreover, following resection of the primary tumor, the EV concentration markedly decreased, indicating its correlation with the tumor presence [236]. However, relying solely on EV concentration lacks specificity as the same observation was made for distinct cancer types [218, 233-236] and, importantly, for non-disease stimuli (e.g. physical exercise [237]). Furthermore, early diagnosis of many cancers will not be possible. Therefore, it is of outstanding interest to look in more detail to the EV cargo (i.e. proteins, miRNA, mRNA,…) as they provide an easy accessible window to monitor the status of the respective producer cell (**section 1.2**). In this respect, the exploitation of comparative omic-studies is fundamental for the detection of new biomarkers. For instance, it was revealed that a panel of eight EV-associated proteins was upregulated in the urine of patients with bladder cancer compared to healthy subjects [238]. Likewise, miRNA profiling of plasma-derived EVs identified a

panel of four tumor-specific miRNAs of potential use in a screening test for lung carcinoma [239]. A comprehensive review on this topic was recently issued by An and colleagues [240].

Isolating EVs from a liquid biopsy prior to molecular analysis enhances the sensitivity (compared to whole blood/urine analysis) as highly abundant serum/plasma proteins (e.g. albumin) and urine proteins (e.g. Tamm–Horsfall glycoprotein) are removed [241]. It is estimated that less than 0.01 % of the proteins present in plasma are EV associated [242]. It is important to realize that in biological fluids, in general, the vast majority of EVs are derived from healthy cells. Hence, it is reasonable to speculate that the sensitivity and specificity can be further enhanced through isolation of cell- or tissue-specific EVs prior to a biomarker assay. Such an approach was explored by Taylor and Gercel-Taylor, who isolated EVs from plasma by antibody-based capturing (using an anti-EPCAM antibody) and subsequently analyzed the miRNA profile in this tumor EV enriched population. The combination of EPCAM-based EV capture and downstream miRNA quantification could be used to distinguish between healthy patients and patients at different stages of ovarian cancer [234]. Another example of the importance of an upstream EV selection was provided by Shi *et al.,* who measured α-synuclein levels in plasma of healthy individuals and patients suffering from Parkinson's disease. When analyzing α-synuclein levels in plasma using the total EV population, no significant difference could be observed between both groups. However, when the quantification was performed on plasma EVs positive for L1 cellular adhesion molecule (L1CAM), which is primarily expressed in the central nervous system, the α-synuclein levels were significantly enhanced in Parkinson's disease patients [243]. Yet, it is important to note that specific cancer markers are not always known or present on the EV surface. Furthermore, population assays neglect an additional level of complexity conferred by the specific composition of individual vesicles, which can provide relevant supplementary information. Therefore, techniques that allow analysis on the single vesicle level are of great interest [244]. For diagnostic purposes such an approach will require screening of large amounts of vesicles, as 'diseased' EVs are rare among the total isolated EV population. One promising approach relies on modifying flow cytometry equipment/protocols to detect single nanosized EVs [245-247]. However, to date flow cytometry is not able to detect the lower size range of EVs and requires antibodies (and hence also knowledge of a particular disease marker) to phenotype EVs. Unfortunately, antibody-independent techniques that combine single vesicle sensitivity and high acquisition speed are not yet available. In **chapter 5** we aim to address this request by designing a new EV analysis platform based on Raman spectroscopy.

3.3. Perspectives

The wide-spread interest from both academia and industry in exploiting EVs in a diagnostic context is evident from ongoing and completed clinical trials (NCT02702856, NCT01779583, NCT02147418, NCT01860118, NCT02439008, NCT02464930, NCT02662621) and extensive investments from the pharmaceutical industry (e.g. Exosomedx, Exosome sciences, Codiak Biosciences, Hansabiomed, *etc.*). These investments are accompanied by a multitude of filed patents claiming technical solutions for the purification and/or readout of this new type of biomarker source. A first diagnostic test (the ExoDx Lung (ALK) by Exosomedx), based on detecting a specific NSCLC-associated mutation present in exosomal RNA, became commercially available at the beginning of 2016 [248].

Nonetheless, various issues still hamper the full exploitation of their biomarker potential. For instance, the lack of standardized purification protocols counteracts reproducibility and strongly influences biomarker identification. Due to this lack of consensus, to date there are no established specialized EV-biobanks, where a specific biofluid/biopsy sample can be correlated to the patient's medical record [249]. Moreover, elaborate purification protocols precludes fast screenings and hence restrains investigation and validation in large patient cohorts. Besides the purification protocol, also other parameters (e.g. the sample collection procedure, specific reagents, sample storage conditions) can influence the outcome of biomarker identification studies [250]. In response to this unmet need, an ISEV position paper was issued, describing guidelines on how to handle different biological fluid samples and emphasizing the importance of a comprehensive experimental description to enhance reproducibility, yet a standardized purification protocol is currently unavailable [251].

4. General conclusions

Inspired by their involvement in many (patho)physiological processes and their role as nature's own intercellular transport vehicles for biomolecules, a multitude of therapeutic and diagnostic applications have been explored for EVs.

To date, EVs have been explored as biological nanocarriers for synthetic drugs ranging from small molecule chemotherapeutics to macromolecular siRNA, proteins and mRNA in various preclinical studies. However, clinical translation will essentially depend on substantial improvements in cost-effective EV isolation methods, improved drug loading techniques and more detailed knowledge on EV composition, heterogeneity and inherent biological effects. Additionally, a knowledgeable assessment of the value of EVs as drug

delivery vehicles will require a direct comparison between EVs and current state-of-the-art synthetic and viral delivery vehicles.

The complex composition of EVs conceivably correlates with off-target effects. On the other hand this inherent complexity, conferred by the many bioactive components associated to EVs, enables them to induce potential beneficial effects likely challenging to mimic with therapeutic formulations containing a single active component. In this respect, MSC-derived EVs have been investigated in the field of regenerative medicine, auto-immune diseases and other inflammatory conditions as a safer alternative to whole cell therapeutics. EVs derived from both antigen-pulsed DC and tumor cells have been tested extensively for vaccination purposes. Despite the fact that the current clinical data show limited effect, pre-clinical reports indicate that modifications (e.g. co-delivery of an adjuvant) can further stimulate the evoked immune response. Nonetheless, it is important to note that safety concerns on the use of tumor-derived EVs are raised as many reports have linked EVs released by tumor cells to disease progression and metastasis. Also here, ample attention should be given to further optimize EV isolation and characterization protocols.

Finally, EVs have great potential to be harnessed in a diagnostic, prognostic and treatment monitoring context. EVs form a reliable and easy accessible window on the physiological status of the parent cell. They contain a vast amount of molecular information, which can be extracted by downstream proteomic, transcriptomic, miRNomic and lipidomic analysis, the feasibility of which has recently been underpinned by the first EV-based diagnostic test acquiring FDA approval. To galvanize further development of EVs as biomarkers, again fast, efficient and standardized purification protocols in combination with sensitive quantification methods will be essential.

Acknowledgments

SS and KR are doctoral and postdoctoral fellows respectively of the Research Foundation – Flanders (FWO). The support of this institution is gratefully acknowledged.

References

[1] P. Wolf, The nature and significance of platelet products in human plasma, Br. J. Haematol., 13 (1967) 269-288.
[2] E. Bonucci, Fine structure of early cartilage calcification, J. Ultrastruct. Res., 20 (1967) 33-50.
[3] M. De Broe, R. Wieme, F. Roels, Letter: Membrane fragments with koinozymic properties released from villous adenoma of the rectum, Lancet, 2 (1975) 1214-1215.

[4] H.F. Dvorak, S.C. Quay, N.S. Orenstein, A.M. Dvorak, P. Hahn, A.M. Bitzer, A.C. Carvalho, Tumor shedding and coagulation, Science, 212 (1981) 923-924.
[5] D.D. Taylor, G.J. Doellgast, Quantitation of peroxidase-antibody binding to membrane fragments using column chromatography, Anal. Biochem., 98 (1979) 53-59.
[6] B.T. Pan, R.M. Johnstone, Fate of the transferrin receptor during maturation of sheep reticulocytes in vitro: selective externalization of the receptor, Cell, 33 (1983) 967-978.
[7] R.M. Johnstone, M. Adam, J.R. Hammond, L. Orr, C. Turbide, Vesicle formation during reticulocyte maturation. Association of plasma membrane activities with released vesicles (exosomes), J. Biol. Chem., 262 (1987) 9412-9420.
[8] R.M. Johnstone, The Jeanne Manery-Fisher Memorial Lecture 1991. Maturation of reticulocytes: formation of exosomes as a mechanism for shedding membrane proteins, Biochem. Cell Biol., 70 (1992) 179-190.
[9] R.M. Johnstone, A. Mathew, A.B. Mason, K. Teng, Exosome formation during maturation of mammalian and avian reticulocytes: evidence that exosome release is a major route for externalization of obsolete membrane proteins, J. Cell. Physiol., 147 (1991) 27-36.
[10] G. Raposo, H.W. Nijman, W. Stoorvogel, R. Liejendekker, C.V. Harding, C.J. Melief, H.J. Geuze, B lymphocytes secrete antigen-presenting vesicles, J. Exp. Med., 183 (1996) 1161-1172.
[11] L. Zitvogel, A. Regnault, A. Lozier, J. Wolfers, C. Flament, D. Tenza, P. Ricciardi-Castagnoli, G. Raposo, S. Amigorena, Eradication of established murine tumors using a novel cell-free vaccine: dendritic cell-derived exosomes, Nat. Med., 4 (1998) 594-600.
[12] T. Pisitkun, R.F. Shen, M.A. Knepper, Identification and proteomic profiling of exosomes in human urine, Proc. Natl. Acad. Sci. U. S. A., 101 (2004) 13368-13373.
[13] J. Skog, T. Wurdinger, S. van Rijn, D.H. Meijer, L. Gainche, M. Sena-Esteves, W.T. Curry, Jr., B.S. Carter, A.M. Krichevsky, X.O. Breakefield, Glioblastoma microvesicles transport RNA and proteins that promote tumour growth and provide diagnostic biomarkers, Nat. Cell Biol., 10 (2008) 1470-1476.
[14] B. Escudier, T. Dorval, N. Chaput, F. Andre, M.P. Caby, S. Novault, C. Flament, C. Leboulaire, C. Borg, S. Amigorena, C. Boccaccio, C. Bonnerot, O. Dhellin, M. Movassagh, S. Piperno, C. Robert, V. Serra, N. Valente, J.B. Le Pecq, A. Spatz, O. Lantz, T. Tursz, E. Angevin, L. Zitvogel, Vaccination of metastatic melanoma patients with autologous dendritic cell (DC) derived-exosomes: results of thefirst phase I clinical trial, J. Transl. Med., 3 (2005) 10.
[15] H. Valadi, K. Ekstrom, A. Bossios, M. Sjostrand, J.J. Lee, J.O. Lotvall, Exosome-mediated transfer of mRNAs and microRNAs is a novel mechanism of genetic exchange between cells, Nat. Cell Biol., 9 (2007) 654-U672.
[16] J. Ratajczak, K. Miekus, M. Kucia, J. Zhang, R. Reca, P. Dvorak, M.Z. Ratajczak, Embryonic stem cell-derived microvesicles reprogram hematopoietic progenitors: evidence for horizontal transfer of mRNA and protein delivery, Leukemia, 20 (2006) 847-856.
[17] E. Cocucci, J. Meldolesi, Ectosomes and exosomes: shedding the confusion between extracellular vesicles, Trends Cell Biol., 25 (2015) 364-372.
[18] A. Saraste, K. Pulkki, Morphologic and biochemical hallmarks of apoptosis, Cardiovasc. Res., 45 (2000) 528-537.
[19] A. Bergsmedh, A. Szeles, M. Henriksson, A. Bratt, M.J. Folkman, A.L. Spetz, L. Holmgren, Horizontal transfer of oncogenes by uptake of apoptotic bodies, Proc. Natl. Acad. Sci. U. S. A., 98 (2001) 6407-6411.

[20] L. Holmgren, A. Szeles, E. Rajnavolgyi, J. Folkman, G. Klein, I. Ernberg, K.I. Falk, Horizontal transfer of DNA by the uptake of apoptotic bodies, Blood, 93 (1999) 3956-3963.
[21] K. Trajkovic, C. Hsu, S. Chiantia, L. Rajendran, D. Wenzel, F. Wieland, P. Schwille, B. Brugger, M. Simons, Ceramide triggers budding of exosome vesicles into multivesicular endosomes, Science, 319 (2008) 1244-1247.
[22] C. D'Souza-Schorey, J.W. Clancy, Tumor-derived microvesicles: shedding light on novel microenvironment modulators and prospective cancer biomarkers, Genes Dev., 26 (2012) 1287-1299.
[23] J. Huotari, A. Helenius, Endosome maturation, EMBO J., 30 (2011) 3481-3500.
[24] A. Savina, M. Vidal, M.I. Colombo, The exosome pathway in K562 cells is regulated by Rab11, J. Cell Sci., 115 (2002) 2505-2515.
[25] C. Lasser, S.E. O'Neil, L. Ekerljung, K. Ekstrom, M. Sjostrand, J. Lotvall, RNA-containing exosomes in human nasal secretions, Am J Rhinol Allergy, 25 (2011) 89-93.
[26] A. Poliakov, M. Spilman, T. Dokland, C.L. Amling, J.A. Mobley, Structural heterogeneity and protein composition of exosome-like vesicles (prostasomes) in human semen, Prostate, 69 (2009) 159-167.
[27] M.P. Caby, D. Lankar, C. Vincendeau-Scherrer, G. Raposo, C. Bonnerot, Exosomal-like vesicles are present in human blood plasma, Int. Immunol., 17 (2005) 879-887.
[28] R. Jahn, R.H. Scheller, SNAREs--engines for membrane fusion, Nat. Rev. Mol. Cell Biol., 7 (2006) 631-643.
[29] J. Lotvall, A.F. Hill, F. Hochberg, E.I. Buzas, D. Di Vizio, C. Gardiner, Y.S. Gho, I.V. Kurochkin, S. Mathivanan, P. Quesenberry, S. Sahoo, H. Tahara, M.H. Wauben, K.W. Witwer, C. Thery, Minimal experimental requirements for definition of extracellular vesicles and their functions: a position statement from the International Society for Extracellular Vesicles, J Extracell Vesicles, 3 (2014) 26913.
[30] A. Llorente, T. Skotland, T. Sylvanne, D. Kauhanen, T. Rog, A. Orlowski, I. Vattulainen, K. Ekroos, K. Sandvig, Molecular lipidomics of exosomes released by PC-3 prostate cancer cells, Biochim. Biophys. Acta, 1831 (2013) 1302-1309.
[31] J.M. Escola, M.J. Kleijmeer, W. Stoorvogel, J.M. Griffith, O. Yoshie, H.J. Geuze, Selective enrichment of tetraspan proteins on the internal vesicles of multivesicular endosomes and on exosomes secreted by human B-lymphocytes, J. Biol. Chem., 273 (1998) 20121-20127.
[32] E.N. Nolte-'t Hoen, H.P. Buermans, M. Waasdorp, W. Stoorvogel, M.H. Wauben, P.A. t Hoen, Deep sequencing of RNA from immune cell-derived vesicles uncovers the selective incorporation of small non-coding RNA biotypes with potential regulatory functions, Nucleic Acids Res., 40 (2012) 9272-9285.
[33] L. Pigati, S.C. Yaddanapudi, R. Iyengar, D.J. Kim, S.A. Hearn, D. Danforth, M.L. Hastings, D.M. Duelli, Selective release of microRNA species from normal and malignant mammary epithelial cells, PLoS One, 5 (2010) e13515.
[34] C. Villarroya-Beltri, C. Gutierrez-Vazquez, F. Sanchez-Cabo, D. Perez-Hernandez, J. Vazquez, N. Martin-Cofreces, D.J. Martinez-Herrera, A. Pascual-Montano, M. Mittelbrunn, F. Sanchez-Madrid, Sumoylated hnRNPA2B1 controls the sorting of miRNAs into exosomes through binding to specific motifs, Nat Commun, 4 (2013) 2980.

[35] M.F. Bolukbasi, A. Mizrak, G.B. Ozdener, S. Madlener, T. Strobel, E.P. Erkan, J.B. Fan, X.O. Breakefield, O. Saydam, miR-1289 and "Zipcode"-like Sequence Enrich mRNAs in Microvesicles, Molecular therapy. Nucleic acids, 1 (2012) e10.
[36] J. Guduric-Fuchs, A. O'Connor, B. Camp, C.L. O'Neill, R.J. Medina, D.A. Simpson, Selective extracellular vesicle-mediated export of an overlapping set of microRNAs from multiple cell types, BMC Genomics, 13 (2012) 357.
[37] F. Collino, M.C. Deregibus, S. Bruno, L. Sterpone, G. Aghemo, L. Viltono, C. Tetta, G. Camussi, Microvesicles derived from adult human bone marrow and tissue specific mesenchymal stem cells shuttle selected pattern of miRNAs, PLoS One, 5 (2010) e11803.
[38] C. Villarroya-Beltri, F. Baixauli, C. Gutierrez-Vazquez, F. Sanchez-Madrid, M. Mittelbrunn, Sorting it out: regulation of exosome loading, Semin. Cancer Biol., 28 (2014) 3-13.
[39] M. Colombo, C. Moita, G. van Niel, J. Kowal, J. Vigneron, P. Benaroch, N. Manel, L.F. Moita, C. Thery, G. Raposo, Analysis of ESCRT functions in exosome biogenesis, composition and secretion highlights the heterogeneity of extracellular vesicles, J. Cell Sci., 126 (2013) 5553-5565.
[40] G. van Niel, S. Charrin, S. Simoes, M. Romao, L. Rochin, P. Saftig, Michael S. Marks, E. Rubinstein, G. Raposo, The Tetraspanin CD63 Regulates ESCRT-Independent and -Dependent Endosomal Sorting during Melanogenesis, Dev. Cell, 21 (2011) 708-721.
[41] D. Koppers-Lalic, M. Hackenberg, I.V. Bijnsdorp, M.A. van Eijndhoven, P. Sadek, D. Sie, N. Zini, J.M. Middeldorp, B. Ylstra, R.X. de Menezes, T. Wurdinger, G.A. Meijer, D.M. Pegtel, Nontemplated nucleotide additions distinguish the small RNA composition in cells from exosomes, Cell reports, 8 (2014) 1649-1658.
[42] J.P. Tosar, F. Gambaro, J. Sanguinetti, B. Bonilla, K.W. Witwer, A. Cayota, Assessment of small RNA sorting into different extracellular fractions revealed by high-throughput sequencing of breast cell lines, Nucleic Acids Res., 43 (2015) 5601-5616.
[43] S. Mathivanan, C.J. Fahner, G.E. Reid, R.J. Simpson, ExoCarta 2012: database of exosomal proteins, RNA and lipids, Nucleic Acids Res., 40 (2012) D1241-1244.
[44] M. Guescini, S. Genedani, V. Stocchi, L.F. Agnati, Astrocytes and Glioblastoma cells release exosomes carrying mtDNA, J Neural Transm, 117 (2010) 1-4.
[45] S. Munich, A. Sobo-Vujanovic, W.J. Buchser, D. Beer-Stolz, N.L. Vujanovic, Dendritic cell exosomes directly kill tumor cells and activate natural killer cells via TNF superfamily ligands, Oncoimmunology, 1 (2012) 1074-1083.
[46] F. Andre, N.E. Schartz, M. Movassagh, C. Flament, P. Pautier, P. Morice, C. Pomel, C. Lhomme, B. Escudier, T. Le Chevalier, T. Tursz, S. Amigorena, G. Raposo, E. Angevin, L. Zitvogel, Malignant effusions and immunogenic tumour-derived exosomes, Lancet, 360 (2002) 295-305.
[47] L. Lugini, S. Cecchetti, V. Huber, F. Luciani, G. Macchia, F. Spadaro, L. Paris, L. Abalsamo, M. Colone, A. Molinari, F. Podo, L. Rivoltini, C. Ramoni, S. Fais, Immune surveillance properties of human NK cell-derived exosomes, J. Immunol., 189 (2012) 2833-2842.
[48] C. Thery, A. Regnault, J. Garin, J. Wolfers, L. Zitvogel, P. Ricciardi-Castagnoli, G. Raposo, S. Amigorena, Molecular characterization of dendritic cell-derived exosomes. Selective accumulation of the heat shock protein hsc73, J. Cell Biol., 147 (1999) 599-610.
[49] N. Koliha, Y. Wiencek, U. Heider, C. Jungst, N. Kladt, S. Krauthauser, I.C. Johnston, A. Bosio, A. Schauss, S. Wild, A novel multiplex bead-based platform highlights the diversity of extracellular vesicles, J Extracell Vesicles, 5 (2016) 29975.

[50] H.W. King, M.Z. Michael, J.M. Gleadle, Hypoxic enhancement of exosome release by breast cancer cells, BMC Cancer, 12 (2012) 421.
[51] P. Kucharzewska, H.C. Christianson, J.E. Welch, K.J. Svensson, E. Fredlund, M. Ringner, M. Morgelin, E. Bourseau-Guilmain, J. Bengzon, M. Belting, Exosomes reflect the hypoxic status of glioma cells and mediate hypoxia-dependent activation of vascular cells during tumor development, Proc. Natl. Acad. Sci. U. S. A., 110 (2013) 7312-7317.
[52] I. Parolini, C. Federici, C. Raggi, L. Lugini, S. Palleschi, A. De Milito, C. Coscia, E. Iessi, M. Logozzi, A. Molinari, M. Colone, M. Tatti, M. Sargiacomo, S. Fais, Microenvironmental pH is a key factor for exosome traffic in tumor cells, J. Biol. Chem., 284 (2009) 34211-34222.
[53] Y. Zhang, D. Liu, X. Chen, J. Li, L. Li, Z. Bian, F. Sun, J. Lu, Y. Yin, X. Cai, Q. Sun, K. Wang, Y. Ba, Q. Wang, D. Wang, J. Yang, P. Liu, T. Xu, Q. Yan, J. Zhang, K. Zen, C.Y. Zhang, Secreted monocytic miR-150 enhances targeted endothelial cell migration, Mol. Cell, 39 (2010) 133-144.
[54] E. Segura, S. Amigorena, C. Thery, Mature dendritic cells secrete exosomes with strong ability to induce antigen-specific effector immune responses, Blood Cells Mol. Dis., 35 (2005) 89-93.
[55] S.H. Kim, E.R. Lechman, N. Bianco, R. Menon, A. Keravala, J. Nash, Z. Mi, S.C. Watkins, A. Gambotto, P.D. Robbins, Exosomes derived from IL-10-treated dendritic cells can suppress inflammation and collagen-induced arthritis, J. Immunol., 174 (2005) 6440-6448.
[56] J. Li, Y. Lee, H.J. Johansson, I. Mager, P. Vader, J.Z. Nordin, O.P. Wiklander, J. Lehtio, M.J. Wood, S.E. Andaloussi, Serum-free culture alters the quantity and protein composition of neuroblastoma-derived extracellular vesicles, J Extracell Vesicles, 4 (2015) 26883.
[57] G. Caracciolo, L. Callipo, S.C. De Sanctis, C. Cavaliere, D. Pozzi, A. Laganà, Surface adsorption of protein corona controls the cell internalization mechanism of DC-Chol–DOPE/DNA lipoplexes in serum, BBA - Biomembranes, 1798 (2010) 536-543.
[58] A. Salvati, A.S. Pitek, M.P. Monopoli, K. Prapainop, F.B. Bombelli, D.R. Hristov, P.M. Kelly, C. Aberg, E. Mahon, K.A. Dawson, Transferrin-functionalized nanoparticles lose their targeting capabilities when a biomolecule corona adsorbs on the surface, Nature nanotechnology, 8 (2013) 137-143.
[59] J.L. Betker, J. Gomez, T.J. Anchordoquy, The effects of lipoplex formulation variables on the protein corona and comparisons with in vitro transfection efficiency, J. Control. Release, 171 (2013) 261-268.
[60] R. van der Meel, M.H. Fens, P. Vader, W.W. van Solinge, O. Eniola-Adefeso, R.M. Schiffelers, Extracellular vesicles as drug delivery systems: lessons from the liposome field, J. Control. Release, 195 (2014) 72-85.
[61] A. Bobrie, M. Colombo, S. Krumeich, G. Raposo, C. Thery, Diverse subpopulations of vesicles secreted by different intracellular mechanisms are present in exosome preparations obtained by differential ultracentrifugation, J Extracell Vesicles, 1 (2012) 18397.
[62] G. van Niel, G. Raposo, C. Candalh, M. Boussac, R. Hershberg, N. Cerf-Bensussan, M. Heyman, Intestinal epithelial cells secrete exosome-like vesicles, Gastroenterology, 121 (2001) 337-349.
[63] E. Willms, H.J. Johansson, I. Mager, Y. Lee, K.E. Blomberg, M. Sadik, A. Alaarg, C.I. Smith, J. Lehtio, S. El Andaloussi, M.J. Wood, P. Vader, Cells release subpopulations of exosomes with distinct molecular and biological properties, Sci. Rep., 6 (2016) 22519.

[64] Z.J. Smith, C. Lee, T. Rojalin, R.P. Carney, S. Hazari, A. Knudson, K. Lam, H. Saari, E.L. Ibanez, T. Viitala, T. Laaksonen, M. Yliperttula, S. Wachsmann-Hogiu, Single exosome study reveals subpopulations distributed among cell lines with variability related to membrane content, J Extracell Vesicles, 4 (2015) 28533.
[65] C. Thery, S. Amigorena, G. Raposo, A. Clayton, Isolation and characterization of exosomes from cell culture supernatants and biological fluids, Curr. Protoc. Cell Biol., Chapter 3 (2006) Unit 3.22.
[66] J. Van Deun, P. Mestdagh, R. Sormunen, V. Cocquyt, K. Vermaelen, J. Vandesompele, M. Bracke, O. De Wever, A. Hendrix, The impact of disparate isolation methods for extracellular vesicles on downstream RNA profiling, J Extracell Vesicles, 3 (2014) 24858.
[67] H.G. Lamparski, A. Metha-Damani, J.Y. Yao, S. Patel, D.H. Hsu, C. Ruegg, J.B. Le Pecq, Production and characterization of clinical grade exosomes derived from dendritic cells, J. Immunol. Methods, 270 (2002) 211-226.
[68] F. Momen-Heravi, L. Balaj, S. Alian, A.J. Trachtenberg, F.H. Hochberg, J. Skog, W.P. Kuo, Impact of biofluid viscosity on size and sedimentation efficiency of the isolated microvesicles, Front. Physiol., 3 (2012) 162.
[69] R.E. Lane, D. Korbie, W. Anderson, R. Vaidyanathan, M. Trau, Analysis of exosome purification methods using a model liposome system and tunable-resistive pulse sensing, Sci. Rep., 5 (2015) 7639.
[70] T. Baranyai, K. Herczeg, Z. Onodi, I. Voszka, K. Modos, N. Marton, G. Nagy, I. Mager, M.J. Wood, S. El Andaloussi, Z. Palinkas, V. Kumar, P. Nagy, A. Kittel, E.I. Buzas, P. Ferdinandy, Z. Giricz, Isolation of Exosomes from Blood Plasma: Qualitative and Quantitative Comparison of Ultracentrifugation and Size Exclusion Chromatography Methods, PLoS One, 10 (2015) e0145686.
[71] J.Z. Nordin, Y. Lee, P. Vader, I. Mager, H.J. Johansson, W. Heusermann, O.P. Wiklander, M. Hallbrink, Y. Seow, J.J. Bultema, J. Gilthorpe, T. Davies, P.J. Fairchild, S. Gabrielsson, N.C. Meisner-Kober, J. Lehtio, C.I. Smith, M.J. Wood, S. El Andaloussi, Ultrafiltration with size-exclusion liquid chromatography for high yield isolation of extracellular vesicles preserving intact biophysical and functional properties, Nanomedicine, 11 (2015) 879-883.
[72] R. Linares, S. Tan, C. Gounou, N. Arraud, A.R. Brisson, High-speed centrifugation induces aggregation of extracellular vesicles, J Extracell Vesicles, 4 (2015) 29509.
[73] D. Maiolo, L. Paolini, G. Di Noto, A. Zendrini, D. Berti, P. Bergese, D. Ricotta, Colorimetric nanoplasmonic assay to determine purity and titrate extracellular vesicles, Anal. Chem., 87 (2015) 4168-4176.
[74] R. Cantin, J. Diou, D. Belanger, A.M. Tremblay, C. Gilbert, Discrimination between exosomes and HIV-1: purification of both vesicles from cell-free supernatants, J. Immunol. Methods, 338 (2008) 21-30.
[75] C.P. Kimpton, G. Corbitt, D.J. Morris, Comparison of polyethylene glycol precipitation and ultracentrifugation for recovery of cytomegalovirus from urine prior to detection of DNA by dot-blot hybridisation, J. Virol. Methods, 28 (1990) 141-145.
[76] C. Lee, R.P. Carney, S. Hazari, Z.J. Smith, A. Knudson, C.S. Robertson, K.S. Lam, S. Wachsmann-Hogiu, 3D plasmonic nanobowl platform for the study of exosomes in solution, Nanoscale, 7 (2015) 9290-9297.

[77] S. Dai, D. Wei, Z. Wu, X. Zhou, X. Wei, H. Huang, G. Li, Phase I clinical trial of autologous ascites-derived exosomes combined with GM-CSF for colorectal cancer, Mol. Ther., 16 (2008) 782-790.
[78] M.A. Morse, J. Garst, T. Osada, S. Khan, A. Hobeika, T.M. Clay, N. Valente, R. Shreeniwas, M.A. Sutton, A. Delcayre, D.H. Hsu, J.B. Le Pecq, H.K. Lyerly, A phase I study of dexosome immunotherapy in patients with advanced non-small cell lung cancer, J. Transl. Med., 3 (2005) 9.
[79] B. Besse, M. Charrier, V. Lapierre, E. Dansin, O. Lantz, D. Planchard, T. Le Chevalier, A. Livartoski, F. Barlesi, A. Laplanche, S. Ploix, N. Vimond, I. Peguillet, C. Théry, L. Lacroix, I. Zoernig, K. Dhodapkar, M. Dhodapkar, S. Viaud, J.-C. Soria, K.S. Reiners, E.P. von Strandmann, F. Vély, S. Rusakiewicz, A. Eggermont, J.M. Pitt, L. Zitvogel, N. Chaput, Dendritic Cell-derived Exosomes as Maintenance Immunotherapy after First Line Chemotherapy in NSCLC, OncoImmunology, 5 (2015) e1071008.
[80] L. Kordelas, V. Rebmann, A.K. Ludwig, S. Radtke, J. Ruesing, T.R. Doeppner, M. Epple, P.A. Horn, D.W. Beelen, B. Giebel, MSC-derived exosomes: a novel tool to treat therapy-refractory graft-versus-host disease, Leukemia, 28 (2014) 970-973.
[81] C.E. Yoo, G. Kim, M. Kim, D. Park, H.J. Kang, M. Lee, N. Huh, A direct extraction method for microRNAs from exosomes captured by immunoaffinity beads, Anal. Biochem., 431 (2012) 96-98.
[82] G. Kim, C.E. Yoo, M. Kim, H.J. Kang, D. Park, M. Lee, N. Huh, Noble Polymeric Surface Conjugated with Zwitterionic Moieties and Antibodies for the Isolation of Exosomes from Human Serum, Bioconjug. Chem., 23 (2012) 2114-2120.
[83] L. Balaj, N.A. Atai, W. Chen, D. Mu, B.A. Tannous, X.O. Breakefield, J. Skog, C.A. Maguire, Heparin affinity purification of extracellular vesicles, Sci. Rep., 5 (2015) 10266.
[84] H. Im, H. Shao, Y.I. Park, V.M. Peterson, C.M. Castro, R. Weissleder, H. Lee, Label-free detection and molecular profiling of exosomes with a nano-plasmonic sensor, Nat. Biotechnol., 32 (2014) 490-495.
[85] L. Grasso, R. Wyss, L. Weidenauer, A. Thampi, D. Demurtas, M. Prudent, N. Lion, H. Vogel, Molecular screening of cancer-derived exosomes by surface plasmon resonance spectroscopy, Anal. Bioanal. Chem., 407 (2015) 5425-5432.
[86] A.N. Boing, E. van der Pol, A.E. Grootemaat, F.A. Coumans, A. Sturk, R. Nieuwland, Single-step isolation of extracellular vesicles by size-exclusion chromatography, J Extracell Vesicles, 3 (2014) 23430.
[87] R.J. Lobb, M. Becker, S.W. Wen, C.S. Wong, A.P. Wiegmans, A. Leimgruber, A. Moller, Optimized exosome isolation protocol for cell culture supernatant and human plasma, J Extracell Vesicles, 4 (2015) 27031.
[88] M. Yanez-Mo, P.R. Siljander, Z. Andreu, A.B. Zavec, F.E. Borras, E.I. Buzas, K. Buzas, E. Casal, F. Cappello, J. Carvalho, E. Colas, A. Cordeiro-da Silva, S. Fais, J.M. Falcon-Perez, I.M. Ghobrial, B. Giebel, M. Gimona, M. Graner, I. Gursel, M. Gursel, N.H. Heegaard, A. Hendrix, P. Kierulf, K. Kokubun, M. Kosanovic, V. Kralj-Iglic, E.M. Kramer-Albers, S. Laitinen, C. Lasser, T. Lener, E. Ligeti, A. Line, G. Lipps, A. Llorente, J. Lotvall, M. Mancek-Keber, A. Marcilla, M. Mittelbrunn, I. Nazarenko, E.N. Nolte-'t Hoen, T.A. Nyman, L. O'Driscoll, M. Olivan, C. Oliveira, E. Pallinger, H.A. Del Portillo, J. Reventos, M. Rigau, E. Rohde, M. Sammar, F. Sanchez-Madrid, N. Santarem, K. Schallmoser, M.S. Ostenfeld, W. Stoorvogel, R. Stukelj, S.G. Van der Grein, M.H. Vasconcelos, M.H. Wauben, O. De Wever, Biological properties of extracellular vesicles and their physiological functions, J Extracell Vesicles, 4 (2015) 27066.

[89] A.J. Abusamra, Z. Zhong, X. Zheng, M. Li, T.E. Ichim, J.L. Chin, W.P. Min, Tumor exosomes expressing Fas ligand mediate CD8+ T-cell apoptosis, Blood Cells Mol. Dis., 35 (2005) 169-173.
[90] L. Muller, M. Mitsuhashi, P. Simms, W.E. Gooding, T.L. Whiteside, Tumor-derived exosomes regulate expression of immune function-related genes in human T cell subsets, Sci. Rep., 6 (2016) 20254.
[91] S.V. Yelamanchili, B.G. Lamberty, D.A. Rennard, B.M. Morsey, C.G. Hochfelder, B.M. Meays, E. Levy, H.S. Fox, MiR-21 in Extracellular Vesicles Leads to Neurotoxicity via TLR7 Signaling in SIV Neurological Disease, PLoS Pathog., 11 (2015) e1005032.
[92] M. Fabbri, A. Paone, F. Calore, R. Galli, E. Gaudio, R. Santhanam, F. Lovat, P. Fadda, C. Mao, G.J. Nuovo, N. Zanesi, M. Crawford, G.H. Ozer, D. Wernicke, H. Alder, M.A. Caligiuri, P. Nana-Sinkam, D. Perrotti, C.M. Croce, MicroRNAs bind to Toll-like receptors to induce prometastatic inflammatory response, Proc. Natl. Acad. Sci. U. S. A., 109 (2012) E2110-2116.
[93] A. Montecalvo, A.T. Larregina, W.J. Shufesky, D.B. Stolz, M.L. Sullivan, J.M. Karlsson, C.J. Baty, G.A. Gibson, G. Erdos, Z. Wang, J. Milosevic, O.A. Tkacheva, S.J. Divito, R. Jordan, J. Lyons-Weiler, S.C. Watkins, A.E. Morelli, Mechanism of transfer of functional microRNAs between mouse dendritic cells via exosomes, Blood, 119 (2012) 756-766.
[94] S. Viaud, C. Thery, S. Ploix, T. Tursz, V. Lapierre, O. Lantz, L. Zitvogel, N. Chaput, Dendritic cell-derived exosomes for cancer immunotherapy: what's next?, Cancer Res., 70 (2010) 1281-1285.
[95] S. Bruno, C. Grange, M.C. Deregibus, R.A. Calogero, S. Saviozzi, F. Collino, L. Morando, A. Busca, M. Falda, B. Bussolati, C. Tetta, G. Camussi, Mesenchymal stem cell-derived microvesicles protect against acute tubular injury, J. Am. Soc. Nephrol., 20 (2009) 1053-1067.
[96] H.C. Zhang, X.B. Liu, S. Huang, X.Y. Bi, H.X. Wang, L.X. Xie, Y.Q. Wang, X.F. Cao, J. Lv, F.J. Xiao, Y. Yang, Z.K. Guo, Microvesicles derived from human umbilical cord mesenchymal stem cells stimulated by hypoxia promote angiogenesis both in vitro and in vivo, Stem cells and development, 21 (2012) 3289-3297.
[97] F. Arslan, R.C. Lai, M.B. Smeets, L. Akeroyd, A. Choo, E.N. Aguor, L. Timmers, H.V. van Rijen, P.A. Doevendans, G. Pasterkamp, S.K. Lim, D.P. de Kleijn, Mesenchymal stem cell-derived exosomes increase ATP levels, decrease oxidative stress and activate PI3K/Akt pathway to enhance myocardial viability and prevent adverse remodeling after myocardial ischemia/reperfusion injury, Stem cell research, 10 (2013) 301-312.
[98] T. Li, Y. Yan, B. Wang, H. Qian, X. Zhang, L. Shen, M. Wang, Y. Zhou, W. Zhu, W. Li, W. Xu, Exosomes derived from human umbilical cord mesenchymal stem cells alleviate liver fibrosis, Stem cells and development, 22 (2013) 845-854.
[99] H. Xin, Y. Li, B. Buller, M. Katakowski, Y. Zhang, X. Wang, X. Shang, Z.G. Zhang, M. Chopp, Exosome-mediated transfer of miR-133b from multipotent mesenchymal stromal cells to neural cells contributes to neurite outgrowth, Stem Cells, 30 (2012) 1556-1564.
[100] E. Favaro, A. Carpanetto, S. Lamorte, A. Fusco, C. Caorsi, M.C. Deregibus, S. Bruno, A. Amoroso, M. Giovarelli, M. Porta, P.C. Perin, C. Tetta, G. Camussi, M.M. Zanone, Human mesenchymal stem cell-derived microvesicles modulate T cell response to islet antigen glutamic acid decarboxylase in patients with type 1 diabetes, Diabetologia, 57 (2014) 1664-1673.
[101] D.G. Phinney, M. Di Giuseppe, J. Njah, E. Sala, S. Shiva, C.M. St Croix, D.B. Stolz, S.C. Watkins, Y.P. Di, G.D. Leikauf, J. Kolls, D.W.H. Riches, G. Deiuliis, N. Kaminski, S.V. Boregowda,

D.H. McKenna, L.A. Ortiz, Mesenchymal stem cells use extracellular vesicles to outsource mitophagy and shuttle microRNAs, Nat. Commun., 6 (2015) 8472.
[102] S. Ferguson, J. Nguyen, Exosomes as therapeutics: The implications of molecular composition and exosomal heterogeneity, J. Control. Release, 228 (2016) 179-90.
[103] S. Rani, A.E. Ryan, M.D. Griffin, T. Ritter, Mesenchymal Stem Cell-derived Extracellular Vesicles: Toward Cell-free Therapeutic Applications, Mol. Ther., 23 (2015) 812-823.
[104] C. Akyurekli, Y. Le, R.B. Richardson, D. Fergusson, J. Tay, D.S. Allan, A systematic review of preclinical studies on the therapeutic potential of mesenchymal stromal cell-derived microvesicles, Stem cell rev, 11 (2015) 150-160.
[105] T. Katsuda, R. Tsuchiya, N. Kosaka, Y. Yoshioka, K. Takagaki, K. Oki, F. Takeshita, Y. Sakai, M. Kuroda, T. Ochiya, Human adipose tissue-derived mesenchymal stem cells secrete functional neprilysin-bound exosomes, Sci. Rep., 3 (2013) 1197.
[106] C. Subra, D. Grand, K. Laulagnier, A. Stella, G. Lambeau, M. Paillasse, P. De Medina, B. Monsarrat, B. Perret, S. Silvente-Poirot, M. Poirot, M. Record, Exosomes account for vesicle-mediated transcellular transport of activatable phospholipases and prostaglandins, J. Lipid Res., 51 (2010) 2105-2120.
[107] A. Waldenstrom, N. Genneback, U. Hellman, G. Ronquist, Cardiomyocyte microvesicles contain DNA/RNA and convey biological messages to target cells, PLoS One, 7 (2012) e34653.
[108] K. Raemdonck, S.C. De Smedt, Lessons in simplicity that should shape the future of drug delivery, Nat. Biotechnol., 33 (2015) 1026-1027.
[109] N. Nayerossadat, T. Maedeh, P.A. Ali, Viral and nonviral delivery systems for gene delivery, Adv Biomed Res, 1 (2012) 27.
[110] J.G. van den Boorn, M. Schlee, C. Coch, G. Hartmann, SiRNA delivery with exosome nanoparticles, Nat. Biotechnol., 29 (2011) 325-326.
[111] T.M. Allen, G.A. Austin, A. Chonn, L. Lin, K.C. Lee, Uptake of liposomes by cultured mouse bone marrow macrophages: influence of liposome composition and size, Biochim. Biophys. Acta, 1061 (1991) 56-64.
[112] E. Teissier, E.I. Pecheur, Lipids as modulators of membrane fusion mediated by viral fusion proteins, Eur. Biophys. J., 36 (2007) 887-899.
[113] A. Jegou, A. Ziyyat, V. Barraud-Lange, E. Perez, J.P. Wolf, F. Pincet, C. Gourier, CD9 tetraspanin generates fusion competent sites on the egg membrane for mammalian fertilization, Proc. Natl. Acad. Sci. U. S. A., 108 (2011) 10946-10951.
[114] F. Martin, D.M. Roth, D.A. Jans, C.W. Pouton, L.J. Partridge, P.N. Monk, G.W. Moseley, Tetraspanins in viral infections: a fundamental role in viral biology?, J. Virol., 79 (2005) 10839-10851.
[115] A. Hoshino, B. Costa-Silva, T.L. Shen, G. Rodrigues, A. Hashimoto, M. Tesic Mark, H. Molina, S. Kohsaka, A. Di Giannatale, S. Ceder, S. Singh, C. Williams, N. Soplop, K. Uryu, L. Pharmer, T. King, L. Bojmar, A.E. Davies, Y. Ararso, T. Zhang, H. Zhang, J. Hernandez, J.M. Weiss, V.D. Dumont-Cole, K. Kramer, L.H. Wexler, A. Narendran, G.K. Schwartz, J.H. Healey, P. Sandstrom, K. Jorgen Labori, E.H. Kure, P.M. Grandgenett, M.A. Hollingsworth, M. de Sousa, S. Kaur, M. Jain, K. Mallya, S.K. Batra, W.R. Jarnagin, M.S. Brady, O. Fodstad, V. Muller, K. Pantel, A.J. Minn, M.J. Bissell, B.A. Garcia, Y. Kang, V.K. Rajasekhar, C.M. Ghajar, I. Matei, H. Peinado, J. Bromberg, D. Lyden, Tumour exosome integrins determine organotropic metastasis, Nature, 527 (2015) 329–335.

[116] Y. Takahashi, M. Nishikawa, H. Shinotsuka, Y. Matsui, S. Ohara, T. Imai, Y. Takakura, Visualization and in vivo tracking of the exosomes of murine melanoma B16-BL6 cells in mice after intravenous injection, J. Biotechnol., 165 (2013) 77-84.
[117] S.C. Saunderson, A.C. Dunn, P.R. Crocker, A.D. McLellan, CD169 mediates the capture of exosomes in spleen and lymph node, Blood, 123 (2014) 208-216.
[118] C.P. Lai, O. Mardini, M. Ericsson, S. Prabhakar, C.A. Maguire, J.W. Chen, B.A. Tannous, X.O. Breakefield, Dynamic biodistribution of extracellular vesicles in vivo using a multimodal imaging reporter, ACS nano, 8 (2014) 483-494.
[119] T. Smyth, M. Kullberg, N. Malik, P. Smith-Jones, M.W. Graner, T.J. Anchordoquy, Biodistribution and delivery efficiency of unmodified tumor-derived exosomes, J. Control. Release, 199C (2014) 145-155.
[120] O.P. Wiklander, J.Z. Nordin, A. O'Loughlin, Y. Gustafsson, G. Corso, I. Mager, P. Vader, Y. Lee, H. Sork, Y. Seow, N. Heldring, L. Alvarez-Erviti, C.E. Smith, K. Le Blanc, P. Macchiarini, P. Jungebluth, M.J. Wood, S.E. Andaloussi, Extracellular vesicle in vivo biodistribution is determined by cell source, route of administration and targeting, J Extracell Vesicles, 4 (2015) 26316.
[121] H. Deschout, K. Raemdonck, S. Stremersch, P. Maoddi, G. Mernier, P. Renaud, S. Jiguet, A. Hendrix, M. Bracke, R. Van den Broecke, M. Roding, M. Rudemo, J. Demeester, S.C. De Smedt, F. Strubbe, K. Neyts, K. Braeckmans, On-chip light sheet illumination enables diagnostic size and concentration measurements of membrane vesicles in biofluids, Nanoscale, 6 (2014) 1741-1747.
[122] A.F. Fomina, T.J. Deerinck, M.H. Ellisman, M.D. Cahalan, Regulation of membrane trafficking and subcellular organization of endocytic compartments revealed with FM1-43 in resting and activated human T cells, Exp. Cell Res., 291 (2003) 150-166.
[123] A. Clayton, C.L. Harris, J. Court, M.D. Mason, B.P. Morgan, Antigen-presenting cell exosomes are protected from complement-mediated lysis by expression of CD55 and CD59, Eur. J. Immunol., 33 (2003) 522-531.
[124] B. Whitehead, L. Wu, M.L. Hvam, H. Aslan, M. Dong, L. Dyrskjot, M.S. Ostenfeld, S.M. Moghimi, K.A. Howard, Tumour exosomes display differential mechanical and complement activation properties dependent on malignant state: implications in endothelial leakiness, J Extracell Vesicles, 4 (2015) 29685.
[125] L. Alvarez-Erviti, Y. Seow, H. Yin, C. Betts, S. Lakhal, M.J. Wood, Delivery of siRNA to the mouse brain by systemic injection of targeted exosomes, Nat Biotechnol, 29 (2011) 341-345.
[126] Y. Tao, J. Han, H. Dou, Brain-targeting gene delivery using a rabies virus glycoprotein peptide modulated hollow liposome: bio-behavioral study, J. Mater. Chem., 22 (2012) 11808-11815.
[127] M.E. Hung, J.N. Leonard, Stabilization of exosome-targeting peptides via engineered glycosylation, J. Biol. Chem., 290 (2015) 8166-8172.
[128] S.A. Kooijmans, L.A. Fliervoet, R. van der Meel, M.H. Fens, H.F. Heijnen, P.M. van Bergen En Henegouwen, P. Vader, R.M. Schiffelers, PEGylated and targeted extracellular vesicles display enhanced cell specificity and circulation time, J. Control. Release, 224 (2016) 77-85.
[129] Y.T. Sato, K. Umezaki, S. Sawada, S.A. Mukai, Y. Sasaki, N. Harada, H. Shiku, K. Akiyoshi, Engineering hybrid exosomes by membrane fusion with liposomes, Sci. Rep., 6 (2016) 21933.
[130] K. Ridder, S. Keller, M. Dams, A.K. Rupp, J. Schlaudraff, D. Del Turco, J. Starmann, J. Macas, D. Karpova, K. Devraj, C. Depboylu, B. Landfried, B. Arnold, K.H. Plate, G. Hoglinger, H. Sultmann, P. Altevogt, S. Momma, Extracellular vesicle-mediated transfer of genetic information

between the hematopoietic system and the brain in response to inflammation, PLoS Biol., 12 (2014) e1001874.
[131] E. Cocucci, G. Racchetti, J. Meldolesi, Shedding microvesicles: artefacts no more, Trends Cell Biol., 19 (2009) 43-51.
[132] T. Yang, P. Martin, B. Fogarty, A. Brown, K. Schurman, R. Phipps, V.P. Yin, P. Lockman, S. Bai, Exosome delivered anticancer drugs across the blood-brain barrier for brain cancer therapy in Danio rerio, Pharm. Res., 32 (2015) 2003-2014.
[133] S.I. Ohno, M. Takanashi, K. Sudo, S. Ueda, A. Ishikawa, N. Matsuyama, K. Fujita, T. Mizutani, T. Ohgi, T. Ochiya, N. Gotoh, M. Kuroda, Systemically Injected Exosomes Targeted to EGFR Deliver Antitumor MicroRNA to Breast Cancer Cells, Mol. Ther., 21 (2012) 185-195.
[134] Y. Tian, S. Li, J. Song, T. Ji, M. Zhu, G.J. Anderson, J. Wei, G. Nie, A doxorubicin delivery platform using engineered natural membrane vesicle exosomes for targeted tumor therapy, Biomaterials, 35 (2014) 2383-2390.
[135] R. Ruiss, S. Jochum, R. Mocikat, W. Hammerschmidt, R. Zeidler, EBV-gp350 Confers B-Cell Tropism to Tailored Exosomes and Is a Neo-Antigen in Normal and Malignant B Cells-A New Option for the Treatment of B-CLL, PLoS One, 6 (2011) e25294.
[136] J.L. Hood, R.S. San, S.A. Wickline, Exosomes released by melanoma cells prepare sentinel lymph nodes for tumor metastasis, Cancer Res., 71 (2011) 3792-3801.
[137] L. Hu, S.A. Wickline, J.L. Hood, Magnetic resonance imaging of melanoma exosomes in lymph nodes, Magn. Reson. Med., 74 (2014) 266–271.
[138] X. Zhuang, X. Xiang, W. Grizzle, D. Sun, S. Zhang, R.C. Axtell, S. Ju, J. Mu, L. Zhang, L. Steinman, D. Miller, H.G. Zhang, Treatment of brain inflammatory diseases by delivering exosome encapsulated anti-inflammatory drugs from the nasal region to the brain, Mol. Ther., 19 (2011) 1769-1779.
[139] M.J. Haney, N.L. Klyachko, Y. Zhao, R. Gupta, E.G. Plotnikova, Z. He, T. Patel, A. Piroyan, M. Sokolsky, A.V. Kabanov, E.V. Batrakova, Exosomes as drug delivery vehicles for Parkinson's disease therapy, J. Control. Release, 207 (2015) 18–30
[140] L.A. Mulcahy, R.C. Pink, D.R. Carter, Routes and mechanisms of extracellular vesicle uptake, J Extracell Vesicles, 3 (2014) 24641.
[141] W. Heusermann, J. Hean, D. Trojer, E. Steib, S. von Bueren, A. Graff-Meyer, C. Genoud, K. Martin, N. Pizzato, J. Voshol, D.V. Morrissey, S.E. Andaloussi, M.J. Wood, N.C. Meisner-Kober, Exosomes surf on filopodia to enter cells at endocytic hot spots, traffic within endosomes, and are targeted to the ER, J. Cell Biol., 213 (2016) 173-184.
[142] T. Tian, Y.L. Zhu, F.H. Hu, Y.Y. Wang, N.P. Huang, Z.D. Xiao, Dynamics of exosome internalization and trafficking, J. Cell. Physiol., 228 (2013) 1487-1495.
[143] T.F. Martens, K. Remaut, J. Demeester, S.C. De Smedt, K. Braeckmans, Intracellular delivery of nanomaterials: How to catch endosomal escape in the act, Nano Today, 9 (2014) 344-364.
[144] V.V. Temchura, M. Tenbusch, G. Nchinda, G. Nabi, B. Tippler, M. Zelenyuk, O. Wildner, K. Uberla, S. Kuate, Enhancement of immunostimulatory properties of exosomal vaccines by incorporation of fusion-competent G protein of vesicular stomatitis virus, Vaccine, 26 (2008) 3662-3672.
[145] K.S. Matlin, H. Reggio, A. Helenius, K. Simons, Pathway of vesicular stomatitis virus entry leading to infection, J. Mol. Biol., 156 (1982) 609-631.

[146] L. Alvarez-Erviti, Y.Q. Seow, H.F. Yin, C. Betts, S. Lakhal, M.J.A. Wood, Delivery of siRNA to the mouse brain by systemic injection of targeted exosomes, Nat. Biotechnol., 29 (2011) 341-U179.
[147] L.L. Zou, J.L. Ma, T. Wang, T.B. Yang, C.B. Liu, Cell-Penetrating Peptide-Mediated Therapeutic Molecule Delivery into the Central Nervous System, Curr. Neuropharmacol., 11 (2013) 197-208.
[148] T. Teesalu, K.N. Sugahara, E. Ruoslahti, Tumor-Penetrating Peptides, Front. Oncol., 3 (2013) 216.
[149] S. Atay, C. Gercel-Taylor, D.D. Taylor, Human trophoblast-derived exosomal fibronectin induces pro-inflammatory IL-1beta production by macrophages, Am. J. Reprod. Immunol., 66 (2011) 259-269.
[150] C. Cossetti, N. Iraci, T.R. Mercer, T. Leonardi, E. Alpi, D. Drago, C. Alfaro-Cervello, H.K. Saini, M.P. Davis, J. Schaeffer, B. Vega, M. Stefanini, C. Zhao, W. Muller, J.M. Garcia-Verdugo, S. Mathivanan, A. Bachi, A.J. Enright, J.S. Mattick, S. Pluchino, Extracellular vesicles from neural stem cells transfer IFN-gamma via Ifngr1 to activate Stat1 signaling in target cells, Mol. Cell, 56 (2014) 193-204.
[151] M. Hedlund, O. Nagaeva, D. Kargl, V. Baranov, L. Mincheva-Nilsson, Thermal- and oxidative stress causes enhanced release of NKG2D ligand-bearing immunosuppressive exosomes in leukemia/lymphoma T and B cells, PLoS One, 6 (2011) e16899.
[152] A. Clayton, S. Al-Taei, J. Webber, M.D. Mason, Z. Tabi, Cancer exosomes express CD39 and CD73, which suppress T cells through adenosine production, J. Immunol., 187 (2011) 676-683.
[153] P. Vader, S.A. Kooijmans, S. Stremersch, K. Raemdonck, New considerations in the preparation of nucleic acid-loaded extracellular vesicles, Ther. Deliv., 5 (2014) 105-107.
[154] J. Wahlgren, L.K.T. De, M. Brisslert, F. Vaziri Sani, E. Telemo, P. Sunnerhagen, H. Valadi, Plasma exosomes can deliver exogenous short interfering RNA to monocytes and lymphocytes, Nucleic Acids Res., 40 (2012) e130.
[155] J.L. Hood, M.J. Scott, S.A. Wickline, Maximizing exosome colloidal stability following electroporation, Anal. Biochem., 448 (2014) 41-49.
[156] I. Nakase, S. Futaki, Combined treatment with a pH-sensitive fusogenic peptide and cationic lipids achieves enhanced cytosolic delivery of exosomes, Sci. Rep., 5 (2015) 10112.
[157] K. Bryniarski, W. Ptak, E. Martin, K. Nazimek, M. Szczepanik, M. Sanak, P.W. Askenase, Free Extracellular miRNA Functionally Targets Cells by Transfecting Exosomes from Their Companion Cells, PLoS One, 10 (2015) e0122991.
[158] G. Fuhrmann, A. Serio, M. Mazo, R. Nair, M.M. Stevens, Active loading into extracellular vesicles significantly improves the cellular uptake and photodynamic effect of porphyrins, J. Control. Release, 205 (2015) 35-44.
[159] D. Sun, X. Zhuang, X. Xiang, Y. Liu, S. Zhang, C. Liu, S. Barnes, W. Grizzle, D. Miller, H.G. Zhang, A novel nanoparticle drug delivery system: the anti-inflammatory activity of curcumin is enhanced when encapsulated in exosomes, Mol. Ther., 18 (2010) 1606-1614.
[160] L. Pascucci, V. Cocce, A. Bonomi, D. Ami, P. Ceccarelli, E. Ciusani, L. Vigano, A. Locatelli, F. Sisto, S.M. Doglia, E. Parati, M.E. Bernardo, M. Muraca, G. Alessandri, G. Bondiolotti, A. Pessina, Paclitaxel is incorporated by mesenchymal stromal cells and released in exosomes that inhibit in vitro tumor growth: A new approach for drug delivery, J. Control. Release, 192 (2014) 262-70.

[161] N. Kosaka, H. Iguchi, Y. Yoshioka, F. Takeshita, Y. Matsuki, T. Ochiya, Secretory mechanisms and intercellular transfer of microRNAs in living cells, J. Biol. Chem., 285 (2010) 17442-17452.
[162] Y. Liu, D. Li, Z. Liu, Y. Zhou, D. Chu, X. Li, X. Jiang, D. Hou, X. Chen, Y. Chen, Z. Yang, L. Jin, W. Jiang, C. Tian, G. Zhou, K. Zen, J. Zhang, Y. Zhang, J. Li, C.Y. Zhang, Targeted exosome-mediated delivery of opioid receptor Mu siRNA for the treatment of morphine relapse, Sci. Rep., 5 (2015) 17543.
[163] A. Zomer, C. Maynard, F.J. Verweij, A. Kamermans, R. Schafer, E. Beerling, R.M. Schiffelers, E. de Wit, J. Berenguer, S.I. Ellenbroek, T. Wurdinger, D.M. Pegtel, J. van Rheenen, In Vivo imaging reveals extracellular vesicle-mediated phenocopying of metastatic behavior, Cell, 161 (2015) 1046-1057.
[164] B. Shen, N. Wu, J.M. Yang, S.J. Gould, Protein targeting to exosomes/microvesicles by plasma membrane anchors, J. Biol. Chem., 286 (2011) 14383-14395.
[165] Z.C. Hartman, J. Wei, O.K. Glass, H. Guo, G. Lei, X.Y. Yang, T. Osada, A. Hobeika, A. Delcayre, J.B. Le Pecq, M.A. Morse, T.M. Clay, H.K. Lyerly, Increasing vaccine potency through exosome antigen targeting, Vaccine, 29 (2011) 9361-9367.
[166] Z. Stickney, J. Losacco, S. McDevitt, Z. Zhang, B. Lu, Development of Exosome Surface Display Technology in Living Human Cells, Biochem. Biophys. Res. Commun., 472 (2016) 53-9.
[167] D.J. Cha, J.L. Franklin, Y. Dou, Q. Liu, J.N. Higginbotham, M. Demory Beckler, A.M. Weaver, K. Vickers, N. Prasad, S. Levy, B. Zhang, R.J. Coffey, J.G. Patton, KRAS-dependent sorting of miRNA to exosomes, eLife, 4 (2015) e07197.
[168] C.A. Maguire, L. Balaj, S. Sivaraman, M.H. Crommentuijn, M. Ericsson, L. Mincheva-Nilsson, V. Baranov, D. Gianni, B.A. Tannous, M. Sena-Esteves, X.O. Breakefield, J. Skog, Microvesicle-associated AAV vector as a novel gene delivery system, Mol. Ther., 20 (2012) 960-971.
[169] E. Hudry, C. Martin, S. Gandhi, B. Gyorgy, D.I. Scheffer, D. Mu, S.F. Merkel, F. Mingozzi, Z. Fitzpatrick, H. Dimant, M. Masek, T. Ragan, S. Tan, A.R. Brisson, S.H. Ramirez, B.T. Hyman, C.A. Maguire, Exosome-associated AAV vector as a robust and convenient neuroscience tool, Gene Ther., 23 (2016) 380-392.
[170] B. Gyorgy, Z. Fitzpatrick, M.H. Crommentuijn, D. Mu, C.A. Maguire, Naturally enveloped AAV vectors for shielding neutralizing antibodies and robust gene delivery in vivo, Biomaterials, 35 (2014) 7598-7609.
[171] H. Potter, Transfection by electroporation, Curr. Protoc. Mol. Biol., Chapter 9 (2003) Unit 9 3.
[172] J.M. Cooper, P.B. Wiklander, J.Z. Nordin, R. Al-Shawi, M.J. Wood, M. Vithlani, A.H. Schapira, J.P. Simons, S. El-Andaloussi, L. Alvarez-Erviti, Systemic exosomal siRNA delivery reduced alpha-synuclein aggregates in brains of transgenic mice, Mov. Disord., 29 (2014) 1476-1485.
[173] G. Chen, J.Y. Zhu, Z.L. Zhang, W. Zhang, J.G. Ren, M. Wu, Z.Y. Hong, C. Lv, D.W. Pang, Y.F. Zhao, Transformation of Cell-Derived Microparticles into Quantum-Dot-Labeled Nanovectors for Antitumor siRNA Delivery, Angew. Chem. Int. Ed. Engl., 54 (2014) 1036–1040.
[174] T.N. Lamichhane, R.S. Raiker, S.M. Jay, Exogenous DNA Loading into Extracellular Vesicles via Electroporation is Size-Dependent and Enables Limited Gene Delivery, Mol. Pharm., 12 (2015) 3650-3657.

[175] T.A. Shtam, R.A. Kovalev, E.Y. Varfolomeeva, E.M. Makarov, Y.V. Kil, M.V. Filatov, Exosomes are natural carriers of exogenous siRNA to human cells in vitro, J Cell Commun Signal., 11 (2013) 88.
[176] H. Saari, E. Lazaro-Ibanez, T. Viitala, E. Vuorimaa-Laukkanen, P. Siljander, M. Yliperttula, Microvesicle- and exosome-mediated drug delivery enhances the cytotoxicity of Paclitaxel in autologous prostate cancer cells, J. Control. Release, 220 (2015) 727-737.
[177] R.W. Yeo, R.C. Lai, B. Zhang, S.S. Tan, Y. Yin, B.J. Teh, S.K. Lim, Mesenchymal stem cell: An efficient mass producer of exosomes for drug delivery, Adv Drug Deliv Rev, 65 (2012) 336-41.
[178] W. Zhu, L. Huang, Y. Li, X. Zhang, J. Gu, Y. Yan, X. Xu, M. Wang, H. Qian, W. Xu, Exosomes derived from human bone marrow mesenchymal stem cells promote tumor growth in vivo, Cancer Lett., 315 (2012) 28-37.
[179] W. Yin, S. Ouyang, Y. Li, B. Xiao, H. Yang, Immature dendritic cell-derived exosomes: a promise subcellular vaccine for autoimmunity, Inflammation, 36 (2013) 232-240.
[180] Q. Wang, Y. Ren, J. Mu, N.K. Egilmez, X. Zhuang, Z. Deng, L. Zhang, J. Yan, D. Miller, H.G. Zhang, Grapefruit-Derived Nanovectors Use an Activated Leukocyte Trafficking Pathway to Deliver Therapeutic Agents to Inflammatory Tumor Sites, Cancer research, 75 (2015) 2520-2529.
[181] R. Munagala, F. Aqil, J. Jeyabalan, R.C. Gupta, Bovine milk-derived exosomes for drug delivery, Cancer Lett., 371 (2016) 48-61.
[182] Q. Wang, X. Zhuang, J. Mu, Z.B. Deng, H. Jiang, L. Zhang, X. Xiang, B. Wang, J. Yan, D. Miller, H.G. Zhang, Delivery of therapeutic agents by nanoparticles made of grapefruit-derived lipids, Nat. commun., 4 (2013) 1867.
[183] W. Jo, D. Jeong, J. Kim, S. Cho, S.C. Jang, C. Han, J.Y. Kang, Y.S. Gho, J. Park, Microfluidic fabrication of cell-derived nanovesicles as endogenous RNA carriers, Lab on a chip, 14 (2014) 1261-1269.
[184] S.C. Jang, O.Y. Kim, C.M. Yoon, D.S. Choi, T.Y. Roh, J. Park, J. Nilsson, J. Lotvall, Y.K. Kim, Y.S. Gho, Bioinspired exosome-mimetic nanovesicles for targeted delivery of chemotherapeutics to malignant tumors, ACS nano, 7 (2013) 7698-7710.
[185] S.A. Kooijmans, P. Vader, S.M. van Dommelen, W.W. van Solinge, R.M. Schiffelers, Exosome mimetics: a novel class of drug delivery systems, Int J Nanomedicine, 7 (2012) 1525-1541.
[186] Y. Akao, A. Iio, T. Itoh, S. Noguchi, Y. Itoh, Y. Ohtsuki, T. Naoe, Microvesicle-mediated RNA molecule delivery system using monocytes/macrophages, Mol. Ther., 19 (2011) 395-399.
[187] A. Mizrak, M.F. Bolukbasi, G.B. Ozdener, G.J. Brenner, S. Madlener, E.P. Erkan, T. Strobel, X.O. Breakefield, O. Saydam, Genetically engineered microvesicles carrying suicide mRNA/protein inhibit schwannoma tumor growth, Mol. Ther., 21 (2013) 101-108.
[188] M. Yang, J. Chen, F. Su, B. Yu, F. Su, L. Lin, Y. Liu, J.D. Huang, E. Song, Microvesicles secreted by macrophages shuttle invasion-potentiating microRNAs into breast cancer cells, Mol. Cancer, 10 (2011) 117.
[189] Y. Zhang, L. Li, J. Yu, D. Zhu, Y. Zhang, X. Li, H. Gu, C.Y. Zhang, K. Zen, Microvesicle-mediated delivery of transforming growth factor beta1 siRNA for the suppression of tumor growth in mice, Biomaterials, 35 (2014) 4390-4400.
[190] A.K. Silva, N. Luciani, F. Gazeau, K. Aubertin, S. Bonneau, C. Chauvierre, D. Letourneur, C. Wilhelm, Combining magnetic nanoparticles with cell derived microvesicles for drug loading and targeting, Nanomedicine, 11 (2015) 645-655.

[191] F. Andre, N. Chaput, N.E. Schartz, C. Flament, N. Aubert, J. Bernard, F. Lemonnier, G. Raposo, B. Escudier, D.H. Hsu, T. Tursz, S. Amigorena, E. Angevin, L. Zitvogel, Exosomes as potent cell-free peptide-based vaccine. I. Dendritic cell-derived exosomes transfer functional MHC class I/peptide complexes to dendritic cells, J. Immunol., 172 (2004) 2126-2136.
[192] C. Thery, L. Duban, E. Segura, P. Veron, O. Lantz, S. Amigorena, Indirect activation of naive CD4+ T cells by dendritic cell-derived exosomes, Nat. Immunol., 3 (2002) 1156-1162.
[193] N. Chaput, N.E. Schartz, F. Andre, J. Taieb, S. Novault, P. Bonnaventure, N. Aubert, J. Bernard, F. Lemonnier, M. Merad, G. Adema, M. Adams, M. Ferrantini, A.F. Carpentier, B. Escudier, T. Tursz, E. Angevin, L. Zitvogel, Exosomes as potent cell-free peptide-based vaccine. II. Exosomes in CpG adjuvants efficiently prime naive Tc1 lymphocytes leading to tumor rejection, J. Immunol., 172 (2004) 2137-2146.
[194] F. Guo, C.K. Chang, H.H. Fan, X.X. Nie, Y.N. Ren, Y.Y. Liu, L.H. Zhao, Anti-tumour effects of exosomes in combination with cyclophosphamide and polyinosinic-polycytidylic acid, J. Int. Med. Res., 36 (2008) 1342-1353.
[195] U. Gehrmann, S. Hiltbrunner, A.M. Georgoudaki, M.C. Karlsson, T.I. Naslund, S. Gabrielsson, Synergistic induction of adaptive antitumor immunity by codelivery of antigen with alpha-galactosylceramide on exosomes, Cancer Res., 73 (2013) 3865-3876.
[196] S. Viaud, S. Ploix, V. Lapierre, C. Thery, P.H. Commere, D. Tramalloni, K. Gorrichon, P. Virault-Rocroy, T. Tursz, O. Lantz, L. Zitvogel, N. Chaput, Updated technology to produce highly immunogenic dendritic cell-derived exosomes of clinical grade: a critical role of interferon-gamma, J. Immunother., 34 (2011) 65-75.
[197] T. Liu, D.E. Mendes, C.E. Berkman, Functional prostate-specific membrane antigen is enriched in exosomes from prostate cancer cells, Int. J. Oncol., 44 (2014) 918-922.
[198] I.S. Zeelenberg, W.W. van Maren, A. Boissonnas, M.A. Van Hout-Kuijer, M.H. Den Brok, J.A. Wagenaars, A. van der Schaaf, E.J. Jansen, S. Amigorena, C. Thery, C.G. Figdor, G.J. Adema, Antigen localization controls T cell-mediated tumor immunity, J. Immunol., 187 (2011) 1281-1288.
[199] X. Gu, U. Erb, M.W. Buchler, M. Zoller, Improved vaccine efficacy of tumor exosome compared to tumor lysate loaded dendritic cells in mice, Int. J. Cancer, 136 (2014) E74–E84.
[200] N. Mahaweni, M. Lambers, J. Dekkers, J. Aerts, J. Hegmans, Tumour-derived exosomes as antigen delivery carriers in dendritic cell-based immunotherapy for malignant mesothelioma, J Extracell Vesicles, 2 (2013) 22492.
[201] C. Yang, P.D. Robbins, The roles of tumor-derived exosomes in cancer pathogenesis, Clin. Dev. Immunol., 2011 (2011) 842849.
[202] J.A. Cho, Y.S. Lee, S.H. Kim, J.K. Ko, C.W. Kim, MHC independent anti-tumor immune responses induced by Hsp70-enriched exosomes generate tumor regression in murine models, Cancer Lett., 275 (2009) 256-265.
[203] S. Dai, X. Zhou, B. Wang, Q. Wang, Y. Fu, T. Chen, T. Wan, Y. Yu, X. Cao, Enhanced induction of dendritic cell maturation and HLA-A*0201-restricted CEA-specific CD8(+) CTL response by exosomes derived from IL-18 gene-modified CEA-positive tumor cells, J. Mol. Med. (Berl.), 84 (2006) 1067-1076.
[204] Y. Zhang, C.L. Luo, B.C. He, J.M. Zhang, G. Cheng, X.H. Wu, Exosomes derived from IL-12-anchored renal cancer cells increase induction of specific antitumor response in vitro: a novel vaccine for renal cell carcinoma, Int. J. Oncol., 36 (2010) 133-140.

[205] G. Andreola, L. Rivoltini, C. Castelli, V. Huber, P. Perego, P. Deho, P. Squarcina, P. Accornero, F. Lozupone, L. Lugini, A. Stringaro, A. Molinari, G. Arancia, M. Gentile, G. Parmiani, S. Fais, Induction of lymphocyte apoptosis by tumor cell secretion of FasL-bearing microvesicles, J. Exp. Med., 195 (2002) 1303-1316.
[206] A. Clayton, J.P. Mitchell, J. Court, M.D. Mason, Z. Tabi, Human tumor-derived exosomes selectively impair lymphocyte responses to interleukin-2, Cancer Res., 67 (2007) 7458-7466.
[207] A. Clayton, J.P. Mitchell, J. Court, S. Linnane, M.D. Mason, Z. Tabi, Human tumor-derived exosomes down-modulate NKG2D expression, J. Immunol., 180 (2008) 7249-7258.
[208] H. Peinado, M. Aleckovic, S. Lavotshkin, I. Matei, B. Costa-Silva, G. Moreno-Bueno, M. Hergueta-Redondo, C. Williams, G. Garcia-Santos, C. Ghajar, A. Nitadori-Hoshino, C. Hoffman, K. Badal, B.A. Garcia, M.K. Callahan, J. Yuan, V.R. Martins, J. Skog, R.N. Kaplan, M.S. Brady, J.D. Wolchok, P.B. Chapman, Y. Kang, J. Bromberg, D. Lyden, Melanoma exosomes educate bone marrow progenitor cells toward a pro-metastatic phenotype through MET, Nat. Med., 18 (2012) 883-891.
[209] A. Ginestra, M.D. La Placa, F. Saladino, D. Cassara, H. Nagase, M.L. Vittorelli, The amount and proteolytic content of vesicles shed by human cancer cell lines correlates with their in vitro invasiveness, Anticancer Res., 18 (1998) 3433-3437.
[210] E.Y. Lee, K.S. Park, Y.J. Yoon, J. Lee, H.G. Moon, S.C. Jang, K.H. Choi, Y.K. Kim, Y.S. Gho, Therapeutic effects of autologous tumor-derived nanovesicles on melanoma growth and metastasis, PLoS One, 7 (2012) e33330.
[211] C. Sedlik, J. Vigneron, L. Torrieri-Dramard, F. Pitoiset, J. Denizeau, C. Chesneau, P. de la Rochere, O. Lantz, C. Thery, B. Bellier, Different immunogenicity but similar antitumor efficacy of two DNA vaccines coding for an antigen secreted in different membrane vesicle-associated forms, J Extracell Vesicles, 3 (2014) 24646.
[212] P.D. Robbins, A.E. Morelli, Regulation of immune responses by extracellular vesicles, Nat. Rev. Immunol., 14 (2014) 195-208.
[213] L. van der Pol, M. Stork, P. van der Ley, Outer membrane vesicles as platform vaccine technology, Biotechnology Journal, 10 (2015) 1689-1706.
[214] K. Strimbu, J.A. Tavel, What are biomarkers?, Curr Opin HIV AIDS, 5 (2010) 463-466.
[215] M.K. Brawer, C.D. Cheli, I.E. Neaman, J. Goldblatt, C. Smith, M.K. Schwartz, D.J. Bruzek, D.L. Morris, L.J. Sokoll, D.W. Chan, K.K. Yeung, A.W. Partin, W.J. Allard, Complexed prostate specific antigen provides significant enhancement of specificity compared with total prostate specific antigen for detecting prostate cancer, The Journal of Urology, 163 (2000) 1476-1480.
[216] R.A. Burrell, N. McGranahan, J. Bartek, C. Swanton, The causes and consequences of genetic heterogeneity in cancer evolution, Nature, 501 (2013) 338-345.
[217] D. Olsen, J.T. Jorgensen, Companion diagnostics for targeted cancer drugs - clinical and regulatory aspects, Front. Oncol., 4 (2014) 105.
[218] G. Rabinowits, C. Gercel-Taylor, J.M. Day, D.D. Taylor, G.H. Kloecker, Exosomal microRNA: a diagnostic marker for lung cancer, Clin. Lung Cancer, 10 (2009) 42-46.
[219] D. Garnier, N. Jabado, J. Rak, Extracellular vesicles as prospective carriers of oncogenic protein signatures in adult and paediatric brain tumours, Proteomics, 13 (2013) 1595-1607.
[220] O.G. de Jong, M.C. Verhaar, Y. Chen, P. Vader, H. Gremmels, G. Posthuma, R.M. Schiffelers, M. Gucek, B.W. van Balkom, Cellular stress conditions are reflected in the protein and RNA content of endothelial cell-derived exosomes, J Extracell Vesicles, 1 (2012) 18396.

[221] A. Suetsugu, K. Honma, S. Saji, H. Moriwaki, T. Ochiya, R.M. Hoffman, Imaging exosome transfer from breast cancer cells to stroma at metastatic sites in orthotopic nude-mouse models, Advanced drug delivery reviews, 65 (2013) 383-390.
[222] C. Lasser, V.S. Alikhani, K. Ekstrom, M. Eldh, P.T. Paredes, A. Bossios, M. Sjostrand, S. Gabrielsson, J. Lotvall, H. Valadi, Human saliva, plasma and breast milk exosomes contain RNA: uptake by macrophages, J. Transl. Med., 9 (2011) 9.
[223] W.M. Dismuke, P. Challa, I. Navarro, W.D. Stamer, Y. Liu, Human aqueous humor exosomes, Exp. Eye Res., 132 (2015) 73-77.
[224] J.M. Street, P.E. Barran, C.L. Mackay, S. Weidt, C. Balmforth, T.S. Walsh, R.T. Chalmers, D.J. Webb, J.W. Dear, Identification and proteomic profiling of exosomes in human cerebrospinal fluid, J. Transl. Med., 10 (2012) 5.
[225] M. Tokuhisa, Y. Ichikawa, N. Kosaka, T. Ochiya, M. Yashiro, K. Hirakawa, T. Kosaka, H. Makino, H. Akiyama, C. Kunisaki, I. Endo, Exosomal miRNAs from Peritoneum Lavage Fluid as Potential Prognostic Biomarkers of Peritoneal Metastasis in Gastric Cancer, PLoS One, 10 (2015) e0130472.
[226] C. Admyre, J. Grunewald, J. Thyberg, S. Gripenback, G. Tornling, A. Eklund, A. Scheynius, S. Gabrielsson, Exosomes with major histocompatibility complex class II and co-stimulatory molecules are present in human BAL fluid, Eur. Respir. J., 22 (2003) 578-583.
[227] K. Al-Nedawi, B. Meehan, J. Micallef, V. Lhotak, L. May, A. Guha, J. Rak, Intercellular transfer of the oncogenic receptor EGFRvIII by microvesicles derived from tumour cells, Nat. Cell Biol., 10 (2008) 619-624.
[228] E.U. Wieckowski, C. Visus, M. Szajnik, M.J. Szczepanski, W.J. Storkus, T.L. Whiteside, Tumor-derived microvesicles promote regulatory T cell expansion and induce apoptosis in tumor-reactive activated CD8+ T lymphocytes, J. Immunol., 183 (2009) 3720-3730.
[229] T. Wurdinger, N.N. Gatson, L. Balaj, B. Kaur, X.O. Breakefield, D.M. Pegtel, Extracellular vesicles and their convergence with viral pathways, Adv. Virol., 2012 (2012) 767694.
[230] E. Colombo, B. Borgiani, C. Verderio, R. Furlan, Microvesicles: novel biomarkers for neurological disorders, Front. Physiol., 3 (2012) 63.
[231] G. Muller, Microvesicles/exosomes as potential novel biomarkers of metabolic diseases, Diabetes Metab. Syndr. Obes., 5 (2012) 247-282.
[232] K.M. Danielson, S. Das, Extracellular Vesicles in Heart Disease: Excitement for the Future ?, Exosomes and microvesicles, 2 (2014).
[233] G. Tavoosidana, G. Ronquist, S. Darmanis, J. Yan, L. Carlsson, D. Wu, T. Conze, P. Ek, A. Semjonow, E. Eltze, A. Larsson, U.D. Landegren, M. Kamali-Moghaddam, Multiple recognition assay reveals prostasomes as promising plasma biomarkers for prostate cancer, Proc. Natl. Acad. Sci. U. S. A., 108 (2011) 8809-8814.
[234] D.D. Taylor, C. Gercel-Taylor, MicroRNA signatures of tumor-derived exosomes as diagnostic biomarkers of ovarian cancer, Gynecol. Oncol., 110 (2008) 13-21.
[235] J. Silva, V. Garcia, M. Rodriguez, M. Compte, E. Cisneros, P. Veguillas, J.M. Garcia, G. Dominguez, Y. Campos-Martin, J. Cuevas, C. Pena, M. Herrera, R. Diaz, N. Mohammed, F. Bonilla, Analysis of exosome release and its prognostic value in human colorectal cancer, Genes Chromosomes Cancer, 51 (2012) 409-418.
[236] W. Wang, H. Li, Y. Zhou, S. Jie, Peripheral blood microvesicles are potential biomarkers for hepatocellular carcinoma, Cancer Biomark., 13 (2013) 351-357.

[237] C. Fruhbeis, S. Helmig, S. Tug, P. Simon, E.M. Kramer-Albers, Physical exercise induces rapid release of small extracellular vesicles into the circulation, Journal of extracellular vesicles, 4 (2015) 28239.
[238] D.M. Smalley, N.E. Sheman, K. Nelson, D. Theodorescu, Isolation and identification of potential urinary microparticle biomarkers of bladder cancer, J. Proteome Res., 7 (2008) 2088-2096.
[239] R. Cazzoli, F. Buttitta, M. Di Nicola, S. Malatesta, A. Marchetti, W.N. Rom, H.I. Pass, microRNAs derived from circulating exosomes as noninvasive biomarkers for screening and diagnosing lung cancer, J. Thorac. Oncol., 8 (2013) 1156-1162.
[240] T. An, S. Qin, Y. Xu, Y. Tang, Y. Huang, B. Situ, J.M. Inal, L. Zheng, Exosomes serve as tumour markers for personalized diagnostics owing to their important role in cancer metastasis, Journal of extracellular vesicles, 4 (2015) 27522.
[241] B.W. van Balkom, T. Pisitkun, M.C. Verhaar, M.A. Knepper, Exosomes and the kidney: prospects for diagnosis and therapy of renal diseases, Kidney Int., 80 (2011) 1138-1145.
[242] S. Pant, H. Hilton, M.E. Burczynski, The multifaceted exosome: Biogenesis, role in normal and aberrant cellular function, and frontiers for pharmacological and biomarker opportunities, Biochem. Pharmacol., 83 (2012) 1484-1494.
[243] M. Shi, C. Liu, T.J. Cook, K.M. Bullock, Y. Zhao, C. Ginghina, Y. Li, P. Aro, R. Dator, C. He, M.J. Hipp, C.P. Zabetian, E.R. Peskind, S.C. Hu, J.F. Quinn, D.R. Galasko, W.A. Banks, J. Zhang, Plasma exosomal alpha-synuclein is likely CNS-derived and increased in Parkinson's disease, Acta Neuropathol., 128 (2014) 639-650.
[244] M.C. DeSantis, W. Cheng, Label-free detection and manipulation of single biological nanoparticles, WIREs Nanomed Nanobiotechnol, (2016).
[245] T. Groot Kormelink, G.J. Arkesteijn, F.A. Nauwelaers, G. van den Engh, E.N. Nolte-'t Hoen, M.H. Wauben, Prerequisites for the analysis and sorting of extracellular vesicle subpopulations by high-resolution flow cytometry, Cytometry. Part A : the journal of the International Society for Analytical Cytology, 89 (2016) 135-147.
[246] A. Arakelyan, O. Ivanova, E. Vasilieva, J.-C. Grivel, L. Margolis, Antigenic composition of single nano-sized extracellular blood vesicles, Nanomedicine: Nanotechnology, Biology and Medicine, 11 (2015) 489-498.
[247] E.N.M. Nolte-'t Hoen, E.J. van der Vlist, M. de Boer-Brouwer, G.J.A. Arkesteijn, W. Stoorvogel, M.H.M. Wauben, Dynamics of dendritic cell-derived vesicles: high-resolution flow cytometric analysis of extracellular vesicle quantity and quality, J. Leukoc. Biol., 93 (2013) 395-402.
[248] C. Sheridan, Exosome cancer diagnostic reaches market, Nat Biotech, 34 (2016) 359-360.
[249] E.M. Mora, S. Alvarez-Cubela, E. Oltra, Biobanking of Exosomes in the Era of Precision Medicine: Are We There Yet?, Int. J. Mol. Sci., 17 (2016) 13.
[250] O. Rubin, D. Crettaz, J.D. Tissot, N. Lion, Pre-analytical and methodological challenges in red blood cell microparticle proteomics, Talanta, 82 (2010) 1-8.
[251] K.W. Witwer, E.I. Buzas, L.T. Bemis, A. Bora, C. Lasser, J. Lotvall, E.N. Nolte-'t Hoen, M.G. Piper, S. Sivaraman, J. Skog, C. Thery, M.H. Wauben, F. Hochberg, Standardization of sample collection, isolation and analysis methods in extracellular vesicle research, J. of extracel. Vesicles, 2 (2013).

2

Electroporation-induced siRNA precipitation obscures the efficiency of siRNA loading into extracellular vesicles

An adapted manuscript of this chapter is published as:

Sander A. A. Kooijmans[1,*], Stephan Stremersch[2,*], Kevin Braeckmans[2,3], Stefaan C. De Smedt[2], An Hendrix[4], Matthew J. A. Wood[5], Raymond M. Schiffelers[1], Koen Raemdonck[2,$], Pieter Vader[1,5,$]. Electroporation-induced siRNA precipitation obscures the efficiency of siRNA loading into extracellular vesicles. *J. Control. Release,* 172(1), 229–238 (2013).

[*]These authors contributed equally to this work

[$]These authors contributed equally to this work

[1]Department of Clinical Chemistry and Haematology, University Medical Center Utrecht, Utrecht, The Netherlands

[2]Laboratory of General Biochemistry and Physical Pharmacy, Ghent University, Ghent, Belgium

[3]Centre for Nano- and Biophotonics, Ghent University, Ghent, Belgium

[4]Laboratory of Experimental Cancer Research, Ghent University Hospital, Ghent, Belgium

[5]Department of Physiology, Anatomy and Genetics, University of Oxford, Oxford, UK

Chapter 2: ToC

Abstract

Extracellular vesicles (EVs) are specialized endogenous carriers of proteins and nucleic acids and are believed to be involved in intercellular communication. EVs are therefore proposed as candidate drug delivery systems for the delivery of nucleic acids and other macromolecules. However, the preparation of EV-based drug delivery systems is hampered by the lack of techniques to load the vesicles with nucleic acids. In this chapter we have characterized in detail the use of electroporation for this purpose. When EVs were electroporated with siRNA, the siRNA retention was comparable with previously published results (~20 – 25 %). Remarkably, when siRNA was electroporated in the absence of EVs, a similar or even greater siRNA retention was measured. Scattering-based single particle tracking and confocal microscopy showed extensive formation of insoluble siRNA aggregates after electroporation, which could be dramatically reduced by addition of ethylenediaminetetraacetic acid (EDTA). Other strategies to reduce aggregate formation, including the use of cuvettes with conductive polymer electrodes and the use of an acidic citrate buffer, resulted in a more efficient reduction of siRNA precipitation than EDTA. However, under these conditions, siRNA retention was below 0.05 % and no significant differences in siRNA retention could be measured between samples electroporated in the presence or absence of EVs. These results show that electroporation of EVs with siRNA is accompanied by extensive siRNA aggregate formation, which may cause overestimation of the amount of siRNA actually loaded into EVs. Overall, the data clearly illustrate that electroporation is far less efficient than previously described, and highlight the necessity for alternative methods to prepare siRNA-loaded EVs.

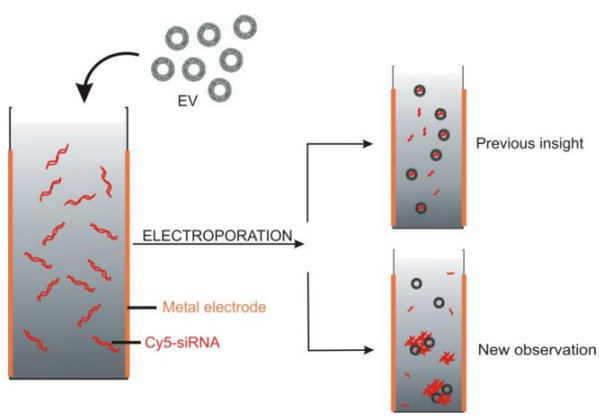

Schematic representation of siRNA-EV mixtures after electroporation in metal electrode cuvettes.

1. Introduction

As discussed in **chapter 1**, EVs are theoretically endowed with many interesting features which rationalizes the exploration of their potential as a drug delivery vehicle. Indeed, after secretion of the vesicles, the lipid bilayer protects the cargo against plasma and immune components, fixes the ratio between biological molecules and assists in functional delivery to target cells, where the vesicular content may provoke functional changes [1-3]. Interestingly, (sub)populations of vesicles may deliver their cargo by direct fusion with the plasma membrane of target cells, circumventing the endosomal-lysosomal pathway and resulting in efficient release of the cargo in the cytoplasm [3, 4]. These characteristics are very attractive for drug delivery purposes, especially in the case of nucleic acid-based drugs, given that endosomal escape is one of the major bottlenecks for the intracellular delivery of nucleic acids [5-7]. Hence, in recent years the exploitation of (endogenous) EVs as delivery vehicle for, amongst others, RNA interference (RNAi)-based therapeutics (i.e. miRNA and siRNA) has gained attention.

RNAi is a highly conserved, natural mechanism used by eukaryotic cells to regulate the gene expression on a post-transcriptional level. The process is mediated by the cell‘s dedicated RNAi machinery that is activated by a small RNA duplex (i.e. siRNA or miRNA) recognizing a specific region in an mRNA strand [8] (**figure 1**). MiRNAs are the product of primary-miRNA (pri-miRNA), which are stem-and-loop RNA strands transcribed from regions in the genomic DNA by RNA polymerase II. These pri-miRNA are recognized and cleaved by Drosha (i.e. a RNase III-like enzyme) into shorter (~70 - 100 nucleotides (nt)) hairpin-like RNAs called precursor-miRNA (pre-miRNA) that are subsequently exported into the cytoplasm by the exportin-5/Ran-GTP heterodimer complex. There, the pre-miRNAs are further processed by Dicer (also a RNase III-like enzyme) into a mature miRNA duplex (~18 - 25 nt). The latter is incorporated in a protein complex termed the RNA-induced silencing complex (RISC) which retains one of the two strands (referred to as the guide or antisense strand). The now activated RISC (RISC*) will scan mRNA strands for regions complementary to the guide strand. Upon (partial) base pairing, the protein expression is inhibited *via* repression of the mRNA translation or *via* Argonaute 2 (AGO2; an endonuclease associated to RISC) mediated cleavage of the phosphodiester backbone of the mRNA strand. SiRNAs are the result of exogenous double stranded RNA (dsRNA) processed by Dicer in the cell’s cytoplasm. Similar to the miRNAs, siRNA is recognized by the RISC complex allowing AGO2-mediated cleavage of the respective mRNA strand. Indeed, siRNAs and miRNAs display many similarities. The major difference between both classes of RNAi effectors relates to specificity. SiRNAs are highly specific with only one theoretical mRNA target, whereas miRNAs generally have multiple targets (some miRNA have up to 100 mRNA targets) [9, 10].

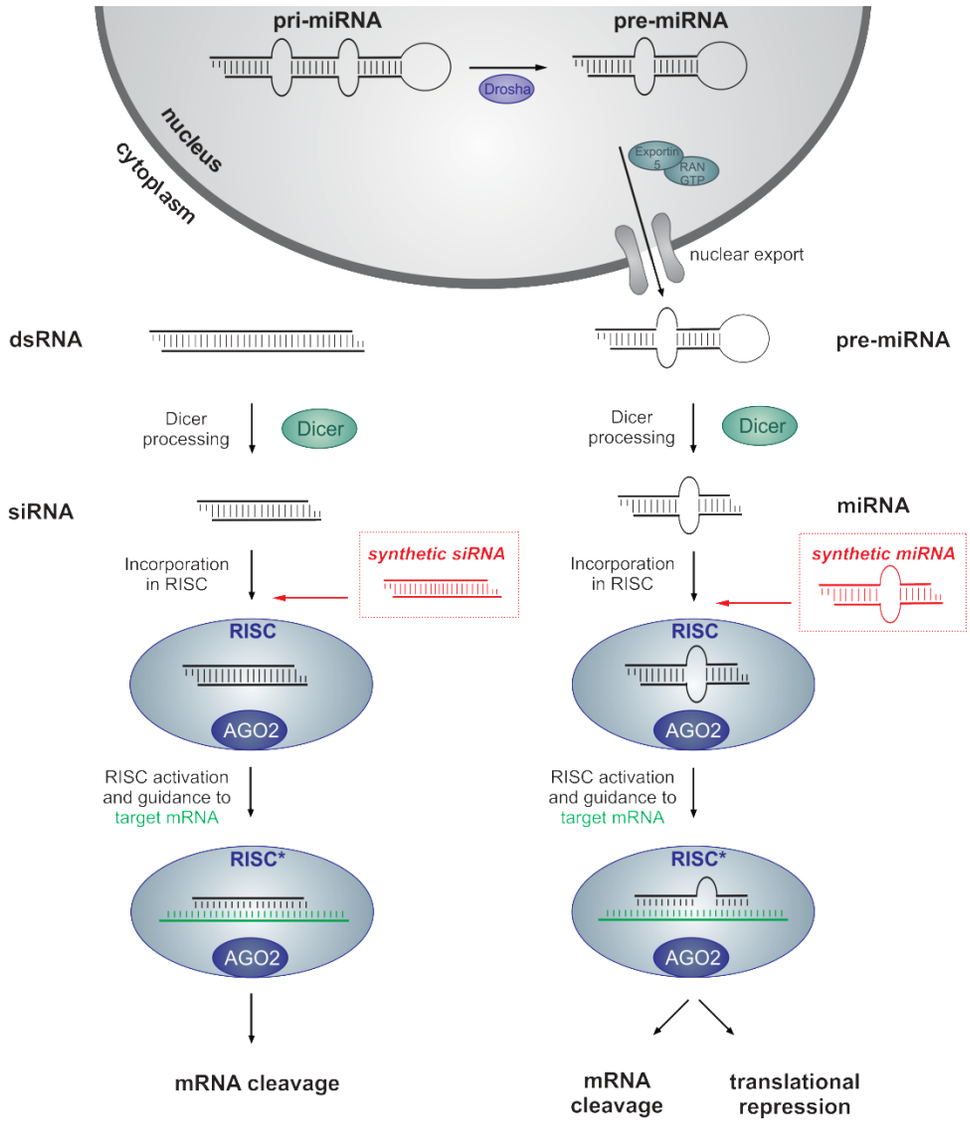

Figure 1. Schematic representation of the RNA interference (RNAi) pathway, activated by small interfering RNA (siRNA) or microRNA (miRNA). The RNAi pathway can be targeted for therapeutic purposes by introducing synthetic siRNA and synthetic miRNA into the cellular cytoplasm (indicated in red). This figure was adopted with permission from ref. [11].

The high specificity, yet broad applicability of the RNAi mechanism makes it a very interesting target for therapeutic intervention. By introducing synthetic siRNA or miRNA in the cytoplasm, the overexpression of specific deregulated genes in a diseased cell can be restored (**figure 1**). However, efficient clinical use of these small RNA duplexes is hampered by some of its inherent characteristics. Unmodified RNA is not stable in (nuclease rich) biological fluids leading to rapid clearance and loss of functionality. Moreover, it can trigger the innate immune system causing unwanted side effects. Additionally, siRNA and miRNA are relatively large (~14 kDa), negatively charged macromolecules that are not able to spontaneously migrate over the cellular membranes and enter the cytoplasm where the RNAi machinery is located. In this respect, many

solutions have been proposed to (partly) counter these adverse features. Careful placement of chemical modifications into the RNA backbone (e.g. substitution of the phosphodiester linkage with phosphorothioate or substitution of the ribose 2'-OH group by 2'-fluoro or 2'-O-methyl) protects RNA against enzymatic degradation and can mitigate interaction with toll-like receptors [12, 13]. Furthermore, much effort is invested in the development of nanosized delivery carriers which shield the RNA cargo from the harsh (extracellular) environment and shuttle the RNA over the different extra- and intracellular biological barriers, finally delivering the cargo to the cytoplasm of the target cell. Although the benefits of packaging siRNA into (nanosized) drug delivery vehicles are indisputable, to date none of the developed approaches address all the multifaceted requirements to efficiently overcome all barriers [7, 10].

In this context, EVs appear as an excellent drug delivery vehicle candidate. Yet, the exploration of their practical use has been limited by the lack of techniques to load them with the desired therapeutics. Several strategies have been proposed to encapsulate siRNA or miRNA into EVs, including transfection-based approaches and electroporation (**chapter 1**). Briefly, in the transfection-based approach, donor cells are transfected with a suitable expression vector, which induces overexpression of the desired small RNA. Subsequently, the RNA is incorporated into EVs and may be transferred to other cells. Using this technique, a number of reports have described the successful loading of a variety of siRNAs and miRNAs into EVs and showed their inhibitory effects in target cells [14-17]. Alternatively, donor cells can be directly transfected with the siRNA or miRNA of choice using conventional transfection reagents. This results in the secretion of EVs, functionally loaded with the selected small RNAs [18-23]. However, a disadvantage of this pre-formation loading technique is that remainders of transfection reagents may influence the encapsulation process and the behavior of the modified EVs. Furthermore, the levels of the desired small RNAs that are secreted into the vesicles are low and vary widely among sequences. Indeed, the biochemical pathways for cargo loading into EVs are still largely elusive and hence uncontrollable. In addition, the transfected miRNA/siRNA may alter target gene expression in the donor cell, which complicates the selection of feasible donor cells and target sequences. By loading small RNAs into purified EVs using electroporation, loading efficiency may be independent of the sequence of the small RNA that is incorporated into EVs. Different groups reported successful loading of EVs with exogenous siRNA by electroporation [24-27]. Wahlgren *et al.* demonstrated that the exogenous siRNA could be detected in up to 85.2 % of the electroporated EVs (however no encapsulation efficiency was reported) *via* bead-based flow cytometry analysis. Loaded EVs induced knockdown of the siRNA target genes when incubated with monocytes or lymphocytes [25]. Alvarez-Erviti *et al.* showed that approximately 25 % of the electroporated siRNA was loaded into EVs and that

retargeted EVs were functional *in vivo*, reducing expression of the *BACE1* target gene in mouse brains by 60 % [24, 26].

Based on these reports it appears that electroporation is able to maintain EV integrity and functionality with concomitant encapsulation of high levels of small RNAs. The reported high encapsulation efficiency after electroporation is intriguing, given that the introduction of nucleic acids into preformed nanosized carrier systems is challenging and not commonly performed. Efficient loading of drug delivery systems with nucleic acids is generally only achieved during assembly of the carriers [28]. The electroporation technique therefore may offer an elegant solution for the loading of EVs with siRNA. However, the biophysical mechanism by which electroporation results in high encapsulation levels of siRNA into EVs remains unclear. In this chapter, we sought to further study and characterize the electroporation process for the loading of siRNA into EVs.

2. Experimental section

2.1. Materials

OptiPrep™ was obtained from Sigma-Aldrich (Steinheim, Germany). Nucleic acids used in this chapter are listed in **table 1** (siRNA) and **table S1** (primers) (see supporting information at the end of this chapter). The Micro BCA Protein Assay Kit was from Thermo Scientific (Rockford, IL). Electroporation cuvettes with aluminum electrodes were from Bio-Rad Laboratories, Inc (Hercules, CA) or VWR (Leuven, Belgium) and cuvettes with conductive polymer electrodes (Nucleocuvettes™) and 4D-Nucleofector electroporation buffers were from Lonza (Basel, Schwitzerland). TRIzol Reagent, GlycoBlue, Taqman miRNA Reverse Transcription Kit, MicroAmp Optical 96-well plates and Lipofectamine 2000 were purchased from Life Technologies (Paisley, UK). FastStart SYBR Green Master was obtained from Roche (Penzberg, Germany) and Rox passive reference dye was from Bio-Rad Laboratories, Inc (Hercules, CA). pCMV-Luc vector was obtained from PlasmidFactory (Bielefeld, Germany) and pGL4.74[hRluc/TK] vector and Dual Luciferase Reporter Assay System kit were from Promega (Leiden, The Netherlands).

Table 1. Sequences and modifications of siRNAs used in this chapter.

Target	Abbreviation	Modification	Manufacturer	Sequence [a)]	
				Sense strand (5'-3')	Antisense strand (5'-3')
Negative control	Cy5-labeled siRNA	Cy5 [b)]	Eurogentec	UGCGCUACGAUCGACGAUG**tt**	CAUCGUCGAUCGUAGCGCA**tt**
Negative control	Cy3-labeled siRNA	Cy3 [b)]	Integrated DNA Technologies	CAGAAGACUGUGGAUGGCC**tt**	GGCCAUCCACAGUCUUCUG**gg**
Luciferase reporter gene	siRNA LUC	/	Integrated DNA Technologies	GAUUAUGUCCGGUUAUGUACG	UACAUAACCGGACAUAAUCGG
Negative control	siRNA CTRL	/	Eurogentec	UGCGCUACGAUCGACGAUG**tt**	CAUCGUCGAUCGUAGCGCA**tt**
eGFP[c)] reporter gene	siRNA GFP	/	Eurogentec	CAAGCUGACCCUGAAGUUC**tt**	GAACUUCAGGGUCAGCUUG**tt**

[a)]lower case bold letters represent deoxyribonucleotides, capital letters represent ribonucleotides; [b)]Cy5 or Cy3 fluorescent label is linked at the 5' end of the sense strand; [c)]enhanced green fluorescent protein

2.2. Cell culture and isolation of extracellular vesicles

Human embryonic kidney (HEK293T) and mouse neuroblastoma (Neuro2A) cell lines were maintained in Dulbecco's modified eagle medium (DMEM; Invitrogen) supplemented with 10 % fetal bovine serum (FBS; Hyclone™), 100 U/ml penicillin and 100 µg/ml streptomycin (Invitrogen). All cells were grown in a humidified atmosphere containing 5 % CO_2 at 37°C.

For EV production, cells were initially cultured in standard cell medium after which they were washed and incubated for 48 hours in EV-depleted medium prepared *via* overnight ultracentrifugation (UC) at 100 000 g. As culture medium is often supplemented with FBS to supply nutrients for cellular growth, it important to note that FBS houses a substantial amount of EVs from bovine origin, for which it has been shown that they can influence the recipient cell's phenotype [29]. To circumvent the presence of these bovine vesicles in the final EV-isolates, different alteration on classic cell culture medium have been used throughout the literature. Researchers have used OptiMEM [30], overnight ultra-centrifuged cell medium (as used in this chapter) [29, 31], ultra-filtrated (UF) cell medium (as used in chapters 3 to 5) [32], commercial vesicle-depleted FBS [33] and cell medium without FBS [19]. This seemingly trivial choice has however shown to influence the protein composition of the produced EVs [34].

Next, conditioned cell medium was harvested and EVs were isolated by a standard differential centrifugation/filtration protocol. Briefly, the medium was centrifuged for 10 minutes at 300 g, followed by 10 minutes at 2 000 g to remove cells and cell debris. Subsequently, the medium was filtered through 0.22 µm syringe filters and EVs were pelleted by centrifugation for 70 minutes at 100 000 g. Pellets were washed with phosphate buffered saline (PBS) and pelleted again by centrifugation for 70 minutes at 100 000 g. Resulting pellets were resuspended in the desired electroporation buffer and the yield was determined using a Micro BCA Protein Assay (Pierce) with bovine serum albumin (BSA) protein standards.

2.3. Electroporation buffers

Citric acid based buffer consisted of 18.6 mM citric acid and 29.4 mM disodium phosphate with a pH of 4.4. Phosphate-free buffer contained 125 mM sodium chloride, 5 mM potassium chloride, 1.5 mM calcium chloride, 10 mM glucose, and 20 mM 4-(2-hydroxyethyl)-1-piperazineethanesulfonic acid (HEPES) adjusted to pH 7.4. OptiPrep-based buffer consisted of 21 % OptiPrep™, 1.25 mM potassium phosphate and 25 mM potassium chloride adjusted to pH 7.2. Cytomix electroporation buffer consisted of 120 mM potassium chloride, 0.15 mM calcium chloride, 10 mM potassium phosphate, 25 mM HEPES, 2 mM EGTA and 5 mM magnesium chloride, adjusted to pH 7.6 with potassium hydroxide.

2.4. Electroporation in metal electrode cuvettes

Electroporations were performed in 0.4 cm cuvettes with aluminum electrodes using a Bio-Rad Gene Pulser II with capacitance extender set at 400 V and 125 µF. For every electroporation the sample volume was fixed at 200 µL, containing 3 µg EVs and 3 µg siRNA unless otherwise stated. After electroporation, all electroporation cuvettes were incubated on ice for at least 30 minutes before further processing.

2.5. Scattering-based single particle tracking

The size and concentration of particle aggregates was determined *via* scattering-based single particle tracking using a NanoSight LM10 instrument (Malvern). Prior to analysis, the samples were diluted in deionized water. For each condition three independent samples were prepared and analyzed. Per measurement a movie of 60 seconds was recorded. To evaluate particle aggregation in conductive polymer cuvettes, the samples were diluted with PBS and analyzed using a Nanosight LM10 instrument connected to a syringe pump device (Malvern) while the temperature was maintained at 22°C. Flow was set at 20 and for each sample a 180 seconds movie was recorded. All data was analyzed with the NTA Analytical Software suite version 2.3.

2.6. Confocal microscopy

Confocal microscopy of aggregates containing Cy5-labeled siRNA was performed using a Nikon Cs1 confocal laser scanning module installed on a motorized Nikon TE2000-E inverted microscope (Nikon Benelux, Brussels, Belgium) equipped with an oil immersion objective lens (60x, NA 1.4, Nikon, Japan). Samples were transferred directly from the electroporation cuvettes into wells of a glass-bottomed 96-well plate (Greiner Bio-one, Frickenhausen, Germany) for analysis. When indicated, EVs present in electroporated samples were labeled using Annexin V – alexa fluor 488 (Molecular probes). To this end, 89 µL of the electroporated sample was mixed with 10 µL of a 10x Annexin binding buffer (100 mM HEPES, 1.4 M NaCl, 25 mM $CaCl_2$, pH 7.4) and 1 µL Annexin V – alexa fluor 488 stock. The mixture was allowed to incubate for 15 minutes at room temperature prior to imaging.

2.7. Fluorescence Fluctuation Spectroscopy

To assess the percentage of encapsulated Cy5-labelled siRNA into EVs by electroporation, fluorescence fluctuation spectroscopy (FFS) was used as previously described [35]. Prior to analysis, the electroporated samples were diluted 10-fold in the respective buffer and 60 µL was transferred to the wells of a glass-bottomed 96-well plate (Greiner Bio-one, Frickenhausen, Germany). The focal volume was positioned in the sample and FFS measurements were performed during a 30 seconds time-interval. A motorized Nikon TE2000-E inverted microscope, equipped with a water immersion

objective lens (60x, NA 1.2, Nikon) and a 637 nm laser line for the excitation of Cy5-siRNA, was used. The fluorescence intensity fluctuations were recorded with the fluorescence correlation spectrometer MicroTime 200 (picoquant GmbH, Berlin, Germany), equipped with SymPhoTime software. For each condition, samples were prepared in triplicate. The fluorescence intensity of the baseline (i.e. the average fluorescence in the focal volume) in the fluctuation profiles was determined as previously described [35]. The siRNA complexation efficiency was subsequently calculated using **equation 1**.

$$siRNA\ complexation\ efficiency\ \ (\%) = 100 - 100 \times \left[\frac{\bar{I}_{after\ electroporation} - \bar{I}_{medium}}{\bar{I}_{before\ electroporation} - \bar{I}_{medium}} \right] \qquad (\textbf{eq.1})$$

Where $\bar{I}_{after\ electroporation}$ is the average intensity of the baseline after electroporation, $\bar{I}_{before electroporation}$ is the average intensity of the baseline before electroporation and $\bar{I}_{medium}$ is the average intensity of the baseline of the medium without fluorescently labeled siRNA.

2.8. eGFP gene silencing assay

eGFP reporter gene silencing experiments were performed using human non-small-cell lung carcinoma cells (H1299_eGFP), which stably express the enhanced green fluorescent protein (eGFP). Cells were grown in RPMI 1640 medium supplemented with 10 % FBS, 2 mM glutamine and 100 U/ml penicillin/streptomycin at 37°C in a humidified atmosphere containing 5 % CO_2. Cells were plated in a 24-well plate in a concentration of 1.36 x 10^4 cells per cm^2. Twenty-four hours after seeding, samples were applied: 3 µg of siRNA targeted against eGFP (siRNA GFP) or siRNA CTRL was electroporated in the presence or absence of 3 µg HEK293T EVs in an OptiPrep™-based electroporation buffer at 400 V and 125 µF in aluminum electroporation cuvettes (0,4 cm, Bio-Rad), diluted with 4 mL PBS and centrifuged at 100 000 g for 70 minutes. Pellets were resuspended in 500 µl OptiMEM and co-incubated with the H1299_eGFP cells. As a positive control, lipofectamine RNAiMAX (Invitrogen) was used in combination with siRNA GFP and siRNA CTRL according to the manufacturer's instructions. After 4h incubation, samples were removed and cells were washed with PBS and incubated in full cell medium for 48h after which eGFP expression was measured using a BD Biosciences FACSCalibur™ (BD Biosciences) flow cytometer. Data analysis was performed by using the BD CellQuest Pro™ (BD Biosciences) analysis software and reported as the average eGFP expression (%) normalized to non-treated cells.

2.9. Statistical data analysis

When applicable, statistical data analysis was done with GraphPad Prism 6 (GraphPad Software). Comparing multiple conditions was done using an ANOVA-test followed by a Tukey post hoc test. Direct comparison between two conditions was done using a student t-test. A p-value < 0.05 was considered as statistically significant. The degree of significance is indicated using ns ($p \geq 0.05$), *($p < 0.05$), **($p < 0.01$), ***($p < 0.001$), ****($p < 0.0001$).

3. Results

3.1. Quantification of siRNA loading into EVs by electroporation

When aiming to use endogenous EVs as nanosized carriers for the delivery of siRNA, it is essential to have an efficient siRNA loading method available. A method proposed by Alvarez-Erviti *et al.* described that about 25 % of fluorescently labeled siRNA could be encapsulated in EVs by electroporation using optimized settings and reagents [24, 26]. We evaluated this loading approach under similar experimental conditions and quantified the amount of retained siRNA in EVs by FFS. Briefly, FFS is a microscopy based technique that monitors fluorescence intensity fluctuations in the excitation volume of a confocal microscope. The fluorescence fluctuations originate from the movement of fluorescently labeled molecules (in this case Cy5-siRNA) in and out of the fixed excitation volume. The average fluorescence signal is proportional to the concentration of freely diffusing fluorescently labeled siRNA in solution. Complexation of siRNA into (nano)particles results in a decrease of the average fluorescence signal. This can be used to quantify siRNA complexation (**section 2.7**) without the need for sample pre-treatment, which has previously been demonstrated for lipo-and polyplexes [35-37]. When FFS was used to quantify Cy5-siRNA loading in EVs after electroporation under the previously reported conditions (3 µg labeled-siRNA and 3 µg EVs electroporated in an OptiPrep™-based buffer), siRNA complexation appeared comparable (~18 %) to what was observed by Alvarez-Erviti and colleagues [26] (**figure 2A**). When no electric pulse was applied, no Cy5-siRNA complexation could be detected. However, when Cy5-siRNA was electroporated in the absence of EVs, an even higher siRNA complexation (~24 %) was measured indicating that other factors than encapsulation in EVs contribute to the observed siRNA complexation (**figure 2A**). To further confirm these observations, EVs were pelleted by ultracentrifugation after electroporation and the amount of siRNA fluorescence in the pellet was assessed by fluorescence spectroscopy (see supporting experimental section). Also in this assay, electroporation in the absence of EVs resulted in high amounts of siRNA retention (**figure S1A**). To verify that these results are not dependent on the fluorescent label associated to the

siRNA strands, the same experiment was repeated with unlabeled siRNA. In this approach the retained siRNA after ultracentrifugation was measured by RT-PCR (see supporting experimental section). It was quantified that 3.7 % of the siRNA was retained in the EV pellet after electroporation (**figure S1B**). Again, when electroporation was performed in the absence of EVs, a substantial portion of siRNA could be recovered from the pellet (2.3 %). This phenomenon appeared to be independent of the EV source as no difference in retained siRNA could be observed between HEK293T- and Neuro2A-derived EVs (**figure S1**). Thus, although absolute values differed between methods, the percentage of retained siRNA following electroporation in the absence of EVs was similar to (or even greater than) the retention obtained in the presence of EVs.

Taken together, these data suggest that electroporation causes siRNA to be retained in particles which could not be distinguished from EVs by FFS, and which co-sediment at centrifugal forces usually applied to pellet EVs. In order to better visualize this phenomenon, electroporated samples were analyzed by confocal microscopy. After electroporation of Cy5-siRNA in the absence of EVs, an excessive number of irregularly shaped insoluble fluorescent aggregates were detected (**figure 2B**). Hence, siRNA appears to strongly aggregate when subjected to electroporation. Moreover, electroporation in the presence of EVs led likewise to massive aggregation in which EVs and siRNA co-precipitate (**figure 2C**).

This effect was not specific for the OptiPrep^{TM}-based electroporation buffer, but was also observed for the previously described Cytomix electroporation buffer [25] by FFS and confocal microscopy (**figure 2A and 2B**), albeit the extent of aggregation was slightly lower compared to the OptiPrep^{TM}-based buffer.

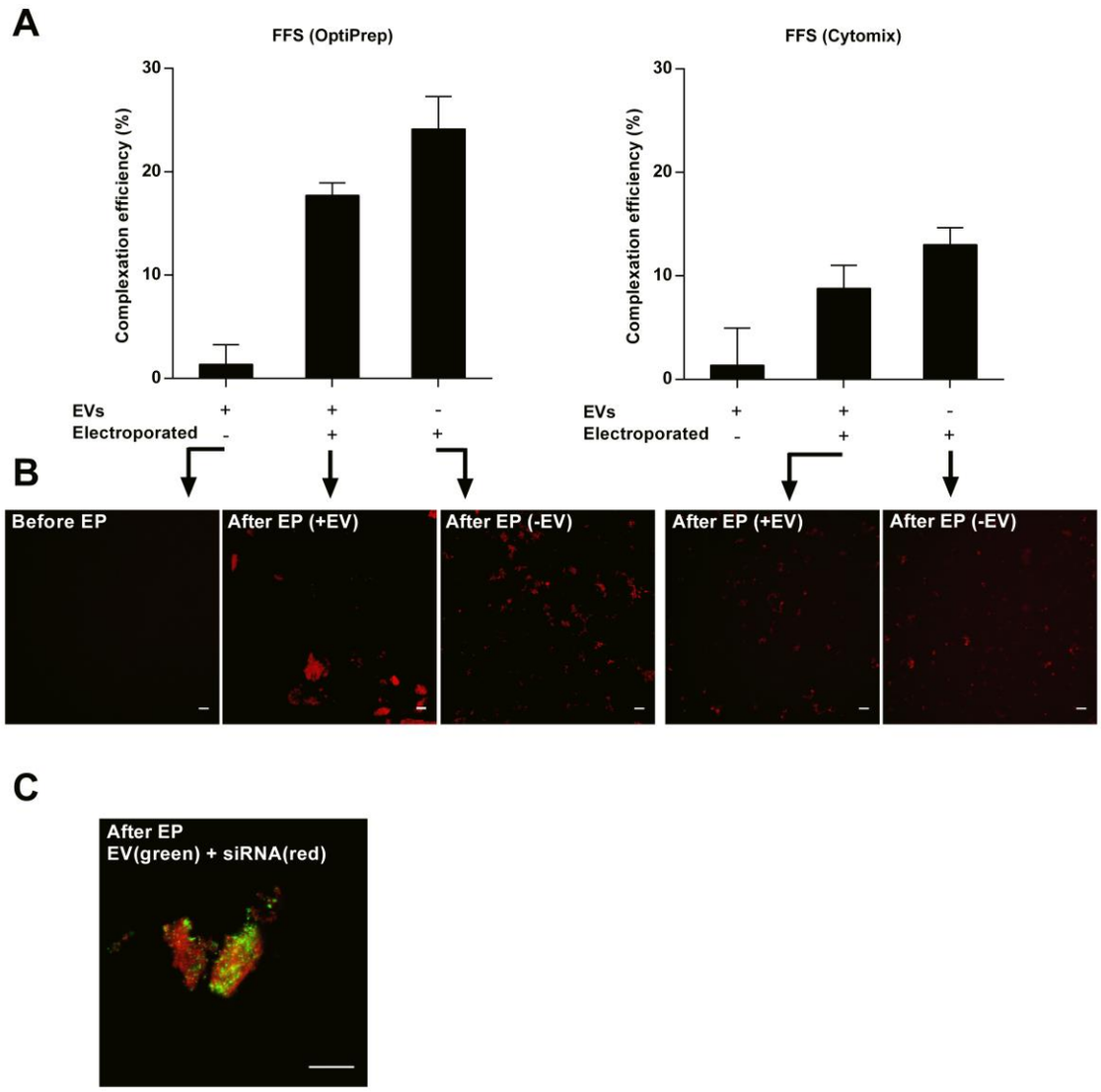

Figure 2. Precipitation of siRNA after electroporation in OptiPrep™-based and Cytomix electroporation buffer in the presence (+) or absence (−) of EVs derived from HEK293T cells. [A] Complexation efficiency of Cy5-siRNA as measured by FFS in OptiPrep™-based and Cytomix electroporation buffer. Experiments were performed in triplicate and data are presented as mean ± SD. [B] Representative confocal microscopy images of aggregate formation of Cy5-siRNA (red) of the indicated mixtures. [C] Representative confocal microscopy image of EVs (Annexin V – alexa fluor 488 labeled; green) and Cy5-siRNA (red) after electroporation in OptiPrep™-based electroporation buffer. The scale bar indicates 10 µm.

3.2. Effect of EV concentration on siRNA precipitation

Interestingly, when increasing concentrations of EVs were added to the electroporation mixture, fluorescence of the EV pellet after electroporation decreased (**figure S1C**). A similar effect was previously reported by Wahlgren *et al.* [25], who showed that the percentage of EVs containing fluorescently labeled siRNA after electroporation decreased from 85.2 % to 0.073 % when the EV concentration in the electroporation cuvettes was

increased from 0.25 µg/µL to 4 µg/µL. These data suggest that the presence of EVs may reduce, but not necessarily remove, the formation of siRNA aggregates after electroporation. To check the possibility that some siRNA aggregates might still be loaded into free EVs (i.e. EVs not incorporated in the large aggregates as depicted in **figure 2C**) or otherwise associated with free EVs, electroporated samples were floated on a sucrose gradient and the siRNA content of each fraction was analyzed by RT-PCR (**figure S2A-C**). Here it was clearly observed that free floating EVs (indicated with the marker CD9 by immunoblotting) did not contain siRNA. The fact that we could not retrieve CD9 expression in the high density fractions (what we would expect based on the observations in **figure 2C**) might be due to the fact that the procedure used to prepare samples for immunoblotting is not disruptive enough to break up the formed aggregates and thus prevents the EV associated proteins to migrate over the SDS-PAGE gel.

These data illustrate that, when not taken into account, electroporation-induced siRNA aggregation causes a severe overestimation of the amount of siRNA actually loaded into EVs. This aggregation needs to be prevented in order to quantitatively analyze the siRNA encapsulation in EVs after electroporation. Furthermore, the formation of siRNA aggregates might inhibit the loading of siRNA into EVs. Therefore, we investigated the mechanism by which siRNA aggregation occurs during electroporation.

3.3. Effect of EDTA on siRNA precipitation and loading efficiency

It has previously been described that electric discharges in electroporation cuvettes containing metal electrodes can cause the release of metal cations (e.g. Al^{3+}-cations, Fe^{3+}-cations) from the electrodes. These multivalent cations can react with phosphate and hydroxide anions present in the electroporation buffer and possibly nucleic acids, causing the formation of insoluble aggregates trapping nucleic acids [38]. Given that in our experiments cuvettes with aluminum electrodes were applied, it was hypothesized that these components caused the siRNA precipitation described in **figure 2**.

To test this hypothesis, the OptiPrep™-based buffer was electroporated without siRNA or EVs and the concentration of formed aggregates was measured by scattering-based single particle tracking. It was confirmed that the buffer was particle-free before electroporation. Strikingly, after electroporation an average of 4×10^9 particles per mL (**figure 3A**) with a broad size distribution could be detected (**figure S3A**). To point out the influence of aluminum cations in the formation of these aggregates, the same buffer was electroporated in the presence of increasing concentrations of EDTA. EDTA acts as a chelator and forms soluble complexes with aluminum ions, which may prevent interactions of these ions with buffer components and macromolecules. Indeed, scattering-based single particle tracking revealed that addition of EDTA to the

electroporation buffer decreased particle formation during electroporation in a concentration-dependent manner (**figure 3A**). Furthermore, when EVs and siRNA were electroporated in the presence of EDTA, RT-PCR showed a similar concentration-dependent inhibition of siRNA retention (**figure S3B**). EDTA at 1 mM concentration reduced particle formation and siRNA precipitation by 98 - 99 % in both experiments. Again similar results were found by FFS and fluorescence spectroscopy (**figures 3B** and **figure S3C**, respectively)**.** These observations are supported by results obtained using the Cytomix electroporation buffer (containing the chelator EGTA), which showed less aggregation after electroporation than the OptiPrep™-based buffer (**figure 2A**). Under the aggregate-reducing conditions depicted in **figures 3B** and **figure S3** retention was again lower in the presence of EVs than in the absence of EVs (approximately 1 % versus 3 %, respectively), supporting the previous finding that increasing concentrations of EVs inhibit aggregate formation. Together, these results strongly suggest that aluminum-induced aggregation, and not encapsulation into EVs, is responsible for the observed complexation of siRNA as depicted in **figure 2** and reported by others [25, 26].

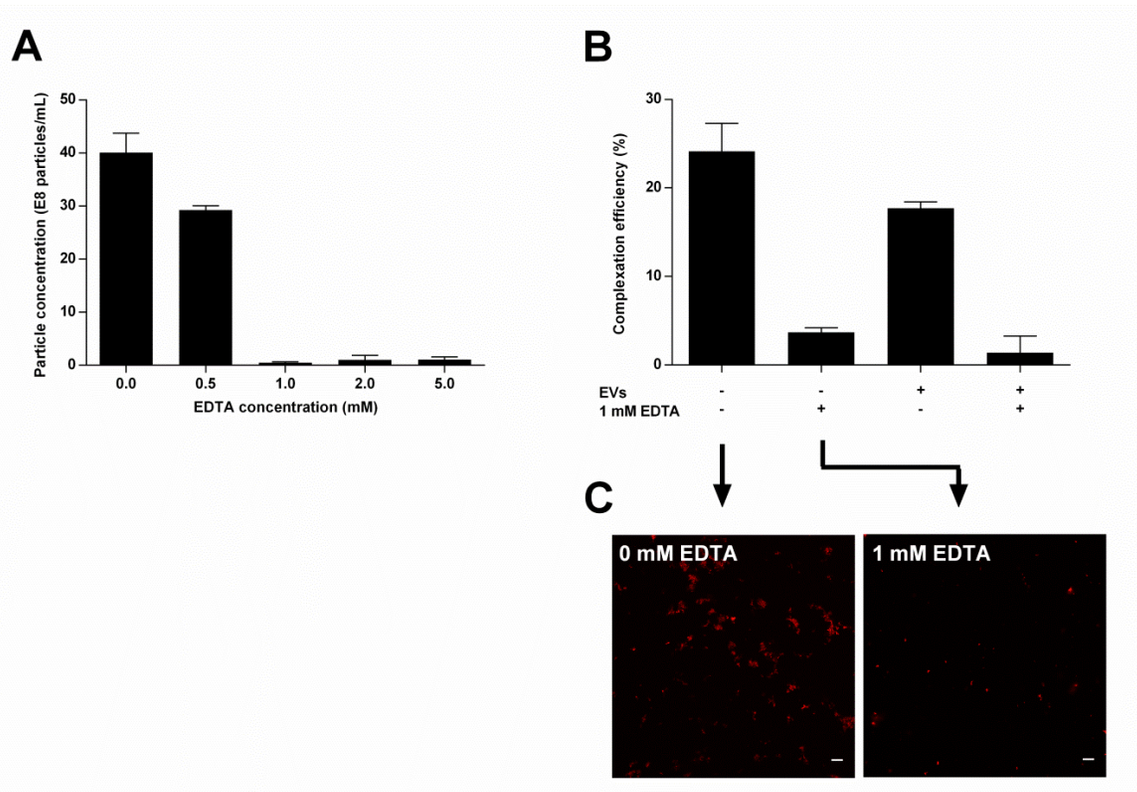

Figure 3. Addition of EDTA to the OptiPrep™-based electroporation buffer affects aggregate formation and retention of siRNA. [A] Concentration of particles formed in OptiPrep™ buffer after electroporation in the presence of increasing concentrations of EDTA as measured by scattering-based single particle tracking. [B] Complexation efficiency of Cy5-siRNA in HEK293T EVs after electroporation as measured by FFS. Experiments were performed in triplicate and data are presented as mean ± SD. [C] Representative confocal microscopy images of aggregate formation of Cy5-siRNA (red) in OptiPrep™ electroporation buffer in the absence or presence of 1 mM EDTA. The scale bar indicates 10 µm.

Of note, while 1 mM EDTA strongly inhibited aggregate formation and reduced the observed retention of siRNA after electroporation, a minor amount of aggregates was still formed (**figure 3A**), which could interfere with accurate determination of loading efficiency in the presence of EVs. These aggregates could be clearly distinguished from the background by confocal microscopy (**figure 3C**), and might account for the 1 % siRNA retention observed with FFS and fluorescence spectroscopy when EVs were electroporated in the presence of EDTA (**figures 3B** and **figure S3C**). Given that increasing EDTA concentrations above 1 mM could not completely inhibit this process (**figure 3A**), our results suggest that chelation of aluminum ions is insufficient to completely inhibit the formation of siRNA aggregates. Therefore alternative methods to reduce background aggregate formation were investigated.

3.4. Effect of electroporation buffer on siRNA precipitation and loading efficiency

As both phosphate and hydroxide anions in the OptiPrep™-based buffer potentially contribute to aggregate formation, using a buffer devoid of these anions could possibly prevent siRNA precipitation. We first evaluated a phosphate-free electroporation buffer for the formation of aggregates. However, the amount of formed aggregates after electroporation in the presence of Cy5-siRNA was comparable to the amount in the OptiPrep™-based buffer (**figure 4A**, left panel). In addition, similar amounts of particles were formed after electroporation in the absence of siRNA (**figure 4B**). This indicates that phosphate anions, in the concentration used in the Optiprep™ based buffer, likely play a minor role in the formation of aggregates. Dabbs *et al.* demonstrated that both acidic pH (implicating low hydroxide concentrations) and the presence of citric acid can prevent the formation of aluminum oxyhydroxide aggregates [39]. Therefore a citric acid based buffer (pH 4.4) was evaluated for aggregate formation after electroporation. Following electroporation of this buffer in the presence of Cy5-siRNA, no fluorescent aggregates could be detected and only minute amounts of particles could be measured *via* scattering-based single particle tracking (**figure 4A**, right panel and **figure 4B**). In agreement with this result, FFS measurements showed near undetectable siRNA complexation following electroporation of Cy5-siRNA without EVs (**figure 4C**). Hence, this buffer could potentially allow for precise measurements of encapsulation of siRNA in EVs. Unfortunately, after siRNA electroporation in the presence of EVs no encapsulation could be detected (**figure 4C**).

However, it can not be excluded that the EV integrity might have been compromised in this acidic environment, possibly reducing siRNA encapsulation. In order to avoid the formation of aggregates while maintaining physiological pH, we next investigated an alternative electroporation strategy.

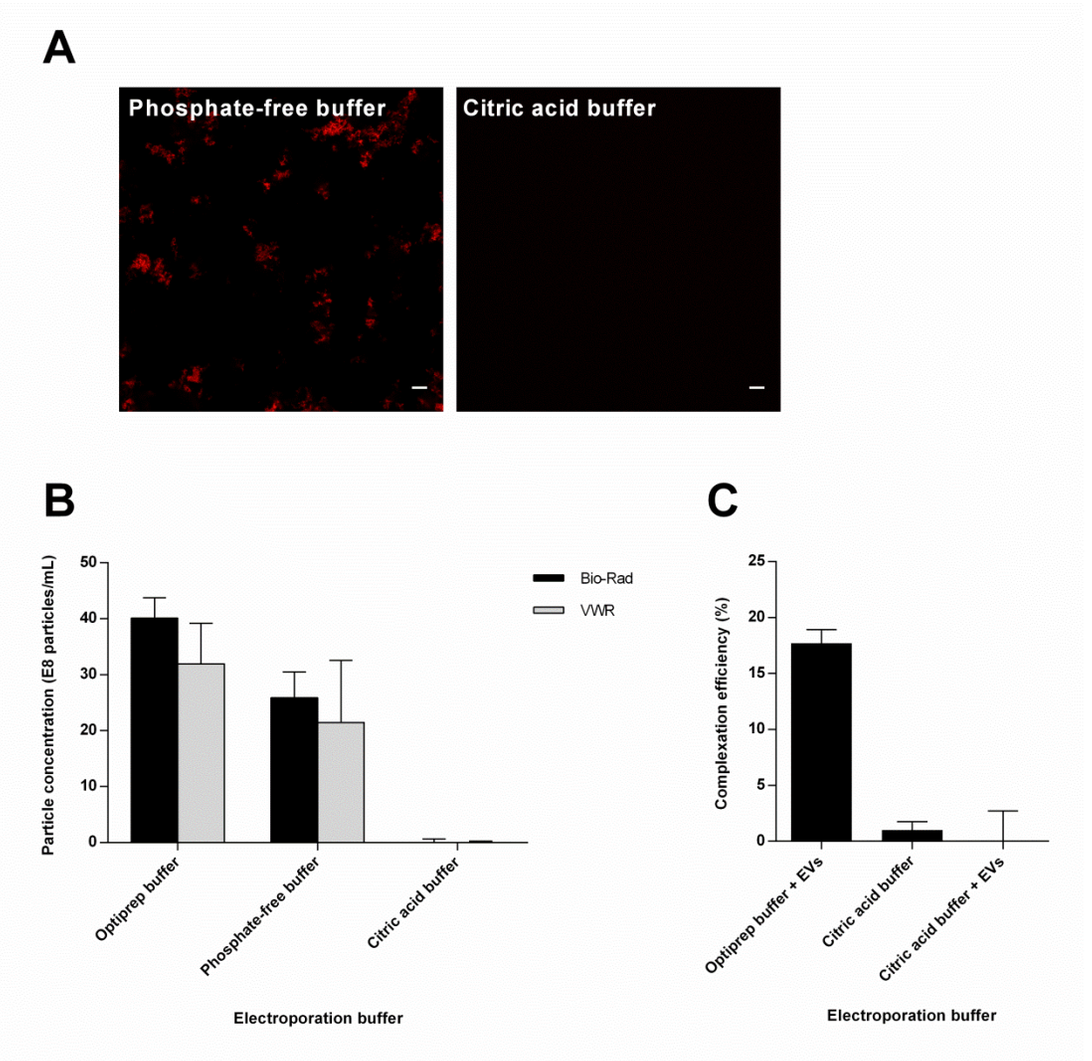

Figure 4. Effect of various electroporation buffers on the formation of aggregates after electroporation. [A] Representative confocal microscopy images of phosphate-free buffer (left) and citric acid buffer (right) after electroporation in the presence of Cy5-siRNA. Scale bars represent 10 µm. [B] Particle concentration after electroporation of OptiPrep™, phosphate-free and citric acid buffers, as measured by scattering-based single particle tracking using electroporation cuvettes of two different manufacturers. [C] Complexation efficiency of Cy5-siRNA after electroporation in OptiPrep™- or citric acid-based buffer in the presence or absence of HEK293T EVs, as measured by FFS. The data are presented as mean ± SD (n=3).

3.5. Effect of electrode material on siRNA precipitation and loading efficiency

Given that metal ions released from the electrodes play a crucial role in the formation of precipitates, it was anticipated that the use of cuvettes with conductive polymer electrodes instead of metal electrodes could prevent aggregate formation. Such polymer cuvettes are commonly used in the Lonza Nucleofector™ technology. Particle formation in the OptiPrep™ buffer after electroporation in these conductive polymer cuvettes was indeed dramatically reduced compared to conventional aluminum cuvettes (**figure**

S4A). This effect was independent of the used voltage and capacitance during electroporation. Polymer cuvettes could thus be valuable for aggregate-free electroporation of EVs.

To optimize loading of siRNA into EVs using these cuvettes, EVs were electroporated with unlabeled siRNA at varying EV:siRNA ratios and siRNA retention was determined by RT-PCR (**figure S4B**). Unfortunately, only minor amounts of siRNA (maximally 0.09 % of total siRNA) could be detected in EV pellets. In addition to siRNA:EV ratios, also electroporation settings of the Lonza 4D-Nucleofector were optimized for the loading of siRNA in EVs. Again, using a variety of electroporation programs, no marked siRNA retention could be measured (**figure S4C**). None of the programs resulted in more than 0.04 % of total siRNA retention in the EV pellet. These findings were confirmed by sucrose gradient flotation of EVs electroporated in conductive polymer cuvettes (**figure S2D**). To determine whether the small amounts of siRNA detected in the EV pellets after electroporation in conductive polymer cuvettes could be attributed to actual siRNA loading into EVs, samples were subjected to either one or two wash steps after which the siRNA present in the pellet was quantified by RT-PCR (**table S2**). After two washes, no significant differences in siRNA retention could be measured between siRNA electroporated in the presence and absence of EVs, albeit siRNA was still detectable in both conditions (average Ct values of 21). Notably, after two washes the endogenous EV enclosed miRNAs (i.e. miR-143 and miR-146a) could still be detected in the washed samples (Ct values ranging from 31 to 34), indicating that EVs were not lost during the extensive wash procedure.

Despite the here observed aggregation effect, previous papers still report functional delivery of the siRNA to recipient cells with associated target gene knockdown [25, 26]. To verify these observations, EVs electroporated in aluminum (**figure 5**) and conductive polymer (**figure S5**) cuvettes were evaluated in a reporter gene silencing assay (i.e. an eGFP and a luciferase assay, respectively) for their ability to functionally deliver siRNAs. As expected by the lack of loading of siRNA into EVs, no siRNA-mediated gene silencing effects was induced. It is interesting to note that in the case of metal electrodes, hence the presence of aluminum aggregates, the eGFP expression was lowered compared to the PBS control. This reduction in eGFP expression was however not siRNA-mediated as both the control sequence (siRNA CTRL) and the targeted sequence (siRNA GFP) showed the same effect. This trend was also observed in a luciferase gene reporter assay indicating that likely the aluminum aggregates influence the gene expression of the recipient cell. The mechanism behind this lowered protein expression is currently not known. Samples electroporated in conductive polymer cuvettes had no influence on the luciferase expression (**figure S5**).

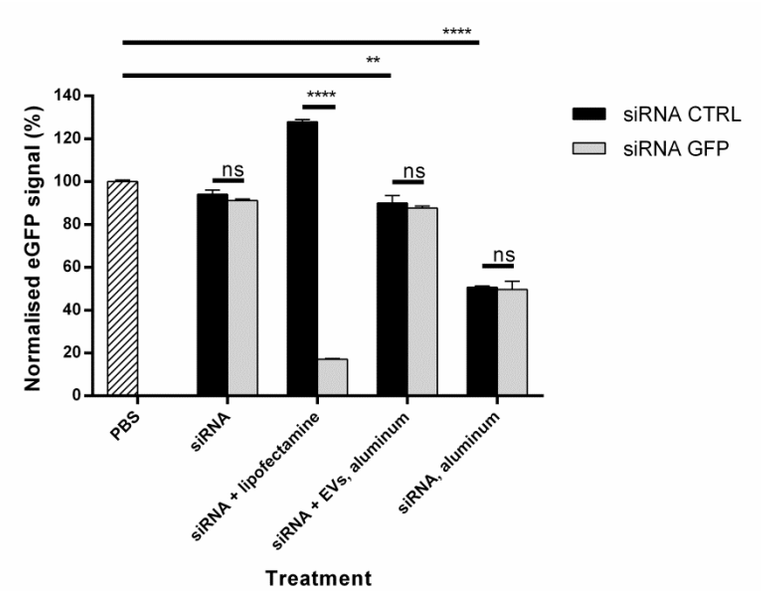

Figure 5. Evaluation of the functionality of siRNA delivery by electroporated samples in metal electrode based cuvettes. Samples containing non-specific control siRNA (siRNA CTRL) or eGFP siRNA (siRNA GFP) were electroporated (using Bio-Rad aluminum electrode cuvettes – 400 V – 125 µF) in the presence or absence of HEK293T EVs in OptiPrep^{TM}-based buffer. H1299_eGFP cells were incubated with the respective samples for 4h in OptiMEM medium. Controls included transfection of siRNA using Lipofectamine RNAiMax and free siRNA (not electroporated). After 48h, eGFP expression was analyzed by flow cytometry and normalized to eGFP expression in PBS treated cells (mean ± SD, n = 3).

4. Discussion

The obtained data provide conclusive evidence that electroporation can induce strong aggregation of siRNA, which might be mistakenly interpreted as encapsulation of siRNA into EVs if proper control experiments are omitted. Complex formation between metal ions from the electrodes and hydroxide ions from the electroporation buffer were shown to be the major cause of siRNA precipitation. While removal of one or both of these components (i.e. metal ions and/or hydroxide ions) almost completely inhibited this process, the loading efficiency of siRNA into EVs in these cases was found to be below 0.05 %. Furthermore, similar siRNA retention was found when siRNA was electroporated in the absence of EVs. These data suggest that any siRNA measured after electroporation and washing of EVs can be attributed to traces of wash solution and not to actual loading of siRNA into EVs. This extremely inefficient encapsulation of siRNA could be expected when performing electroporations under these conditions. According to scattering-based single particle tracking measurements and corresponding to a previous report [40], an electroporation volume of 200 µL with 15 µg/mL EVs contains approximately 2.5 x 10^{10} vesicles. Based on the size distribution of the EVs, and assuming they exist as perfect spherical structures in the electroporation buffer, the total volume of EVs can be calculated. When this calculation was performed using the EV

size distributions commonly measured (median size of 110 nm), it was found that the total internal volume of EVs comprised 0.04 % of the total electroporation volume (200 µL). Hence, assuming that loading of siRNA by electroporation occurs by passive diffusion of the macromolecules through pores in the EV membrane, no more than 0.04 % of the siRNA molecules would be expected to enter the lumen of the EVs. In practice this is likely to be even lower, given that pores are only temporarily formed during electroporation and that the calculation is based on empty spherical structures, while EVs are dense vesicles already enriched in macromolecules. This theory is supported by the findings in this work, that show that when electroporation artefacts are effectively prevented, no encapsulation of siRNA into EVs could be detected. Although unlikely, it should be noted that loading efficiencies might differ depending of the source of the EVs. Despite our findings that loading efficiencies were similar among EVs derived from two different cell lines, EVs derived from primary cells may show different loading behavior during electroporation.

In this work we show that extensive aggregate formation occurs during electroporation, resulting in precipitation of siRNA and EVs. This finding is consistent with a previous report, which showed that electric discharges through a solution cause DNA, RNA and some proteins to precipitate [38]. Furthermore, we showed that aggregate formation decreased with increasing concentrations of EVs. This effect may be due to the capturing of multivalent ions on the negatively charged EV membrane, or by changes in buffer conductivity upon addition of EVs. Furthermore, the formed siRNA-EV-aluminum complexes were not able to induce a RNAi-mediated gene knockdown under the tested conditions. Our findings demonstrate the importance of a variety of analysis techniques for the determination of loading efficiency. The main techniques used in this work (i.e. FFS, fluorescence spectroscopy and RT-PCR) revealed similar trends as a function of electroporation conditions, but absolute values for loading efficiency varied between fluorescence based measurements and RT-PCR. FFS and fluorescence spectroscopy generally showed over 5-fold higher siRNA retention or complexation than RT-PCR. The reason for this discrepancy is unclear. After electroporation siRNA could potentially be damaged or unavailable due to association with metal ions, resulting in less copies to be detected *via* RT-PCR. Indeed, aggregation of siRNA may cause the critical 3’ ends of siRNA to become unavailable for reverse transcription and subsequent PCR, resulting in an underestimation of the siRNA concentrations. Alternatively, fluorescently labeled siRNA might be more prone to aggregation than unlabeled siRNA. Nevertheless, these discrepancies warrant the use of multiple analysis techniques and controls to adequately measure loading of siRNA in EVs.

5. Conclusion

In contrast to previous reports we show that electroporation of siRNA into EVs results in extensive precipitation of siRNA. Due to this process, encapsulation efficiency is easily overestimated when commonly used electroporation conditions and analysis techniques are employed. The presented data further show that electroporation is far less efficient than previously believed. This work highlights an important complication of the electroporation technique and demonstrates the necessity for alternative methods to load EVs with macromolecules such as siRNA, in order to maximize the therapeutic applicability of EVs as a drug delivery vehicle.

Acknowledgements

Experimental work/design was done in close collaboration with Dr. P. Vader from the Department of Physiology, Anatomy and Genetics, University of Oxford and with Prof. R. Schiffelers and S. Kooijmans from the Department of Clinical Chemistry and Haematology, University Medical Center Utrecht. PV executed the fluorescence spectroscopy experiments and SK was responsible for data obtained *via* qPCR and electroporation experiments in polymer cuvettes. The experimental details and obtained results are listed in the supporting information section at the end of this chapter.

References

[1] K. Al-Nedawi, B. Meehan, J. Micallef, V. Lhotak, L. May, A. Guha, J. Rak, Intercellular transfer of the oncogenic receptor EGFRvIII by microvesicles derived from tumour cells, Nat Cell Biol, 10 (2008) 619-624.

[2] J. Skog, T. Wurdinger, S. van Rijn, D.H. Meijer, L. Gainche, M. Sena-Esteves, W.T. Curry, Jr., B.S. Carter, A.M. Krichevsky, X.O. Breakefield, Glioblastoma microvesicles transport RNA and proteins that promote tumour growth and provide diagnostic biomarkers, Nat Cell Biol, 10 (2008) 1470-1476.

[3] A. Montecalvo, A.T. Larregina, W.J. Shufesky, D. Beer Stolz, M.L. Sullivan, J.M. Karlsson, C.J. Baty, G.A. Gibson, G. Erdos, Z. Wang, J. Milosevic, O.A. Tkacheva, S.J. Divito, R. Jordan, J. Lyons-Weiler, S.C. Watkins, A.E. Morelli, Mechanism of transfer of functional microRNAs between mouse dendritic cells via exosomes, Blood, 119 (2012) 756-766.

[4] J.G. van den Boorn, M. Schlee, C. Coch, G. Hartmann, SiRNA delivery with exosome nanoparticles, Nat. Biotechnol., 29 (2011) 325-326.

[5] S.A. Kooijmans, P. Vader, S.M. van Dommelen, W.W. van Solinge, R.M. Schiffelers, Exosome mimetics: a novel class of drug delivery systems, International journal of nanomedicine, 7 (2012) 1525-1541.

[6] A. Wittrup, A. Ai, X. Liu, P. Hamar, R. Trifonova, K. Charisse, M. Manoharan, T. Kirchhausen, J. Lieberman, Visualizing lipid-formulated siRNA release from endosomes and target gene knockdown, Nat. Biotechnol., 33 (2015) 870-876.
[7] K. Raemdonck, R.E. Vandenbroucke, J. Demeester, N.N. Sanders, S.C. De Smedt, Maintaining the silence: reflections on long-term RNAi, Drug Discov Today,, 13 (2008) 917-931.
[8] N. Agrawal, P.V. Dasaradhi, A. Mohmmed, P. Malhotra, R.K. Bhatnagar, S.K. Mukherjee, RNA interference: biology, mechanism, and applications, Microbiol. Mol. Biol. Rev., 67 (2003) 657-685.
[9] L.P. Lim, N.C. Lau, P. Garrett-Engele, A. Grimson, J.M. Schelter, J. Castle, D.P. Bartel, P.S. Linsley, J.M. Johnson, Microarray analysis shows that some microRNAs downregulate large numbers of target mRNAs, Nature, 433 (2005) 769-773.
[10] J.K. Lam, M.Y. Chow, Y. Zhang, S.W. Leung, siRNA Versus miRNA as Therapeutics for Gene Silencing, Molecular therapy. Nucleic acids, 4 (2015) e252.
[11] L. De Backer, Exploring bio-inspired nanocomposites of nanogels and pulmonary surfactant for small interfering RNA delivery, Doctoral thesis, Faculty of Pharmaceutical Sciences, Ghent University, Ghent (2015).
[12] F. Eckstein, Phosphorothioates, essential components of therapeutic oligonucleotides, Nucleic Acid Ther., 24 (2014) 374-387.
[13] C.R. Allerson, N. Sioufi, R. Jarres, T.P. Prakash, N. Naik, A. Berdeja, L. Wanders, R.H. Griffey, E.E. Swayze, B. Bhat, Fully 2'-modified oligonucleotide duplexes with improved in vitro potency and stability compared to unmodified small interfering RNA, J. Med. Chem., 48 (2005) 901-904.
[14] N. Kosaka, H. Iguchi, Y. Yoshioka, F. Takeshita, Y. Matsuki, T. Ochiya, Secretory mechanisms and intercellular transfer of microRNAs in living cells, J. Biol. Chem., 285 (2010) 17442-17452.
[15] N. Kosaka, H. Iguchi, Y. Yoshioka, K. Hagiwara, F. Takeshita, T. Ochiya, Competitive interactions of cancer cells and normal cells via secretory microRNAs, J. Biol. Chem., 287 (2012) 1397-1405.
[16] Q. Pan, V. Ramakrishnaiah, S. Henry, S. Fouraschen, P.E. de Ruiter, J. Kwekkeboom, H.W. Tilanus, H.L. Janssen, L.J. van der Laan, Hepatic cell-to-cell transmission of small silencing RNA can extend the therapeutic reach of RNA interference (RNAi), Gut, 61 (2012) 1330-1339.
[17] S.D. Olson, A. Kambal, K. Pollock, G.M. Mitchell, H. Stewart, S. Kalomoiris, W. Cary, C. Nacey, K. Pepper, J.A. Nolta, Examination of mesenchymal stem cell-mediated RNAi transfer to Huntington's disease affected neuronal cells for reduction of huntingtin, Mol. Cell. Neurosci., 49 (2012) 271-281.
[18] S.S. Luo, O. Ishibashi, G. Ishikawa, T. Ishikawa, A. Katayama, T. Mishima, T. Takizawa, T. Shigihara, T. Goto, A. Izumi, A. Ohkuchi, S. Matsubara, T. Takeshita, T. Takizawa, Human villous trophoblasts express and secrete placenta-specific microRNAs into maternal circulation via exosomes, Biol. Reprod., 81 (2009) 717-729.
[19] Y. Akao, A. Iio, T. Itoh, S. Noguchi, Y. Itoh, Y. Ohtsuki, T. Naoe, Microvesicle-mediated RNA molecule delivery system using monocytes/macrophages, Mol. Ther., 19 (2011) 395-399.
[20] M. Yang, J. Chen, F. Su, B. Yu, F. Su, L. Lin, Y. Liu, J.D. Huang, E. Song, Microvesicles secreted by macrophages shuttle invasion-potentiating microRNAs into breast cancer cells, Molecular cancer, 10 (2011) 117.

[21] P. Mocharla, S. Briand, G. Giannotti, C. Dorries, P. Jakob, F. Paneni, T. Luscher, U. Landmesser, AngiomiR-126 expression and secretion from circulating CD34+ and CD14+ PBMCs: role for proangiogenic effects and alterations in type 2 diabetics, Blood, 121 (2013) 226-236.
[22] S. Ohno, M. Takanashi, K. Sudo, S. Ueda, A. Ishikawa, N. Matsuyama, K. Fujita, T. Mizutani, T. Ohgi, T. Ochiya, N. Gotoh, M. Kuroda, Systemically Injected Exosomes Targeted to EGFR Deliver Antitumor MicroRNA to Breast Cancer Cells, Mol Ther, 21 (2013) 185-191.
[23] Y. Zhang, D. Liu, X. Chen, J. Li, L. Li, Z. Bian, F. Sun, J. Lu, Y. Yin, X. Cai, Q. Sun, K. Wang, Y. Ba, Q. Wang, D. Wang, J. Yang, P. Liu, T. Xu, Q. Yan, J. Zhang, K. Zen, C.Y. Zhang, Secreted monocytic miR-150 enhances targeted endothelial cell migration, Mol. Cell, 39 (2010) 133-144.
[24] S. El-Andaloussi, Y. Lee, S. Lakhal-Littleton, J. Li, Y. Seow, C. Gardiner, L. Alvarez-Erviti, I.L. Sargent, M.J. Wood, Exosome-mediated delivery of siRNA in vitro and in vivo, Nat. Protoc., 7 (2012) 2112-2126.
[25] J. Wahlgren, L.K.T. De, M. Brisslert, F. Vaziri Sani, E. Telemo, P. Sunnerhagen, H. Valadi, Plasma exosomes can deliver exogenous short interfering RNA to monocytes and lymphocytes, Nucleic Acids Res., 40 (2012) e130.
[26] L. Alvarez-Erviti, Y.Q. Seow, H.F. Yin, C. Betts, S. Lakhal, M.J.A. Wood, Delivery of siRNA to the mouse brain by systemic injection of targeted exosomes, Nat. Biotechnol., 29 (2011) 341-U179.
[27] T.A. Shtam, R.A. Kovalev, E.Y. Varfolomeeva, E.M. Makarov, Y.V. Kil, M.V. Filatov, Exosomes are natural carriers of exogenous siRNA to human cells in vitro, J Cell Commun Signal., 11 (2013) 88.
[28] X. Yuan, S. Naguib, Z. Wu, Recent advances of siRNA delivery by nanoparticles, Expert Opin Drug Deliv, 8 (2011) 521-536.
[29] G.V. Shelke, C. Lasser, Y.S. Gho, J. Lotvall, Importance of exosome depletion protocols to eliminate functional and RNA-containing extracellular vesicles from fetal bovine serum, J Extracell Vesicles, 3 (2014) 24783.
[30] J.Z. Nordin, Y. Lee, P. Vader, I. Mager, H.J. Johansson, W. Heusermann, O.P. Wiklander, M. Hallbrink, Y. Seow, J.J. Bultema, J. Gilthorpe, T. Davies, P.J. Fairchild, S. Gabrielsson, N.C. Meisner-Kober, J. Lehtio, C.I. Smith, M.J. Wood, S. El Andaloussi, Ultrafiltration with size-exclusion liquid chromatography for high yield isolation of extracellular vesicles preserving intact biophysical and functional properties, Nanomedicine, 11 (2015) 879-883.
[31] J. Van Deun, P. Mestdagh, R. Sormunen, V. Cocquyt, K. Vermaelen, J. Vandesompele, M. Bracke, O. De Wever, A. Hendrix, The impact of disparate isolation methods for extracellular vesicles on downstream RNA profiling, Journal of extracellular vesicles, 3 (2014) 24858.
[32] M.L. Heinemann, M. Ilmer, L.P. Silva, D.H. Hawke, A. Recio, M.A. Vorontsova, E. Alt, J. Vykoukal, Benchtop isolation and characterization of functional exosomes by sequential filtration, J. Chromatogr. A, 1371C (2014) 125-135.
[33] Y. Connor, S. Tekleab, S. Nandakumar, C. Walls, Y. Tekleab, A. Husain, O. Gadish, V. Sabbisetti, S. Kaushik, S. Sehrawat, A. Kulkarni, H. Dvorak, B. Zetter, R.E. E, S. Sengupta, Physical nanoscale conduit-mediated communication between tumour cells and the endothelium modulates endothelial phenotype, Nat. Commun., 6 (2015) 8671.
[34] J. Li, Y. Lee, H.J. Johansson, I. Mager, P. Vader, J.Z. Nordin, O.P. Wiklander, J. Lehtio, M.J. Wood, S.E. Andaloussi, Serum-free culture alters the quantity and protein composition of neuroblastoma-derived extracellular vesicles, J Extracell Vesicles, 4 (2015) 26883.

[35] K. Buyens, B. Lucas, K. Raemdonck, K. Braeckmans, J. Vercammen, J. Hendrix, Y. Engelborghs, S.C. De Smedt, N.N. Sanders, A fast and sensitive method for measuring the integrity of siRNA-carrier complexes in full human serum, J. Control. Release, 126 (2008) 67-76.
[36] K. Buyens, J. Demeester, S.S. De Smedt, N.N. Sanders, Elucidating the encapsulation of short interfering RNA in PEGylated cationic liposomes, Langmuir, 25 (2009) 4886-4891.
[37] K. Raemdonck, B. Naeye, K. Buyens, R.E. Vandenbroucke, A. Høgset, J. Demeester, S.C. De Smedt, Biodegradable Dextran Nanogels for RNA Interference: Focusing on Endosomal Escape and Intracellular siRNA Delivery, Adv. Funct. Mater., 19 (2009) 1406-1415.
[38] R. Stapulionis, Electric pulse-induced precipitation of biological macromolecules in electroporation, Bioelectrochem. Bioenerg., 48 (1999) 249-254.
[39] D.M. Dabbs, U. Ramachandran, S. Lu, J. Liu, L.Q. Wang, I.A. Aksay, Inhibition of aluminum oxyhydroxide precipitation with citric acid, Langmuir, 21 (2005) 11690-11695.
[40] J. Webber, A. Clayton, How pure are your vesicles?, J Extracell Vesicles, 2 (2013) 19861.
[41] C. Chen, D.A. Ridzon, A.J. Broomer, Z. Zhou, D.H. Lee, J.T. Nguyen, M. Barbisin, N.L. Xu, V.R. Mahuvakar, M.R. Andersen, K.Q. Lao, K.J. Livak, K.J. Guegler, Real-time quantification of microRNAs by stem-loop RT-PCR, Nucleic Acids Res, 33 (2005) e179.

Supporting information

Supporting experimental section

Electroporation in polymer cuvettes

Electroporations were performed using a Bio-rad Gene Pulser I with capacitance extender set at 400 V and 125 µF. For every electroporation the sample volume was fixed at 100 µL, containing 1.5 µg EVs and 1.5 µg siRNA unless otherwise stated. A custom designed adapter was used to properly connect the electrodes to the electroporator. Electroporations of 16-well 20 µL Nucleocuvette™ strips were performed in a Lonza 4D-Nucleofector™ X unit. EVs where suspended in 4D-Nucleofector buffer P3 with supplement 1 and electroporated in a total volume of 20 µL containing 0.6 µg EVs and 0.6 µg siRNA. After electroporation, all electroporation cuvettes were incubated on ice for at least 30 minutes before further processing.

Fluorescence spectroscopy

To evaluate the encapsulation of siRNA in EVs using fluorescence spectroscopy, 3 µg EVs were mixed with 3 µg Cy3-labelled siRNA in OptiPrep™-based electroporation buffer and electroporated in 0.4 cm cuvettes with aluminium electrodes. Samples were diluted 10-fold with PBS and centrifuged for 70 minutes at 100 000 g to remove unbound siRNA. Pellets were resuspended in PBS and siRNA fluorescence (excitation 560 nm; emission 610 nm) was determined using a fluorescence plate reader. A calibration curve of free Cy3-siRNA was used to calculate the percentage of encapsulation.

Quantitative reverse transcription polymerase chain reactions

Encapsulation of non-fluorescent siRNA (siRNA LUC) in EVs was analysed by quantitative reverse transcription PCR (RT-PCR). After electroporation, samples were diluted 10x with PBS and centrifuged at 100 000 g for 70 minutes to remove unbound siRNA. RNA was isolated from pellets with TRIzol Reagent according to the manufacturer's recommendations, with minor modifications. In brief, pellets were dissolved in TRIzol and solution was spiked with 10 fmol of internal control siRNA (siRNA GFP), followed by chloroform extraction. Isopropanol and 1 µL GlycoBlue were added to the aqueous phase and sample was stored overnight at -20°C for maximal RNA recovery. RNA was pelleted by centrifugation at 12 000 g and 4°C for 30 minutes, washed with 80 % ethanol and air dried. Dry RNA pellets were reconstituted in 20 µL nuclease-free water and stored at -20°C until analysis. Standard solutions of siRNA LUC and siRNA GFP were prepared by serially diluting 10 µM stocks of both siRNAs in 10-fold dilution steps (range

10 µM – 100 pM). Standard solutions were also purified with TRIzol Reagent according to described protocol to ensure equal PCR efficiency among samples and standards.

Reverse transcription of standards and samples was performed in a GeneAmp PCR System 9700 (Applied Biosystems, Foster City, CA) thermocycler using a Taqman MicroRNA Reverse Transcription Kit, according to manufacturer's instructions. Each 7.5 µL reverse transcription reaction contained 1 µL of RNA template, 1 mM dNTPs, 1.9 U RNAse Inhibitor, 50 nM reverse stemloop primer (custom designed as described by Chen *et al*. [41], see **table S1**) and 25 U MultiScribe Reverse Transcriptase in 1x Reverse Transcription buffer.

Quantitative PCR was performed in 10 µL reactions containing 1 µL of reverse transcription product, 0.625 µM of sequence-specific forward primer, 0.625 µM of stemloop-specific reverse primer (**table S1**) and 0.013 µL of Rox passive reference dye in 1x FastStart SYBR Green master. Reactions were prepared in MicroAmp Optical 96-well plates and were run on a Viia™ 7 Real Time PCR System (Applied Biosystems, Foster City, CA) using the following settings: 10 minutes at 95°C; 40 cycles of 15 seconds at 95°C, 30 seconds at 60°C and 20 seconds at 72°C; melting curve analysis; store at 4°C. Amplification curves were analysed with Viia 7 software version 1.2.1 and Ct values were determined for siRNA LUC and siRNA GFP. Each plate contained a set of siRNA LUC and siRNA GFP standard solutions which were used to construct calibration curves. Total copy number (Cn) of siRNA LUC and siRNA GFP in each sample was calculated and $Cn_{siRNALUC}$ was normalised for $Cn_{siRNAGFP}$ using **eq. S1**. From normalised $Cn_{siGFPLUC}$ the loading efficiency of siGFP LUC in each sample was calculated. All electroporation samples for RT-PCR were prepared in triplicate and each RNA isolate was analysed in duplicate. Using this method, traces of siRNA could still be accurately quantified.

$$Normalised\ Cn_{siRNALUC} = Cn_{siRNALUC} \times \frac{\overline{Cn}_{siRNAGFP}}{Cn_{siRNAGFP}} \qquad (\textbf{eq. S1})$$

where $\overline{Cn}_{siRNAGFP}$ is the mean $Cn_{siRNAGFP}$ of all samples processed in the same experiment.

table S1. Primers for RT-PCR.

Name	Sequence (5'-3')	manufacturer
Reverse_stemloop_ siRNA LUC	GTCGTATCCAGTGCAGGGTCCGAGGTATTCGCACTGGATACGACCCGATT	Sigma-Aldrich
Forward_siRNA LUC	CCGCTAATACATAACCGGACAT	Sigma-Aldrich
Reverse_stemloop_ siRNA GFP	GTCGTATCCAGTGCAGGGTCCGAGGTATTCGCACTGGATACGACAAGCAC	Sigma-Aldrich
Forward_siRNA GFP	CCGCTAAGGACTTGAAGAAGTC	Sigma-Aldrich
Reverse_miR-143	GTCGTATCCAGTGCAGGGTCCGAGGTATTCGCACTGGATACGACGAGCTA	Sigma-Aldrich
Forward_miR-143	CGCTAATGAGATGAAGCACTG	Sigma-Aldrich
Reverse_miR-146a	GTCGTATCCAGTGCAGGGTCCGAGGTATTCGCACTGGATACGACAACCCA	Sigma-Aldrich
Forward_miR-146a	CGCTAATGAGAACTGAATTCC	Sigma-Aldrich
Reverse_stemloop	GTGCAGGGTCCGAGGT	Sigma-Aldrich

Fractionation using sucrose gradients

EVs were electroporated in OptiPrep-based buffer as described before, using 15 µg/mL EVs and 15 µg/mL siGFP LUC in 200 µL total volume for cuvettes with aluminium electrodes, or 100 µL total volume for cuvettes with conductive polymer electrodes. After electroporation, duplicate samples were combined to 400 µL electroporation samples (corresponding to 6 µg EVs/siRNA LUC) and mixed with 1.5 mL of 2.5 M sucrose in PBS in SW40 tubes (Beckman Instruments). Samples were overlaid with a linear gradient of 0.4 - 2 M sucrose in PBS in SW40 tubes (Beckman Instruments) and centrifuged for 15 hours at 202 000 g. Gradient fractions of 1 mL were collected from the top of the gradients and sucrose densities measured by refractometry. Subsequent fractions were pooled in pairs of two and 60 µL aliquots were collected for RNA isolation. Each 60 µL aliquot was mixed with 300 µL Trizol, RNA was isolated, and RT-PCR was performed according to the method described before. The siRNA content of each fraction was expressed as a relative concentration compared to the fraction with the lowest sucrose density (top fraction), using **eq. S2**. Remainders of pooled sucrose fractions (1940 µL) were diluted to 4 mL with PBS and centrifuged at 100 000 g for 70 minutes. Pellets were dissolved in 25 µL sample buffer for immunoblot analysis.

$$relative\ siRNA\ concentration_{fraction\ X} = \frac{Cn_{fraction\ X}}{Cn_{fraction\ top}} \qquad \textbf{(eq. S2)}$$

$Cn_{fraction\ X}$ is the measured copy number of siRNA in the 60 µL sample of fraction X and $Cn_{fraction\ top}$ is the measured copy number of siRNA in the 60 µL sample of the top fraction of the gradient.

Immunoblotting

Stored samples were heated to 95°C for 10 minutes, snap cooled on ice and subjected to 12 % SDS-PAGE. Proteins were electrotransferred to Immobilon-FL polyvinylidene difluoride (PVDF) membranes (Millipore). Blots were blocked with 50 % v/v Odyssey Blocking Buffer (LI-COR Biosciences) in Tris buffered saline (TBS). CD9 immunolabelling was performed with 50 % v/v Odyssey Blocking Buffer in TBS containing 0.1 % Tween20 and rabbit anti-CD9 antibody (Abcam, ab92726, 1:4000 dilution). Primary antibodies were probed with Alexa Fluor 680-conjugated anti-rabbit antibodies (Invitrogen, 1:7500 dilution) and bands were visualised using an Odyssey Infrared Imager (LI-COR Biosciences, Leusden, the Netherlands) at 700 nm.

Dual luciferase reporter assay

Neuro2A cells were transfected during 24 hours with a combination of pCMV-Luc and pGL4.74[hRluc/TK] (driving expression of *Firefly* luciferase and *Renilla* luciferase, respectively) using Lipofectamine 2000 according to manufacturer's instructions. Subsequently cells were washed with PBS, trypsinised and seeded in a gelatin-coated 96-well plate at a density of 3 x 10^4 cells per well. Cells were allowed to attach for 24 hours, and medium was replaced with EV-depleted medium. 3 µg of siRNA against *Firefly* luciferase (siRNA LUC) or non-specific control (siRNA CTRL) siRNA was electroporated in the presence or absence of 3 µg Neuro2A EVs in OptiPrep-based electroporation buffer at 400 V and 125 µF, diluted with 4 mL PBS and centrifuged at 100 000 g for 70 minutes. Pellets were resuspended in 50 µL PBS and added to the cells. As controls, 10 pmol of both siRNAs were complexed with Lipofectamine 2000 according to manufacturer's instructions and added to the cells in antibiotic-free medium. Cells were incubated for 48 hours and lysed with Passive Lysis Buffer (Promega). Lysates were mixed with substrates from the Dual Luciferase Reporter Assay System kit (Promega) according to manufacturer's instructions and activities of both luciferases were sequentially measured at room temperature for 5 seconds using a SpectraMax L luminescence microplate reader (Molecular Devices). *Firefly* luciferase activity was normalised to *Renilla* luciferase activity and expressed as a percentage of normalised *Firefly* luciferase activity in untreated cells.

Supporting results

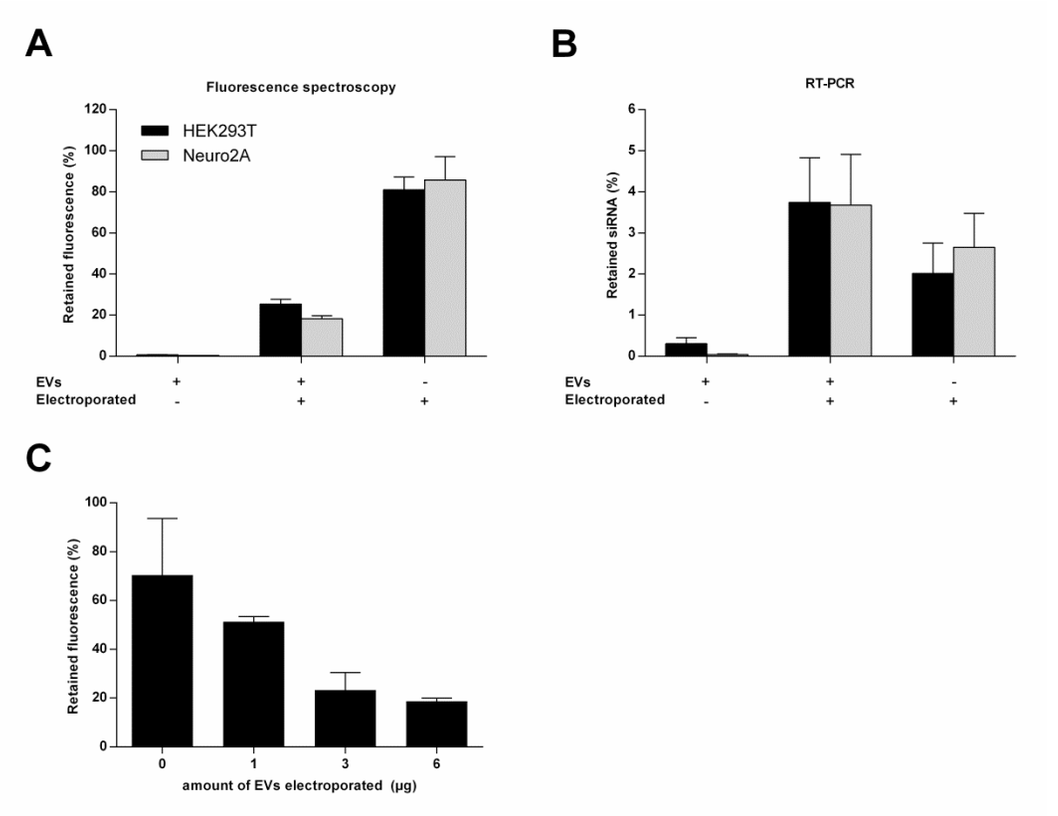

Figure S1. **Retained siRNA after electroporation in OptiPrep™-based buffer in the presence (+) or absence (−) of EVs from HEK293T or Neuro2A cells.** [A] Retained percentage of Cy3-siRNA in 100 000 g pellets before (−) or after (+) electroporation as measured by fluorescence spectroscopy. [B] Retained percentage of unlabeled siRNA in 100 000 g pellets as measured by RT-PCR. [C] Retained percentage of Cy3-siRNA in 100 000 g pellets in the presence of increasing amounts of EVs as measured by fluorescence spectroscopy. Experiments were all performed in triplicate and data are presented as mean ± SEM.

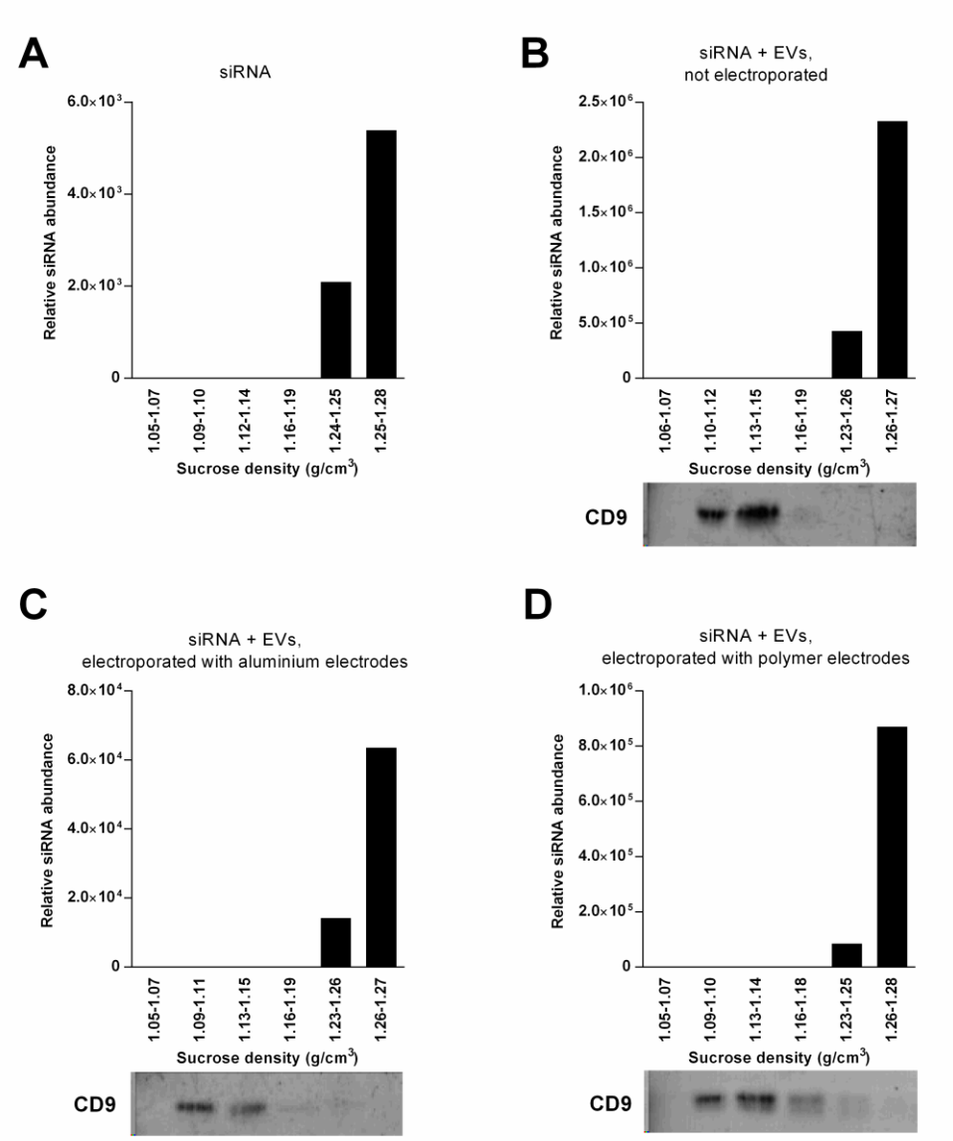

Figure S2. Fractionation of electroporation samples on sucrose gradients. Unlabeled siRNA was electroporated in OptiPrep™ buffer in the absence [A] or presence [B–D] of Neuro2A EVs in cuvettes with aluminum electrodes [A, C] or conductive polymer electrodes [D] at 400 V and 125 µF. Electroporation samples were floated on a sucrose gradient and RT-PCR was used to determine relative concentrations of siRNA in each sucrose fraction compared to siRNA concentrations in fractions with the lowest sucrose density (bar charts). Immunoblotting shows the presence of the EV marker CD9 in the 100 000 g pellet of each fraction. Bars in the bar charts correspond to the lanes on the immunoblots below. Most representative data of three independent experiments is shown.

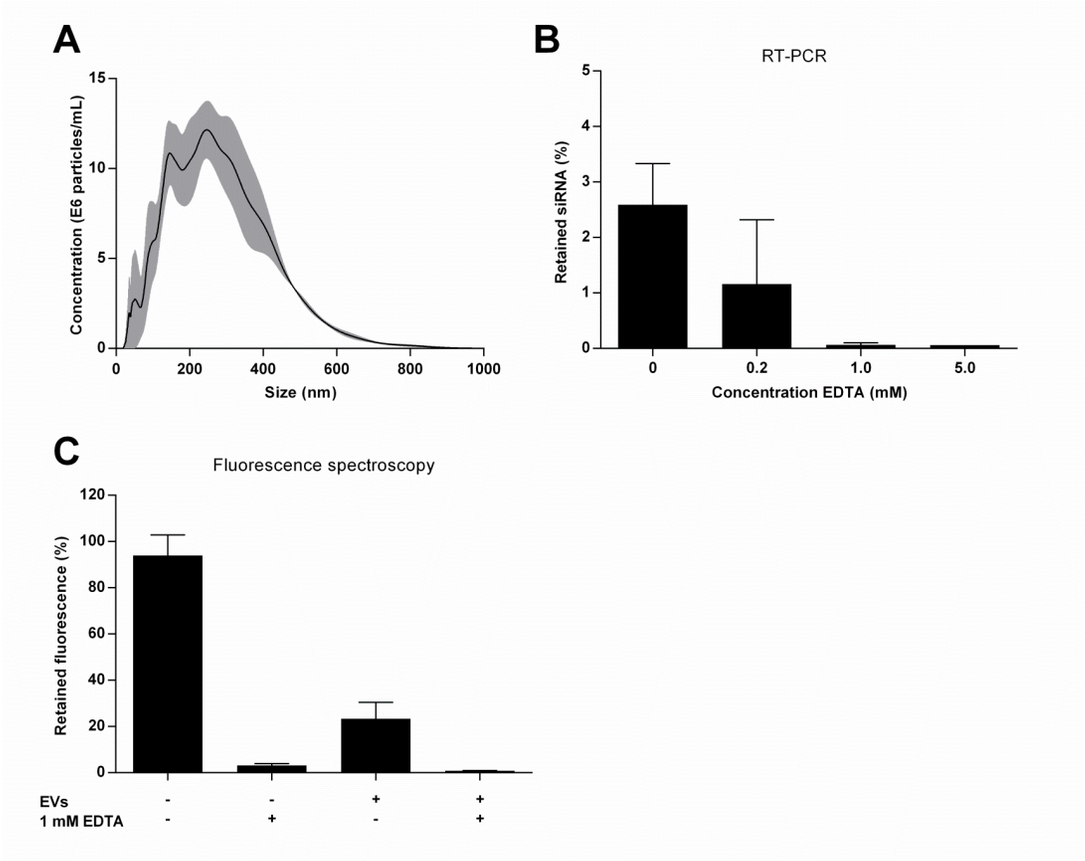

Figure S3. Electroporation in the absence or presence of a chelating agent. [A] Size distribution of aggregates in OptiPrep™ buffer after electroporation, as measured by scattering-based single particle tracking. The experiment was performed in triplicate and data are presented as mean ± SEM (grey area). [B] Percentage of retained unlabeled siRNA in 100 000 g pellet after electroporation of Neuro2A EVs in the presence of increasing concentrations of EDTA as measured by RT-PCR. [C] Percentage of retained Cy3-siRNA in the 100 000 g pellet after electroporation in the presence (+) or absence (−) of HEK293T EVs and 1 mM EDTA as measured by fluorescence spectroscopy. Experiments were performed in triplicate and the data are presented as mean ± SEM.

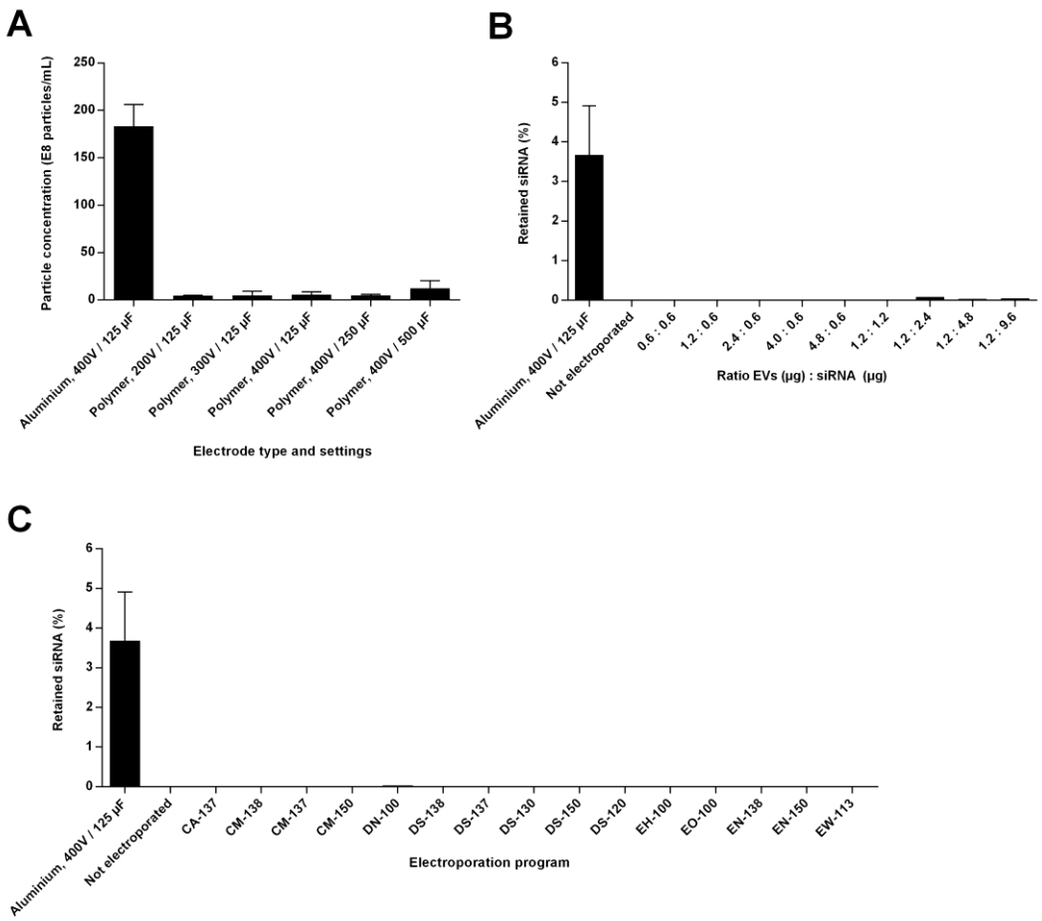

Figure S4. The influence of cuvettes with conductive polymer electrodes on the aggregate formation and siRNA retention in Neuro2A EVs. [A] Concentration of particles in OptiPrep™ electroporation buffer after electroporation in cuvettes with aluminum electrodes (at standard settings) or conductive polymer electrodes (at a range of voltages and capacitances), as measured by scattering-based single particle tracking. [B] Percentage of retained unlabeled siRNA in 100 000 g pellet at various EVs:siRNA ratios after electroporation in a 4D-Nucleofector using the EH-100 program compared to electroporation in the Bio-Rad Gene Pulser, as measured by RT-PCR. [C] Percentage of retained unlabeled siRNA in 100 000 g pellet after electroporation of 0.6 µg EVs with 0.6 µg siRNA in the 4D-Nucleofector using various programs. Data are presented as mean ± SEM (n = 3).

Table S2. Retained percentage of unlabeled siRNA in 100 000 g pellets after electroporation of siRNA in the presence or absence of Neuro2A EVs in cuvettes with conductive polymer electrodes, as measured by RT-PCR. After electroporation in OptiPrep™ electroporation buffer at 400 V and 125 µF, samples were centrifuged at 100 000 g (washed once), or subsequently resuspended in PBS and centrifuged again (washed twice).

Sample	Retained siRNA (%)[a]	
	Washed once	Washed twice
siRNA, electroporated	0.2411 ± 0.0394	0.0008 ± 0.0005[b]
EVs + siRNA, not electroporated	0.0736 ± 0.0274	0.0001 ± 0.0001[b]
EVs + siRNA, electroporated	0.0856 ± 0.0255	0.0014 ± 0.0009[b]

[a]Data are presented as mean percentage of total siRNA ± SD, n = 3. [b]Retained siRNA did not significantly differ among conditions when analyzed by an one-way ANOVA (p = 0.099).

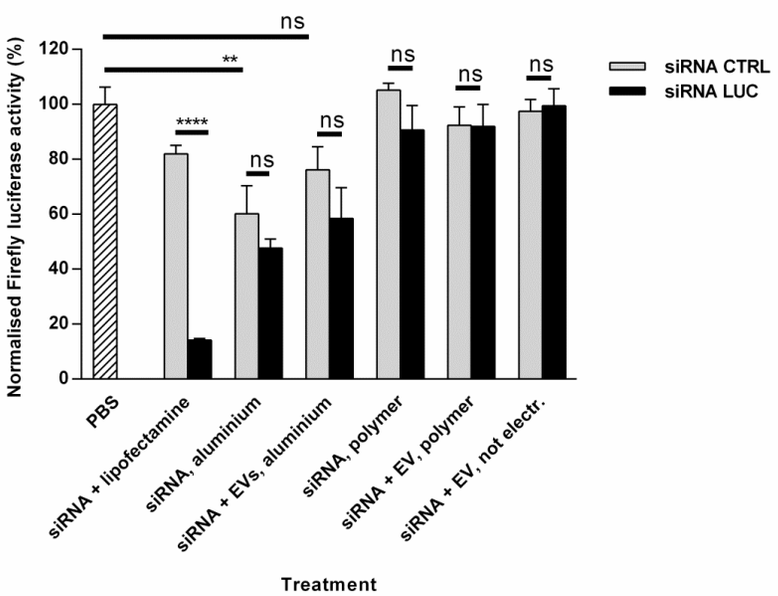

Figure S5. Evaluation of the functionality of siRNA delivery by electroporated samples in metal and polymer cuvettes. Neuro2A cells expressing Firefly luciferase and Renilla luciferase were incubated with siRNA which was electroporated in the presence or absence of Neuro2A EVs in cuvettes with aluminum or conductive polymer electrodes at 400 V and 125 µF. Controls included transfection of siRNA using Lipofectamine 2000 and siRNA mixed with EVs (not electroporated). After 48h, activities of both luciferases were analyzed and Firefly luciferase activity was normalized to Renilla luciferase activity. Luciferase activities are expressed as the percentage of activity relative to the PBS control (mean ± SEM, n=3–6).

3

Inadequate purification of extracellular vesicles can lead to misinterpretation of downstream experimental data

Stephan Stremersch[1], Kevin Braeckmans[1,2], Stefaan de Smedt[1], Koen Raemdonck[1]

[1]Laboratory of General Biochemistry and Physical Pharmacy, Ghent University, Ghent, Belgium

[2]Centre for Nano- and Biophotonics, Ghent University, Ghent, Belgium

Chapter 3: ToC

Abstract

Despite the growing interest in the (patho)physiological function and potential pharmaceutical application of extracellular vesicles (EVs), there is no general consensus regarding the most optimal protocol to separate EVs from non-vesicular components. In this chapter we provide a comparative analysis of different EV isolation strategies, discussing the purity of the final isolate and highlighting the importance of purity on downstream experimental readouts. First we show that ultracentrifugation (UC), which is one of the most exploited strategies and has long been considered as the gold standard, co-purifies protein(complexes) with nuclease activity that should be taken into account when focusing on (EV-associated) nucleic acids. In a second part of this chapter three commonly used purification strategies (i.e. precipitation, UC and density gradient) were evaluated for their ability to remove non-incorporated fluorescent dye. For both types of impurities, endogenous and exogenous, density gradient purification outperforms the other evaluated strategies. Overall these results demonstrate that the implementation of stringent purification techniques and adequate control experiments is of pivotal importance to draw reliable conclusions from downstream experiments performed with EV isolates.

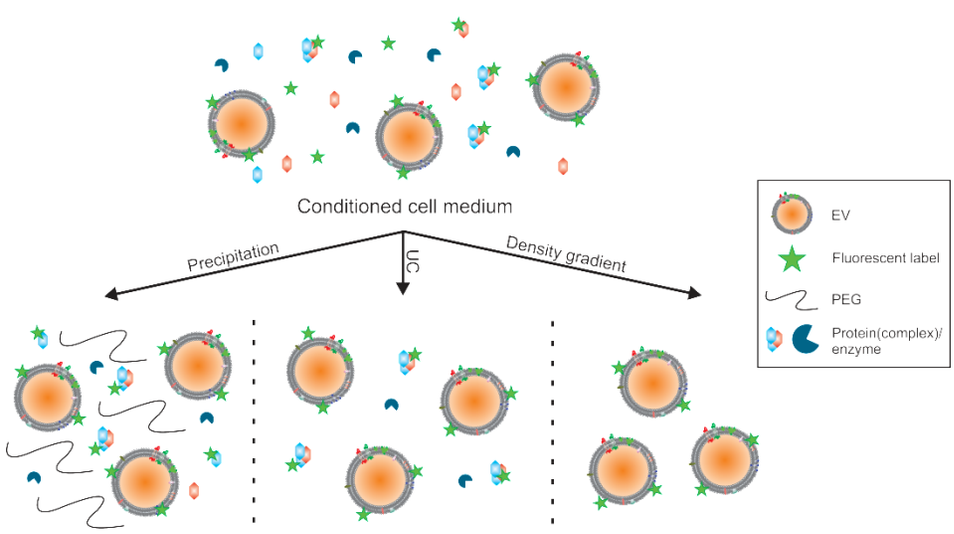

Schematic representation of the purity of EV samples after isolation from conditioned cell medium using precipitation, ultracentrifugation (UC) or a density gradient protocol.

1. Introduction

Since their discovery in the late 1960s, EVs have been linked to many physiological processes and are scrutinized for potential pharmaceutical applications in different areas (i.e. biomarker discovery [1], nucleic acid delivery [2], immunotherapy [3] and as cell surrogate for regenerative therapy [4]) as comprehensively overviewed in **chapter 1**. Especially the last couple of years, since the identification of EVs as nature's own RNA transporters [5], interest in these vesicles as a bio-inspired nanocarrier is exponentially growing with many new research groups entering the field, studying their extra- and intracellular behavior and developing new approaches to harness these vesicles for therapeutic applications, e.g. as siRNA delivery vehicle.

One of the major bottlenecks still hampering the development of EVs as nanosized carriers is the inability to efficiently load them with synthetic therapeutics. In **chapter 2** we critically evaluated a previously published method based on electroporation (EP) [2, 6]. However, duplication of these experiments under identical experimental conditions revealed that the aforementioned siRNA encapsulation was largely due to unspecific aggregate formation, independent of the presence of EVs. After blocking aggregate formation, by virtue of an acidic citrate EP buffer or the use of polymer based EP cuvettes, no significant encapsulation of siRNA could be measured [7]. Alternative to EP, it was reported by Bryniarski and colleagues that antibody-coated EVs released by B1a cells could internalize free miRNA-150 after simple co-incubation at 37°C and subsequently functionally deliver this to effector T-cells [8, 9]. Yet this approach of active uptake of free RNA by EVs has not been thoroughly characterized, nor reported by others. In this chapter we will evaluate the extrapolation of this principle to EVs derived from other origins for siRNA loading.

Besides methods to load EVs with therapeutics, tools to study their interaction with cells are highly desired. In this respect, fluorescence microscopy is an important tool to understand the cellular internalization and subsequent intracellular trafficking of EVs [10]. In analogy with the cell-like architecture of EVs many labeling strategies are equivalent to cell labeling techniques. The type of dyes most often used throughout the literature are equipped with a lipophilic tail allowing insertion in the lipid membrane of EVs (e.g. PKH26 [11], PKH67 [12-15], R18 [16, 17], DiI [18]). Alternatively, EVs have been labeled with carboxyfluorescein diacetate succinimidyl ester (CFDA-SE), which is a membrane permeable molecule responsive to esterase activity present in the lumen of (a subtype of) EVs. After cleavage of the acetate group the molecule can bind covalently to amino acids present inside the EV lumen, becomes fluorescent and membrane impermeable [19]. Finally, the nucleic acid cargo of EVs can be labeled using the membrane permeable acridine orange [20] and SYTO RNASelect dyes [21]. The above mentioned labeling strategies are indeed able to fluorescently tag certain EV

components. However, protocols to wash away unbound or non-EV associated labels are insufficiently characterized, which might lead to incorrect interpretation of downstream experimental results and observations.

In the past, the use of stringent purification protocols was mainly emphasized in a diagnostic context where co-purification of non-vesicular RNAs or proteins influences the reproducibility of biomarker discovery [22]. In this chapter, we demonstrate how non-EV contaminants present in EV isolates can lead to misinterpretation of downstream data regarding EV post-formation loading with nucleic acid based therapeutics and fluorescent dyes. Consequently, we postulate that stringent purification strategies, such as density gradient isolation, are essential to unambiguously investigate EV-mediated processes.

2. Experimental section

2.1. Materials

Nucleic acids used in this chapter are listed in **table 1**. Exoquick-TC™ was purchased from SBI Biosciences. The broad range RNase inhibitor (SUPERase In™ RNase Inhibitor) was purchased from ThermoFisher Scientific. 4-(2-hydroxyethyl)-1-piperazineethanesulfonic acid (HEPES), Iodixanol (Optiprep™) and boric acid were purchased from Sigma-Aldrich. $Na_2EDTA.2H_2O$ and Tris(hydroxymethyl)aminomethane (Tris) were purchased from Merck.

Table 1. Nucleic acids

Abbreviation	Modification	Manufacturer	Sense strand[1] / Antisense strand[1]
Cy5-siRNA	Cy5 label[2]	Eurogentec	5′-UGCGCUACGAUCGACGAUG**tt**-3′/ 5′-CAUCGUCGAUCGUAGCGCA**tt**-3′
siRNA	/	Eurogentec	5′-CAAGCUGACCCUGAAGUUC**tt**-3′/ 5′-GAACUUCAGGGUCAGCUUG**tt**-3′
siDNA	deoxyribonucleotides	Eurogentec	5′-**caagctgaccctgaagttctt**-3′/ 5′-**gaacttcagggtcagcttgtt**-3′
ssRNA	/	Eurogentec	5′-UUAUCUGUGAGCAUUCUUCUU-3′/ N.A.
siRNA (stabilized)	stabilized[3]	GE Dharmacon	5′-CAAGCUGACCCUGAAGUUCUU-3′/ 5′-GAACUUCAGGGUCAGCUUGUU-3′

[1]Lowercase bold letters represent deoxyribonucleotides; [2]Cy5 dye is linked at the 5′ end of the sense strand; [3]RNA strand modified for the use in nuclease-rich environments (siSTABLE modification; GE Dharmacon)

2.2. Cell culture

B16F10 melanoma cells (ATCC® CRL-6475™) and H1299 non-small-cell lung carcinoma cells (ATCC® CRL-5803™) were cultured in Dulbecco's Modified Eagle Medium (DMEM) (Invitrogen) supplemented with 2 mM L-glutamine, 10 % fetal bovine serum (FBS; Hyclone™), 1 mM sodium pyruvate (Invitrogen) and 100 U/ml penicillin, 100 µg/ml streptomycin. The cells were grown in a humidified atmosphere containing 5 % CO_2 at 37°C.

2.3. EV purification

Prior to the purification of EVs, the B16F10 melanoma cells were washed with phosphate buffered saline (PBS; Invitrogen) and incubated for 24h with vesicles depleted medium after which the conditioned cell medium was harvested for EV purification. To prepare vesicle depleted medium, the normal cell medium was ultra-filtrated through a 300 kDa filter (Millipore) using an Amicon stirred cell (Millipore) under nitrogen pressure. Using ultrafiltration to generate vesicle-depleted cell medium was previously described by Heinemann *et al*. [23]. Cell viability, at the moment of conditioned cell medium harvesting, was determined by means of trypan blue (Sigma-Aldrich) staining. The viability was always higher than 95 %.

EVs were purified from conditioned cell medium by differential (ultra)centrifugation as schematically represented in **figure 1A**. Conditioned cell medium was centrifuged for 10 minutes at 300 g and 10 minutes at 3 000 g. Next, the supernatant was concentrated by ultrafiltration using a 30 kDa filter (Millipore) in an Amicon stirred cell under nitrogen pressure. The concentrated sample was next centrifuged at 10 000 g (k = 1811) for 15 minutes using a SW55ti rotor (Beckman instruments). Finally the supernatant was ultracentrifugated (UC) twice for 70 minutes at 120 000 g (k = 116) with a washing step in-between and resuspended in PBS.

If indicated, EVs were further purified by iodixanol-based (Optiprep™, Axis-Shield) density gradient UC. The gradient was produced by carefully laying 1 ml of different dilutions of iodixanol (12.5 %, 25 %, 37.5 % and 50 % in 250 mM sucrose, 1 mM EDTA, 10 mM Tris-HCl buffer; pH = 7.4) underneath one another, creating a density gradient. Next 1 ml concentrated, conditioned cell medium (after the 10 000 g UC step) was carefully placed on top of the gradient and centrifuged at 150 000 g (k = 92) for 15h. Next, the gradient was fractionated per 0.5 ml. The fractions with a density between 1.11 and 1.15 g/ml were diluted 10x in PBS buffer and centrifuged at 150 000 g for 150 minutes. Finally, the pellet was washed one more time and resuspended in PBS buffer.

2.4. Concentration measurements

The amount of EVs obtained after purification was estimated by measuring the total amount of proteins using a Pierce™ BCA protein determination assay (Thermo scientific) as prescribed by the manufacturer. The absolute amount of EVs was determined by scattering-based single particle tracking (SPT) using a Nanosight LM10 device equipped with the NTA 3.0 software (Malvern). Alternatively, fluorescently labeled EV concentrations were determined by recording videos (31.5 f/s) using a Nikon C1si confocal scanning module installed on a motorized TE2000-E inverted microscope (35 µm slit; Nikon), equipped with a 60x oil immersion objective lens (NA 1.4; Nikon), using a 488 nm laser line. Fluorescent particle concentration was estimated using previously published software [24].

2.5. Size and zeta potential measurements

The size of the EVs was determined *via* scattering-based SPT using a NanoSight LM10 instrument (Malvern). Movies of 60 seconds were recorded and analyzed with the NTA version 3.0 software (Malvern).

The zeta-potential was measured by dynamic light scattering (DLS) using a Zetasizer Nano ZS (Malvern), equipped with Dispersion Technology Software. The samples were diluted in HEPES buffer (20 mM; pH 7.4).

2.6. Gel retention assay

Association between EVs and small nucleic acids was assessed by polyacrylamide gel electrophoresis (PAGE). Ten pmol siRNA (or, if indicated, another small nucleic acid) was incubated with increasing amounts of EVs for 1h at 37°C (unless otherwise indicated) in PBS (unless otherwise indicated) after which a 10x gel loading solution (AM8556; Ambion) was added to each sample. The samples were loaded onto a 20 % non-denaturing polyacrylamide gel prepared in TBE-buffer (10.8 g/L Tris base, 5.5 g/L boric acid, 0.74 g/L $Na_2EDTA.2H_2O$). Electrophoresis was performed at 120 V during 40 minutes. Free migrating nucleic acids were visualized by incubating the gel in SYBR Green II RNA staining solution (ThermoFisher Scientific) for 45 minutes at room temperature followed by UV transillumination and gel photography. Gel images were cropped for clarity using ImageJ software.

2.7. Immunoblotting

The EV pellet was resuspended in RIPA buffer (Sigma-Aldrich) supplemented with MS-SAFE protease and phosphatase inhibitor cocktail (Sigma-Aldrich), vortexed and placed on ice for 30 minutes. Next, the samples were placed in a sonication bath (Branson 2510) for 3x 5 minutes with vortexing in-between. The protein concentration was

determined using the DC™ protein assay (Bio-Rad) according to the manufacturer's instructions. The samples were diluted in 2x laemmli buffer (Bio-Rad) with 5 % 2-mercaptoethanol (Sigma-Aldrich) and heated to 95°C for 5 minutes. Ten µg protein was loaded on a 10 % mini-protean TGX precasted gel (Bio-Rad). Proteins were separated at 100 V for 60 minutes in running buffer (Tris-Glycine-SDS). Blotting was done on an immune-blot® PVDF 0.2 µm membrane (Bio-Rad) at 100 V for 90 minutes in blotting buffer (Tris-Glycine-Methanol-SDS). The blot was blocked for 1h in PBS supplemented with 3 % bovine serum albumin (BSA) and 0.1 % Tween20. Next, the anti-Hsp70 antibody (1/1000; LS-C24142; LS biosciences Inc.) was incubated overnight at 4°C under gentle shaking. The secondary antibody (1/50 000; AP307P; Millipore), conjugated to Horseradish peroxidase, was incubated for 1h at room temperature. Visualization was done using the SuperSignal West Dura chemiluminescent kit (Thermo-Scientific). To estimate the protein size, a precision plus protein dual color standard (Bio-Rad) was ran along with the sample. Protein bands were cropped for clarity using ImageJ software.

2.8. Dynabead® assay

Thirty µg isolated EVs (after incubation with Cy5-labeled siRNA if indicated) were mixed with anti-CD63 coated dynabeads® (Invitrogen) and incubated overnight at 4°C under gentle shaking according to the manufacturer's protocol. The next day, samples were incubated with anti-CD63-FITC (312003; Biolegend), FITC-labeled isotype control (400107; Biolegend) or immediately washed. Bead-associated FITC or Cy5 fluorescence was quantified by flow cytometry (FACSCalibur; BD Biosciences).

2.9. Fluorescent labeling

B16F10-derived concentrated conditioned cell medium (after the 10 000 g spin) was mixed with an equal volume of 6 µM PKH67 (Sigma-Aldrich) in Diluent C (Sigma-Aldrich) and incubated for 30 minutes at 37°C. Next, the samples were divided in three equal volumes and further purified according to one of the protocols (i.e. precipitation, UC and density gradient) as schematically represented in **figure 6**.

2.10. Density gradient flotation (bottom-up)

Fluorescently labeled EV samples were mixed with the iodixanol stock to obtain a 50 % iodixanol solution (1 ml). This mixture was carefully placed underneath the previously described 0 – 37.5 % iodixanol gradient and centrifuged for 15h at 150 000 g. Next, 250 µl fractions (20 fractions per gradient) were carefully collected and pipetted in a black 96-well plate (Greiner bio-one) and fluorescence was evaluated in each fraction using an EnVision plate reader (PerkinElmer).

2.11. Quantification of the background fluorescence

Movies of 150 frames (31.5 f/s) were recorded from labeled and purified EV samples using a Nikon C1si confocal scanning module installed on a motorized TE2000-E inverted microscope (35 µm slit; Nikon), equipped with a 60x oil immersion objective lens (NA 1.4; Nikon). In each frame the average background fluorescence (i.e. after exclusion of the detected nanoparticles) was determined as a measure for non-EV associated dye.

2.12. Cell uptake experiments

H1299 cells (1.36×10^4 cells per cm^2) were grown in a 24-well plate and allowed to attach overnight. The next day, cells were incubated with an equal amount (determined by scattering-based SPT, **section 2.4**) of labeled EVs in OptiMEM reduced serum medium (Invitrogen) for the indicated time period. Next, the sample containing medium was removed and the cells were washed with PBS before being detached by means of trypsin/EDTA (Invitrogen). The detached cells were washed twice with flow buffer (1 % BSA, 0.1 % sodium azide in PBS) and analyzed for PKH67 fluorescence by flow cytometry (CytoFLEX; Beckman Coulter) recording at least 10 000 events per sample. Alternatively, H1299 cells were plated at the same cellular density in glass bottom plates for microscopy (Greiner bio-one). After sample incubation, the cells were washed thrice with PBS after which the cells were incubated with CellMask™ deep red plasma membrane stain (ThermoFisher Scientific) for 10 minutes at room temperature. Finally, the cells were again washed with PBS and fixed using 4 % paraformaldehyde for 15 minutes at room temperature, washed 3x with PBS and mounted with Vectashield Antifade mounting medium containing DAPI (Vector Laboratories). Images were recorded using a Nikon C1si confocal scanning module installed on a motorized TE2000-E inverted microscope (35 µm slit; Nikon), equipped with a 60x oil immersion objective lens (NA 1.4; Nikon), using a 405 nm, 488 nm and 637 nm laser line for the excitation of DAPI, PKH67 and CellMask™ deep red, respectively.

2.13. Statistical analysis

When applicable, statistical data analysis was done with GraphPad Prism 6 (GraphPad Software). Comparing multiple conditions was done using an ANOVA-test followed by a Tukey post hoc test. Direct comparison between two conditions was done using a student t-test. P-values < 0.05 were considered as statistically significant. The degree of significance is indicated using ns ($p \geq 0.05$), *($p < 0.05$), **($p < 0.01$), ***($p < 0.001$), ****($p < 0.0001$).

3. Results

3.1. EVs purified by conventional UC contain considerable nuclease activity

EVs were isolated out of conditioned cell culture medium from *in vitro* cultured B16F10 melanoma cells utilizing the currently most adopted protocol, which is based on differential UC [25]. The sequential centrifugation steps are depicted in **figure 1A** and exist initially out of low centrifugal forces to remove dead cells and larger vesicles such as apoptotic bodies. Theoretically, all vesicles larger than 350 nm should be pelleted in the described set-up considering a particle density of 1.14 g/ml [26]. Next, the smaller sized vesicles (exosomes and remaining ectosomes) are pelleted using high speed UC. Isolated EVs showed a typical size ranging from 30 nm up to 350 nm as determined by scattering-based SPT **(figure 1B)**, and a negative zeta potential of around -20 mV **(figure 1C)**. Moreover, the presence of the tetraspanin CD63 (an exosomal marker) was shown by bead-based flow cytometry **(figure 1D)** and the presence of Hsp70 was shown by immunoblotting **(figure 1E)**.

Loading purified EVs with synthetic nucleic acids is the subject of intensive research [2, 6, 8, 27, 28]. This can be driven by the objective to attribute a certain effect to EV-mediated transport/delivery of nucleic acids or to exploit EVs as a drug delivery vehicle. To date, few methods are available that allow to load purified vesicles with exogenous macromolecules. The previously reported method of EP [2, 29, 30] appears very inefficient (**chapter 2**) [7]. Likewise, loading EVs by mixing them with synthetic lipofection agents has important limitations as it significantly alters the EV composition [31]. A report from Bryniarski *et al.* indicated that simple mixing of synthetic miRNA with purified vesicles at 37°C is sufficient to load EVs with the respective miRNA [8, 9]. Indeed, when mixing siRNA with mounting concentrations of B16F10 EVs at 37°C, siRNA appears to bind to the vesicles, as demonstrated by a gel retention assay **(figure 2A)**. This assay is often used in the field of synthetic drug carriers to verify the association between a nanocarrier and the nucleic acid cargo as only non-associated RNA is small enough to migrate through the gel pores and hence can be visualized [32]. Moreover, we observed that the outcome of the gel retention assay was dependent on the nucleic acid type, incubation temperature and pH, suggesting an active process **(figure 2B-D)**.

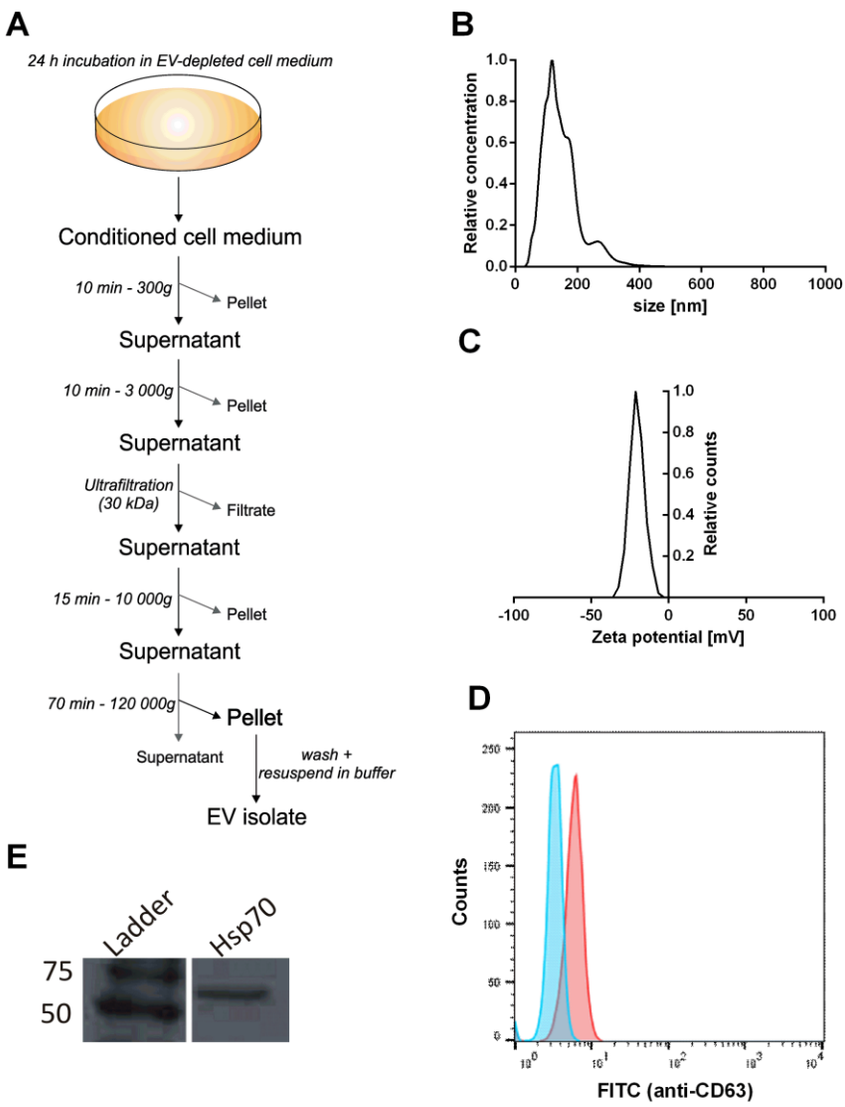

Figure 1. Purification and characterization of extracellular vesicles (EVs) isolated from B16F10 melanoma cells. [A] Schematic overview of the UC-based purification protocol. [B] Representative size and [C] zeta potential distribution of purified B16F10-derived EVs. [D] Flow cytometry analysis of anti-CD63 coated dynabeads® incubated with B16F10-derived EVs and mixed with FITC anti-CD63 (red) or FITC control antibody (blue), respectively. [E] Immunoblotting of isolated EVs using an anti-Hsp70 antibody. The molecular weight of the reference ladder proteins is indicated in kDa.

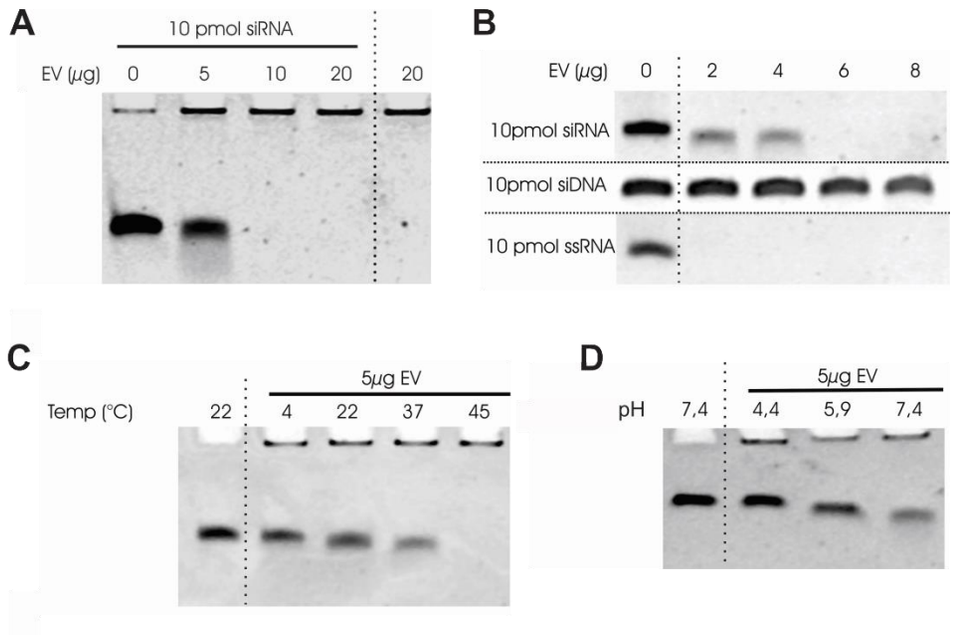

Figure 2. The influence of incubation conditions on small nucleic acid 'retention' by EVs, evaluated by a gel retention assay. [A] Representative PAGE of siRNA mixed with different amounts of B16F10 EVs after one hour incubation at 37°C. [B] Influence of small nucleic acid type (siRNA = a small RNA duplex, siDNA = a small DNA duplex and ssRNA = a single stranded small RNA; **see table 1**) on the retention by increasing amounts of EVs at 37°C and pH 7.4. [C] Influence of incubation temperature on the retention of siRNA when co-incubating 10 pmol siRNA and 5 µg EVs at pH 7.4. [D] Influence of pH during co-incubation of 10 pmol siRNA and 5 µg EVs at 37°C. Nucleic acids were visualized by incubating the gel in SYBR Green II staining solution.

However, as the gel retention assay does not provide conclusive evidence regarding the association between EVs and siRNA, we incubated B16F10-derived EVs with Cy5-labeled siRNA prior to capturing the EVs with CD63-coated dynabeads®. As shown by **figure 3**, no bead-associated Cy5 fluorescence could be observed *via* subsequent flow cytometric analysis, indicating that the siRNA is not associated with CD63-positive EVs. To verify if the observations in **figure 2** could be explained by remaining nuclease activity in the purified vesicle samples (as this can also explain the disappearance of siRNA bands on PAGE), we repeated the loading experiment following a heat-inactivation step or addition of a broad range RNase inhibitor. A short heat treatment of the EV sample to inhibit enzymatic activity prior to the incubation with siRNA corroborated the lack of interaction with the vesicles **(figure 4A)**. As the vesicle structure was not compromised during heat inactivation **(figure 4A)**, the latter results are suggestive of nuclease contamination in the EV isolates. Indeed, upon inactivation of nuclease activity through addition of a broad range RNase inhibitor, no association of siRNA with EVs could be detected **(figure 4B)** which was further confirmed by the inability of chemically stabilized siRNA to be retained by EVs on a gel retention assay **(figure 4C)**.

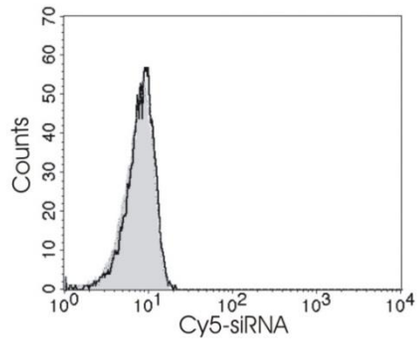

Figure 3. Anti-CD63 bead-based assay to determine EV-siRNA association. Anti-CD63 antibody coated dynabeads® were incubated with an EV + Cy5-siRNA mixture (black line), EVs only (gray full) and Cy5-siRNA without EVs (gray dotted line), respectively.

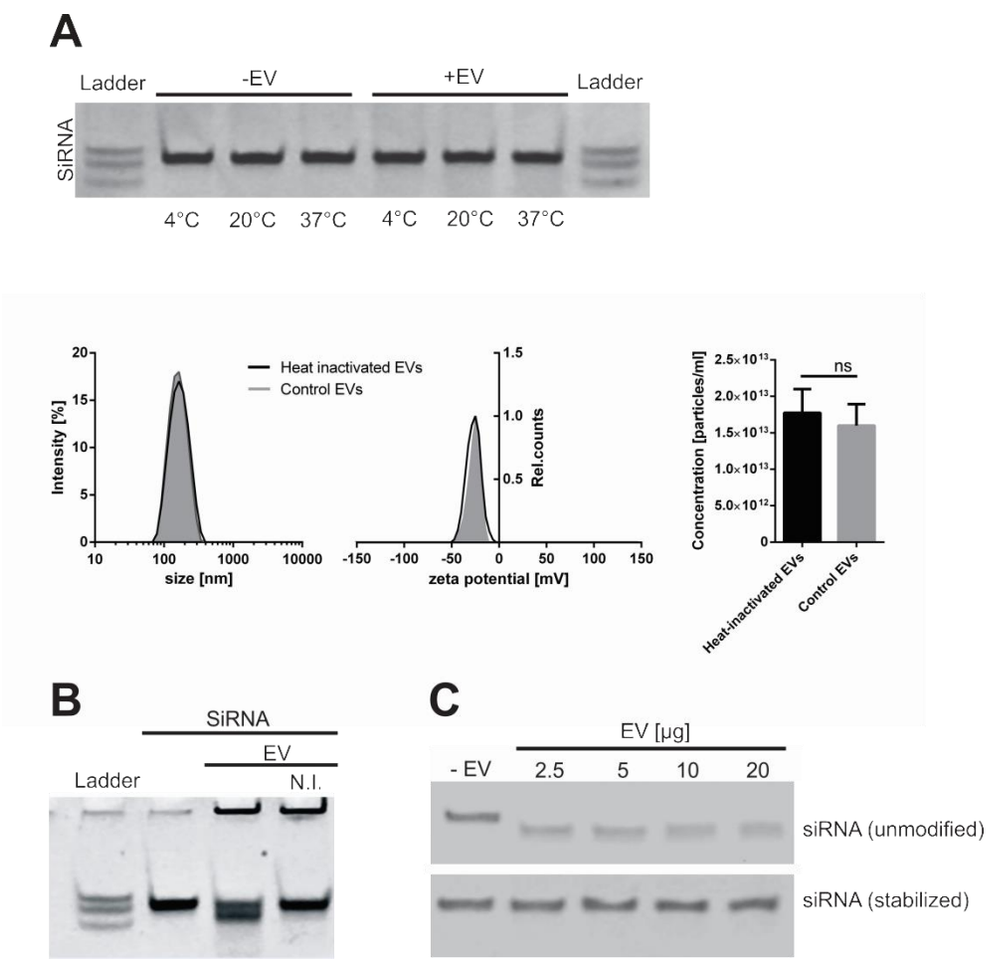

Figure 4. Nuclease activity in B16F10-derived EVs purified by differential UC. [A] *(upper)* PAGE of 10 pmol siRNA with and without 10 µg heat-inactivated EVs. *(lower)* Characterization of heat-inactivated EVs. Size, zeta potential and concentration of the vesicles before and after heat inactivation. Error bars represents the standard deviation of three technical replicates. [B] Gel retention assay of EV-siRNA with and without a nuclease inhibitor (N.I). The ladder contains strands of 25, 21 and 17 base pairs, respectively. [C] Comparing the behavior of unmodified and stabilized siRNA (siSTABLE, GE Dharmacon, **table 1**) after incubation with mounting concentrations of UC-purified EVs.

3.2. Density gradient purification removes non-EV associated nuclease activity

To verify if the observed nuclease activity is associated to vesicles (as previously reported for other enzymes [33-37]) or whether it is merely a contamination in our EV isolate, a more stringent purification protocol was used. To this end, following the differential centrifugation steps, the EV concentrate was layered on top of an iodixanol density gradient and fractionated by overnight UC to obtain higher purity vesicles and minimize co-purification of e.g. protein aggregates. Interestingly, the vesicles obtained *via* a density gradient contained much lower nuclease activity compared to conventional UC purified vesicles **(figure 5)**, suggesting that nucleases are not associated with the vesicular membrane. However, as nucleic acid degradation could not be completely avoided, it is advisable to work with chemically modified RNA as this was shown to be resistant to degradation by nuclease present in EV samples **(figure 4C)**.

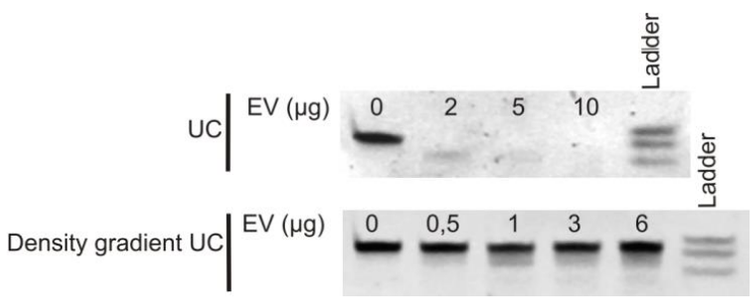

Figure 5. Comparing nuclease activity in EV isolates purified by differential UC (upper) and density gradient ultracentrifugation (lower). The ladder contains strands of 25, 21 and 17 base pairs, respectively. The samples were incubated for 2h at 37°C. Nucleic acids were visualized by incubating the gel in SYBR Green II staining solution.

3.3. The fluorescent labeling of EVs requires stringent purification protocols

The observation that non-vesicular components co-isolate with EVs when using differential UC, i.e. a method often used to wash away non incorporated molecules (e.g. fluorescent dyes) [13, 38, 39], lead us to hypothesize that free or non-vesicular associated fluorescent dye might remain in the EV isolate, possibly leading to false assumptions regarding EV uptake and intracellular trafficking. To this end we compared three purification strategies (i.e. precipitation [40], UC [41, 42] and density gradient [43, 44]) for their efficiency to render high purity isolates. All three techniques have previously been used in the literature and their theoretical background has been discussed in **chapter 1**.

Conditioned cell medium from B16F10 melanoma cells was again deprived of larger particles by sequential centrifugation and the sample was concentrated (~130x) to workable volumes by ultrafiltration (30 kDa). Next, the concentrated conditioned cell

medium (cCCM) was incubated with a lipophilic dye. In this chapter we opted for PKH67 as a fluorescent dye as this is often used throughout the literature to evaluate and quantify the interaction of EVs with recipient cells [13, 45-47]. Next, the labeled cCCM was divided in three equal fractions and purified with one of the following methods: (1) precipitation using a commercial kit (i.e. Exoquick-TC™), (2) pelleting by UC (120 000 g – 70 minutes) and (3) density gradient purification (0.0 % – 50.0 % iodixanol gradient) as schematically represented in **figure 6**.

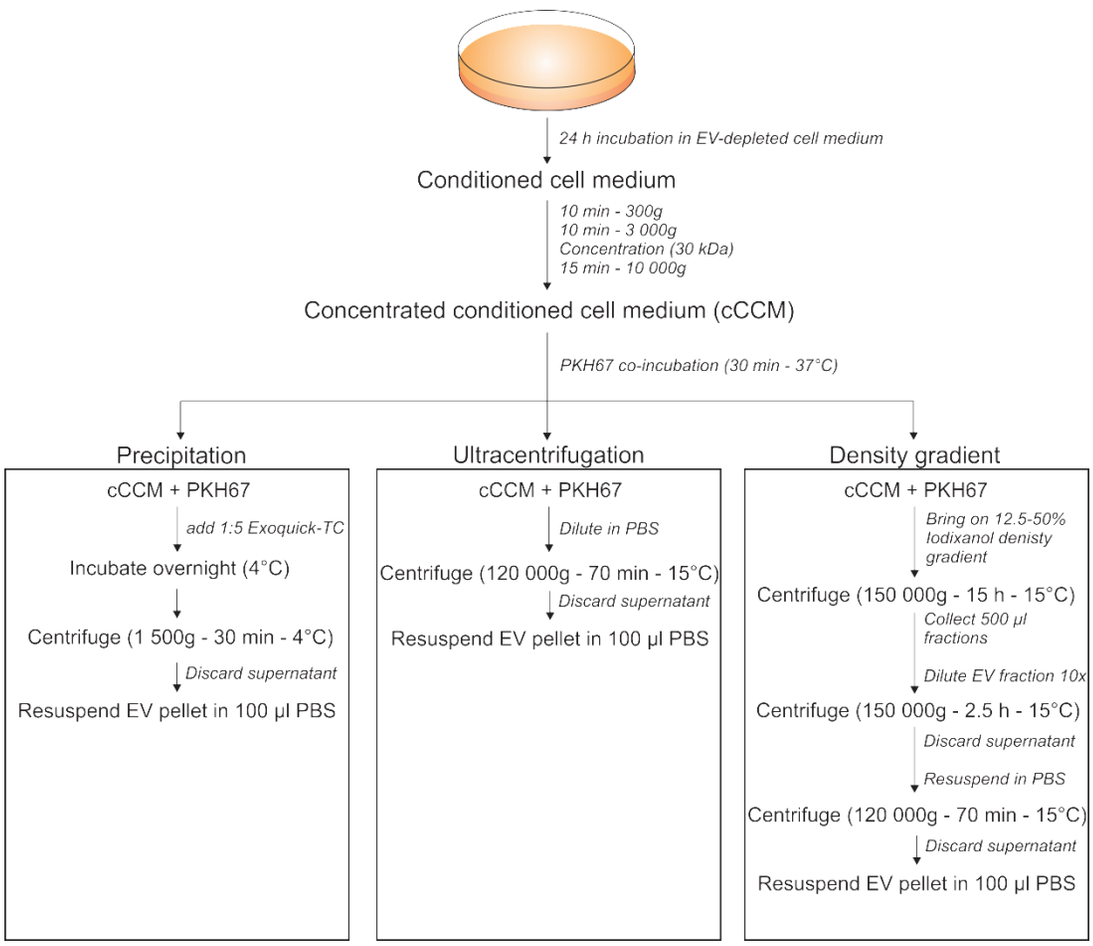

Figure 6. Schematic representation of the different purification strategies used to wash away non-EV associated PKH67 dye.

EV isolation by precipitation results in the highest number of particles (~2.4x) followed by UC (~1.9x) and density gradient (normalized to 1.0), as measured by scattering-based SPT (**figure 7**). The same trend is seen for the total amount of fluorescence that is retained, yet the fold increase relative to density gradient purification is much more pronounced (36.4x and 3.4x using precipitation and UC, respectively) (**figure 7**). This can have two distinct reasons: (1) The precipitation method isolates EVs with more fluorescent molecules per vesicle compared to UC and density gradient purification.

However this is unlikely as one batch of (an equal volume of) PKH67-labeled cCCM was applied as starting material for all three isolation strategies (**figure 6**). (2) Alternatively, the additional fluorescence of the precipitation- and UC-obtained isolates is a consequence of free or non-EV associated (e.g. albumin) dye which would imply that precipitation, and to a lesser extent UC, leads to less pure isolates compared to density gradient purification confirming our results for nuclease contamination in differential UC purified isolates (**section 3.2**).

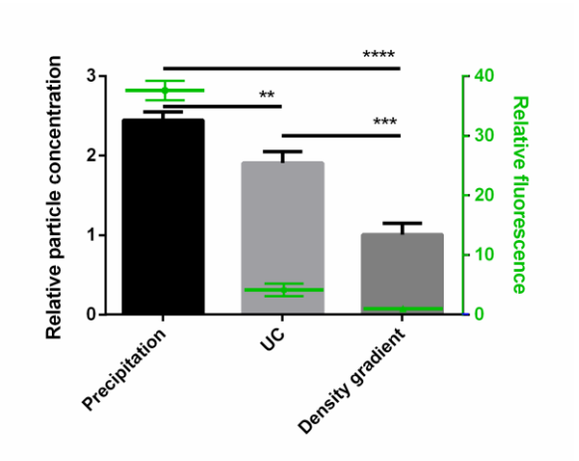

Figure 7. Particle and fluorescence yield using different purification protocols. The relative amount of particles (*left axis*) obtained for each purification strategy using scattering-based SPT (Nanosight, Malvern instruments) normalized to the amount of particles obtained using the density gradient purification protocol. For each purification strategy the relative amount of fluorescence is indicated (*right axis; green*) again normalized to density gradient purification. The data is represent the mean ± SD (n=3).

In order to verify the latter hypothesis, the vesicular purity of each isolation strategy was estimated by plotting the amount of scattering particles (i.e. a measure for the amount of retained EVs) relative to the total amount of proteins. This methods was proposed by Webber and Clayton as a semi-quantitative method to express the vesicular purity [48] and clearly shows that the purity is inversely proportional to the total amount of retained fluorescence (**figure 8A**). This is a first indication that precipitation and, to a lesser extent, UC are insufficient to wash away non-EV associated or even free fluorescent dye. To confirm this, fluorescent confocal images of the isolated, labeled samples were recorded using a swept field confocal microscope in combination with particle detection, using in-house developed software as previously described by Deschout *et al.* [49]. This allows to determine the background fluorescence which can be used as a measure for the amount of non-nanoparticle associated PKH67 label (**figure 8B**). Here, again the same trend could be observed with a high background signal for the precipitation obtained EV isolate followed by UC and finally density gradient purification not showing a significant difference from the non-fluorescent

control (i.e. PBS) indicating that all non-incorporated PKH67 was efficiently washed away.

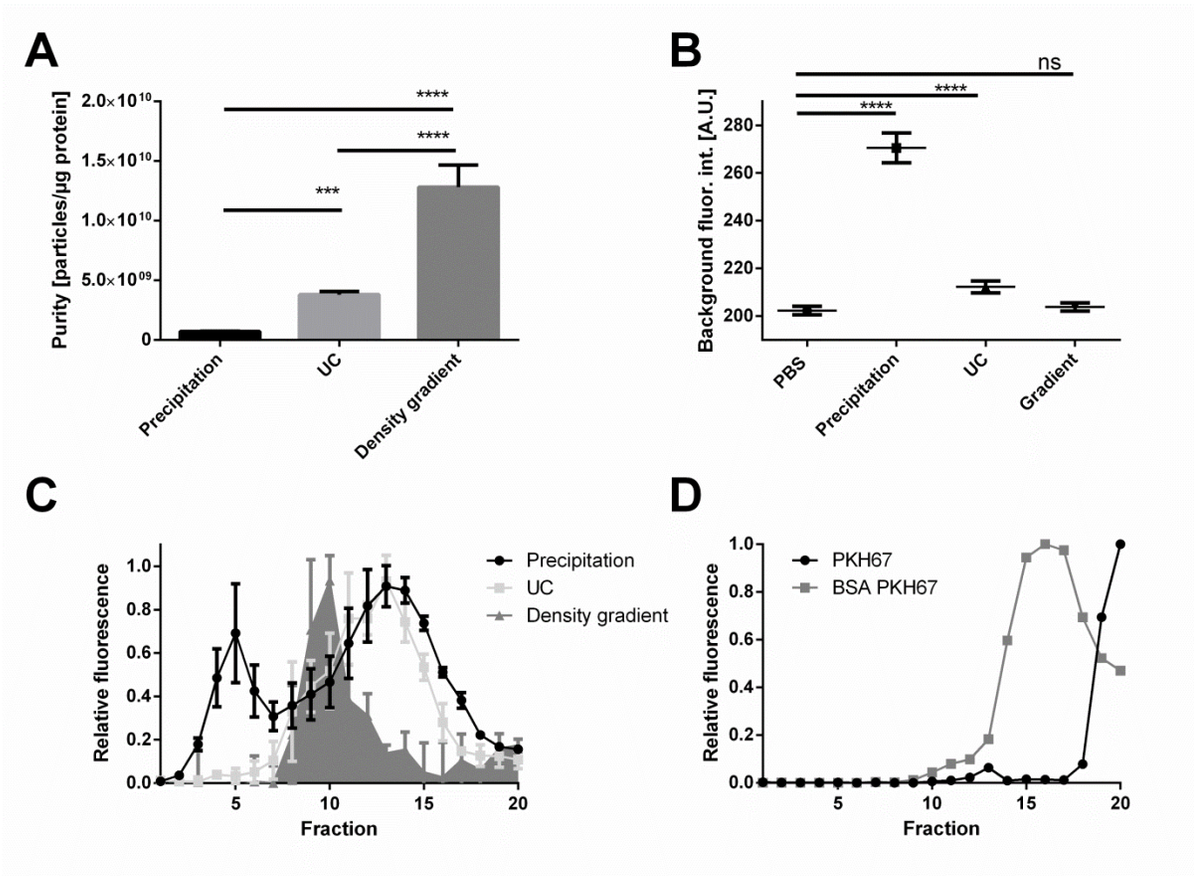

Figure 8. Characterization of the purity of each isolation strategy. [A] Particle concentration (measured *via* scattering-based SPT) over protein concentration (measured *via* a BCA-protein assay kit). The data is represented as mean ± SD (n=3). [B] Fluorescent background signal (i.e. the average fluorescence per frame excluding the particles). The results (mean ± SD) represent two independent experiments analyzing > 3000 frames per condition. [C] Relative PKH67-derived fluorescence for each fraction (20 fractions in total, fraction 1 being the lowest density) after a bottom-up density gradient flotation over a 0 - 50 % iodixanol gradient for each purification strategy. The results are represented as mean ± SD (n=3). [D] Relative PKH67-derived fluorescence for each fraction after bottom-up density gradient flotation of unbound PKH67 and BSA-bound PKH67.

In an attempt to better understand the association profile of the non-vesicular PKH67, the labeled isolates were floated (bottom-up) on a density gradient (0 – 50 % iodixanol). A clear difference in fluorescence distribution over the density gradient is apparent between the different isolation strategies (**figure 8C**). For both UC and precipitation a large fraction of the fluorescence is present at higher densities. A recent observation by Willms *et al.* shows that using this bottom-up flotation approach, a higher density EV fraction can be separated from the 'normal' EV density fraction (i.e. fraction 9 – 10, see **chapter 4**), which is not visible using the top-down approach [50].

However, we observed (*via* scattering-based SPT) that this higher density fractions contain far less particles (~18 % and ~21 % for precipitation and UC, respectively) compared to the EV fraction (i.e. fraction 9 and 10) whereas the fluorescence (expressed as AUC) is around 2 times higher, implying that next to vesicles it are mainly other components that are associated to PKH67 and hence responsible for the flotation of the dye at higher densities. Likely, albumin is one of these contaminants as we (**figure 8D**) and others [51] confirmed that albumin floats at higher densities. Moreover, the presence of albumin in both UC and precipitation isolates has been described in the literature while this is not the case for density gradient-based isolates [43]. The fluorescent peak visible at fraction 4 and 5 using the precipitation protocol appeared not of vesicular origin (<1 % vesicles for 1.5x fluorescence, compared to the EV fraction) yet can originate from dye associated to alternative components as free dye does not float (**figure 8D**).

Based on the obtained results it appears that, dependent on the used isolation strategy, the fluorescent dye can be present under different forms (i.e. EV-associated, protein(complex) associated, …). It is likely that this altered association profile interferes with cell interaction experiments. To this end, equal amount of scattering particles from each purification strategy were added to H1299 lung carcinoma cells as a model recipient cell. It is interesting to note that normalization (i.e. diluting the isolates to obtain an equal amount of EVs for each purification strategies) on the amount of scattering nanoparticles corresponds with normalization on the amount of fluorescent nanoparticles for the EVs purified with UC and density gradient (data not shown). For isolates obtained using precipitation, the fluorescence-based SPT approach underestimates the amount of particles relative to the scattering-based SPT which is likely due to the high PKH67 background (**figure 8B**) making some weakly labeled particles disappear in the fluorescent background.

When quantifying the uptake of EVs in recipient cells as a function of time, a comparable profile was seen between UC and precipitation with a fast internalization of fluorescent label. In contrast, the gradient-purified EVs show a much slower, linear uptake profile. When analyzing free PKH67 dye in the same concentration as present in the EV isolates, the fast uptake profile of the UC and precipitation obtained samples could be mimicked (**figure 9A**). Looking in more detail to the cellular uptake using confocal microscopy, the intracellular distribution following 20h co-incubation appears comparable between the different purification strategies (**figure 9B**). However, we believe drawing reliable conclusions regarding the origin of this dotted profile is not feasible as we observed a comparable punctuated appearance for the free PKH67 dye as well (**figure 9B**).

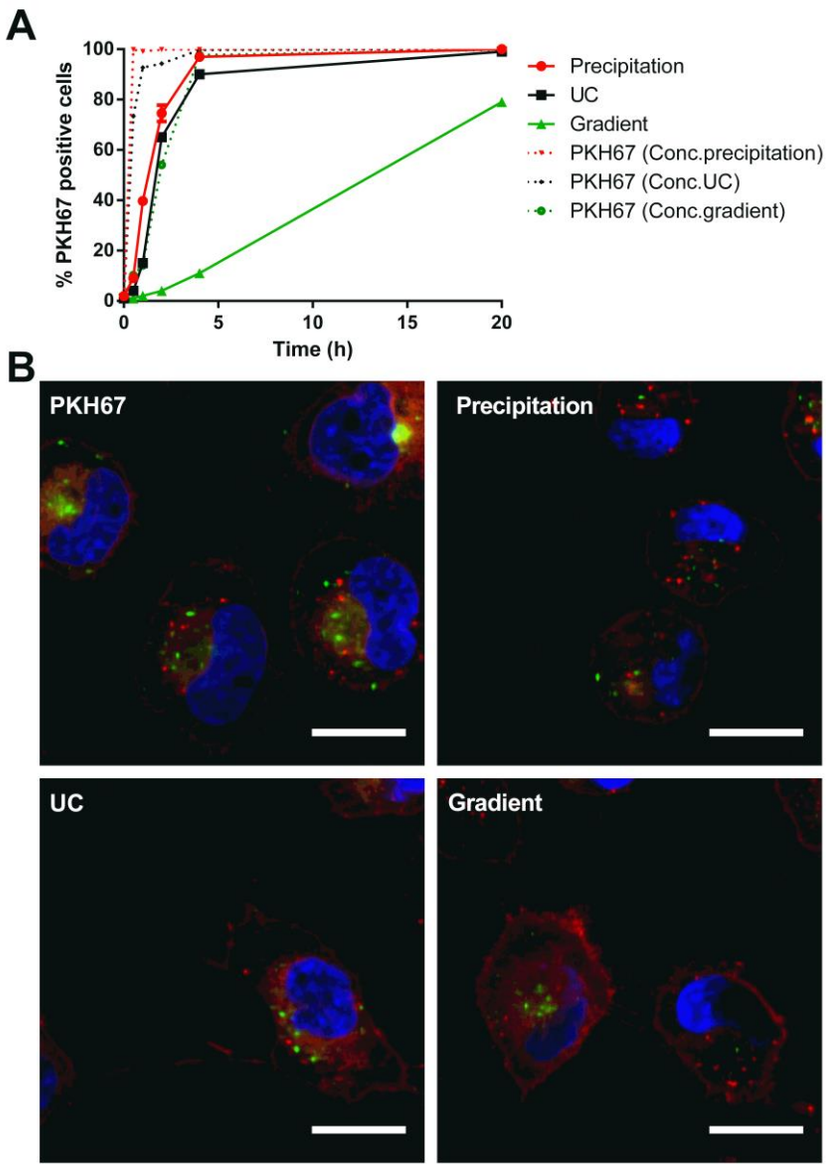

Figure 9. Uptake of PKH67-labeled B16F10-derived EVs by H1299 cells after different isolation strategies. Percentage positive H1299 cells after co-incubation with the same concentration (measured by scattering-based SPT; ~1.5 x 10^{10} particles/ml) of PKH67-labeled EVs purified by precipitation, UC and density gradient, respectively. The dotted lines indicate the uptake of unbound PKH67 incubated with the cells at the same concentration as present in the respective EV fractions (determined by fluorescence intensity). Representative confocal microscopy images of H1299 cells after 20h incubation with PKH67-labeled EVs (green) purified using the indicated isolation strategy or unbound PKH67. The nuclei are labeled with DAPI (blue) and cells are labeled with CellMask™ deep red plasma membrane stain (red). The scale bars represents 20 µm.

4. Discussion

Our results demonstrate that the currently most used purification protocol (i.e. differential UC followed by a washing step) is prone to co-purification of (protein) contaminants including ribonucleases (RNase), i.e. endogenously present in FBS supplemented medium and/or secreted by cultured cells [52]. In this respect, it is important to note that standard approaches to determine the association between the therapeutic nucleic acid cargo and a nanocarrier (e.g. a gel retention assay, as often used in the field of synthetic drug delivery vehicles [32]) have to be interpreted with caution, especially when no measures have been taken to block this nuclease activity (e.g. working at 4°C as was done in **chapter 2**). By performing additional control experiments (e.g. an antibody-based EV capture approach), we were able to show that loading purified EVs by simple incubation with small RNA duplexes, as previously shown for Ba1 cell-derived EVs and miR-150 [9], is not an universal mechanism applicable to all EVs and small RNA duplexes. Likely this phenomenon is limited to a certain niche of EVs, RNAs or specific circumstances. Additionally, the unanticipated detection of RNase activity in EV isolates prompted us to switch from unmodified to chemically stabilized siRNA as therapeutic cargo in the next chapter and underscores the importance of EV isolate purity, e.g. when contemplating downstream (post-formation) loading with nucleic acid therapeutics.

In the literature, the importance of EV purity is mainly emphasized in biomarker identification studies as it appears to severely affect the reproducibility of biomarker identification [43, 53]. However, we demonstrated here that EV isolates of high purity are not only important in a diagnostic context but are also vital to reliably probe the physiological behavior of EVs. Fluorescent labeling of EVs is an important tool to study the interaction between EVs and cells, e.g. to quantify the uptake of (drug-loaded) EVs, to evaluate intracellular trafficking and to assess cell type specificity of EV-cell interactions. Unfortunately, the strategies to remove non-EV incorporated or free dye are often insufficiently characterized before downstream experiments are executed. In this respect, three purification approaches were evaluated in a comparative analysis for the overall purity of the final isolate and their ability to wash away non-incorporated fluorescent dye. In addition to the biological relevance of studying the dye-EV association, the addition of a fluorescent dye prior to the actual purification appeared an elegant tool to study the purity of the final EV isolate.

We observed that precipitation and UC retained a higher amount of fluorescence compared to density gradient purification. This appeared not only to be due to a difference in EV yield but was mainly a consequence of contaminating, non-EV-associated dye. The particle to protein ratio gave a first indication that density gradient purification renders isolates with the highest purity. This was further confirmed by

background fluorescence analysis and corroborates with other reports in the literature [43, 54]. This implies that the fluorescent dye not only associates with EVs but also with non-vesicular components. Importantly, this unspecific dye association and difference in purity translates into a modified uptake profile in recipient cells as a function of time. We observed that the EVs isolated with techniques categorized as less stringent (i.e. precipitation and to a lesser extent UC) show a very fast cellular uptake, which is comparable to free PKH dye. On the other hand, EVs purified using more stringent purification protocols (i.e. density gradient) showed a much slower, linear uptake profile. As the vesicle isolate obtained *via* density gradient purification contains the least non-EV associated label, this likely is more representative for the actual uptake profile. However, it is also possible that the density gradient purification protocol impairs the EV-cell interactions. Yet, we consider this as less likely as a comparable protocol has recently been used to purify adeno-associated viruses and showed that they maintained their ability to functionally deliver their gene content to receptive cells [55].

Due to the commercialization of the easy-to-use precipitation kits, often these low quality EV isolates are used as EV source for further experiments. For example the use of Exoquick-TC™ is advised by the manufacturer to wash away non-incorporated label [56] which, based on our data, is insufficient to obtain clean isolates of labeled EVs. Consequently, this can have a strong impact on studies evaluating EV-cell interaction specificity [10]. Other purification strategies, including size based purification strategies (**chapter 1**), are likely also able to remove non-incorporated dye. Generally, these techniques are, just as density gradient, categorized as stringent [57, 58] and from our own experience with amphiphilic molecules (MPLA adjuvant; **figures S1**) we know that size exclusion chromatography (SEC) is able to wash away non-EV associated components.

It is also interesting to note that EVs can be labeled using fusion protein constructs consisting of an inherent EV-associated protein (e.g. CD63) and a fluorescent protein (e.g. GFP) [59, 60]. This restricts the fluorescent molecule to EVs with no background fluorescence, yielding reliable information on cellular interaction (e.g. uptake and intracellular trafficking) [61]. However, such an approach could restrict labeling to certain EV subtypes and moreover requires the biotechnological alteration of the EV producer cell which is not always feasible (e.g. when working with EVs obtained from biofluids or working with difficult-to-transfect cells).

5. Conclusion

Overall our data demonstrate that inadequate purification strategies can lead to misinterpretation of downstream experiments on EV isolates, e.g. post-formation loading with nucleic acid therapeutics and fluorescent labeling. From the here tested purification strategies, density gradient purification rendered EV isolates with the highest purity followed by UC and finally precipitation.

Acknowledgements

SS and KR are doctoral and postdoctoral fellows respectively of the Research Foundation - Flanders (FWO). The support of this institution is gratefully acknowledged. Dr. Toon Brans is thanked for his help with the analysis of the background fluorescence. Dr. Heleen Dewitte is thanked for providing primary bone marrow-derived DC and assistance in the DC-maturation assay. We also thank Dr. An Hendrix from the Laboratory of Experimental Cancer Research – University hospital Ghent for the use of the Nanosight LM10 equipment and Prof. T. Coenye of the laboratory of microbiology – Ghent University for the use of the PerkinElmer envision plate reader.

References

[1] J. Skog, T. Wurdinger, S. van Rijn, D.H. Meijer, L. Gainche, M. Sena-Esteves, W.T. Curry, Jr., B.S. Carter, A.M. Krichevsky, X.O. Breakefield, Glioblastoma microvesicles transport RNA and proteins that promote tumour growth and provide diagnostic biomarkers, Nat. Cell Biol., 10 (2008) 1470-1476.

[2] L. Alvarez-Erviti, Y.Q. Seow, H.F. Yin, C. Betts, S. Lakhal, M.J.A. Wood, Delivery of siRNA to the mouse brain by systemic injection of targeted exosomes, Nat. Biotechnol., 29 (2011) 341-U179.

[3] L. Zitvogel, A. Regnault, A. Lozier, J. Wolfers, C. Flament, D. Tenza, P. Ricciardi-Castagnoli, G. Raposo, S. Amigorena, Eradication of established murine tumors using a novel cell-free vaccine: dendritic cell-derived exosomes, Nat. Med., 4 (1998) 594-600.

[4] R.C. Lai, F. Arslan, M.M. Lee, N.S. Sze, A. Choo, T.S. Chen, M. Salto-Tellez, L. Timmers, C.N. Lee, R.M. El Oakley, G. Pasterkamp, D.P. de Kleijn, S.K. Lim, Exosome secreted by MSC reduces myocardial ischemia/reperfusion injury, Stem cell Res., 4 (2010) 214-222.

[5] H. Valadi, K. Ekstrom, A. Bossios, M. Sjostrand, J.J. Lee, J.O. Lotvall, Exosome-mediated transfer of mRNAs and microRNAs is a novel mechanism of genetic exchange between cells, Nat. Cell Biol., 9 (2007) 654-U672.

[6] J. Wahlgren, L.K.T. De, M. Brisslert, F. Vaziri Sani, E. Telemo, P. Sunnerhagen, H. Valadi, Plasma exosomes can deliver exogenous short interfering RNA to monocytes and lymphocytes, Nucleic Acids Res., 40 (2012) e130.

[7] S.A. Kooijmans, S. Stremersch, K. Braeckmans, S.C. de Smedt, A. Hendrix, M.J. Wood, R.M. Schiffelers, K. Raemdonck, P. Vader, Electroporation-induced siRNA precipitation obscures the efficiency of siRNA loading into extracellular vesicles, J. Control. Release, 172 (2013) 229-238.
[8] K. Bryniarski, W. Ptak, A. Jayakumar, K. Pullmann, M.J. Caplan, A. Chairoungdua, J. Lu, B.D. Adams, E. Sikora, K. Nazimek, S. Marquez, S.H. Kleinstein, P. Sangwung, Y. Iwakiri, E. Delgato, F. Redegeld, B.R. Blokhuis, J. Wojcikowski, A.W. Daniel, T. Groot Kormelink, P.W. Askenase, Antigen-specific, antibody-coated, exosome-like nanovesicles deliver suppressor T-cell microRNA-150 to effector T cells to inhibit contact sensitivity, J. Allergy Clin. Immunol., 132 (2013) 170-181.
[9] K. Bryniarski, W. Ptak, E. Martin, K. Nazimek, M. Szczepanik, M. Sanak, P.W. Askenase, Free Extracellular miRNA Functionally Targets Cells by Transfecting Exosomes from Their Companion Cells, PLoS One, 10 (2015) e0122991.
[10] L.A. Mulcahy, R.C. Pink, D.R. Carter, Routes and mechanisms of extracellular vesicle uptake, J Extracell Vesicles, 3 (2014) 24641.
[11] H.C. Christianson, K.J. Svensson, T.H. van Kuppevelt, J.P. Li, M. Belting, Cancer cell exosomes depend on cell-surface heparan sulfate proteoglycans for their internalization and functional activity, Proc. Natl. Acad. Sci. U. S. A., 110 (2013) 17380-17385.
[12] D. Feng, W.L. Zhao, Y.Y. Ye, X.C. Bai, R.Q. Liu, L.F. Chang, Q. Zhou, S.F. Sui, Cellular internalization of exosomes occurs through phagocytosis, Traffic, 11 (2010) 675-687.
[13] L. Zhu, L. Bao, X. Zhang, X. Xia, H. Sun, Inhibition of porcine reproductive and respiratory syndrome virus replication with exosome-transferred artificial microRNA targeting the 3' untranslated region, J. Virol. Methods, 223 (2015) 61-68.
[14] K. Ekstrom, H. Valadi, M. Sjostrand, C. Malmhall, A. Bossios, M. Eldh, J. Lotvall, Characterization of mRNA and microRNA in human mast cell-derived exosomes and their transfer to other mast cells and blood CD34 progenitor cells, J Extracell Vesicles, 1 (2012).
[15] K.J. Svensson, H.C. Christianson, A. Wittrup, E. Bourseau-Guilmain, E. Lindqvist, L.M. Svensson, M. Morgelin, M. Belting, Exosome Uptake Depends on ERK1/2-Heat Shock Protein 27 Signaling and Lipid Raft-mediated Endocytosis Negatively Regulated by Caveolin-1, J. Biol. Chem., 288 (2013) 17713-17724.
[16] A. Montecalvo, A.T. Larregina, W.J. Shufesky, D.B. Stolz, M.L. Sullivan, J.M. Karlsson, C.J. Baty, G.A. Gibson, G. Erdos, Z. Wang, J. Milosevic, O.A. Tkacheva, S.J. Divito, R. Jordan, J. Lyons-Weiler, S.C. Watkins, A.E. Morelli, Mechanism of transfer of functional microRNAs between mouse dendritic cells via exosomes, Blood, 119 (2012) 756-766.
[17] I. Parolini, C. Federici, C. Raggi, L. Lugini, S. Palleschi, A. De Milito, C. Coscia, E. Iessi, M. Logozzi, A. Molinari, M. Colone, M. Tatti, M. Sargiacomo, S. Fais, Microenvironmental pH is a key factor for exosome traffic in tumor cells, J. Biol. Chem., 284 (2009) 34211-34222.
[18] C. Obregon, B. Rothen-Rutishauser, S.K. Gitahi, P. Gehr, L.P. Nicod, Exovesicles from human activated dendritic cells fuse with resting dendritic cells, allowing them to present alloantigens, Am. J. Pathol., 169 (2006) 2127-2136.
[19] V.V. Temchura, M. Tenbusch, G. Nchinda, G. Nabi, B. Tippler, M. Zelenyuk, O. Wildner, K. Uberla, S. Kuate, Enhancement of immunostimulatory properties of exosomal vaccines by incorporation of fusion-competent G protein of vesicular stomatitis virus, Vaccine, 26 (2008) 3662-3672.
[20] A. Waldenstrom, N. Genneback, U. Hellman, G. Ronquist, Cardiomyocyte microvesicles contain DNA/RNA and convey biological messages to target cells, PLoS One, 7 (2012) e34653.

[21] M. Li, E. Zeringer, T. Barta, J. Schageman, A. Cheng, A.V. Vlassov, Analysis of the RNA content of the exosomes derived from blood serum and urine and its potential as biomarkers, Philos. Trans. R. Soc. Lond. B Biol. Sci., 369 (2014) 20130502.
[22] J. Van Deun, P. Mestdagh, R. Sormunen, V. Cocquyt, K. Vermaelen, J. Vandesompele, M. Bracke, O. De Wever, A. Hendrix, The impact of disparate isolation methods for extracellular vesicles on downstream RNA profiling, J Extracell Vesicles, 3 (2014) 24858.
[23] M.L. Heinemann, M. Ilmer, L.P. Silva, D.H. Hawke, A. Recio, M.A. Vorontsova, E. Alt, J. Vykoukal, Benchtop isolation and characterization of functional exosomes by sequential filtration, J. Chromatogr. A, 1371C (2014) 125-135.
[24] M. Roding, H. Deschout, K. Braeckmans, M. Rudemo, Measuring absolute number concentrations of nanoparticles using single-particle tracking, Phys. Rev. E Stat. Nonlin. Soft Matter Phys., 84 (2011) 031920.
[25] C. Thery, S. Amigorena, G. Raposo, A. Clayton, Isolation and characterization of exosomes from cell culture supernatants and biological fluids, Curr. Protoc. Cell Biol., Chapter 3 (2006) U3.22.
[26] M.A. Livshts, E. Khomyakova, E.G. Evtushenko, V.N. Lazarev, N.A. Kulemin, S.E. Semina, E.V. Generozov, V.M. Govorun, Isolation of exosomes by differential centrifugation: Theoretical analysis of a commonly used protocol, Sci. Rep., 5 (2015) 17319.
[27] Q. Pan, V. Ramakrishnaiah, S. Henry, S. Fouraschen, P.E. de Ruiter, J. Kwekkeboom, H.W. Tilanus, H.L. Janssen, L.J. van der Laan, Hepatic cell-to-cell transmission of small silencing RNA can extend the therapeutic reach of RNA interference (RNAi), Gut, 61 (2012) 1330-1339.
[28] S.I. Ohno, M. Takanashi, K. Sudo, S. Ueda, A. Ishikawa, N. Matsuyama, K. Fujita, T. Mizutani, T. Ohgi, T. Ochiya, N. Gotoh, M. Kuroda, Systemically Injected Exosomes Targeted to EGFR Deliver Antitumor MicroRNA to Breast Cancer Cells, Mol. Ther., 21 (2012) 185–191.
[29] J. Wahlgren, L. Karlson Tde, M. Brisslert, F. Vaziri Sani, E. Telemo, P. Sunnerhagen, H. Valadi, Plasma exosomes can deliver exogenous short interfering RNA to monocytes and lymphocytes, Nucleic Acids Res., 40 (2012) e130.
[30] T.A. Shtam, R.A. Kovalev, E.Y. Varfolomeeva, E.M. Makarov, Y.V. Kil, M.V. Filatov, Exosomes are natural carriers of exogenous siRNA to human cells in vitro, Cell Commun. Signal., 11 (2013) 88.
[31] P. Vader, S.A. Kooijmans, S. Stremersch, K. Raemdonck, New considerations in the preparation of nucleic acid-loaded extracellular vesicles, Ther. Deliv., 5 (2014) 105-107.
[32] L. De Backer, K. Braeckmans, J. Demeester, S.C. De Smedt, K. Raemdonck, The influence of natural pulmonary surfactant on the efficacy of siRNA-loaded dextran nanogels, Nanomedicine, 8 (2013) 1625-1638.
[33] J. Esser, U. Gehrmann, F.L. D'Alexandri, A.M. Hidalgo-Estevez, C.E. Wheelock, A. Scheynius, S. Gabrielsson, O. Radmark, Exosomes from human macrophages and dendritic cells contain enzymes for leukotriene biosynthesis and promote granulocyte migration, J. Allergy Clin. Immunol., 126 (2010) 1032-1040.
[34] S.A. Melo, H. Sugimoto, J.T. O'Connell, N. Kato, A. Villanueva, A. Vidal, L. Qiu, E. Vitkin, L.T. Perelman, C.A. Melo, A. Lucci, C. Ivan, G.A. Calin, R. Kalluri, Cancer exosomes perform cell-independent microRNA biogenesis and promote tumorigenesis, Cancer Cell, 26 (2014) 707-721.

[35] A. Bulloj, M.C. Leal, H. Xu, E.M. Castano, L. Morelli, Insulin-degrading enzyme sorting in exosomes: a secretory pathway for a key brain amyloid-beta degrading protease, J. Alzheimers Dis., 19 (2010) 79-95.
[36] A. Savina, M. Vidal, M.I. Colombo, The exosome pathway in K562 cells is regulated by Rab11, J. Cell Sci., 115 (2002) 2505-2515.
[37] V. Dolo, A. Ginestra, D. Cassara, S. Violini, G. Lucania, M.R. Torrisi, H. Nagase, S. Canevari, A. Pavan, M.L. Vittorelli, Selective localization of matrix metalloproteinase 9, beta1 integrins, and human lymphocyte antigen class I molecules on membrane vesicles shed by 8701-BC breast carcinoma cells, Cancer Res., 58 (1998) 4468-4474.
[38] S.H. Kim, N. Bianco, R. Menon, E.R. Lechman, W.J. Shufesky, A.E. Morelli, P.D. Robbins, Exosomes derived from genetically modified DC expressing FasL are anti-inflammatory and immunosuppressive, Mol. Ther., 13 (2006) 289-300.
[39] K. Yuyama, H. Sun, S. Sakai, S. Mitsutake, M. Okada, H. Tahara, J. Furukawa, N. Fujitani, Y. Shinohara, Y. Igarashi, Decreased amyloid-beta pathologies by intracerebral loading of glycosphingolipid-enriched exosomes in Alzheimer model mice, J. Biol. Chem., 289 (2014) 24488-24498.
[40] K.J. Kelly, J. Zhang, L. Han, M. Kamocka, C. Miller, V.H. Gattone, 2nd, J.H. Dominguez, Improved Structure and Function in Autosomal Recessive Polycystic Rat Kidneys with Renal Tubular Cell Therapy, PLoS One, 10 (2015) e0131677.
[41] A. Zomer, C. Maynard, F.J. Verweij, A. Kamermans, R. Schafer, E. Beerling, R.M. Schiffelers, E. de Wit, J. Berenguer, S.I. Ellenbroek, T. Wurdinger, D.M. Pegtel, J. van Rheenen, In Vivo imaging reveals extracellular vesicle-mediated phenocopying of metastatic behavior, Cell, 161 (2015) 1046-1057.
[42] D. Fitzner, M. Schnaars, D. van Rossum, G. Krishnamoorthy, P. Dibaj, M. Bakhti, T. Regen, U.K. Hanisch, M. Simons, Selective transfer of exosomes from oligodendrocytes to microglia by macropinocytosis, J. Cell Sci., 124 (2011) 447-458.
[43] J. Van Deun, P. Mestdagh, R. Sormunen, V. Cocquyt, K. Vermaelen, J. Vandesompele, M. Bracke, O. De Wever, A. Hendrix, The impact of disparate isolation methods for extracellular vesicles on downstream RNA profiling, J Extracell Vesicles, 3 (2014) 24858.
[44] S. Rana, S. Yue, D. Stadel, M. Zoller, Toward tailored exosomes: the exosomal tetraspanin web contributes to target cell selection, Int. J. Biochem. Cell Biol., 44 (2012) 1574-1584.
[45] E.J. van der Vlist, E.N. Nolte-'t Hoen, W. Stoorvogel, G.J. Arkesteijn, M.H. Wauben, Fluorescent labeling of nano-sized vesicles released by cells and subsequent quantitative and qualitative analysis by high-resolution flow cytometry, Nat. Protoc., 7 (2012) 1311-1326.
[46] D.M. Pegtel, K. Cosmopoulos, D.A. Thorley-Lawson, M.A. van Eijndhoven, E.S. Hopmans, J.L. Lindenberg, T.D. de Gruijl, T. Wurdinger, J.M. Middeldorp, Functional delivery of viral miRNAs via exosomes, Proc. Natl. Acad. Sci. U. S. A., 107 (2010) 6328-6333.
[47] H. Vallhov, C. Gutzeit, S.M. Johansson, N. Nagy, M. Paul, Q. Li, S. Friend, T.C. George, E. Klein, A. Scheynius, S. Gabrielsson, Exosomes containing glycoprotein 350 released by EBV-transformed B cells selectively target B cells through CD21 and block EBV infection in vitro, J. Immunol., 186 (2011) 73-82.
[48] J. Webber, A. Clayton, How pure are your vesicles?, J Extracell Vesicles, 2 (2013) 19861.

[49] H. Deschout, T. Martens, D. Vercauteren, K. Remaut, J. Demeester, S.C. De Smedt, K. Neyts, K. Braeckmans, Correlation of dual colour single particle trajectories for improved detection and analysis of interactions in living cells, Int J Mol Sci, 14 (2013) 16485-16514.
[50] E. Willms, H.J. Johansson, I. Mager, Y. Lee, K.E. Blomberg, M. Sadik, A. Alaarg, C.I. Smith, J. Lehtio, S. El Andaloussi, M.J. Wood, P. Vader, Cells release subpopulations of exosomes with distinct molecular and biological properties, Sci. Rep., 6 (2016) 22519.
[51] M.S. Yee, D.V. Pavitt, T. Tan, S. Venkatesan, I.F. Godsland, W. Richmond, D.G. Johnston, Lipoprotein separation in a novel iodixanol density gradient, for composition, density, and phenotype analysis, J. Lipid Res., 49 (2008) 1364-1371.
[52] M. Moenner, E. Hatzi, J. Badet, Secretion of ribonucleases by normal and immortalized cells grown in serum-free culture conditions, In Vitro Cell. Dev. Biol. Anim., 33 (1997) 553-561.
[53] K.W. Witwer, E.I. Buzas, L.T. Bemis, A. Bora, C. Lasser, J. Lotvall, E.N. Nolte-'t Hoen, M.G. Piper, S. Sivaraman, J. Skog, C. Thery, M.H. Wauben, F. Hochberg, Standardization of sample collection, isolation and analysis methods in extracellular vesicle research, J Extracell Vesicles, 2 (2013) 20360.
[54] H. Kalra, C.G. Adda, M. Liem, C.S. Ang, A. Mechler, R.J. Simpson, M.D. Hulett, S. Mathivanan, Comparative proteomics evaluation of plasma exosome isolation techniques and assessment of the stability of exosomes in normal human blood plasma, Proteomics, 13 (2013) 3354-3364.
[55] B. Strobel, F.D. Miller, W. Rist, T. Lamla, Comparative Analysis of Cesium Chloride- and Iodixanol-Based Purification of Recombinant Adeno-Associated Viral Vectors for Preclinical Applications, Hum Gene Ther Methods, 26 (2015) 147-157.
[56] SBI System Biosciences, Exo-Glow™ Tracking Labels, URL: https://www.systembio.com/downloads/Exo-Glow-prod-sheet.pdf (2014).
[57] R.J. Lobb, M. Becker, S.W. Wen, C.S. Wong, A.P. Wiegmans, A. Leimgruber, A. Moller, Optimized exosome isolation protocol for cell culture supernatant and human plasma, J Extracell Vesicles, 4 (2015) 27031.
[58] A.N. Boing, E. van der Pol, A.E. Grootemaat, F.A. Coumans, A. Sturk, R. Nieuwland, Single-step isolation of extracellular vesicles by size-exclusion chromatography, J Extracell Vesicles, 3 (2014) 23430.
[59] C.P. Lai, E.Y. Kim, C.E. Badr, R. Weissleder, T.R. Mempel, B.A. Tannous, X.O. Breakefield, Visualization and tracking of tumour extracellular vesicle delivery and RNA translation using multiplexed reporters, Nat. Commun., 6 (2015) 7029.
[60] A. Suetsugu, K. Honma, S. Saji, H. Moriwaki, T. Ochiya, R.M. Hoffman, Imaging exosome transfer from breast cancer cells to stroma at metastatic sites in orthotopic nude-mouse models, Adv Drug Deliv Rev, 65 (2013) 383-390.
[61] W. Heusermann, J. Hean, D. Trojer, E. Steib, S. von Bueren, A. Graff-Meyer, C. Genoud, K. Martin, N. Pizzato, J. Voshol, D.V. Morrissey, S.E. Andaloussi, M.J. Wood, N.C. Meisner-Kober, Exosomes surf on filopodia to enter cells at endocytic hot spots, traffic within endosomes, and are targeted to the ER, J. Cell Biol., 213 (2016) 173-184.
[62] H. Dewitte, S. Van Lint, C. Heirman, K. Thielemans, S.C. De Smedt, K. Breckpot, I. Lentacker, The potential of antigen and TriMix sonoporation using mRNA-loaded microbubbles for ultrasound-triggered cancer immunotherapy, J. Control. Release, 194 (2014) 28-36.

Supporting information

The experiments represented in **figure S1** were conducted in the context of EV-based immunotherapy using tumor-derived EVs. In this respect the goal was to load EVs with toll-like receptor (TLR) agonists, in this case monophosphoryl lipid A (MPLA; a TLR4 agonist). The data are presented in this chapter as they illustrate the ability of size exclusion chromatography (SEC) to wash away non-incorporated amphiphilic molecules. The graph indicates the amount of MPLA (expressed as MPLA-induced dendritic cell maturation by virtue of CD86 expression) that was retained after the indicated purification strategies (i.e. UC or SEC). A single UC step is not sufficient to wash away free MPLA as is evident from the high amount of maturation induced in the absence of EVs. An additional UC washing step already deprived a large fraction of the non-incorporated MPLA, yet is not sufficient to inhibit all maturation. SEC on the other hand was able to completely abrogate MPLA-induced maturation in the absence of EVs. When EVs are present, MPLA is incorporated in the EV membrane and MPLA-loaded EVs are able to induce DC maturation. The DC isolation protocol, culture conditions and CD86 expression assay were conducted according to ref. [62].

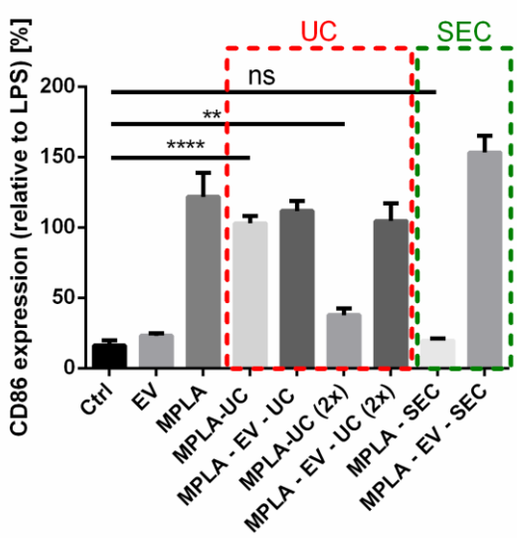

Figure S1. Associating an amphiphilic components (i.e. MPLA) to EVs requires sufficient stringent purification protocols to wash away non-incorporated molecules. Mouse bone marrow-derived dendritic cells (DC) were incubated (overnight) with EVs, MPLA (1 µg/ml; Avanti polar lipids), MPLA washed by UC (70 minutes – 120 000 g), MPLA incubated with B16F10-derived EVs (1 µg MPLA per 10 µg EV) for 1h at 37°C followed by an UC wash, MPLA washed 2x by UC, MPLA incubated with EVs and washed 2x by UC, flow-through of MPLA over a commercially available SEC column (Exosome Spin Columns; Invitrogen) or flow-through of MPLA incubated with EVs over a SEC column. After incubation, the expression of CD86 (a marker for DC maturation) was evaluated using flow cytometry and expressed relative to the CD86 expression induced by *Escherichia coli* derived lipopolysaccharide (LPS; 1 µg/ml). The data are represented as mean ± SD (n=3).

4

Comparing exosome-like vesicles with liposomes for the functional cellular delivery of small RNAs

A manuscript of this chapter is published as:

Stephan Stremersch[1], Roosmarijn E. Vandenbroucke[2,3], Elien Van Wonterghem[2,3], An Hendrix[4], Stefaan C. De Smedt[1,$], Koen Raemdonck[1,$]. Comparing exosome-like vesicles with liposomes for the functional cellular delivery of small RNAs. *J. Control. Release,* 232 (2016) 51-61.

[1]Laboratory of General Biochemistry and Physical Pharmacy, Ghent University, Ghent, Belgium
[2]Inflammation Research Center, VIB, Ghent, Belgium
[3]Department of Biomedical Molecular Biology, Ghent University, Ghent, Belgium
[4]Laboratory of Experimental Cancer Research, Ghent University Hospital, Ghent, Belgium
[$]Equal last author contribution

Chapter 4: ToC

Abstract

Exosome-like vesicles (ELVs) play an important role in intercellular communication by acting as natural carriers for biomolecule transfer between cells. This unique feature rationalizes their exploitation as bio-inspired drug delivery systems. However, the therapeutic application of ELVs is hampered by the lack of efficient and reproducible drug loading methods, in particular for therapeutic macromolecules. To overcome this limitation, we present a generic method to attach siRNA to the surface of isolated ELVs by means of a cholesterol anchor. Despite a feasible uptake in both a dendritic and lung epithelial cell line, B16F10- and JAWSII-derived ELVs were unable to functionally deliver the associated small RNAs, neither exogenous cholesterol-conjugated siRNA nor endogenous miRNA derived from the melanoma producer cell. The latter results were confirmed both for purified ELVs and ELVs delivered *via* a transwell® co-culture set-up. In contrast, simple anionic fusogenic liposomes were able to induce a marked siRNA-mediated gene knockdown under equal experimental conditions, both indicating successful cytosolic delivery of surface-bound cholesterol-conjugated siRNA and further underscoring the incapacity of the here evaluated ELVs to guide cytosolic delivery of small RNAs. In conclusion, we demonstrate that a more in-depth understanding of the biomolecular delivery mechanism and specificity is required before ELVs can be envisioned as a generic siRNA carrier.

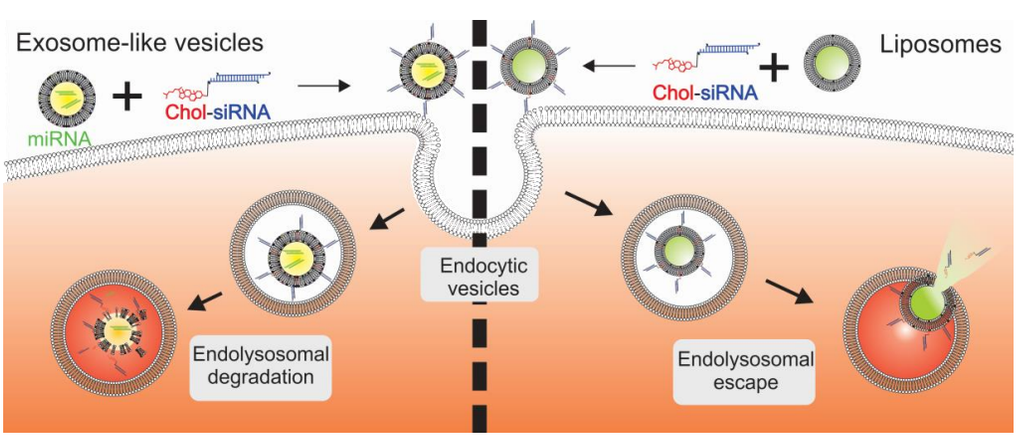

Schematic representation of the intracellular fate of RNAi-based therapeutics after delivery by exosome-like vesicles and CHEMS:DOPE liposomes.

1. Introduction

As already highlighted in **chapter 1** and **2**, extracellular vesicles (EVs) are being intensively explored as bio-inspired drug delivery vehicles [1, 2]. Yet an efficient loading strategy for macromolecular drugs is still missing. In **chapter 3**, we also showed the importance of an adequate purification strategy to prevent experimental misconceptions due to co-isolation of non-EV components. In this respect, density gradient purification appeared a valuable technique to obtain high-purity EV isolates. This technique focusses on EVs with a specific buoyant density typically attributed to exosomes [3]. Nonetheless, also ectosomes (partially) float at this density, consequently leading to a mixture of both vesicle types. Additionally, exosomes and ectosomes share many physicochemical characteristics, and selective markers to discriminate both vesicle types are currently lacking [3, 4]. Therefore, we will use the term exosome-like vesicles (ELVs) throughout the next two chapters to indicate EVs purified by a density gradient protocol [4, 5].

The role of ELVs as a waste disposal mechanism to maintain cellular homeostasis has long been recognized [6]. Nonetheless, their involvement in intercellular communication, thus contribution to many physiological and pathological processes, has only recently been appreciated [7]. The ability of ELVs to functionally transfer biomolecules (lipids, proteins, nucleic acids) to recipient cells evoked a surge of interest within the drug delivery community to exploit ELVs as delivery systems, e.g. to enhance the cellular delivery of therapeutic nucleic acids like siRNA and miRNA [8]. Such small RNA-based therapeutics harbor great promise because of their ability to selectively silence disease-causing genes [9]. Delivery of siRNA across cellular barriers is typically facilitated by synthetic polymer- or lipid-based nanomedicines [10]. Unfortunately, such delivery systems often fail to merge biocompatibility and efficacy [11]. Owing to both their endogenous nature as well as their intrinsic physiological activity and cell transfection properties, ELVs could be regarded as a bio-inspired alternative for siRNA delivery.

When envisioning ELVs as nucleic acid delivery systems, one of the most important issues to address is the feasibility of loading them with nucleic acids of interest. As mentioned previously, ELVs share important physicochemical features with synthetic liposomes, i.e. a (phospho)lipid bilayer that encloses an aqueous lumen [12]. However, in contrast to liposomes, ELVs are not optimally suited for encapsulating exogenous hydrophilic macromolecules. To date, different loading strategies have been explored which can largely be categorized in pre- (during ELV biogenesis) and post- (after ELV isolation) formation loading methods [13]. In a pre-formation loading approach, the endogenous cell machinery for RNA sorting in ELVs is exploited. Several studies evaluated the feasibility of transfecting cells with high concentrations of small RNAs,

followed by their ELV-mediated secretion in the extracellular fluid [14-16]. However, as the mechanisms for RNA sorting in ELVs are not yet fully understood [17-20], such a loading approach is difficult to control and rather inefficient [13, 21, 22]. A valuable alternative might be a post-formation loading approach. In this respect, two distinct methods have been previously reported. Employing a commercial fusogenic lipofection reagent to transfer complexed siRNA to purified ELVs requires cumbersome additional purification steps and might drastically alter the original vesicle composition [23]. A second, more widely-adopted approach involves loading of siRNA into ELVs through electroporation [23-25]. However, as thoroughly investigated and discussed in **chapter 2** we have strong doubts regarding the efficiency and validity of this approach [26]. Considering the above, alternative methods to load ELVs with hydrophilic macromolecular drugs like siRNA are required to evaluate their drug delivery potential. In this chapter we envisage a distinct post-formation loading method based on the insertion of a lipid-modified siRNA [27] in the vesicular membrane of isolated ELVs.

Here, we successfully demonstrated the association of cholesterol-modified siRNA with ELVs from both a melanoma and a monocyte/dendritic cell (DC) line and assessed their siRNA delivery potential in distinct target cells. In addition, given the structural analogy between ELVs and liposomes [12, 28], which have been widely investigated as drug delivery carriers, we also aimed to compare the ELV-mediated siRNA delivery efficiency with state-of-the-art anionic fusogenic liposomes by employing the same loading approach. This is of pivotal importance to truly assess the efficacy with which ELVs transfect cells. Finally, we also evaluated the cellular delivery of endogenously encapsulated miRNAs by melanoma ELVs.

2. Experimental section

2.1. Cell lines and culture conditions

The JAWSII cell line (ATCC® CRL-11904™) is composed of immortalized DCs and monocytes and was cultured in RPMI 1640 (Invitrogen) supplemented with 2 mM L-glutamine (Gibco), 10 % fetal bovine serum (FBS, Hyclone™), 0.05 mM 2-mercaptoethanol (Invitrogen), 100 U/ml penicillin, 100 µg/ml streptomycin (Gibco), 1 mM sodium pyruvate (Gibco) and 5 ng/ml murine GM-CSF (PeproTech). B16F10 melanoma cells (ATCC® CRL-6475™) cells and H1299 non-small-cell lung carcinoma cells (ATCC® CRL-5803™) were cultured in Dulbecco's Modified Eagle Medium (DMEM) (Gibco) supplemented with 2 mM L-glutamine, 10 % FBS, 1 mM sodium pyruvate (Gibco) and 100 U/ml penicillin, 100 µg/ml streptomycin. H1299_eGFP cells stably

express the enhanced green fluorescent protein (eGFP) [29]. All cells were grown in a humidified atmosphere containing 5 % CO_2 at 37 °C.

Prior to ELV purification, the cells were washed with phosphate buffered saline (PBS) (Invitrogen) and incubated for 24h in vesicle-depleted medium after which the thus obtained conditioned cell medium was harvested for ELV purification. To prepare vesicle-depleted medium, cell culture medium was ultrafiltrated through a 300 kDa filter (Millipore) using an Amicon® stirred cell (Millipore) under nitrogen pressure [30]. Cell viability, at the moment of medium harvesting, was determined by means of 0.4 % Trypan blue (Sigma-Aldrich) staining. The cell viability was always higher than 95 %.

2.2. ELV purification, concentration measurements and fluorescent labeling

ELVs were purified from conditioned cell medium by differential centrifugation followed by density gradient ultracentrifugation (UC). Conditioned cell medium was centrifuged for 10 minutes at 300 g and 10 minutes at 3 000 g (Heraeus Multifuge 1S-R). Next, the supernatant was concentrated by ultrafiltration using a 30 kDa filter (Millipore) in an Amicon® stirred cell (Millipore) under nitrogen pressure. Next, the concentrated sample was centrifuged at 10 000 g for 15 minutes using a SW55ti rotor in a L8-M Beckman ultracentrifuge. One milliliter of this concentrated cell medium was placed on top of an iodixanol (OptiPrep™, Axis-Shield) density gradient. The gradient was produced according to the manufacturer's instruction. Briefly, by careful placing 1 ml of different iodixanol dilutions (12.5 %, 25 %, 37.5 % and 50 % in 250 mM sucrose, 1 mM EDTA, 10 mM Tris-HCl buffer; pH = 7.4) underneath one another, a density gradient was created. The gradient was subjected to UC at 150 000 g for 15h. Next, the gradient was fractionated per 0.5 ml, diluted 10x in PBS and centrifuged again at 150 000 g for 150 minutes. Finally, the pellet was washed and resuspended in PBS. The average density of the individual fractions was determined by diluting each fraction 2x in ultrapure water (Milli-q, Millipore) and measuring the absorbance at 340 nm using an EnVision plate reader (PerkinElmer).

To estimate the amount of ELVs obtained after purification, a Pierce™ BCA protein determination assay (ThermoFisher Scientific) was executed as described by the manufacturer. Alternatively, the absolute amount of particles was determined by scattering-based single particle tracking using a NanoSight LM10 device equipped with the NTA 2.3 software (Malvern).

ELVs were fluorescently labeled using the membrane permeable Syto RNASelect dye (Molecular Probes, Invitrogen) to label the RNA present inside the vesicles. The labeling was done as described by the manufacturer. Briefly, purified ELVs were incubated at 37°C for 20 minutes with Syto RNASelect at a final concentration of 40 µM. Next, the remaining free dye was removed by an exosome spin column (MWCO 3 000,

Invitrogen). Alternatively, ELVs (diluted in Diluent C) were incubated with 4 µM PKH26 (Sigma-Aldrich) for 15 minutes at 37°C. Non-associated dye was washed away using UC (120 000 g for 70 minutes in Diluent C). The quality of the fluorescent labeling was assessed each time by fluorescent single particle tracking using a swept field confocal microscope (LiveScan SFC, Nikon) equipped with a 100x oil immersion lens (NA 1.40; Nikon). The ELVs were irradiated with 488 nm (Syto RNASelect) or 561 nm (PKH26) laser light and movies of labeled ELVs were recorded with an iXon Ultra EMCCD camera (Andor) as an additional control to verify the labeling quality.

2.3. Immunoblotting

Cells were washed 3 times with ice cold PBS and detached by means of a cell scraper. Next, the cells were centrifuged for 5 minutes at 300 g and resuspended in RIPA buffer (Sigma-Aldrich) supplemented with MS-SAFE protease and phosphatase inhibitor cocktail (Sigma-Aldrich), vortexed and placed on ice for 30 minutes. Next, the cells were sonicated 3x 5 minutes with vortexing in between. Finally, the cell lysate was centrifuged at 13 000 g for 5 minutes and the supernatant retained for further analysis. The same protocol was used for ELV sample preparation.

The protein concentration was determined using the DC™ protein assay (Bio-Rad) according to the manufacturer's instructions. Samples were diluted in 2x laemmli buffer (Bio-Rad) with or without 5 % 2-mercaptoethanol (Sigma-Aldrich) and heated to 95°C for 5 minutes. Equal protein amounts (10 µg per lane) were loaded on a 10 % mini-protean TGX precasted gel (Bio-Rad). Proteins were separated at 100 V for 60 minutes in running buffer (Tris-Glycine-SDS). Blotting was done on an immune-blot® PVDF 0.2 µm membrane (Bio-Rad) at 100 V for 90 minutes in blotting buffer (Tris-Glycin-Methanol-SDS). The blot was blocked for 1h in PBS supplemented with 3 % bovine serum albumin (BSA) and 0.1 % Tween20. Next, primary antibodies (**table 1**) were incubated overnight at 4°C under gentle shaking. The secondary antibody, conjugated to horseradish peroxidase (HRP), was incubated for 1h at room temperature. Visualization was done using the SuperSignal West Dura chemiluminescent kit (ThermoFisher Scientific) in combination with a VersaDoc™ imaging system (Bio-Rad).

Table 1. Antibodies used for immunoblotting.

Target	Dilution	Supplier	Cat.#	Reducing conditions [2]
CD81	1:1 000	LS biosciences Inc.	LS-C108453	No
CD63	1:500	Tebu-bio	GTX37555	No
β-actin	1:1 000	Cell Signaling Techn.	#4970	Yes
Hsp70	1:1 000	LS biosciences Inc.	LS-C24142	Yes
Calnexin	1:1 000	LS biosciences Inc.	LS-C92236	Both
GM130	1:14 000	LS biosciences Inc.	LS-C49800	Both
Rabbit IgG[1]	1:50 000	Millipore	AP307P	/

[1]The secondary antibody is conjugated to horseradish peroxidase; [2]Samples are mixed with 5 % 2-mercaptoethanol and heated at 95°C for 5 minutes

2.4. siRNA

An overview of the siRNAs used throughout this chapter can be found in **table S1**. Chol-siRNA was fluorescently labeled by means of a covalent coupling with Cy5 dye using a *Label* IT *siRNA tracker* kit (Mirus Bio). The coupling was done according to the manufacturer's instructions. The final RNA concentration was determined with a Nanodrop 2000c (ThermoFisher Scientific) spectrophotometer at 260 nm.

2.5. Preparation of CHEMS:DOPE liposomes

1,2-dioleoyl-*sn*-glycero-3-phosphoethanolamine (DOPE) and 3β-hydroxy-5-cholestene 3-hemisuccinate (CHEMS) were purchased from Avanti Polar Lipids and Sigma-Aldrich, respectively. Both lipids were dissolved in chloroform and mixed in a molar ratio of 6:4 (DOPE:CHEMS) in a round-bottomed flask. A lipid film was formed by evaporating the chloroform under vacuum at 45°C. The film was hydrated in PBS reaching a final lipid concentration of 10 mg/ml. To obtain uniformly sized liposomes, the lipids were extruded 21x through a 200 nm pore sized polycarbonate filter (Whatmann). Concentration measurements were done by scattering-based single particle tracking using a NanoSight LM10 device equipped with the NTA 2.3 software (Malvern). The zeta potential was measured in 4-(2-hydroxyethyl)-1-piperazineethanesulfonic acid (HEPES) buffer (20 mM, pH 7.4) by dynamic light scattering using a Zetasizer Nano ZS (Malvern), equipped with Dispersion Technology Software. Liposomes were labeled using PKH26 (Sigma-Aldrich) as described for ELV labeling using the same particle to dye ratio.

2.6. Gel retention assay

Semi-quantification of (chol-)siRNA retained by ELV/liposomes was assessed by polyacrylamide gel electrophoresis (PAGE). Ten pmol (chol-)siRNA was incubated with

increasing amounts of ELVs/liposomes for 1h at 37°C in PBS after which 10x gel loading solution (AM8556, Ambion) was added to each sample. The samples were loaded onto a 20 % non-denaturing polyacrylamide gel prepared in TBE buffer (10.8 g/L Tris-base, 5.5 g/L boric acid, 0.74 g/L $Na_4EDTA.2H_2O$). Electrophoresis was performed at 120 V during 40 minutes. (Chol-)siRNA was visualized by SYBR Green II RNA staining solution (Molecular Probes, Invitrogen) for 45 minutes at room temperature followed by UV transillumination and gel photography. Band density of the free migrating nucleic acids was determined by ImageJ software and compared to non-retained siRNA to estimate the amount of vesicle associated siRNA.

2.7. Anti-CD63 dynabeads® assay

Qualitative association between ELVs and Cy5-labeled (chol-)siRNA was assessed by bead-based flow cytometry. Chol-siRNA loaded ELVs were subjected to UC (120 000 g – 70 minutes) to wash away non-incorporated chol-siRNA. The respective sample and controls were mixed with anti-CD63 coated dynabeads® (Invitrogen) and incubated overnight at 4°C under gentle mixing (HulaMixer®, ThermoFisher Scientific) according to the manufacturer's protocol. Bead-associated Cy5 fluorescence was quantified by flow cytometry (FACSCalibur; BD Biosciences).

2.8. Density gradient co-localization

Binding of Cy5-labeled chol-siRNA to isolated ELVs was additionally assessed by density gradient co-localization. To this end, 30 µg ELVs were incubated with 20 pmol Cy5-labeled chol-siRNA for 1h at 37°C. Next, the samples were placed on top of an iodixanol-based density gradient and centrifuged for 15h at 150 000 g. Fractions of 0.5 ml were carefully pipetted and analyzed for Cy5 fluorescence on an EnVision plate reader (PerkinElmer). The same procedure was followed to assess the buoyant density of free chol-siRNA and Syto RNASelect labeled ELVs and represented as normalized fluorescence intensity per fraction.

2.9. Quantification of ELV and chol-siRNA cell uptake by flow cytometry

JAWSII cells (4.5×10^4 cells per cm^2) and H1299 cells (1.36×10^4 cells per cm^2) were seeded in a 24-well plate and allowed to attach overnight. The next day, cells were incubated with the respective fluorescently labeled sample in vesicle-depleted cell medium. After 24h, the sample containing medium was removed and the cells were washed with PBS before being detached by means of 0.05 % Trypsin/EDTA (Gibco). Next, the detached cells were washed twice in flow buffer (1 % BSA, 0.1 % sodium azide in PBS) and analyzed for chol-siRNA (Cy5) or ELV (Syto RNASelect, PKH26 or CD63-GFP) fluorescence by flow cytometry (CytoFLEX; Beckman Coulter or FACSCalibur; BD Biosciences) recording at least 10 000 events per sample.

2.10. Visualization of ELV and liposome cell uptake by confocal microscopy

JAWSII cells (4.5 x 10^4 cells per cm^2) and H1299 cells (1.36 x 10^4 cells per cm^2) were plated in 8-well Lab-Tek Chamber Slides (ThermoFisher Scientific). The next day, cells were incubated with Cy5-labeled chol-siRNA, chol-siRNA loaded liposomes, chol-siRNA loaded ELVs in vesicle-depleted cell medium. After 24h incubation, the samples were removed and the cells were washed thrice with PBS after which the cells were incubated with fresh cell medium supplemented with Hoechst 33342 (ThermoFisher Scientific) for 30 minutes at 37°C. Finally, cells were again washed with PBS and fixed using 4 % paraformaldehyde for 15 minutes at room temperature. Images were recorded using a Nikon C1si confocal scanning module installed on a motorized TE2000-E inverted microscope (22 µm slit; Nikon), equipped with a 100x oil immersion objective lens (NA 1.4; Nikon), using a 405 nm, 561 nm and 637 nm laser line for the excitation of Hoechst 33342, PKH26 and Cy5, respectively.

2.11. CD45 gene silencing assay

JAWSII cells were plated in a 24-well plate (4.5 x 10^4 cells per cm^2) and allowed to attach overnight. Next, the cell medium was replaced by vesicle-depleted medium. The cells were co-cultured for 24h with chol-siRNA loaded ELVs, chol-siRNA loaded liposomes or chol-siRNA at the indicated concentration. Next, the cells were washed with PBS and cultured for an additional day in full cell medium before being detached with non-enzymatic cell dissociation buffer (Sigma-Aldrich), incubated for 5 minutes in blocking buffer (5 % FBS in PBS) and stained with PerCP-Cy™5.5 Rat Anti-Mouse CD45 (BD biosciences) for 45 minutes on ice. After 3 washing steps, fluorescence was monitored *via* flow cytometry (FACSCalibur, BD Biosciences). A minimum of 10 000 events was recorded for each sample. For the long term silencing conditions, the cells were detached and replated at half the cell density every two days. Lipofectamine RNAiMAX (Invitrogen) was used as a positive control following the manufacturer's instructions. The chol-siCD45 induced gene silencing was normalized to CD45 expression obtained after identical treatment of the cells with chol-siCTRL.

2.12. eGFP gene silencing assay

H1299_eGFP cells were plated in a 24-well plate (1.36 x 10^4 cells per cm^2) and allowed to attach overnight. Next, the cell medium was replaced by vesicle-depleted medium. The same samples and procedures were followed as indicated above **(section 2.11)**. To quantify eGFP expression, cells were detached using 0.05 % trypsin/EDTA (Gibco), washed with flow buffer and eGFP fluorescence was monitored (MFI of ≥ 10 000 events) using a flow cytometer (CytoFLEX, Beckman Coulter). The chol-siGFP induced eGFP silencing was normalized to eGFP expression after identical treatment with chol-siCTRL.

2.13. Chloroquine treatment to induce endolysosomal destabilization

H1299_eGFP cells were plated in a 24-well plate (1.36 x 10^4 cells per cm^2) and allowed to attach overnight. Next, the cell medium was replaced by vesicle-depleted medium and incubated with chol-siRNA (50 nM) loaded ELVs. After 6h, the samples were removed and replaced by cell medium in the absence or presence of 40 μM chloroquine (Sigma-Aldrich) for 12h after which the medium was again replaced by fresh culture medium. After an additional 24h of incubation, eGFP expression was quantified *via* flow cytometry (CytoFLEX, Beckman Coulter). The chol-siGFP induced eGFP silencing was normalized to eGFP expression obtained after identical treatment with chol-siCTRL.

2.14. Luciferase assay using purified ELVs

JAWSII and H1299_eGFP cells were transfected using lipofectamine 2000 (Invitrogen) in 24-well plates (4.5 x 10^4 or 1.36 x 10^4 cells per cm^2, respectively) with 100 ng or 20 ng of a reporter plasmid containing a *HMGA2* 3'UTR wt luciferase (Luc-wt) (Addgene plasmid # 14785) or *HMGA2* 3'UTR m7 luciferase (Luc-m7) (Addgene plasmid # 14788) insert, respectively [31]. Twenty-four hours later, cells were incubated with 3.3 x 10^{11} B16F10-derived ELV per ml for 24h in vesicle-depleted cell medium or with miRIDIAN mmu-*let-7a* miRNA mimic (GE Dharmacon) complexed to lipofectamine RNAiMAX (Invitrogen) in OptiMEM reduced serum medium for 4h. Next, the cells were washed with PBS and cultured for an additional day before analyzing the luciferase expression using the *Renilla* luciferase assay (Promega) with a GloMax®96 microplate luminometer (Promega) according to the manufacturer's instructions. The *HMGA2* 3'UTR wt luciferase expression is normalized to the *HMGA2* 3'UTR m7 luciferase expression for each condition.

2.15. Luciferase assay using a transwell® insert

H1299_eGFP cells were plated in a 6-well plate (1.36 x 10^4 cells per cm^2) and transfected with a luc-wt or luc-m7 plasmid using lipofectamine 2000 as stated above. An equal number of B16F10 melanoma cells were plated in a transwell® permeable support (24 mm – pore size 3 μm, Corning) and co-cultured with the plasmid-transfected H1299_eGFP cells. After 3 days, luciferase expression in H1299_eGFP cells was evaluated as described above.

2.16. Statistical analysis

Statistical analysis was done with GraphPad Prism 6 (GraphPad Software). Comparing multiple conditions was done using an ANOVA-test followed by a Tukey post hoc test. Direct comparison between two conditions was done using a student t-test. A p-value <

0.05 is regarded as statistically significant. The degree of significance is indicated using ns ($p \geq 0.05$), *($p < 0.05$), **($p < 0.01$), ***($p < 0.001$), ****($p < 0.0001$).

3. Results

3.1. Isolation and characterization of ELVs

Exosome-like vesicles (ELVs) were isolated from conditioned cell medium of B16F10 melanoma cells and JAWSII immortalized monocyte/DC using an iodixanol-based density gradient UC protocol [32]. After overnight UC, the density gradient was collected in 10 fractions. Screening each fraction by immunoblotting revealed that especially fractions 4 to 6 contained the conventional ELV-associated markers (Hsp70, CD63, β-actin and CD81) (**figure 1A**). Fractions 4 and 5 are typically selected for further experiments as they show the highest vesicle purity, expressed as the ratio of vesicle number to total protein concentration (**figure 1B**) [33]. Moreover, the density of these fractions lies around 1.12 to 1.14 g/ml and corresponds to the typical buoyant density of exosomes [34]. Furthermore, these fractions are devoid of protein markers for intracellular organelles (i.e. calnexin and GM130 for the endoplasmic reticulum and Golgi apparatus, respectively) providing additional evidence of the isolate's purity (**figure 1C**). Pooling of both ELV fractions and collection *via* UC revealed a size distribution ranging from 30 to 300 nm as measured with single particle tracking, comparable to the size distribution observed by cryo-TEM imaging and corroborating earlier reports in the literature (**figure 1D and 1E**) [32].

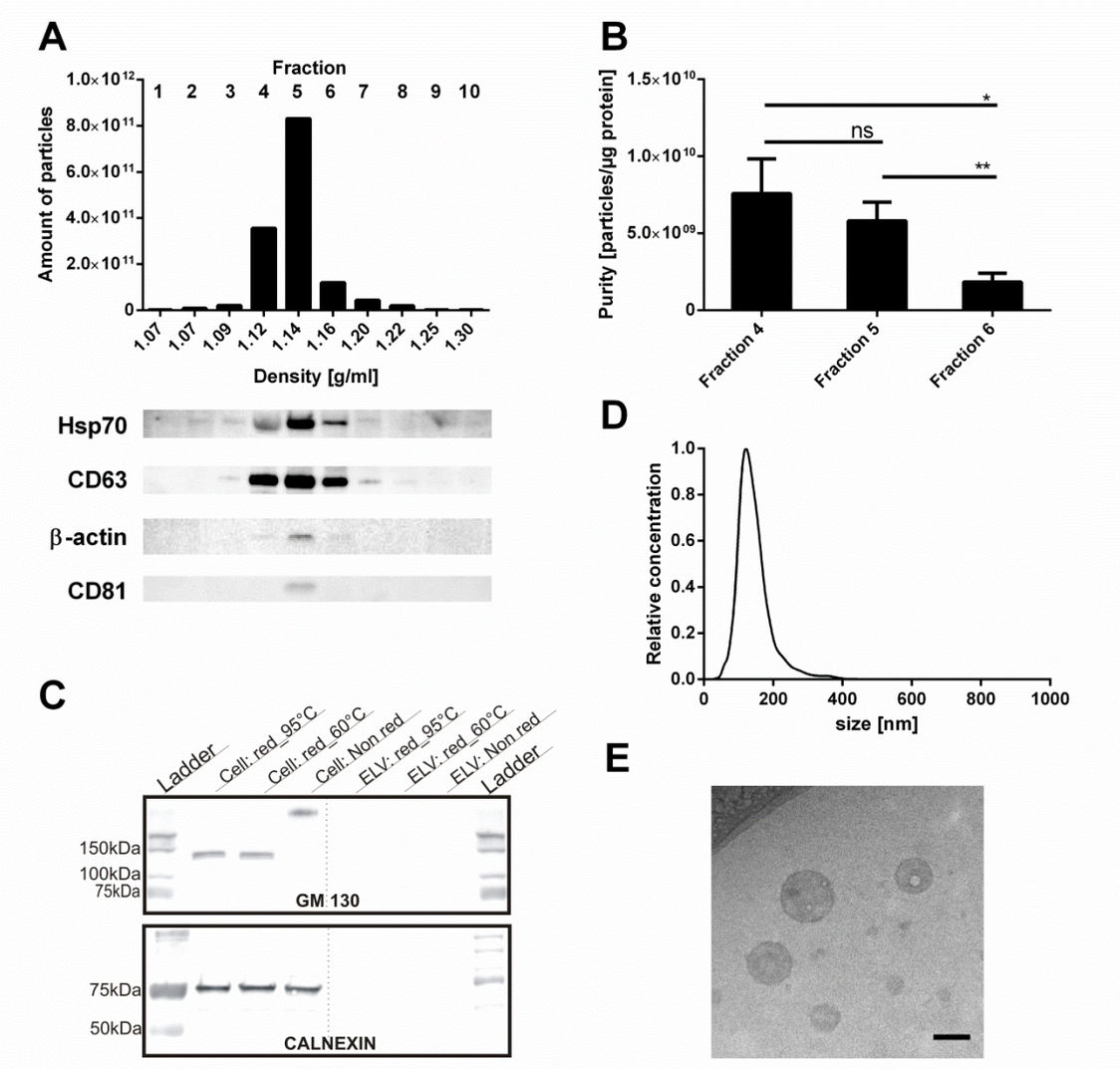

Figure 1. Characterization of gradient-purified B16F10-derived ELVs. [A] Amount of particles and ELV-associated protein markers in the different fractions of an iodixanol density gradient after overnight UC. [B] Quantification of the vesicle purity of the ELV-containing fractions (i.e. 4, 5 and 6) by measuring the amount of particles by scattering-based single particle tracking relative to the protein concentration. The purity is thus expressed as particles/µg total protein as suggested by ref. [33]. The data is represented as mean ± SD (n=4). [C] Immunoblotting of GM130 and calnexin on 10 µg B16F10 cell- and 10 µg ELV-lysate (derived from fraction 4 and 5) under (non-) reducing (red) conditions. [D] Representative size distribution of density gradient purified B16F10-derived ELVs measured by scattering-based single particle tracking. [E] Cryo-TEM image of density gradient purified B16F10 ELVs. The scale bar indicates 100 nm.

3.2. Cholesterol conjugation enables siRNA association to isolated ELVs

In analogy with earlier reports on lipophilic siRNAs [27], we used cholesterol-conjugated siRNA (chol-siRNA) to allow post-formation loading of ELVs *via* insertion into the outer vesicular membrane. In addition, we opted for a nuclease resistant siRNA backbone (**table S1**) to avoid siRNA degradation by possible nuclease contamination of the

sample (**chapter 3**). To validate that chol-siRNA was indeed bound to the ELVs, three distinct yet complementary methods were used. First, efficient binding of chol-siRNA to B16F10 ELVs was demonstrated by a polyacrylamide gel retention assay (**figure 2A**). Semi-quantitative analysis of the unbound chol-siRNA revealed that 15 µg of ELVs, which relates to ~6.6 x 10^{10} vesicles, is able to bind ~80 % of the 10 pmol chol-siRNA (i.e. ~8 pmol), corresponding with about 73 chol-siRNA molecules per vesicle. Importantly, unconjugated siRNA did not show any interaction with the ELVs under the given experimental conditions, implying that the cholesterol moiety governs the siRNA-ELV association (**figure S1**). Second, an immunobead-based assay was developed in which we aimed to exploit the CD63 expression on (a subpopulation of) ELVs [32, 35]. To this end, purified ELVs were mixed with Cy5-labeled chol-siRNA prior to incubation with anti-CD63-functionalized micrometer beads. Flow cytometric analysis of the beads indeed revealed a clear Cy5 fluorescent signal indicating the association of chol-siRNA to CD63-positive ELVs (**figure 2B**). Finally, a mixture of ELVs and Cy5-labeled chol-siRNA was placed on top of an iodixanol density gradient and subjected to overnight UC. **Figure 2C** shows that the chol-siRNA largely migrates to the fraction that corresponding with the typical buoyant density of the ELVs, of which the presence was additionally confirmed by immunoblotting. In contrast, in the absence of ELVs, the labeled chol-siRNA could only be detected in the upper, low density fractions (**figure S2**). Moreover, the profile of the ELV-associated chol-siRNA corresponds well with the fluorescence profile obtained by tracking ELVs labeled with Syto RNASelect, i.e. a membrane-permeable RNA dye (**figure 2C**) [36]. Altogether, these data clearly indicate the anchoring of siRNA to the surface of isolated ELVs through insertion of the cholesteryl moiety in the vesicular membrane. The same method for loading ELVs with siRNA proved also feasible for vesicles derived from a JAWSII cell line (**figure S3**).

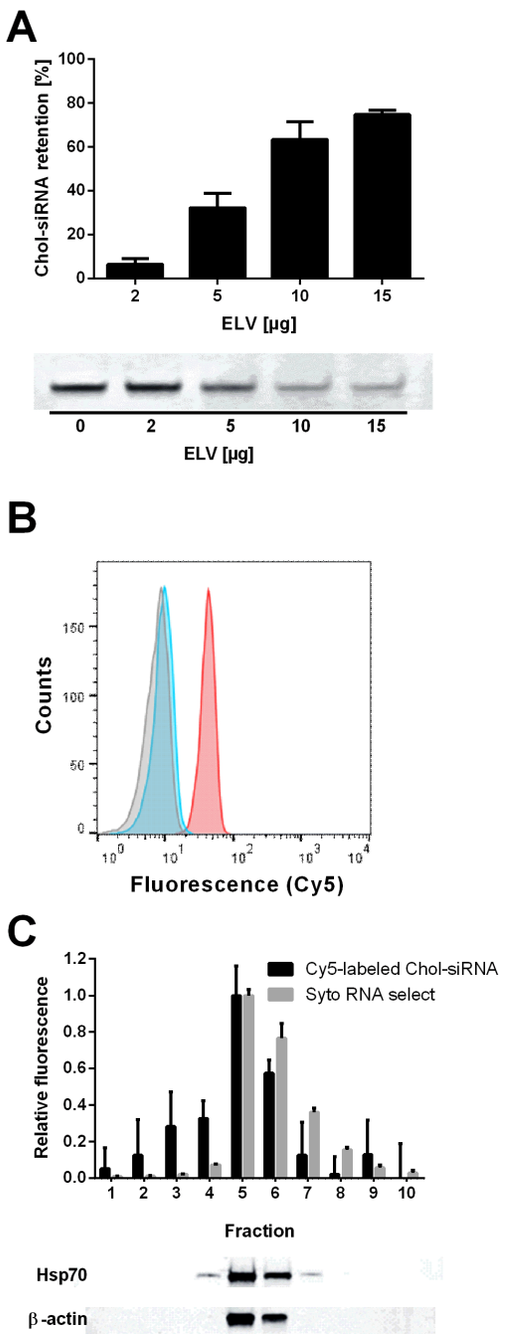

Figure 2. Chol-siRNA association to B16F10-derived ELVs. [A] Percentage of chol-siRNA retained by the ELVs after 1h incubation at 37°C, as analyzed *via* a polyacrylamide gel retention assay. In each well 10 pmol chol-siRNA, mixed with the indicated amount of ELVs, was loaded. The data are represented as mean ± SD (n=3). The free, migrating chol-siRNA bands of one representative PAGE experiment is displayed underneath. [B] Flow cytometry of anti-CD63 coated dynabeads® incubated with Cy5-labeled chol-siRNA loaded ELVs (red), ELVs (gray) and Cy5-labeled chol-siRNA without ELVs (blue), respectively. [C] Relative Cy5 (chol-siRNA-associated) and Syto RNASelect (ELV-associated) fluorescence intensity for each density fraction after laying chol-siRNA loaded ELVs and Syto RNASelect labeled ELVs on top of an iodixanol density gradient after overnight UC. Data is represented as mean ± SD (n=3). For each fraction immunoblotting against ELV markers (Hsp70 and β-actin) was done to confirm the presence of the vesicles.

3.3. Anionic fusogenic liposomes outperform ELVs in chol-siRNA delivery *in vitro*

Having optimized ELVs as carriers for chol-siRNA, we next sought to evaluate their potential to deliver the associated siRNA into recipient cells, including JAWSII (a monocytic cell line) and H1299 (a non-small cell lung carcinoma cell line). In addition, we aimed to compare the siRNA delivery efficiency of the ELVs with synthetic fusogenic liposomes, equipped with a pH-sensitive fusogenic lipid (i.e. cholesteryl hemisuccinate; CHEMS) [37]. These liposomes displayed comparable physicochemical characteristics as the ELVs, i.e. a negative surface charge and a comparable size distribution and polydispersity (**figure 3A and 3B**) and equally have the ability to retain chol-siRNA (**figure 3C**).

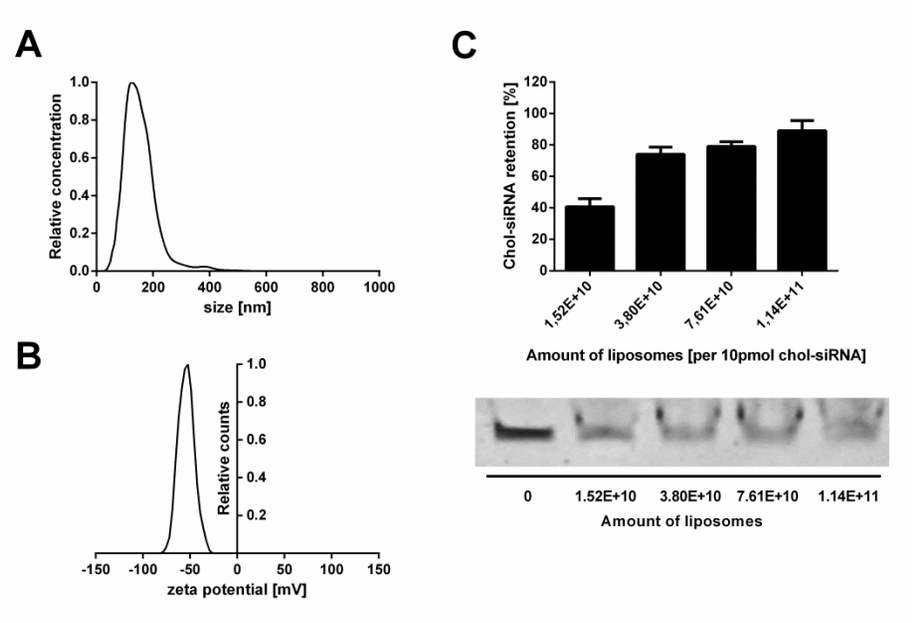

Figure 3. CHEMS:DOPE liposome characterization and chol-siRNA loading. [A] Size distribution and [B] zeta potential of CHEMS:DOPE (4:6 molar ratio) liposomes determined by scattering-based single particle tracking and dynamic light scattering, respectively. [C] Chol-siRNA retention by CHEMS:DOPE liposomes evaluated using a polyacrylamide gel retention assay. The quantification was performed in triplicate, of which one representative gel is shown underneath the graph. For each well 10 pmol chol-siRNA, incubated with the indicated amount of liposomes, was loaded. Data is represented as mean ± SD (n=3).

First, cellular uptake of B16F10-derived ELVs and CHEMS:DOPE liposomes by two recipient cells (i.e. JAWSII and H1299) was verified by confocal fluorescence microscopy and flow cytometry, for which the ELV and liposomal membrane was stained by insertion of the lipophilic dye PKH26 (**figure S4A and S4B**). To confirm that the observed ELV uptake was not an artifact of the here used labeling approach (i.e. lipophilic insertion in the membrane), ELVs were fluorescently labeled by different

approaches. To this end, B16F10 cells were stably transfected with a CD63-GFP plasmid (see supporting information). ELVs purified from this cell line were equipped with a GFP-tag which allowed to track the uptake in JAWSII cells (**figure S4C**). Another approach using a membrane permeable, RNA binding dye (Syto RNASelect) again corroborates the ELV (and its endogenous RNA cargo) internalization by JAWSII cells [38, 39]. Furthermore, comparing the uptake of chol-siRNA loaded ELVs to unloaded ELVs showed no influence of the chol-siRNA cargo on the vesicle uptake by JAWSII cells (**figure S5**).

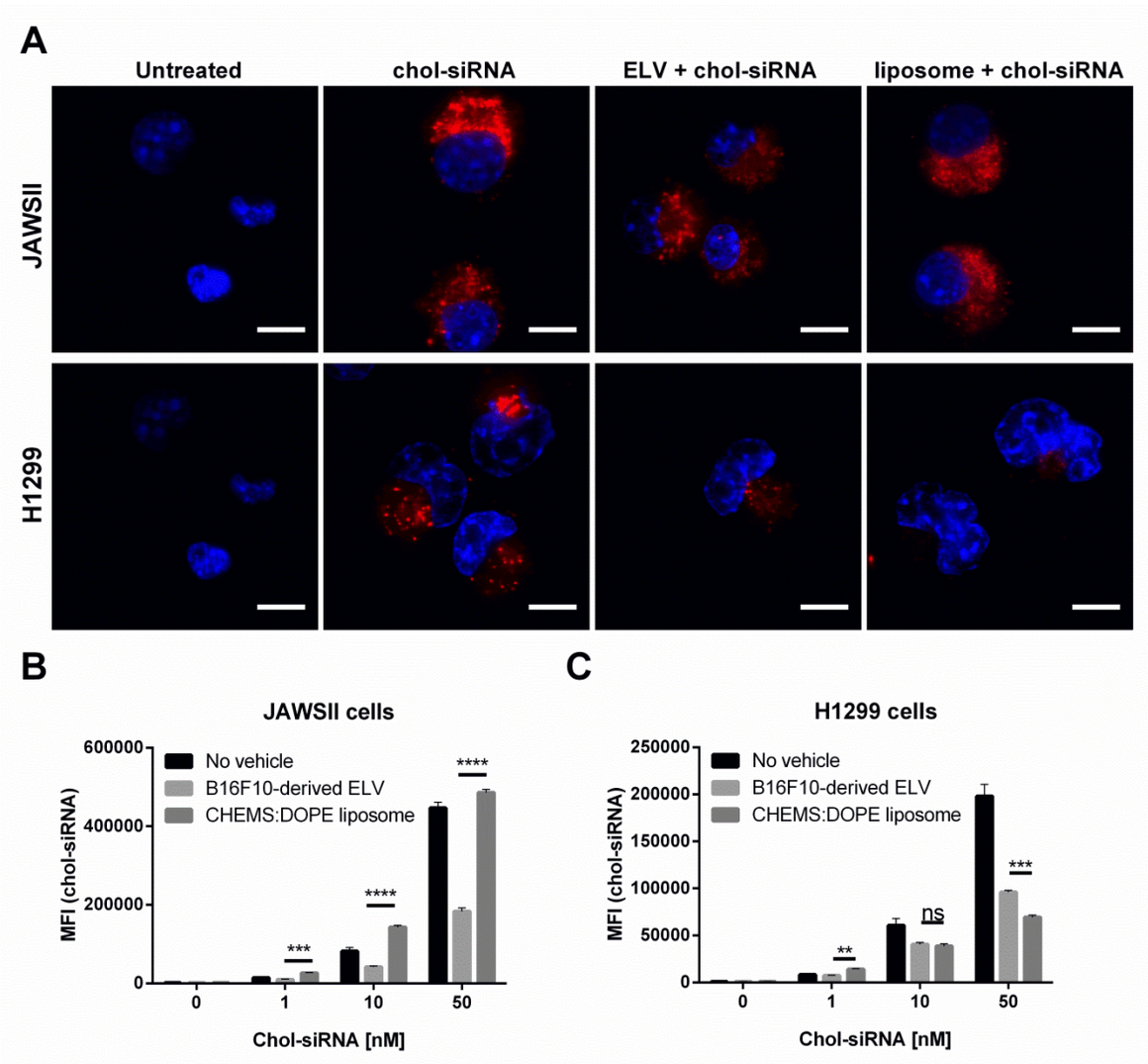

Figure 4. Chol-siRNA delivery by B16F10-derived ELVs and CHEMS:DOPE liposomes. [A] Confocal imaging of Cy5-labeled (red) chol-siRNA (free, associated to ELVs or liposomes) uptake (50 nM) by JAWSII and H1299 cells (nucleus labeled with Hoechst 33342 (blue)) after 24h incubation. The scale bar indicates 10 µm. Quantification by flow cytometry of Cy5-labeled chol-siRNA uptake by [B] JAWSII and [C] H1299 cells after 24h incubation. The ratio vehicle:chol-siRNA (i.e. 6.6 x 10^9 particles/pmol chol-siRNA) was constant for each condition. MFI is the mean fluorescent intensity is expressed in arbitrary units. The error bars represent the SD (n=3).

In agreement with the cellular uptake observed for the B16F10 ELVs and CHEMS:DOPE liposomes, the associated chol-siRNA was likewise internalized by both JAWSII and H1299 cells (**figure 4**). When quantifying and comparing the chol-siRNA delivery potential of ELVs and liposomes between both recipient cells, it is clear that JAWSII cells take up more chol-siRNA compared to H1299 cells. This corresponds with the vesicle uptake microscopy data (**figure S4A**) and is likely related to the phagocytic activity of the monocytic/DC cell line. The fact that phagocytic cells tend to take up more ELVs is also in agreement with previous reports [40]. Additionally, the fusogenic liposomes deliver noticeably more chol-siRNA compared to ELVs in JAWSII cells whereas in H1299 cells the opposite holds true for the highest chol-siRNA concentration tested, though less pronounced (**figure 4B and 4C**). Overall, both cell lines effectively internalize both ELVs and anionic liposomes with their respective cargo, yet to a different extent.

Next, the functional *in vitro* siRNA delivery capacity of the chol-siRNA loaded ELVs was evaluated, again using different ELV producer-recipient cell pairs. Chol-siRNA delivery *via* B16F10-derived ELVs was assessed in JAWSII cells and in H1299_eGFP cells, using the CD45 pan-leucocyte marker (chol-siCD45) and eGFP (chol-siGFP) as a model gene target, respectively [29]. Additionally, JAWSII-derived ELVs were tested for autocrine siRNA delivery in recipient JAWSII cells. Remarkably, comparing equal particle and siRNA concentrations, only the fusogenic liposomes were able to downregulate gene expression both in JAWSII (CD45) and H1299_eGFP (GFP) target cells (**figure 5A and 5B**). This inability of B16F10-derived ELVs to functionally deliver the associated chol-siRNA was also confirmed as a function of time (up to 6 days after co-incubation) (**figure 5C**). Comparable results were obtained for ELVs derived from the JAWSII cells (**figure S6**). Of note, 50 nM chol-siRNA in the absence of a nanocarrier induced a moderate knockdown in H1299_eGFP cells, yet following association to ELVs this effect was largely lost (**figure 5B**). This not only shows the inability of ELVs to functionally deliver chol-siRNA when attached to the vesicular surface, it also provides indirect proof of the stability of the association between ELVs and the chol-siRNA under the reported culturing conditions. Interestingly, when incubating the ELV-transfected cells with chloroquine, an endosomolytic compound [41], the eGFP expression was silenced to a comparable level as achieved by the CHEMS:DOPE liposomes (**figure 6**)**.**

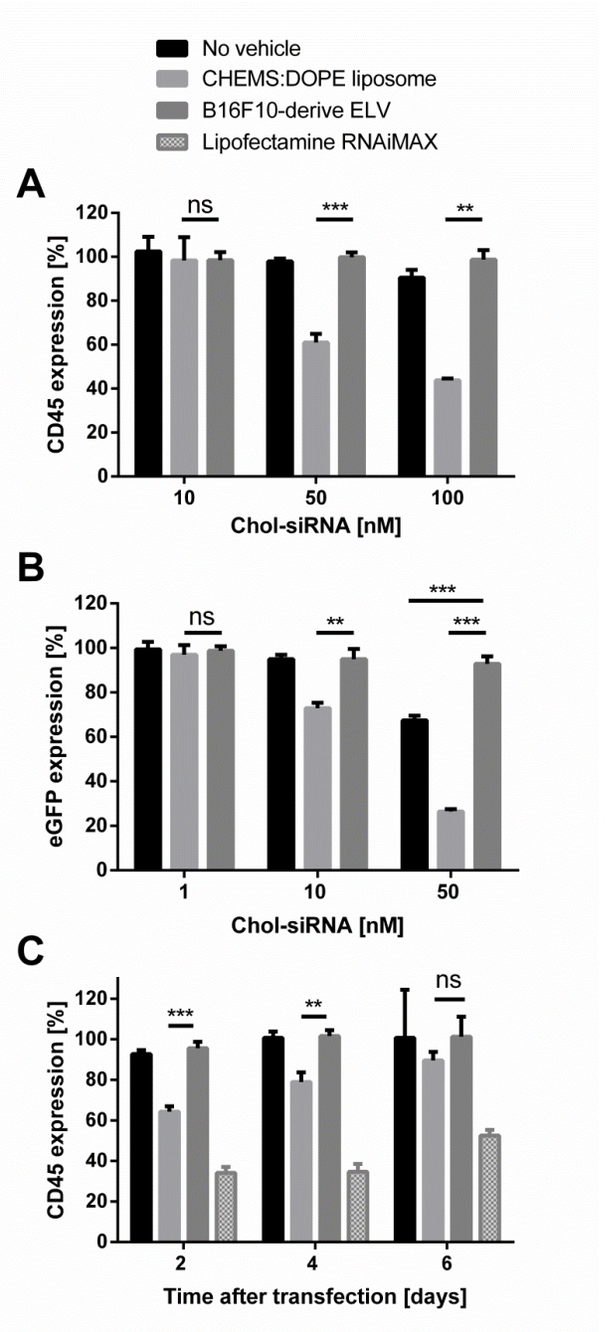

Figure 5. Chol-siRNA mediated gene silencing. Target gene expression in [A] JAWSII cells and [B] H1299_eGFP cells after treatment (24h) with chol-siRNA, chol-siRNA associated to liposomes or chol-siRNA associated to ELVs. The target gene expression levels following chol-siCD45 or chol-siGFP treatment are normalized to the levels obtained with chol-siCTRL. [C] Time-dependent CD45 knockdown in JAWSII cells after treatment with chol-siRNA (50 nM), chol-siRNA loaded liposomes, chol-siRNA loaded ELVs or chol-siRNA complexed to lipofectamine RNAiMAX. The ratio vesicle:chol-siRNA (i.e. 6.6 x 10^9 particles/pmol chol-siRNA) was constant for each condition. All data are represented as mean ± SD (n=3).

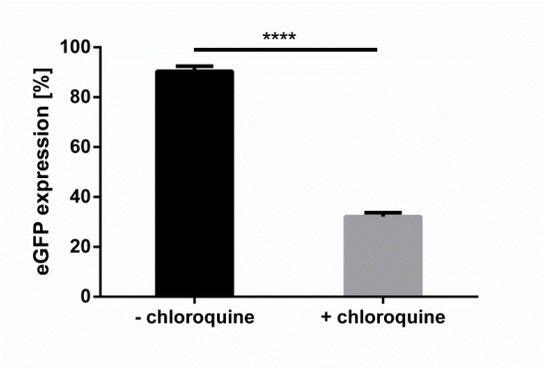

Figure 6. Chol-siRNA loaded ELVs induce gene silencing in the presence of an endosomolytic agent. eGFP expression in H1299_eGFP cells after treatment with chol-siRNA associated to B16F10-derived ELVs followed by overnight incubation with cell culture medium supplemented with or without chloroquine. The target gene expression levels following chol-siGFP treatment are normalized to the levels obtained with chol-siCTRL.

3.4. Functional delivery of endogenous ELV-associated miRNA

Many reports in the literature describe functional ELV-mediated transfer of endogenous miRNAs [7, 42]. Therefore, we aimed to assess if the isolated B16F10 ELVs can successfully deliver their miRNA payload to recipient cells. To identify the predominant miRNA species in melanoma ELVs, a high-throughput miRNA analysis was performed (**figure S7**). For the most abundant miRNAs (**figure 7**), experimentally validated target transcripts were determined using the miRTarBase database (**table 2**) [43]. Next, the expression of different selected target transcripts was assessed *via* RT-qPCR in JAWSII recipient cells after 24h incubation with the purified B16F10-derived ELVs. High mobility group A2 mRNA (*HMGA2*) is a known target for *mmu-let-7a* miRNA, which is abundantly present in B16F10 ELVs (**figure 7**). The latter seemed to enable functional *let-7a* delivery into JAWSII cells, judging from the two-fold knockdown of *HMGA2* transcripts. However, and more importantly, when summarizing data for all selected transcripts, no clear trend could be observed as some validated targets show significant downregulation as a function of the ELV concentration (e.g. *HMGA2, MTPN, Ywhaz*), while others show no response (e.g. *Bcl2, CDC25c, ARL2*) or are even markedly upregulated (e.g. *MAPK14*) (**figure 8 and S8**). We anticipate that the lack of a negative control to account for vesicle induced off-target effects substantially impedes unambiguous analysis of miRNA-related target transcript silencing.

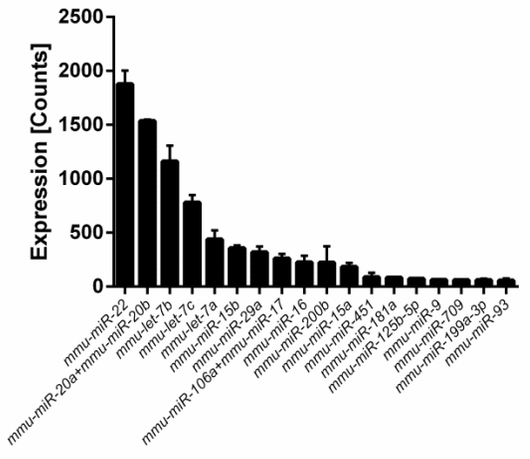

Figure 7. Overview of the most abundant miRNAs present in B16F10-derived ELVs determined by the nCounter miRNA expression assay. Error bars indicate the SD of 2 technical replicates of 3 pooled biological replicates.

Table 2. Experimentally validated targets of a selection of the most abundant miRNA present in B16F10-derived ELVs [43].

miRNA	Gene Target
mmu-miR-22	*Ywhaz*
mmu-miR-15a	*Bcl2*
mmu-miR-22	*IRF8*
mmu-let-7a	*HMGA2*
mmu-let-7b	*Bsg*
mmu-miR-15b; mmu-miR-16	*Arl2*
mmu-miR-181a; mmu-miR-9; mmu-miR-199-3p	*Runx1*
mmu-miR-29a	*Dnmt3*
mmu-miR-20a+20b; mmu-miR-17	*MAPK14*
mmu-miR-22	*ERBB3*
mmu-miR-106a; mmu-miR-17; mmu-miR-93; mmu-miR-125b-5p	*Stat3*
mmu-let-7c; mmu-miR-451; mmu-miR-709	*Myc*
mmu-miR-22	*CDC25c*
mmu-let-7b	*MTPN*

To resolve this issue, a luciferase reporter assay was utilized for *mmu-let-7a*, using a reporter construct that contains the 3'-UTR of the murine *HMGA2* transcript that is appended to the *renilla* luciferase ORF [31]. Luciferase expression is compared with a control plasmid containing a *HMGA2* 3'-UTR in which all seven *mmu-let7* binding sites are mutated. Both JAWSII and H1299_eGFP cells were transfected with the above mentioned plasmids, prior to 24h co-culture with B16F10 ELVs. As JAWSII cells appeared to be highly refractory to plasmid transfection with commercial lipofection reagents (i.e. lipofectamine 2000, data not shown), we focused on the H1299_eGFP cells as recipient cells. The same amount of B16F10 ELVs as used in the previous

experiments was incubated for 24h with H1299_eGFP cells, which were transfected beforehand with the luciferase reporter plasmids. In contrast to the *HMGA2* knockdown previously observed, no significant downregulation of luciferase activity, normalized to the mutated control construct, was measured. As a positive control for this assay, a commercial lipofection reagent (i.e. lipofectamine RNAiMAX) was employed to complex synthetic *mmu-let-7a* and was incubated with the plasmid-transfected H1299_eGFP cells, which resulted in a significant reduction in luciferase expression (**figure 9A**).

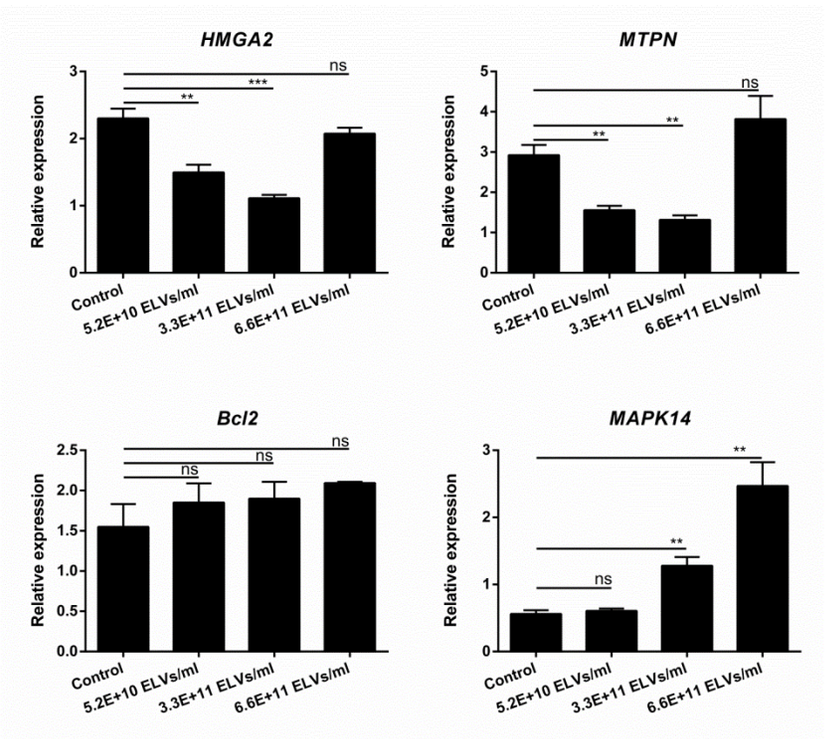

Figure 8. Alternations in gene expression profile in JAWSII cells after treatment with B16F10-derived EVs. Relative expression levels (determined by RT-qPCR) of the indicated genes in JAWSII cells after incubation for 24h with B16F10-derived ELVs. The data are reported as mean ± SD (n=4).

Additionally, in an attempt to more closely mimic the *in vivo* situation and to circumvent the harsh ELV purification protocol, a cell co-culture experiment using a transwell® insert (pore size: 3 µm) was initiated. B16F10 cells were seeded in the transwell® insert while an equal amount of plasmid-transfected H1299_eGFP cells were seeded at the bottom. Using this set-up, transport of CD63-positive B16F10 ELVs through the pores of the insert and subsequent internalization by H1299_eGFP cells in the bottom compartment was confirmed by using a B16F10 melanoma cell line stably expressing CD63-GFP (**figure S9**). Following 3 days of co-culture, luciferase expression in the recipient cells was evaluated. However, also *via* this experimental set-up, no functional ELV-mediated transfer of *mmu-let-7a* could be observed (**figure 9B**).

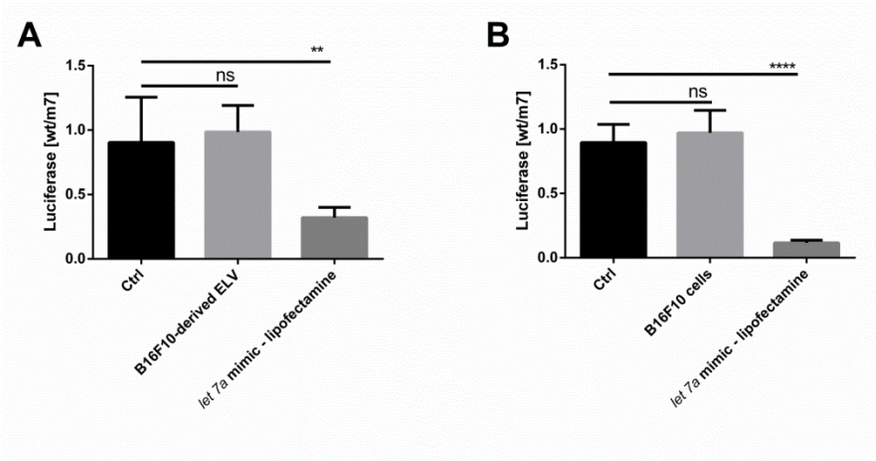

Figure 9. *Mmu-let-7a* responsive luciferase reporter assay. Relative luciferase signal (expressed as wt- over m7-signal) in plasmid-transfected H1299_eGFP cells after co-culture with [A] purified B16F10-derived ELVs (24h incubation; 3.3 x 10^{11} particles/ml), [B] B16F10 cells seeded in a transwell insert (72h incubation; cell ratio 1:1) or synthetic *mmu-let-7a* miRNA complexed to lipofectamine RNAiMAX (4h). The data are reported as mean ± SD (n=4).

4. Discussion

In this chapter an efficient and reproducible post-formation loading method is reported to associate exogenous siRNA to ELVs by means of a cholesterol anchor. ELVs are under intensive scrutiny for biomedical purposes, e.g. as diagnostic biomarkers and as bio-inspired drug delivery nanocarriers [44]. The latter application originates from the observation that ELVs can efficiently transfer biomolecules (nucleic acids, lipids or proteins) from a donor cell to a recipient cell, thus playing an important role in intercellular communication [7]. However, to exploit ELVs as a generic nanocarrier for delivery of exogenous macromolecular therapeutics, like siRNA, novel methods to efficiently load isolated ELVs with the siRNA of interest are highly sought after [12, 13, 28].

Wolfrum *et al.* previously observed that cholesterol-modified siRNA (chol-siRNA) efficiently binds to lipoprotein particles such as high and low density lipoprotein (HDL and LDL), which are rich in phospholipids and cholesterol, leading to functional siRNA delivery *in vitro* and *in vivo* [27, 45]. Interestingly, cancer-derived EVs likewise contain high amounts of phospholipids and cholesterol [46]. Hence, we anticipated that a cholesterol moiety (covalently linked to the siRNA of interest) could similarly insert in the outer leaflet of the ELV lipid bilayer, thus anchoring the siRNA to the surface of the vesicles. Analogous to HDL and LDL, we could clearly demonstrate efficient binding of chol-siRNA to the surface of B16F10- and JAWSII-derived ELVs using three complementary methodologies. Of note, the ELVs were purified according to state-of-the-art density gradient UC and subjected to extensive characterization prior to use, in

order to minimize chol-siRNA binding to co-purified protein aggregates. We also opted to work with stabilized siRNAs to exclude possible nuclease degradation during sample preparation (**chapter 3**). Moreover, all cell experiments were performed in vesicle-depleted cell culture medium (see materials and methods) to avoid interference of ELVs or lipoproteins endogenously present in bovine serum.

ELVs express a variety of membrane proteins on their surface, some of which engage in specific receptor-ligand interactions with recipient cells [47, 48]. The molecular expression pattern of ELVs is believed to be producer cell-type dependent and, in concert with the type of recipient cell, this further defines the nature of the receptor-ligand binding as well as the downstream cellular processing. Hence, as the choice of producer-recipient cell pair might influence the efficiency of ELV-mediated biomolecule transfer, we selected cancer cell-DC [49, 50], DC-DC [51, 52] and cancer cell-cancer cell [53-56] pairs, previously reported in the literature as enabling a functional, ELV-based intercellular interactions. Moreover, Parolini *et al.* showed that melanoma-derived ELVs display considerable fusogenic properties, further contributing to the hypothesis that melanoma-derived ELVs are efficient toward intercellular biomolecule delivery [54]. Although our results indicate efficient binding of chol-siRNA to isolated ELVs and efficient cellular delivery of the siRNA cargo to recipient cells, we could not observe a significant knockdown effect. In contrast, employing the exact same protocol to formulate chol-siRNA in synthetic liposomes did result in significant downregulation of target gene expression. Here, we opted for CHEMS:DOPE liposomes as a control liposomal formulation as it mimics the most important physicochemical features of ELVs, i.e. size, surface charge and fusogenic properties. Thus, a simple synthetic anionic and fusogenic liposomal formulation clearly outperformed our purified ELVs in terms of functional chol-siRNA delivery.

We hypothesized that this inability to functionally deliver the chol-siRNA might pertain to the cargo location. Our post-formation loading approach inherently confines the siRNA on the surface of the vesicle while endogenously the miRNA cargo is likely present inside the ELV lumen [7]. We therefore sought to investigate if the B16F10-derived ELVs were able to functionally deliver their natural miRNA payload. The miRNA profile obtained for B16F10-derived vesicles is comparable to what was previously reported for highly metastatic cancer cell lines, e.g. a strong abundance of the *let-7* miRNA family [57, 58]. Following exposure of JAWSII cells with the isolated melanoma ELVs, the change in expression levels of validated target transcripts for the most abundant ELV miRNAs varied substantially. Indeed, where the expression of some target genes was significantly suppressed, the expression of others remained unaffected or was even markedly upregulated. These inconsistent results can likely be explained by unspecific effects induced by ELV-associated lipids and proteins which might influence the

expression profile of the examined target gene [59, 60]. Therefore, we subsequently implemented a luciferase reporter assay in the recipient cells. Using a luciferase reporter construct containing the wild-type 3'-UTR of the *HMGA2* transcript (a documented *let-7* target) and a mutated 3'-UTR with all seven *let-7* binding sites disrupted through point mutations, allowed us to account for ELV-induced unspecific effects [31]. Nonetheless, also when using this more controllable reporter assay, once more no functional miRNA delivery was observed with the melanoma ELVs. Finally, this was also confirmed in a transwell® set-up, more closely resembling the *in vivo* intercellular ELV transfer, through which we could verify that the multi-step ELV purification protocol was likely not responsible for the inability of the ELV to functionally deliver their miRNA cargo.

Given the absence of a miRNA/siRNA induced knockdown effect despite efficient ELV cellular uptake, it is reasonable to speculate that under the given experimental conditions the ELV content remains trapped in the endolysosomal degradation pathway. In addition, a too stable anchoring of the chol-siRNA into the ELV membrane might hamper activation of the RNAi machinery. Efficient escape from the endosome is a major barrier for cellular delivery of macromolecular therapeutics in general [61]. Importantly, when adding a lysosomotropic agent (i.e. chloroquine) that induces endolysosomal membrane perturbation [41] to H1299_eGFP cells, previously transfected with chol-siRNA loaded ELVs, a marked eGFP knockdown could be observed. This result supports the hypothesis that endolysosomal entrapment is the predominant barrier that limits ELV-mediated small RNA delivery. To date it still remains an open question why under some conditions ELVs are very efficient in delivering their cargo [51] while in other circumstances they appear dysfunctional. Yet it is conceivable that, due to the vast complexity of these vesicles, their functionality is restricted to a particular cell type or even cell status. The latter has already been demonstrated for viral particles, with which ELVs share many features [62, 63]. Therefore, the observations reported here cannot simply be extrapolated to other ELVs or ELV-cell interactions. Nonetheless, our results question the therapeutic value of ELVs as a universal siRNA delivery vehicle.

5. Conclusion

Overall, we could show that purified ELVs can be loaded with cholesterol-modified siRNA. The association of the siRNA on the surface of the vesicles did not interfere with their uptake by recipient cells. However, using distinct experimental set-ups and carefully selected controls, we were able to unambiguously conclude that the ELVs used in this study did not allow functional delivery of small RNAs, neither the exogenously added siRNA nor the endogenously encapsulated miRNAs. In contrast and surprisingly, simple anionic fusogenic liposomes were able to induce a marked siRNA-mediated target

gene knockdown under the same experimental conditions. Safe and efficient cellular delivery of macromolecular therapeutics requires innovative delivery technologies. ELVs have been proposed as a bio-inspired alternative for state-of-the-art synthetic nanomedicines. Despite the available reports in the literature that support this claim, the results obtained for the ELV producer-recipient cell pairs tested here imply that synthetic liposomes are still preferred [64]. Future research on ELVs should focus more on elucidating the cellular mechanisms behind successful ELV-mediated transfection before generic adoption of natural ELVs or synthetic ELV mimicking nanomedicines as a competing drug delivery tool can be considered.

Acknowledgements

REV and EVW have executed the nCounter miRNA profiling and qPCR assays. We thank Dr. Pieter Baatsen from the EM-facility (VIB-KULeuven Bio Imaging Core and Center for Human Genetics, KULeuven, Belgium) for his support with the cryo-TEM imaging and Prof. Dieter Deforce from the laboratory of Pharmaceutical Biotechnology (UGent, Belgium) for the use of the VersaDoc™ imaging system. SS and KR are doctoral and postdoctoral fellows respectively of the Research Foundation - Flanders (FWO). AH is supported by the Vlaamse Liga tegen Kanker (VLK). The support of these institutions is gratefully acknowledged.

References

[1] J.G. van den Boorn, J. Dassler, C. Coch, M. Schlee, G. Hartmann, Exosomes as nucleic acid nanocarriers, Adv Drug Deliv Rev, 65 (2013) 331-335.
[2] C. Lasser, Exosomes in diagnostic and therapeutic applications: biomarker, vaccine and RNA interference delivery vehicle, Expert Opin. Biol. Ther., 15 (2015) 103-117.
[3] C.P. Lai, X.O. Breakefield, Role of exosomes/microvesicles in the nervous system and use in emerging therapies, Front. Physiol., 3 (2012) 228.
[4] G. Raposo, W. Stoorvogel, Extracellular vesicles: exosomes, microvesicles, and friends, J. Cell Biol., 200 (2013) 373-383.
[5] L. Montermini, B. Meehan, D. Garnier, W.J. Lee, T.H. Lee, A. Guha, K. Al-Nedawi, J. Rak, Inhibition of Oncogenic Epidermal Growth Factor Receptor Kinase Triggers Release of Exosome-like Extracellular Vesicles and Impacts Their Phosphoprotein and DNA Content, J. Biol. Chem., 290 (2015) 24534-24546.
[6] R.M. Johnstone, A. Mathew, A.B. Mason, K. Teng, Exosome formation during maturation of mammalian and avian reticulocytes: evidence that exosome release is a major route for externalization of obsolete membrane proteins, J. Cell. Physiol., 147 (1991) 27-36.

[7] H. Valadi, K. Ekstrom, A. Bossios, M. Sjostrand, J.J. Lee, J.O. Lotvall, Exosome-mediated transfer of mRNAs and microRNAs is a novel mechanism of genetic exchange between cells, Nat. Cell Biol., 9 (2007) 654-U672.
[8] P. Vader, E.A. Mol, G. Pasterkamp, R.M. Schiffelers, Extracellular vesicles for drug delivery, Adv Drug Deliv Rev, in press (2016).
[9] S.L. Uprichard, The therapeutic potential of RNA interference, FEBS Lett., 579 (2005) 5996-6007.
[10] K. Raemdonck, R.E. Vandenbroucke, J. Demeester, N.N. Sanders, S.C. De Smedt, Maintaining the silence: reflections on long-term RNAi, Drug discovery today, 13 (2008) 917-931.
[11] K.B. Knudsen, H. Northeved, P.E. Kumar, A. Permin, T. Gjetting, T.L. Andresen, S. Larsen, K.M. Wegener, J. Lykkesfeldt, K. Jantzen, S. Loft, P. Moller, M. Roursgaard, In vivo toxicity of cationic micelles and liposomes, Nanomedicine, 11 (2015) 467-477.
[12] R. van der Meel, M.H. Fens, P. Vader, W.W. van Solinge, O. Eniola-Adefeso, R.M. Schiffelers, Extracellular vesicles as drug delivery systems: lessons from the liposome field, J. Control. Release, 195 (2014) 72-85.
[13] P. Vader, S.A. Kooijmans, S. Stremersch, K. Raemdonck, New considerations in the preparation of nucleic acid-loaded extracellular vesicles, Ther. Deliv., 5 (2014) 105-107.
[14] N. Kosaka, H. Iguchi, Y. Yoshioka, F. Takeshita, Y. Matsuki, T. Ochiya, Secretory mechanisms and intercellular transfer of microRNAs in living cells, J. Biol. Chem., 285 (2010) 17442-17452.
[15] S.D. Olson, A. Kambal, K. Pollock, G.M. Mitchell, H. Stewart, S. Kalomoiris, W. Cary, C. Nacey, K. Pepper, J.A. Nolta, Examination of mesenchymal stem cell-mediated RNAi transfer to Huntington's disease affected neuronal cells for reduction of huntingtin, Mol. Cell. Neurosci., 49 (2012) 271-281.
[16] Q. Pan, V. Ramakrishnaiah, S. Henry, S. Fouraschen, P.E. de Ruiter, J. Kwekkeboom, H.W. Tilanus, H.L. Janssen, L.J. van der Laan, Hepatic cell-to-cell transmission of small silencing RNA can extend the therapeutic reach of RNA interference (RNAi), Gut, 61 (2012) 1330-1339.
[17] A.O. Batagov, V.A. Kuznetsov, I.V. Kurochkin, Identification of nucleotide patterns enriched in secreted RNAs as putative cis-acting elements targeting them to exosome nano-vesicles, BMC Genomics, 12 Suppl 3 (2011) S18.
[18] D. Koppers-Lalic, M. Hackenberg, I.V. Bijnsdorp, M.A. van Eijndhoven, P. Sadek, D. Sie, N. Zini, J.M. Middeldorp, B. Ylstra, R.X. de Menezes, T. Wurdinger, G.A. Meijer, D.M. Pegtel, Nontemplated nucleotide additions distinguish the small RNA composition in cells from exosomes, Cell reports, 8 (2014) 1649-1658.
[19] C. Villarroya-Beltri, C. Gutierrez-Vazquez, F. Sanchez-Cabo, D. Perez-Hernandez, J. Vazquez, N. Martin-Cofreces, D.J. Martinez-Herrera, A. Pascual-Montano, M. Mittelbrunn, F. Sanchez-Madrid, Sumoylated hnRNPA2B1 controls the sorting of miRNAs into exosomes through binding to specific motifs, Nat. Commun., 4 (2013) 2980.
[20] Mario L. Squadrito, C. Baer, F. Burdet, C. Maderna, Gregor D. Gilfillan, R. Lyle, M. Ibberson, M. De Palma, Endogenous RNAs Modulate MicroRNA Sorting to Exosomes and Transfer to Acceptor Cells, Cell Reports, 8 (2014) 1432-1446.
[21] J.R. Chevillet, Q. Kang, I.K. Ruf, H.A. Briggs, L.N. Vojtech, S.M. Hughes, H.H. Cheng, J.D. Arroyo, E.K. Meredith, E.N. Gallichotte, E.L. Pogosova-Agadjanyan, C. Morrissey, D.L. Stirewalt, F. Hladik, E.Y. Yu, C.S. Higano, M. Tewari, Quantitative and stoichiometric analysis of the microRNA content of exosomes, Proc Natl Acad Sci U S A, 111 (2014) 14888-93.

[22] A. Turchinovich, L. Weiz, A. Langheinz, B. Burwinkel, Characterization of extracellular circulating microRNA, Nucleic Acids Res., 39 (2011) 7223-7233.
[23] J. Wahlgren, L.K.T. De, M. Brisslert, F. Vaziri Sani, E. Telemo, P. Sunnerhagen, H. Valadi, Plasma exosomes can deliver exogenous short interfering RNA to monocytes and lymphocytes, Nucleic Acids Res., 40 (2012) e130.
[24] L. Alvarez-Erviti, Y.Q. Seow, H.F. Yin, C. Betts, S. Lakhal, M.J.A. Wood, Delivery of siRNA to the mouse brain by systemic injection of targeted exosomes, Nat. Biotechnol., 29 (2011) 341–345.
[25] T.N. Lamichhane, R.S. Raiker, S.M. Jay, Exogenous DNA Loading into Extracellular Vesicles via Electroporation is Size-Dependent and Enables Limited Gene Delivery, Mol. Pharm., 12 (2015) 3650-3657.
[26] S.A. Kooijmans, S. Stremersch, K. Braeckmans, S.C. de Smedt, A. Hendrix, M.J. Wood, R.M. Schiffelers, K. Raemdonck, P. Vader, Electroporation-induced siRNA precipitation obscures the efficiency of siRNA loading into extracellular vesicles, J. Control. Release, 172 (2013) 229-238.
[27] C. Wolfrum, S. Shi, K.N. Jayaprakash, M. Jayaraman, G. Wang, R.K. Pandey, K.G. Rajeev, T. Nakayama, K. Charrise, E.M. Ndungo, T. Zimmermann, V. Koteliansky, M. Manoharan, M. Stoffel, Mechanisms and optimization of in vivo delivery of lipophilic siRNAs, Nat. Biotechnol., 25 (2007) 1149-1157.
[28] M. Duechler, Vehicles for Small Interfering RNA transfection: Exosomes versus Synthetic Nanocarriers, DNA and RNA Nanotechnology, (2013) 16-28.
[29] L. De Backer, K. Braeckmans, J. Demeester, S.C. De Smedt, K. Raemdonck, The influence of natural pulmonary surfactant on the efficacy of siRNA-loaded dextran nanogels, Nanomedicine, 8 (2013) 1625-1638.
[30] M.L. Heinemann, M. Ilmer, L.P. Silva, D.H. Hawke, A. Recio, M.A. Vorontsova, E. Alt, J. Vykoukal, Benchtop isolation and characterization of functional exosomes by sequential filtration, J. Chromatogr. A, 1371C (2014) 125-135.
[31] C. Mayr, M.T. Hemann, D.P. Bartel, Disrupting the pairing between let-7 and Hmga2 enhances oncogenic transformation, Science, 315 (2007) 1576-1579.
[32] J. Van Deun, P. Mestdagh, R. Sormunen, V. Cocquyt, K. Vermaelen, J. Vandesompele, M. Bracke, O. De Wever, A. Hendrix, The impact of disparate isolation methods for extracellular vesicles on downstream RNA profiling, J Extracellr Vesicles, 3 (2014) 24858.
[33] J. Webber, A. Clayton, How pure are your vesicles?, J Extracell Vesicles, 2 (2013) 19861.
[34] D.M. Pegtel, L. Peferoen, S. Amor, Extracellular vesicles as modulators of cell-to-cell communication in the healthy and diseased brain, Philos. Trans. R. Soc. Lond. B Biol. Sci., 369 (2014) 20130516.
[35] M. Logozzi, A. De Milito, L. Lugini, M. Borghi, L. Calabro, M. Spada, M. Perdicchio, M.L. Marino, C. Federici, E. Iessi, D. Brambilla, G. Venturi, F. Lozupone, M. Santinami, V. Huber, M. Maio, L. Rivoltini, S. Fais, High levels of exosomes expressing CD63 and caveolin-1 in plasma of melanoma patients, PLoS One, 4 (2009) e5219.
[36] A.M. Nicola, S. Frases, A. Casadevall, Lipophilic dye staining of Cryptococcus neoformans extracellular vesicles and capsule, Eukaryotic cell, 8 (2009) 1373-1380.
[37] S. Cho, H. Lee, J.-C. Kim, pH-dependent release property of dioleoylphosphatidyl ethanolamine liposomes, Korean J. Chem. Eng., 25 (2008) 390-393.

[38] N. Ismail, Y. Wang, D. Dakhlallah, L. Moldovan, K. Agarwal, K. Batte, P. Shah, J. Wisler, T.D. Eubank, S. Tridandapani, M.E. Paulaitis, M.G. Piper, C.B. Marsh, Macrophage microvesicles induce macrophage differentiation and miR-223 transfer, Blood, 121 (2013) 984-995.
[39] M. Li, E. Zeringer, T. Barta, J. Schageman, A. Cheng, A.V. Vlassov, Analysis of the RNA content of the exosomes derived from blood serum and urine and its potential as biomarkers, Philos. Trans. R. Soc. Lond. B Biol. Sci., 369 (2014) 20130502.
[40] D. Feng, W.L. Zhao, Y.Y. Ye, X.C. Bai, R.Q. Liu, L.F. Chang, Q. Zhou, S.F. Sui, Cellular internalization of exosomes occurs through phagocytosis, Traffic, 11 (2010) 675-687.
[41] A. El-Sayed, S. Futaki, H. Harashima, Delivery of macromolecules using arginine-rich cell-penetrating peptides: ways to overcome endosomal entrapment, The AAPS journal, 11 (2009) 13-22.
[42] D.M. Pegtel, K. Cosmopoulos, D.A. Thorley-Lawson, M.A. van Eijndhoven, E.S. Hopmans, J.L. Lindenberg, T.D. de Gruijl, T. Wurdinger, J.M. Middeldorp, Functional delivery of viral miRNAs via exosomes, Proc. Natl. Acad. Sci. U. S. A., 107 (2010) 6328-6333.
[43] S.D. Hsu, Y.T. Tseng, S. Shrestha, Y.L. Lin, A. Khaleel, C.H. Chou, C.F. Chu, H.Y. Huang, C.M. Lin, S.Y. Ho, T.Y. Jian, F.M. Lin, T.H. Chang, S.L. Weng, K.W. Liao, I.E. Liao, C.C. Liu, H.D. Huang, miRTarBase update 2014: an information resource for experimentally validated miRNA-target interactions, Nucleic Acids Res., 42 (2014) D78-85.
[44] C. Lasser, Exosomes in diagnostic and therapeutic applications: biomarker, vaccine and RNA interference delivery vehicle, Expert Opin. Biol. Ther., 15 (2015) 103-117.
[45] Y. Ding, Y. Wang, J. Zhou, X. Gu, W. Wang, C. Liu, X. Bao, C. Wang, Y. Li, Q. Zhang, Direct cytosolic siRNA delivery by reconstituted high density lipoprotein for target-specific therapy of tumor angiogenesis, Biomaterials, 35 (2014) 7214-7227.
[46] A. Llorente, T. Skotland, T. Sylvanne, D. Kauhanen, T. Rog, A. Orlowski, I. Vattulainen, K. Ekroos, K. Sandvig, Molecular lipidomics of exosomes released by PC-3 prostate cancer cells, Biochim. Biophys. Acta, 1831 (2013) 1302-1309.
[47] S. Rana, M. Zoller, Exosome target cell selection and the importance of exosomal tetraspanins: a hypothesis, Biochem. Soc. Trans., 39 (2011) 559-562.
[48] K.B. Johnsen, J.M. Gudbergsson, M.N. Skov, L. Pilgaard, T. Moos, M. Duroux, A comprehensive overview of exosomes as drug delivery vehicles — Endogenous nanocarriers for targeted cancer therapy, Biochim. Biophys. Acta – Rev on Cancer, 1846 (2014) 75-87.
[49] A. Marton, C. Vizler, E. Kusz, V. Temesfoi, Z. Szathmary, K. Nagy, Z. Szegletes, G. Varo, L. Siklos, R.L. Katona, V. Tubak, O.M. Howard, E. Duda, J. Minarovits, K. Nagy, K. Buzas, Melanoma cell-derived exosomes alter macrophage and dendritic cell functions in vitro, Immunol. Lett., 148 (2012) 34-38.
[50] S. Yu, C. Liu, K. Su, J. Wang, Y. Liu, L. Zhang, C. Li, Y. Cong, R. Kimberly, W.E. Grizzle, C. Falkson, H.G. Zhang, Tumor exosomes inhibit differentiation of bone marrow dendritic cells, J. Immunol., 178 (2007) 6867-6875.
[51] A. Montecalvo, A.T. Larregina, W.J. Shufesky, D.B. Stolz, M.L. Sullivan, J.M. Karlsson, C.J. Baty, G.A. Gibson, G. Erdos, Z. Wang, J. Milosevic, O.A. Tkacheva, S.J. Divito, R. Jordan, J. Lyons-Weiler, S.C. Watkins, A.E. Morelli, Mechanism of transfer of functional microRNAs between mouse dendritic cells via exosomes, Blood, 119 (2012) 756-766.

[52] M. Alexander, R. Hu, M.C. Runtsch, D.A. Kagele, T.L. Mosbruger, T. Tolmachova, M.C. Seabra, J.L. Round, D.M. Ward, R.M. O'Connell, Exosome-delivered microRNAs modulate the inflammatory response to endotoxin, Nat. Commun., 6 (2015) 7321.
[53] A. Zomer, C. Maynard, F.J. Verweij, A. Kamermans, R. Schafer, E. Beerling, R.M. Schiffelers, E. de Wit, J. Berenguer, S.I. Ellenbroek, T. Wurdinger, D.M. Pegtel, J. van Rheenen, In Vivo imaging reveals extracellular vesicle-mediated phenocopying of metastatic behavior, Cell, 161 (2015) 1046-1057.
[54] I. Parolini, C. Federici, C. Raggi, L. Lugini, S. Palleschi, A. De Milito, C. Coscia, E. Iessi, M. Logozzi, A. Molinari, M. Colone, M. Tatti, M. Sargiacomo, S. Fais, Microenvironmental pH is a key factor for exosome traffic in tumor cells, J. Biol. Chem., 284 (2009) 34211-34222.
[55] W.X. Chen, X.M. Liu, M.M. Lv, L. Chen, J.H. Zhao, S.L. Zhong, M.H. Ji, Q. Hu, Z. Luo, J.Z. Wu, J.H. Tang, Exosomes from drug-resistant breast cancer cells transmit chemoresistance by a horizontal transfer of microRNAs, PLoS One, 9 (2014) e95240.
[56] M.T. Le, P. Hamar, C. Guo, E. Basar, R. Perdigao-Henriques, L. Balaj, J. Lieberman, miR-200-containing extracellular vesicles promote breast cancer cell metastasis, J. Clin. Invest., 124 (2014) 5109-5128.
[57] K. Ohshima, K. Inoue, A. Fujiwara, K. Hatakeyama, K. Kanto, Y. Watanabe, K. Muramatsu, Y. Fukuda, S. Ogura, K. Yamaguchi, T. Mochizuki, Let-7 microRNA family is selectively secreted into the extracellular environment via exosomes in a metastatic gastric cancer cell line, PLoS One, 5 (2010) e13247.
[58] G. Falcone, A. Felsani, I. D'Agnano, Signaling by exosomal microRNAs in cancer, J. Exp. Clin. Cancer Res., 34 (2015) 32.
[59] I. Lazar, E. Clement, M. Ducoux-Petit, L. Denat, V. Soldan, S. Dauvillier, S. Balor, O. Burlet-Schiltz, L. Larue, C. Muller, L. Nieto, Proteome characterization of melanoma exosomes reveals a specific signature for metastatic cell lines, Pigment Cell Melanoma Res, 28 (2015) 464-475.
[60] M. Record, K. Carayon, M. Poirot, S. Silvente-Poirot, Exosomes as new vesicular lipid transporters involved in cell-cell communication and various pathophysiologies, Biochim. Biophys. Acta, 1841 (2014) 108-120.
[61] T.F. Martens, K. Remaut, J. Demeester, S.C. De Smedt, K. Braeckmans, Intracellular delivery of nanomaterials: How to catch endosomal escape in the act, Nano Today, 9 (2014) 344-364.
[62] J. Grove, M. Marsh, The cell biology of receptor-mediated virus entry, J. Cell Biol., 195 (2011) 1071-1082.
[63] H.M. van Dongen, N. Masoumi, K.W. Witwer, D.M. Pegtel, Extracellular Vesicles Exploit Viral Entry Routes for Cargo Delivery, Microbiol. Mol. Biol. Rev., 80 (2016) 369-386.
[64] K. Raemdonck, S.C. De Smedt, Lessons in simplicity that should shape the future of drug delivery, Nat. Biotechnol., 33 (2015) 1026-1027.
[65] J. Vandesompele, K. De Preter, F. Pattyn, B. Poppe, N. Van Roy, A. De Paepe, F. Speleman, Accurate normalization of real-time quantitative RT-PCR data by geometric averaging of multiple internal control genes, Genome Biol., 3 (2002) r34.1-r34.11.

Supporting information

Supporting experimental section

Cryo-TEM imaging

The ELV sample (3.5 µl) was applied to 300 mesh quantifoil grids and incubated for 30 to 60 seconds. Next, excess buffer was removed by blotting the grids for 3 seconds using a Whatmann no.1 filter paper and the sample was snap frozen by plunging in liquid ethane at a temperature of -180°C and stored in liquid nitrogen until visualization. Next, the samples were transferred to a Gatan 914 cryoholder and imaged at low dose conditions at -177°C, using a JEOL JEM1400 TEM equipped with a 11 Mpxl Olympus SIS Quemesa camera.

CD63-GFP transfection in B16F10 melanoma cells

pCT-CD63-GFP (pCMV, exosome CD63 tetraspanin Tag, Virus) was purchased from SBI system biosciences. B16F10 melanoma cells were plated in a 24-well plate (2.8 x 10^4 cells/cm²). After 24h, cell culture medium was replaced by TransDux™ (SBI System biosciences) supplemented cell medium and cells were incubated with viral particles at a multiplicity of infection (MOI) of 20. Seventy-two hours post transfection, cells were washed with PBS and cultured in medium supplemented with 2 µg/ml puromycin (Invitrogen) during one week to select transduced cells. These cells were termed B16F10_CD63-GFP cells throughout this chapter.

To confirm (CD63-GFP positive) ELV transport through the transwell® permeable support and subsequent cellular internalization, B16F10_CD63-GFP cells were seeded in a 6-well plate insert (24 mm – pore size 3 µm). Recipient cells (JAWSII) were seeded in the bottom compartment of the 6-well plate. After 3 days of co-culture the bottom cells were washed 3x with PBS, detached using 0.05 % trypsin-EDTA (Gibco) and analyzed for GFP fluorescence using a flow cytometer (CytoFLEX, Beckman Coulter).

miRNA profiling of B16F10-derived ELVs

Three independent isolates of B16F10-derived ELVs were pooled and analyzed in duplicate. nCounter™ assays were carried out according to the manufacturer's protocol v.20090807 (Nanostring Technologies). In brief, in a first annealing and ligation step, a unique miRNA specific miRtag was ligated to the miRNA molecules in the total RNA sample. Subsequently, a mastermix containing Reporter CodeSet and hybridization buffer was prepared. An aliquot of 5 µl from the miRNA sample preparation in the first step was added to 20 µl mastermix. Just before hybridization, 5 µl of Capture CodeSet was added and hybridization was carried out in a PCR machine for 23h at 65°C.

Immediately after hybridization, the post-hybridization process was started in the nCounter™ Prep-Station according to the manufacturer's protocol v.20081003 (Nanostring Technologies) using the High Sensitivity Protocol (software version 4.0.9), and excess probes were washed away using a two-step magnetic bead-based purification. Finally, the purified target/probe complexes were eluted and immobilized in the cartridge for data collection. Data were collected in the nCounter™ Digital Analyzer. Each flow cell (sample) was scanned at the highest resolution of 1150 fields of view using a microscope objective and a CCD camera yielding hundreds of thousands of target molecule counts. After processing the digital images on the nCounter™ Digital Analyzer, the barcode counts were tabulated in a comma separated value format.

RT-qPCR

JAWSII cells were plated in a 24-well plate (4.5 x 10^4 cells per cm^2) and allowed to attach overnight. The next day, the indicated concentration of B16F10-derived ELVs (without chol-siRNA loading) were incubated with the cells for 24h after which the cells were washed with PBS and total RNA was purified using a RNeasy Mini Kit (Qiagen) according to the manufacturer's instructions. cDNA was made using the iScript™ cDNA Synthesis Kit (Bio-Rad) with 1000 ng starting material. qPCR was done using the SensiFAST™ SYBR No-ROX kit (Bioline) on the Light Cycler 480 system (Roche). Expression levels were normalized to the expression of the two most stable genes β-actin and GAPDH, which were determined using the geNorm Software [65]. Primer sequences can be found in **table S2.**

Supporting figures

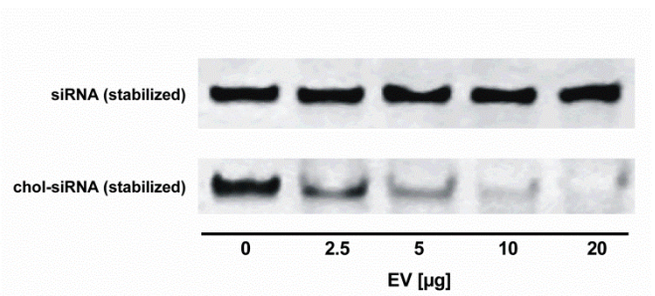

Figure S1. Comparing siRNA and chol-siRNA association to B16F10-derived ELV. Increasing amounts of B16F10-derived ELVs incubated with 10 pmol chemically stabilized siRNA and chol-siRNA for 1h at 37°C.

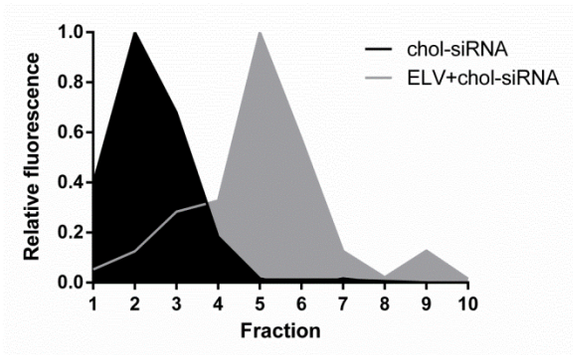

Figure S2. Chol-siRNA flotation on an iodixanol density gradient after overnight UC. Relative Cy5 fluorescence in the different density fractions when layering chol-siRNA (black) and ELV-associated chol-siRNA (gray), respectively on top of an iodixanol density gradient after overnight UC.

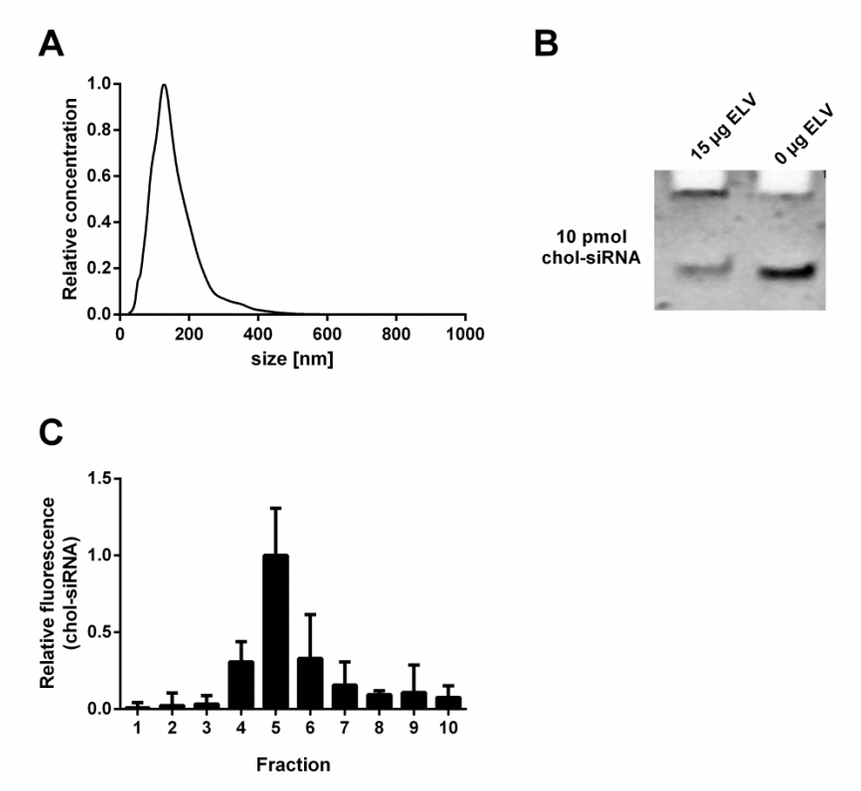

Figure S3. JAWSII-derived ELV characterization and chol-siRNA loading. [A] Representative size distribution of JAWSII-derived ELVs, determined by scattering-based single particle tracking. [B] Polyacrylamide gel retention assay of chol-siRNA mixed with JAWSII-derived ELVs and chol-siRNA without ELVs, respectively, after 1h incubation at 37°C. [C] Relative fluorescence intensity distribution of Cy5-labeled chol-siRNA following incubation with JAWSII-derived ELVs when placed on top of an iodixanol density gradient after overnight UC. The results are represented as mean ± SD (n=3).

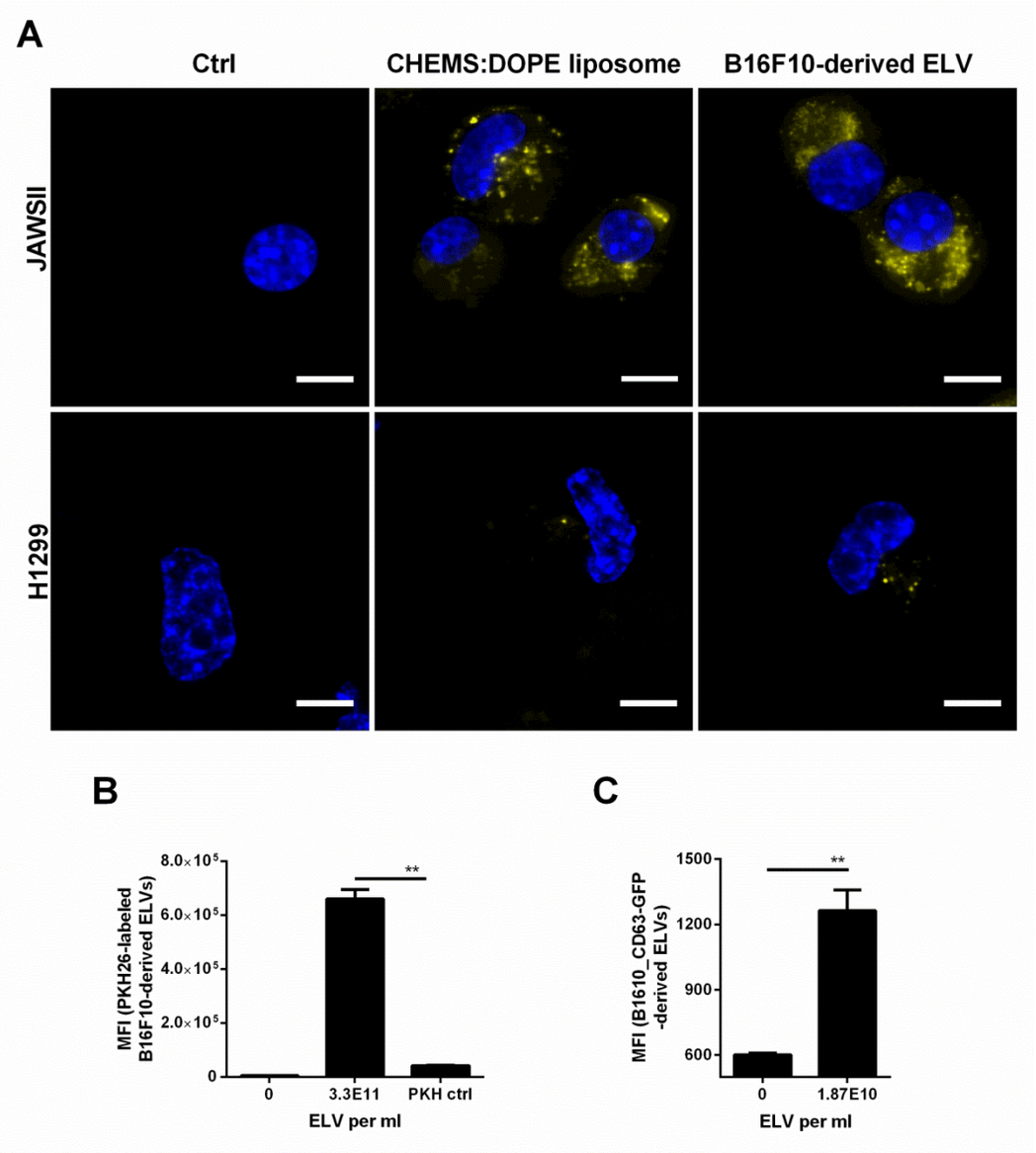

Figure S4. Cellular uptake of B16F10-derived ELVs and CHEMS:DOPE liposomes. [A] Representative confocal images of the internalization of chol-siRNA loaded CHEMS:DOPE liposomes and B16F10-derived ELVs (3.3 x 10^{11} particles/ml, vesicles are PKH26 labeled and depicted in yellow, nuclei are Hoechst 33342 labeled and depicted in blue)) into recipient cells after 24h incubation in vesicle-depleted cell medium. The scale bar indicates 10 µm. Confirmation of B16F10-derived ELVs uptake by JAWSII cells using different ELV labeling strategies: [B] PKH26-labeled ELVs and [C] ELVs derived from B16F10_CD63-GFP cells. MFI represents the mean fluorescence intensity per cell determined by flow cytometry and expressed in arbitrary units (mean ± SD; n=3).

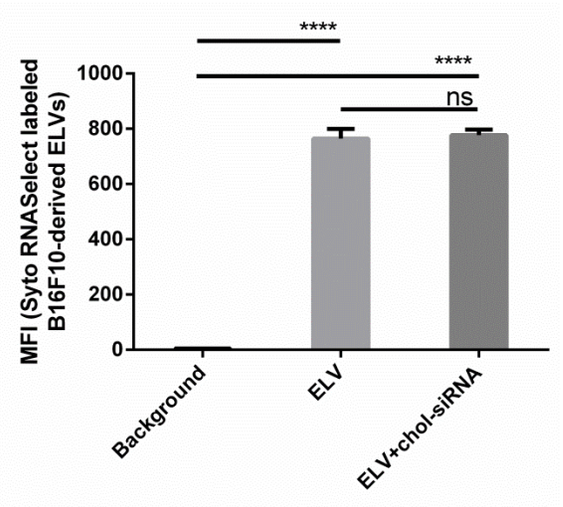

Figure S5. Quantification by flow cytometry of B16F10-derived ELV (Syto RNASelect-labeled) uptake by JAWSII cells, comparing chol-siRNA loaded and unloaded ELVs after 24h incubation. MFI represents the mean fluorescence intensity. The data are represented as mean ± SD (n=3).

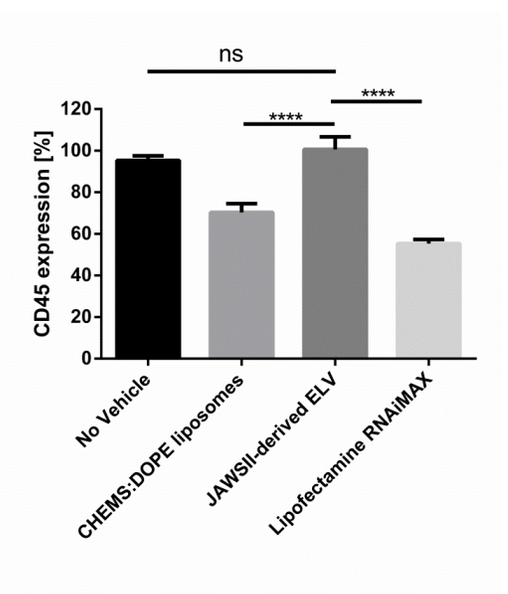

Figure S6. Chol-siRNA mediated gene silencing in JAWSII cells. CD45 expression in JAWSII cells after treatment with chol-siRNA, chol-siRNA associated to CHEMS:DOPE liposomes, chol-siRNA associated to JAWSII-derived ELVs and chol-siRNA associated to lipofectamine RNAiMAX. The expression of the target protein CD45 following chol-siCD45 transfection is represented relatively to identical treatment with a chol-siCTRL sequence. Chol-siRNA (50 nM) with, if applicable, ~3.3 x 10^{11} liposomes or ELVs per ml were incubated with the cells for 24h in vesicle-depleted medium. In case of the lipofectamine RNAiMAX treatment, the concentration advised by the manufacturer was used (i.e. 10 nM chol-siRNA; 4h incubation time).

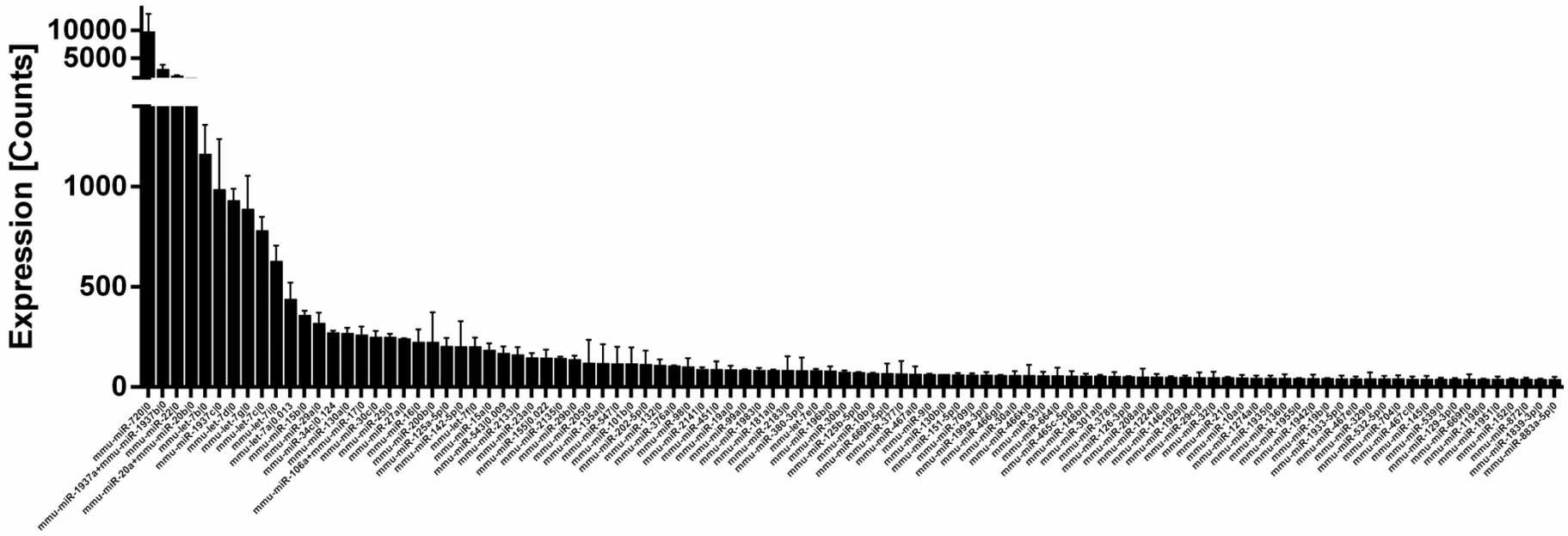

Figure S7. miRNAs present in B16F10-derived ELVs determined by the nCounter miRNA expression assay. miRNAs are included if the expression is higher than the average plus 2x SD of the signal generated by different negative controls. Error bars indicate the SD of 2 technical replicates of 3 pooled biological replicates.

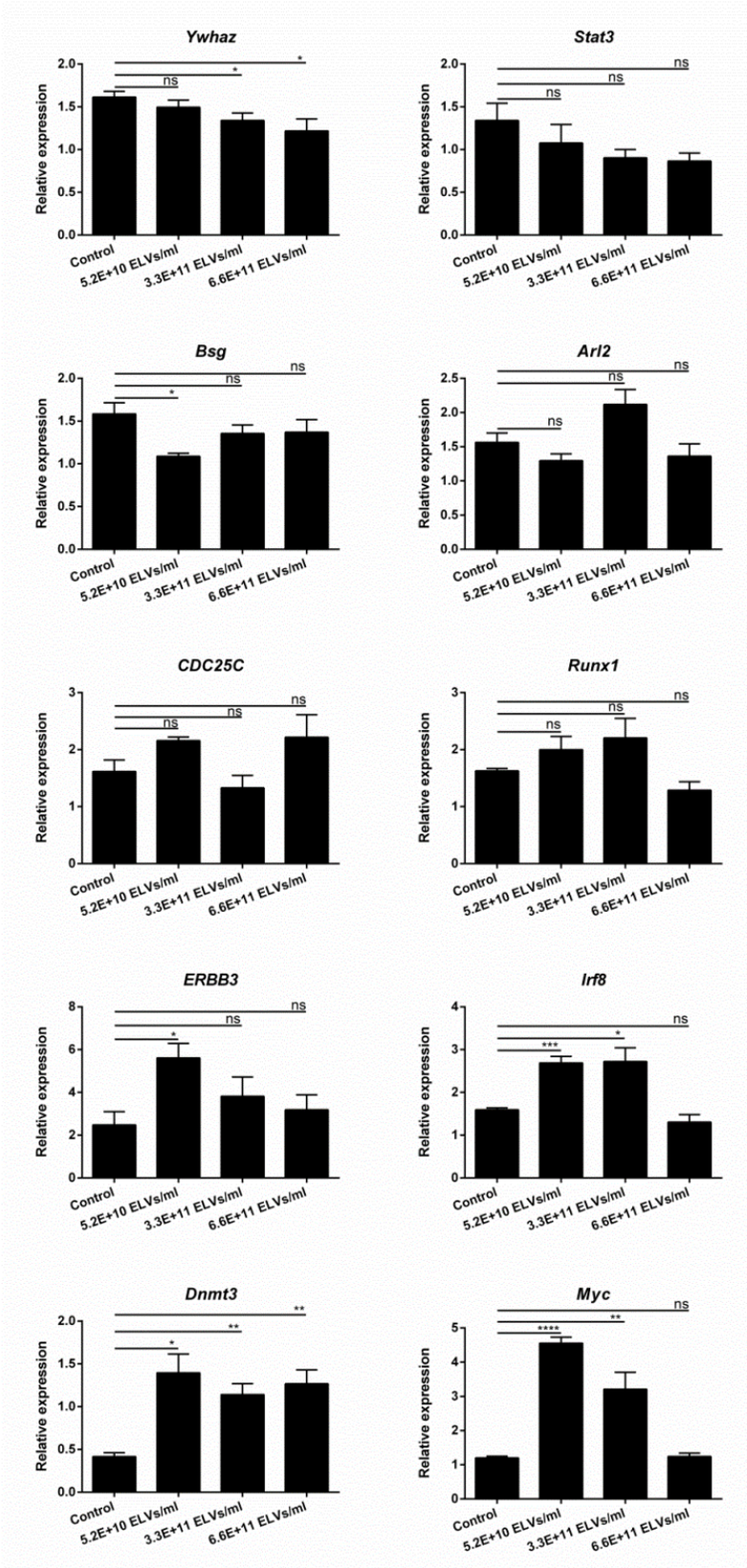

Figure S8. Alterations in gene expression profile in JAWSII cells after treatment with B16F10-derived EVs. mRNA expression profile of validated gene targets of some of the most abundant miRNAs present in B16F10-derived ELVs (*cfr.* **table 2**). JAWSII cells were incubated with mounting concentrations of purified B16F10-derived ELVs for 24h. The next day, expression levels of the indicated transcripts were determined using RT-qPCR. The data are represented as mean ± SD (n=4).

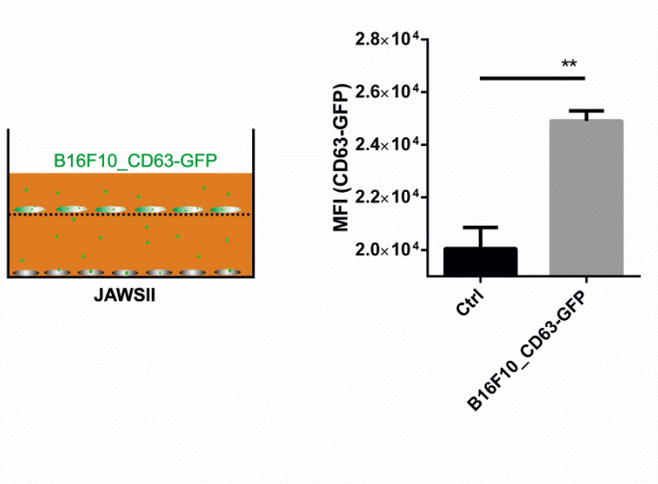

Figure S9. Validation of ELV transport through a transwell® insert. Uptake of CD63-GFP positive vesicles released by B16F10_CD63-GFP cells (seeded in a transwell® insert) by recipient cells (JAWSII seeded at the bottom) after 72h co-culture, as determined by flow cytometry (CytoFLEX; Beckman Coulter). The data are represented as mean ± SD (n=3).

Supporting tables

Table S1. Modifications and sequences of siRNAs used in this chapter

Target	Abbreviation	Modification	Manufacturer	Sequence	
				Sense strand (5'-3')	Antisense strand (5'-3')
Negative control	Chol-siCTRL	Cholesteryl [1] / stabilized [2]	GE Dharmacon™	Not available	Not available
Pan-leukocyte marker CD45	Chol-siCD45	Cholesteryl [1] / stabilized [2]	GE Dharmacon™	GAAGAAUGCUCACAGAUAAUU	UUAUCUGUGAGCAUUCUUCUU
eGFP [3]	Chol-siGFP	Cholesteryl [1] / stabilized [2]	GE Dharmacon™	CAAGCUGACCCUGAAGUUCUU	GAACUUCAGGGUCAGCUUGUU
eGFP [3]	siGFP	stabilized [2]	GE Dharmacon™	CAAGCUGACCCUGAAGUUCUU	GAACUUCAGGGUCAGCUUGUU

[1]cholesteryl-tetraethyleneglycol linker modification at the 5' end of the sense strand, purchased from GE Dharmacon; [2]RNA strand modified for the use in nuclease-rich environments (siSTABLE modification; GE Dharmacon); [3]enhanced green fluorescent protein

Table S2. Primers used throughout the qPCR experiments.

Gene name	Forward primer	Reversed primer
β-actin	GCTTCTAGGCGGACTGTTACTGA	GCCATGCCAATGTTGTCTCTTAT
GAPDH	TGAAGCAGGCATCTGAGGG	CGAAGGTGGAAGAGTGGGAG
HMGA2	GAGCCCTCTCCTAAGAGACCC	TTGGCCGTTTTTCTCCAATGG
MTPN	CCCTGAAAAACGGAGACTTGG	GAAACATGACCCTCATAGACAGC
Ywhaz	GAAAAGTTCTTGATCCCCAATGC	TGTGACTGGTCCACAATTCCTT
Bcl2	ATGCCTTTGTGGAACTATATGGC	GGTATGCACCCAGAGTGATGC
CDC25c	ATGTCTACAGGACCTATCCCAC	ACCTAAAACTGGGTGCTGAAAC
ARL2	GCACTGTCCTGTAATGCTATTCA	GCAGTAAAGACACGACTGGAAAT
MAPK14	GGCTCGGCACACTGATGAT	TGGGGTTCCAACGAGTCTTAAA

5

Identification of individual exosome-like vesicles by surface enhanced Raman spectroscopy

A manuscript of this chapter is published as:

Stephan Stremersch[1], Monica Marro[2], Bat-El Pinchasik[3], Pieter Baatsen[4], An Hendrix[5], Stefaan C. De Smedt[1], Pablo Loza-Alvarez[2], Andre G. Skirtach[3,6,7], Koen Raemdonck[1], Kevin Braeckmans[1,7]. Identification of Individual Exosome-Like Vesicles by Surface Enhanced Raman Spectroscopy*, Small*, 12 (2016) 3292-301.

[1]Laboratory of General Biochemistry and Physical Pharmacy, Ghent University, Ghent, Belgium
[2]ICFO-Institut de Ciencies Fotoniques, The Barcelona Institute of Science and Technology, Castelldefels, Spain
[3]Department of Interfaces and Biomaterials, Max Planck Institute of Colloids and Interfaces, Potsdam, Germany
[4]EM-facility EMoNe, VIB-KULeuven, Leuven, Belgium
[5]Laboratory of Experimental Cancer Research, Ghent University Hospital, Ghent, Belgium
[6]Department of Molecular Biotechnology, Ghent University, Ghent, Belgium
[7]Centre for Nano- and Biophotonics, Ghent University, Ghent, Belgium

Chapter 5: ToC

Abstract

Exosome-like vesicles (ELVs) are a novel class of biomarkers that are receiving a lot of attention for the early stage detection and monitoring of cancer. In this study the feasibility of using a Surface Enhanced Raman Spectroscopy (SERS) based method to distinguish between ELVs derived from different cellular origins is evaluated. A gold nanoparticle based shell is deposited on the surface of ELVs derived from cancerous and healthy cells which enhances the Raman signal while maintaining a colloidal suspension of individual vesicles. This nano-coating allows the recording of SERS spectra from single vesicles. By using Partial Least Square Discriminative Analysis (PLS-DA) on the obtained spectra, vesicles from different origin can be distinguished, even when present in the same mixture.

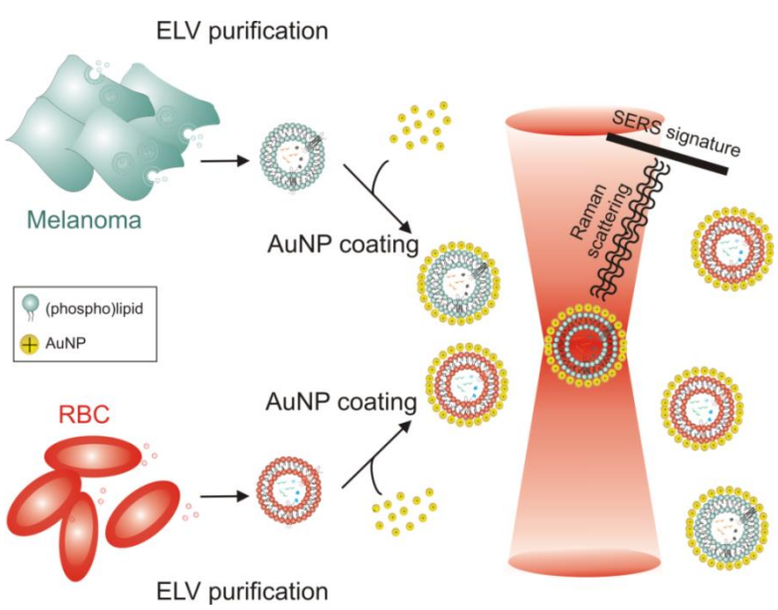

Schematic representation of the gold nanoparticle (AuNP) coating and subsequent surface-enhanced Raman spectroscopy measurements of purified exosome-like vesicles (ELV).

1. Introduction

To maximize the impact of current cancer treatments it is essential to detect carcinogenic cells in an early stage. To this end, the discovery of sufficiently sensitive and specific biomarkers is of foremost importance. Recently, circulating extracellular vesicles (EVs), especially exosomes, have emerged as a potential new class of biomarkers for early detection and treatment monitoring in cancer and other diseases [1, 2]. As contextualized in **chapter 1**, exosomes are of interest for diagnostic and prognostic applications as they contain molecules derived directly from the parent cell [3]. In addition, they are fairly easily accessible as they are found in various body fluids (e.g. blood, salvia, urine, breast milk, ascites, etc.) [4-6]. Currently, most exosome-based diagnostic approaches focus on identifying specific molecular components by elaborate 'omics' studies [7]. Examples are elevated levels of miR-21 in exosomes of hepatocellular cancer patients [8] and the presence of EGFRvIII mutant proteins on exosomes derived from a specific glioblastoma subtype [9]. Despite the fact that these techniques provide detailed information on the molecular composition of exosomes, they rely on complicated and time-consuming protocols. Moreover, these analyses are performed on the overall EV population level which makes it less likely to find low abundant subpopulations. Indeed, considering that most cells secrete EVs as part of their normal function, it is to be expected that the amount of vesicles derived from diseased cells is comparatively low. Accordingly, the detection of altered levels of low abundant components in a bulk analysis is quite challenging. Furthermore, it is becoming apparent that one cell type may release multiple subtypes of EVs (**chapter 1**) due to which bulk analysis is prone to missing specific subtypes or subtype ratios of vesicles [10-12]. Therefore, techniques capable of identifying individual exosomes could prove very valuable, but are currently lacking.

In this chapter, a new approach is explored for single vesicle identification based on surface enhanced Raman spectroscopy (SERS) for diagnostic applications. Raman spectroscopy is a label-free technique based on inelastic scattering of laser light due to the interaction of photons with molecular vibrations. As such, the Raman spectrum of inelastic scattered photons contains information on the molecular composition of the sample. Raman spectroscopy has been used before to characterize EVs [13, 14]. However, as it is a very inefficient process (only 1 in 10^{6-8} photons is scattered inelastically), a high sample concentration is required in combination with high laser power and long signal integration times [15]. High throughput screening of single vesicles by Raman spectroscopy is therefore not feasible.

Fortunately, the Raman signal can be strongly enhanced (up to 10^{14-15} times) by using surface enhanced Raman spectroscopy (SERS) [16]. SERS is based on the enhancement

of the incident and scattered electromagnetic field by plasmon excitation on irregular (metal) surfaces, typically composed of Au or Ag [17-19]. As it has single molecule sensitivity, SERS is increasingly applied for the characterization of biological samples [20, 21]. In this respect, different types of SERS-substrates have been developed to obtain plasmon enhancement and record Raman spectra from (sub)cellular components down to the single biomolecule level [22]. These can be, but are not limited to, well defined nanostructured surfaces of gold [23] or silver [24], (intracellular) aggregated Ag- [25] or Au nanoparticles (AuNP) [26]. Both Ag-nanograin coated chips and precipitated AuNP clusters were previously applied for bulk EV measurements [27, 28]. These few reports show the feasibility of obtaining SERS spectra from an EV sample and the capability to differentiate between EVs from different origin [27, 28]. However, it is important to note that these previous analyses were still performed on bulk vesicles from a single cell type. Yet, clinical samples contain EVs from different origin in a mixture, hampering the further implementation of bulk Raman measurements for diagnostic applications.

To enable true single vesicle SERS identification, here we demonstrate to the best of our knowledge for the first time that EVs can be functionalized with AuNP on their surface, forming an irregularly shaped nanoshell that enables the generation of an enhanced Raman signal while maintaining a colloidal suspension of individual vesicles. As proof-of-concept of the discriminative potential of this approach, we show that vesicles derived from B16F10 melanoma cells can be successfully identified and quantified in a mixture with red blood cell (RBC)-derived vesicles.

2. Experimental section

2.1. Cell culturing and ELV purification

B16F10 melanoma cells (ATCC® CRL-6475™) were cultured in Dulbecco's Modified Eagle Medium (Invitrogen), supplemented with glutamine (2 mM), 10 % fetal bovine serum (Hyclone™), sodium pyruvate (1 mM), penicillin (100 U/mL) and streptomycin (100 µg/ml) (Invitrogen) at 37 °C in a humidified atmosphere containing 5 % CO_2. For the purification of ELVs, cells were first washed with phosphate buffered saline (PBS, Invitrogen) and the cell medium was replaced with vesicle-depleted medium. The latter was prepared by ultrafiltration of complete cell culture medium through a 300 kDa filter (Millipore) using an Amicon stirred cell set-up (Millipore) under three bar nitrogen pressure to remove bovine EVs. Cells were incubated for 24 hours after which the conditioned cell medium was harvested for vesicle isolation.

RBC were isolated out of blood from a healthy volunteer as described previously [29] with minor modifications. Briefly, blood was collected in K_2EDTA coated tubes (Venosafe) and spun at 1 500g for 15 minutes (Heraeus Multifuge 1S-R) within 15 minutes after blood collection. RBC were retained, washed twice and suspended in Ringer buffer (NaCl (150 mM), KCl (5 mM), $CaCl_2$ (2 mM), $MgCl_2$ (1mM), NaH_2PO_4 (2 mM), 4-(2-hydroxyethyl)-1-piperazineethanesulfonic acid (HEPES) buffer (10 mM), Glucose (10 mM), pH=7.2) for 2 days at 37°C while shaking.

Vesicles derived from B16F10 melanoma cells and RBC were purified from conditioned cell medium or Ringer buffer, respectively by differential centrifugation followed by density gradient ultracentrifugation (UC) (**figure S1**). First, conditioned cell medium/Ringer buffer was centrifuged for 10 minutes at 300 g and 10 minutes at 3 000 g. Next, the supernatant was concentrated by ultrafiltration using a 30 kDa filter (Millipore) in a Amicon stirred cell set-up (Millipore) under nitrogen pressure. The concentrated sample was centrifuged (Beckman® L8-70M ultracentrifuge) at 10 000 g for 10 minutes using a SW55ti rotor (Beckman instruments) and the supernatant was placed on top of an iodixanol (Optiprep™, Axis-Shield) based density gradient. The gradient was produced according to the manufacturer's instruction. Briefly, 1 ml of different iodixanol dilutions (12.5 %, 25 %, 37.5 % and 50 % in sucrose (250 mM), EDTA (1 mM), Tris-HCl (10 mM) buffer; pH = 7.4) were carefully laid underneath one another using a 21G needle. The samples were then centrifuged at 150 000 g for 15 hours. Next, the gradient was fractionated per 0.5 ml, diluted 10x in ultrapure water and centrifuged at 150 000 g for 150 minutes. Finally, the pellet was washed one more time and suspended in ultrapure water. The fraction containing the highest exosome associated proteins was used for further characterization and Raman spectroscopy experiments and the respective vesicles are referred to as ELVs.

2.2. Immunoblotting

In order to determine the density fraction containing the exosomes, pelleted vesicles from each fraction were resuspended in ice cold RIPA buffer (Sigma-Aldrich) mixed with MS-SAFE protease and phosphatase inhibitor cocktail (Sigma-Aldrich) and vortexed. Next, the samples were sonicated for 10 minutes and centrifuged at 13 000 g for 5 minutes. For protein separation, samples were diluted in 2x laemmli buffer (Bio-Rad) with or without 5 % 2-mercaptoethanol (Sigma-Aldrich), heated at 95°C for 5 minutes and loaded on a 10 % mini-protean TGX precasted gel (Bio-Rad). The polyacrylamide gel was ran at 100 V for 60 minutes in running buffer (Tris (25 mM) – Glycine (200 mM) – 0.1 % SDS). The blotting was done on an immunoblot PVDF 0.2 µm membrane (Bio-Rad) at 100 V for 90 minutes in blotting buffer (Tris (25 mM) – Glycine (200 mM) – 20 % Methanol – 0.05 % SDS). The blot was blocked for 1 hour using 3 % BSA, 0.1 % Tween20 (Sigma-Aldrich) in PBS buffer (Invitrogen). Next, primary antibodies were

incubated overnight at 4°C on a shaker. After washing the blots with blocking buffer they were incubated with a secondary antibody conjugated to horseradish peroxidase (HRP) for 1 hour at room temperature (**table S1**). Visualization was done using the SuperSignal West Dura chemiluminscent kit (Thermo-Scientific) in combination with a VersaDoc^{TM} imaging system (Bio-Rad). All density fractions were loaded on one gel using equal volumes for objective comparison and the respective protein bands were cropped using ImageJ and aligned underneath one another for clarity.

2.3. DMAP coated AuNP

AuNP coated with 4-dimethylaminopyridine (DMAP) were prepared as described by Gittins and Caruso [30]. Briefly, a $HAuCl_4$ aqueous solution was added to a tetraoctylammonium bromide in toluene solution under gentle stirring. Next, $NaBH_4$ was added to the mixture. After 30 minutes the toluene phase was separated from the aqueous phase and washed 3 times using H_2SO_4, NaOH and ultrapure water. Equal volumes of the AuNP in toluene solution and an aqueous DMAP solution were mixed and left to equilibrate for 1 hour. During this period the AuNP transfer from the organic toluene phase to the aqueous phase concomitantly exchanging the tetraoctylammonium bromide coat for a DMAP coating (**figure S2**). Finally the aqueous phase, containing the AuNP coated with DMAP, is separated from the toluene phase. The final AuNP concentration was estimated by UV/VIS spectroscopy based on the optical density of the surface plasmon resonance peak (SPR)-peak (Nanodrop 2000c; ThermoFisher Scientific), assuming that the AuNP are spherical with a molar extinction coefficient of 1.03 x 10^8 M^{-1} cm^{-1} as calculated from **equation 1** reported by Liu *et al.* [31].

$$\ln(\varepsilon) = 3.3211 \times \ln(d) + 10.80505 \qquad (\textbf{eq.1})$$

In which ε represents the molar extinction coefficient and *d* the diameter of the AuNP (10 nm).

2.4. AuNP coating of ELVs

ELVs were mixed with DMAP-coated AuNP at different AuNP:vesicle ratios by mixing equal volumes using a pipette. After 10 minutes incubation at room temperature, the samples were diluted in ultrapure water/buffer and analyzed by different techniques (i.e. dynamic light scattering and cryo-transmission electron microscopy (cryo-TEM)).

2.5. Concentration, size and zeta potential measurements

The concentration and size distribution of purified ELVs was determined by scattering-based single particle tracking using a NanoSight LM10 instrument (Malvern instruments

Ltd.) equipped with a 405 nm laser. Prior to analysis, the concentrated vesicles were diluted in HEPES buffer (pH 7.4; 20 mM) to obtain a concentration in the range of 1.0 to 9.0 x 10^8 particles/ml to guarantee reliable measurements. Movies of 60 seconds were recorded and analyzed with the NTA Analytical Software version 2.3 (Malvern instruments Ltd.).

The size and zeta potential of ELVs and ELVs coated with AuNP (after dilution in HEPES-buffer) were measured by dynamic light scattering using a Zetasizer Nano ZS (Malvern instruments Ltd.), equipped with Dispersion Technology Software.

2.6. Cryo-TEM

Each ELV (with our without AuNP) sample (3.5 µL) was applied to a 300 mesh quantifoil grid and incubated for 30 - 60 seconds. Next, excess buffer was removed by blotting the grids for 3 seconds using a Whatmann 1 filter paper and the sample was snap frozen by plunging in liquid ethane at a temperature of -180°C and stored in liquid nitrogen until visualization. Next, the samples were transferred to a Gatan 914 cryoholder and imaged at low dose conditions at -177°C, using a JEOL JEM1400 TEM equipped with a 11 Mpxl Olympus SIS Quemesa camera.

2.7. Fluorescent labeling and confocal microscopy of ELVs

Purified B16F10- and RBC-derived vesicles were incubated for 15 minutes at 37°C with Vibrant DiD (Invitrogen) or PKH67 (Sigma-Aldrich), respectively (final dye concentration is 5 µM; in Diluent C (Sigma-Aldrich)). Next, non-incorporated dye and diluent C was removed using exosome spin columns (MWCO 3 000) pre-incubated with ultrapure water according to the manufacturer's instructions (Invitrogen).

The labeled ELVs were mixed with AuNP in the indicated ratios (*cfr.* SERS measurements) and visualized using a swept field confocal microscope (LiveScan SFC, Nikon Belux) equipped with a 60x oil immersion lens (NA = 1.4, Nikon). The ELVs were alternately irradiated with 488 nm and 647 nm laser light and images were recorded with an iXon Ultra EMCCD camera (Andor). Particle detection was done with in-house developed software in Matlab as previously described by Deschout *et al.* [32]. The ratio of B16F10 to RBC vesicles (B16F10:RBC ratio) was determined for each mixture by particle counting in at least 20 individual frames at different spatial locations.

2.8. SERS measurements

ELVs (unlabeled) were mixed with DMAP coated AuNP at a fixed AuNP:vesicle ratio (i.e. ~800 for B16F10-derived ELVs and ~1200 for RBC-derived ELVs). Next, samples were diluted in ultrapure water to ≤ 5 x 10^7 vesicles per µl to minimize the possibility that more than one vesicle is present in the focal detection volume. A droplet (60 µl) of the

diluted sample was placed on a quartz substrate and SERS spectra were recorded using an inVia confocal Raman microscope (Renishaw, UK) equipped with a 60x WI lens (NA = 1, Nikon) and a 785 nm laser using a 10 second integration time and 15 mW power. Alternatively, a Raman microscope (Zeiss) equipped with a piezo-scanner (P500, physick instrumente) and a 785 nm laser focused through a 60x WI lens (NA = 1, Nikon) was used. The spectra were acquired with a Spectra Pro500i (Acton Research) monochromator/spectrograph (integration time 500 ms). The 785 nm laser was chosen to limit photodegradation and autofluorescence [33, 34]. All spectra were recorded at different locations in the sample. The presence of a gold coated ELV in the focal volume was confirmed by Rayleigh scattering (**figure 4A**).

2.9. Analysis of SERS spectra

The statistical modeling in this chapter was done by Dr. Monica Marro at the ICFO-institute for photonical sciences. Briefly, the obtained spectra were pre-processed as described previously [35]. To assess the ability of Raman spectroscopy to discriminate RBC- and B16F10 melanoma-derived ELVs, PLS-DA was performed using the PLS toolbox from Eigenvector Research in MatLab. Cross-validation analysis was computed by venetian blinds (10 splits and one sample per split). The number of retained latent variables was chosen to minimize the root mean square error of cross validation curves. Additionally, a Multivariate Curve Resolution Alternating Least Squares (MCR-ALS) algorithm was used to analyze the spectra.

3. Results

3.1. ELV purification and characterization

The potential of SERS to distinguish between vesicles released by two distinct cell types was explored using ELVs from RBC and B16F10 melanoma cancer cells. B16F10 cells were cultured *in vitro* and after 24h incubation, the conditioned cell medium was harvested and used for ELV purification. An iodixanol density gradient based UC protocol was used (**figure S1**) to obtain ELVs with a high purity with minimal protein contamination (**chapter 3**) [36] or residuals of commercial precipitation kit reagents [37]. After density gradient UC the fraction containing the ELVs was determined by immunoblotting against typical exosome-associated protein markers (Hsp70, β-actin, CD63, CD81) on each fraction of the density gradient [38]. In this respect, fraction 5 contained the highest amount of exosomal markers. Moreover, the average density of this fraction was ~1.14 g/ml, which corresponds with earlier reports on the typical buoyant density of exosomes [39] (**figure 1A**). This fraction was used further for characterization and Raman spectroscopy experiments. As a 'healthy' vesicle source,

RBC were used as they are abundantly present in patient-derived blood samples. The same ELV purification protocol was used as described for the B16F10 melanoma cell-derived vesicles (**figure S1**).

After two additional washing steps by UC, the ELV pellet was suspended in ultrapure water (Millipore) and analyzed for size and zeta potential by scattering-based single particle tracking analysis and dynamic light scattering, respectively. The majority of the B16F10 melanoma-derived ELVs had a hydrodynamic diameter of approximately 0.12 µm. RBC-derived vesicles were slightly larger with a size of approximately 0.17 µm. Both types of vesicles had a negative surface charge (**figure 1B**). Finally, cryo-TEM was used as an additional confirmation of the presence of membranous structures in the purified samples (**figure 1C**).

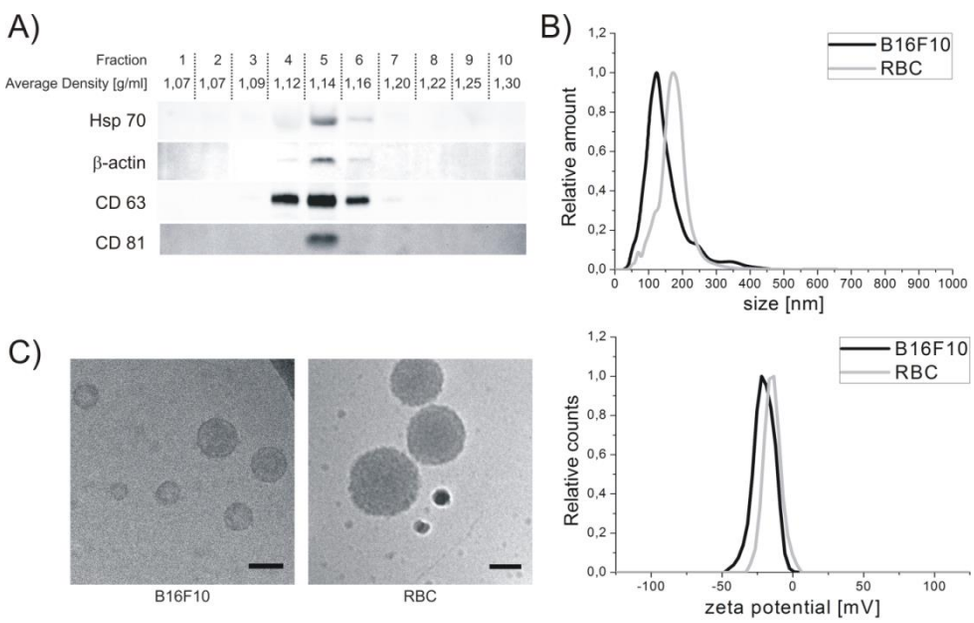

Figure 1. Characterization of purified B16F10 melanoma- and RBC-derived ELVs. [A] Immunoblotting against exosomal markers Hsp70, β-actin, CD63 and CD81 on the different density fractions after overnight density gradient UC of B16F10 melanoma-derived conditioned medium. For each fraction the average density is reported [g/ml]. [B] Representative size (upper) and zeta potential (lower) of B16F10 melanoma- (black) and RBC- (gray) derived ELVs determined by single particle tracking analysis and dynamic light scattering, respectively. [C] Cryo-TEM images of B16F10 melanoma (left) and RBC-derived (right) ELVs. The scale bar indicates 100 nm.

3.2. Gold nanoparticle coating of ELVs

As a next step, we investigated if it would be possible to coat ELVs with AuNP while maintaining a colloidal single vesicle suspension. Specifically, we explored a coating strategy that is based on the electrostatic adsorption of cationic (due to a DMAP coating), 10 nm AuNP (**figure 2A and 2B**) onto the anionic surface of ELVs. AuNP were

mixed with vesicles at increasing particle over vesicle ratios. It was observed that increasing the ratio of AuNP:vesicles causes an initial increase in size due to the zeta potential becoming more neutral (i.e. agglomeration). When increasing the ratio of AuNP:vesicles further, the zeta potential became strongly positive, resulting in a dispersion of individual AuNP coated ELVs, as confirmed by dynamic light scattering size measurements (**figure 3A and 3B**) and cryo-TEM imaging (**figure 3C and 3D**). The latter also confirms the association between the negatively charged ELVs and the positively charged AuNP. Around 600 AuNP per B16F10 vesicle (**figure 3A**) and 1200 AuNP per RBC vesicle (**figure 3B**) were required to obtain a colloidal stable suspension. The fact that more AuNP per vesicles were needed to coat the RBC compared to the B16F10 melanoma vesicles is in accordance with the larger surface area of a RBC-derived vesicles. Moreover, these numbers approach the average theoretical amount of AuNP (i.e. 912 AuNP per B16F10- and 1291 AuNP per RBC-derived vesicle) needed to coat an entire vesicle in a monolayer as can be calculated from **equation 2**. To obtain a SERS signal, AuNP need to be in close proximity to one another [19]. In this respect, high amounts of AuNP to vesicles were mixed (i.e. ~800 for B16F10 and ~1200 for RBC) for the SERS measurements. Indeed, for these higher ratios, cryo-TEM imaging showed nearly complete coating of both vesicle types with AuNP (**figure 3C and 3D**).

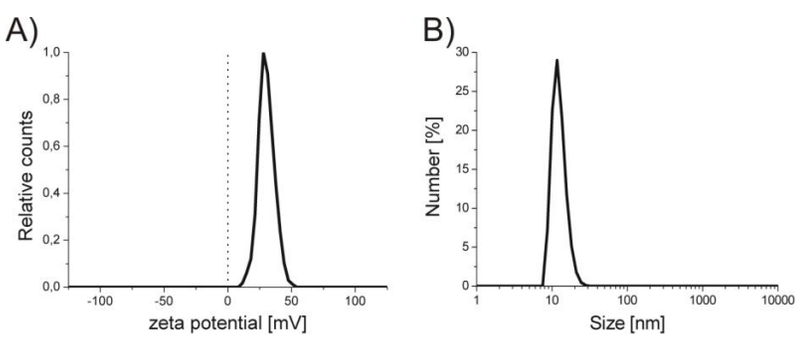

Figure 2. Characterization of DMAP coated AuNP. [A] Zeta potential and [B] hydrodynamic diameter of DMAP-coated gold nanoparticles, as determined by dynamic light scattering.

$$\frac{\overline{AuNP}}{ELV} = \frac{\sum_{i=1}^{n}\left[S_{ELV,i}\cdot\eta / SS_{AuNP}\right]}{n} \qquad \textbf{(eq.2)}$$

Equation 2. Equation used to calculate the theoretical average amount of AuNP needed to coat an entire vesicle surface in a monolayer, with *n* as the total amount of vesicles, $S_{ELV,i}$ as the surface of a vesicle i, η is the maximum packing density of a sphere which was fixed at 0.9 (hexagonal packing was assumed) and SS_{AuNP} as the surface of the section occupied by one AuNP. Calculations were based on the size distribution for each ELV type as depicted in **figure 1B**.

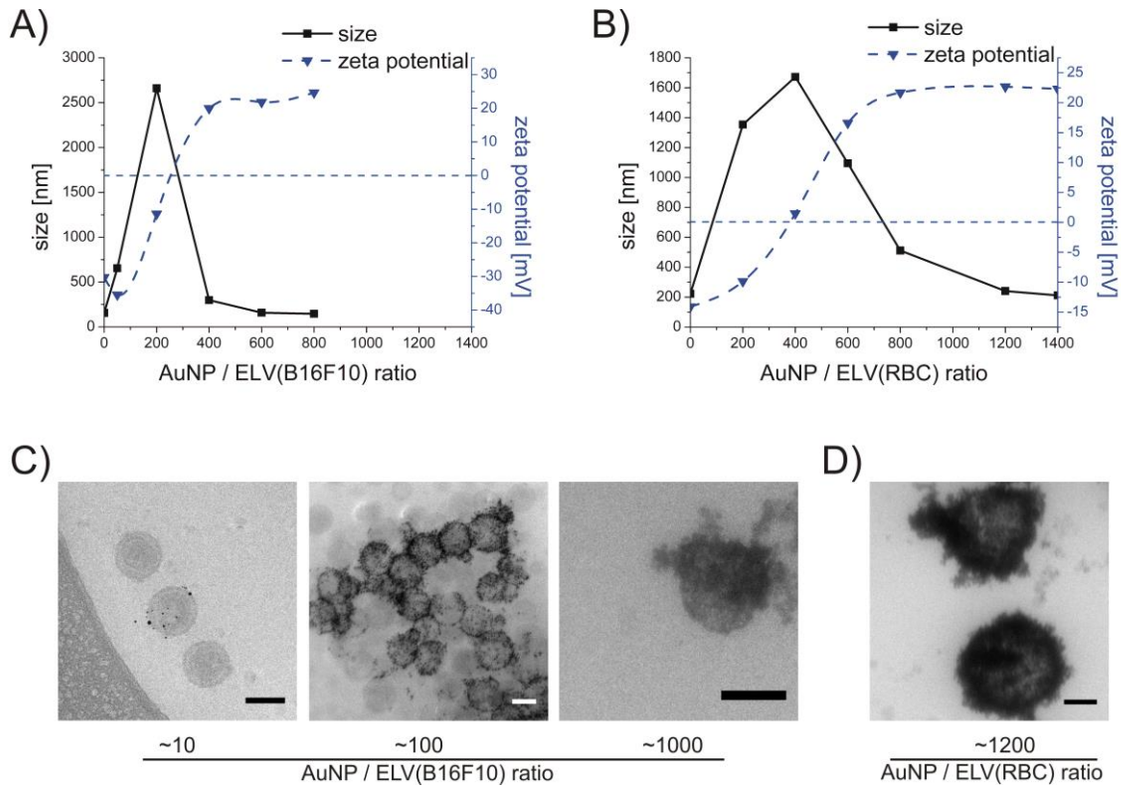

Figure 3. AuNP coating of ELVs. Average size and zeta potential of AuNP coated [A] B16F10 melanoma-derived ELVs and [B] RBC-derived ELVs, as a function of mounting AuNP:vesicle ratios. [C] Cryo-TEM images of AuNP coated B16F10-derived ELVs. Mounting AuNP:vesicle ratios are indicated underneath the respective pictures. [D] Cryo-TEM confirmation of full coating conditions for RBC-derived ELVs. The scale bars indicate 100 nm.

3.3. Recording SERS spectra of individual ELVs

Next, we investigated if this dense packing of AuNP on the vesicular surface indeed allows to generate a SERS spectral fingerprint. For these experiments we worked under high AuNP:vesicle ratios as described above. Spectra were recorded from individual AuNP coated ELVs adsorbed on a quartz surface as schematically represented in **figure 4A**. Peaks from (ELV) biomolecules (green arrows) could be clearly identified in the spectra from B16F10 melanoma-derived vesicles (**figure 4B**) and RBC-derived vesicles (**figure 4C**), apart from peaks arising from the DMAP coating of the AuNP (red arrows; cfr. **figure S3**). **Table 1** gives an overview of the identified biomolecule peaks with their tentative molecular origin. Most classes of biomolecules seem to be present, i.e. lipids, proteins, nucleic acids and carbohydrates. It is of note that ELVs without AuNP coating could not generate a clear Raman signal under the same conditions, underscoring the importance of SERS for enhancing the signal of single vesicles.

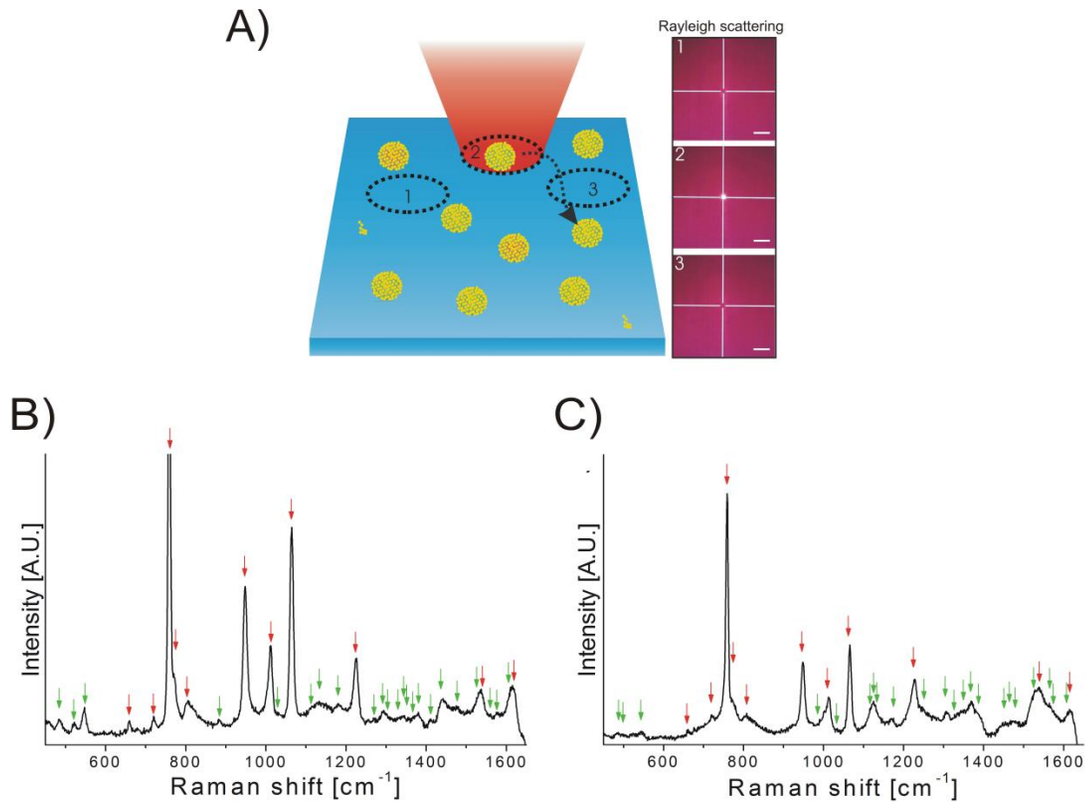

Figure 4. SERS spectra of individual ELVs. [A] Schematic representation of the SERS measurements of AuNP coated ELVs. Each recorded spectrum is derived from another vesicle by moving the laser to a different spatial location (e.g. 1, 2, 3). The presence of a gold coated ELV was confirmed by a Rayleigh scattering signal (*cfr.* location 2). The scale bar indicates 10 µm. [B] Representative, unmodified SERS spectrum of a B16F10 melanoma-derived ELV coated with AuNP and [C] a RBC-derived ELV coated with AuNP. Red arrows indicate peaks arising from the DMAP AuNP coating. Green arrows indicate ELV-related peaks.

Table 1. Enumeration and tentative assignment of SERS peaks for AuNP-coated B16F10 ELVs (B16F10_AuNP) and AuNP-coated RBC ELVs (RBC_AuNP).

Raman shift [cm^{-1}]	**RBC_AuNP** [1]	**B16F10_AuNP** [1]	**Previously identified in EV isolates**	**Presumed origin [40]** [2]
486	w	m		polysaccharide
521	w	m		S-S stretching (e.g. protein)
546	w	m		cholesterol
883		w	[13, 37]	$\rho(CH_2)$ (e.g. protein)
989	sh		[28]	
1032	w	sh	[13, 27]	CH_2CH_3 bending (e.g. phospholipid); ν(C-C) (e.g. polysaccharide)
1115	sh	sh	[37]	C-O in ribose (e.g. nucleic acid)

Raman shift [cm^{-1}]	RBC_AuNP [1]	B16F10_AuNP [1]	Previously identified in EV isolates	Presumed origin [40] [2]
1124	s	m	[13, 14]	v_{22} (porphyrin half ring; typical for RBC) / C-C stretch (e.g. lipid, protein) / C-N (e.g. protein)
1134	sh	m	[27]	v(C-C) (e.g. lipid)
1172	m	sh	[37]	δ(C-H) (e.g. protein)
1179		m		v(C-C) or v(C-O) (e.g. phospholipids)
1243	sh		[13]	amide III (e.g. protein) / asymmetric phosphate stretching (e.g. nucleic acid)
1271		w	[13]	amide III (e.g. protein) / C=C (e.g. fatty acids)
1293		m	[14]	cytosine (nucleic acid) / CH_2 deformation (e.g. lipids)
1307	m	sh	[13, 28, 37]	C-N asymmetric stretching (e.g. protein) / CH_3CH_2 twisting (e.g. lipid)
1326	sh	sh	[37]	ω(CH_3CH_2) (e.g. nucleic acid)
1346	sh	w		
1354		w		guanine (nucleic acid)
1367	sh	sh		v(CH_3) (e.g. phospholipid)
1370	s	m		carbohydrate
1381	sh	m		δCH_3 symmetric (e.g. lipid)
1411		w		
1443	sh	s	[13, 14, 37]	δ(CH_2/CH_3) (e.g. protein, lipid)
1465	w		[37]	lipid
1477	w	w	[27]	DMAP + δ(C-H) (e.g. lipid, protein)
1528	w	sh	[13]	v(-C=C-) $_{conjugated}$
1563	sh	w		tryptophan
1576	w	w	[14]	guanine (nucleic acid)
1608	sh	sh	[13]	cytosine (nucleic acid) / phenylalanine (protein)
1618	s	s	[28]	DMAP/v(C=C) (e.g. protein)

[1] s: strong, m: medium, w: weak, sh: shoulder; [2] v: vibration, δ: deformation, ω: wagging, ρ: in plane rocking, DMAP: 4-dimethylaminopyridine

3.4. Identification of individual ELVs by spectral analysis

The obtained Raman spectra were subjected to two previously published dedicated statistical models: a PLS-DA and a MCR-ALS [35, 41]. Both models were trained and calibrated by Raman spectra obtained from pure/unmixed samples i.e. AuNP alone, AuNP coated B16F10-derived vesicles and AuNP coated RBC-derived vesicles. The potential of Raman spectroscopy to discriminate between B16F10 melanoma and RBC-derived ELVs in an unbiased fashion was quantified by the PLS-DA model. A sensitivity of 95.8 %, 88.0 %, 95.1 % and specificity of 95.5 %, 95.4 % and 98.0 % for AuNP, B16F10 and RBC-derived ELVs, respectively was obtained (**table 2**). The here reported specificity and sensitivity of the model to discriminate among the different types of vesicles was assessed by cross-validation. Moreover, a parallel experiment was performed with a different Raman microscope allowing shorter acquisition times (500 ms compared to 10 s for the above measurements). Analysis of the obtained data was again performed using the PLS-DA model. The results show that the ability to separate between samples based on their SERS fingerprint was maintained (**table S2**).

Table 2. PLS-DA classification of the Raman spectra of pure/unmixed samples (i.e. AuNP, B16F10 ELVs coated with AuNP and RBC ELVs coated with AuNP) .

Sample	n[1]	PLS-DA prediction			
		Correct identification	Wrong identification	Sensitivity (%)	Specificity (%)
AuNP	24	24	0	100^2 / 95.8^3	97.0^2 / 95.5^3
B16F10_AuNP	25	23	2	92.0^2 / 88.0^3	96.9^2 / 95.4^3
RBC_AuNP	41	39	2	95.1^2 / 95.1^3	100^2 / 98.0^3

[1]n is the amount of spectra recorded for each sample. Sensitivity and specificity were computed with[3] and without[2] cross validation.

Additionally, a MCR-ALS algorithm was applied on the obtained spectra (**figure S4**). Here it is important to note that the MCR-ALS model requires minimal constraints and prior information about the sample and is an unsupervised methodology. Nonetheless, the algorithm was able to deconvolve spectra (**figure S4A**) which can be attributed (based on the score plots represented in **figure S4B** and spectra in **figure 4**) to: Quartz (surface), DMAP (AuNP coating), B16F10 and RBC vesicles respectively. Indeed, this objectively shows the spectral discrepancy between ELVs from different origin.

3.5. Identification and quantification of B16F10 ELVs in a mixture with RBC ELVs

Finally, to provide evidence of the diagnostic potential of this approach, mixtures of AuNP functionalized B16F10 cancerous- and RBC-derived ELVs were prepared at two different ratios. This set-up is a first step towards mimicking the *in vivo* situation where cancerous vesicles need to be detected in patient samples containing a variety of vesicle types, especially highly abundant RBC-derived ELVs. To determine as a reference the exact ratio of both types of vesicles in the prepared mixtures, ELVs were fluorescently labeled with lipophilic dyes (RBC ELVs = green; B16F10 ELVs = red) and subsequently coated with AuNP. The suspension was placed on a microscopy cover slip and confocal microscopy images were recorded. With in-house developed particle detection software the number of green and red fluorescent spots were identified and counted (**figure 5A**). It was calculated that mixture 1 contained 51 ± 17 % cancerous ELVs and mixture 2 contained 15 ± 6 % cancerous ELVs, respectively (**figure 5B**). From these images it could also be confirmed that the two types of AuNP coated vesicles did not agglomerate with one another as no co-localization of green and red spots could be seen.

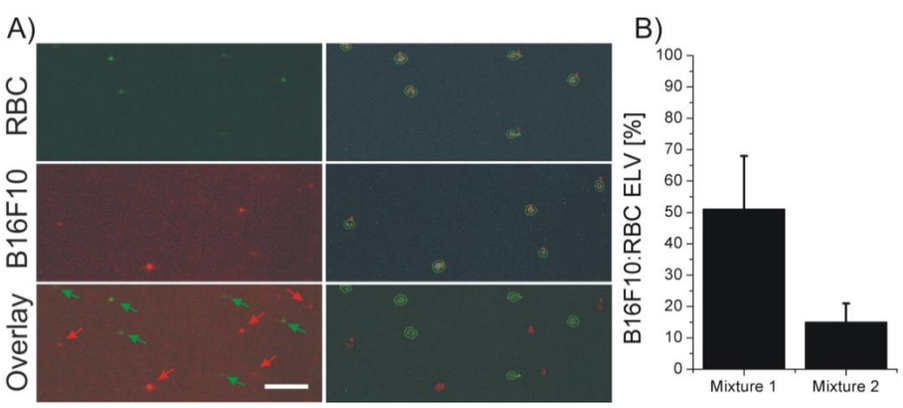

Figure 5. Mixtures of AuNP coated, fluorescently labeled RBC- (green) and B16F10 melanoma- (red) derived ELVs. [A] A representative confocal image of mixture 1 (left) with particle location analysis (right). The scale bar indicates 20 µm. [B] Percentage B16F10 melanoma-derived ELVs of the two B16F10:RBC mixtures based on fluorescence particle counting. The data is represented as mean ± SD of 20 technical replicates.

Identical mixtures without fluorescent labels were subsequently prepared for SERS measurements. For each mixture between 60 and 80 spectra were recorded of AuNP coated vesicles. Using the previously build PLS-DA model, each spectrum was assigned to one of the following groups: Unbound AuNP, RBC-derived ELVs or B1610-derived ELVs (**figure 6A**). In mixture 1 and 2, 38 % and 6.3 % cancerous vesicles were retrieved, respectively (**figure 6B**). A few of the spectra were found to originate from unbound AuNP clusters. These values reasonably correspond to the ratios as determined

by fluorescence microscopy and clearly demonstrate the potential of identifying and quantifying vesicles from different origins in a mixture using the developed SERS platform.

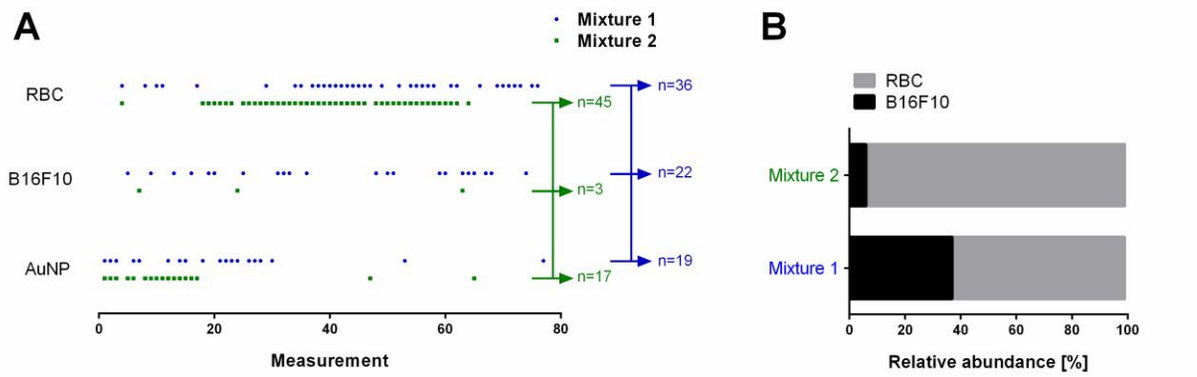

Figure 6. PLS-DA analysis of SERS measurements executed on two B16F10:RBC ELV mixtures. [A] Each point represents an individual spectrum allocated to one of the three classes (unbound AuNP, AuNP coated B16F10 ELVs or AuNP coated RBC ELVs). *n* Represents the amount of spectra allocated to a specific class within a mixture. For the first mixture 77 spectra were recorded, for the second mixture 65 spectra were recorded. [B] The results, as represented in panel A, plotted as percentage B16F10-derived EVs to the total amount of ELVs measured (with exclusion of spectra allocated to AuNP only).

4. Discussion

In this chapter we investigated the possibility of identifying single ELVs by SERS. In contrast to previous diagnostic approaches, where the focus lies on detecting the presence or modified expression of a single exosomal component (i.e. a specific nucleic acid, lipid or protein) [42] using elaborate and time-consuming 'omics' studies, here the potential of SERS was tested to generate an optical fingerprint of individual ELVs coated with AuNP. If successful, such a method holds great potential for the identification of vesicles from different cellular origin in a quantitative manner from patient samples.

As an initial proof-of-concept, ELV were purified from two distinct cell types. A skin-derived, B16F10 melanoma cell line was used as a model for carcinogenic cells and primary RBC as a model for healthy cells that are highly abundant in blood samples. To obtain vesicular concentrates as pure as possible, an iodixanol density gradient based UC protocol was used [36]. This is essential as it was previously shown that residuals of commercial purification kits can interfere with the Raman fingerprint [37]. Moreover, as shown in **chapter 3**, other less stringent purification protocols (i.e. UC and commercial precipitation kits) suffer from limited purity due to co-purification of vesicle-independent

proteins and nucleic acids, which might preclude the AuNP from interacting with the ELVs and interfere with the Raman fingerprint [43].

In a next step, the purified vesicles were functionalized with ~10 nm AuNP to generate the SERS signal. The small diameter ensures that a large number of hot-spots are created in close proximity to the ELV surface. The AuNP carry a cationic surface charge due to the DMAP coating which allows adsorption onto the anionic ELVs surface. Likely this association is charge based though it is also possible that the DMAP molecules are exchanged for thiol-containing proteins present on the ELV surface [44]. Although aggregation was observed initially at low AuNP:vesicle ratios, at higher ratios a colloidal suspension of individual AuNP coated vesicles could be obtained. Indeed, once the overall surface charge of the AuNP coated ELVs became firmly positive (due to the DMAP coating), a mutual repulsion between the coated vesicles was created. This was confirmed using dynamic light scattering, cryo-electron microscopy and indirectly by confocal fluorescence microscopy. Additionally, as DMAP is a small molecule, the AuNP can reside in close contact with the ELV surface. To the best of our knowledge this is the first time that single ELVs were enveloped with a gold coating. On average ~800 AuNP were used to coat the B16F10 melanoma vesicles, while ~1200 for RBC vesicles which is in agreement with the fact that RBC ELVs have a larger surface area and approaches the theoretical amount of AuNP to create a monolayer. This nanoshell of AuNP allowed to generate a SERS signal emanating from the ELVs due to a strong localized surface plasmon between the closely packed AuNP present on the vesicular surface [45].

The Raman peaks in the SERS spectra of single ELVs were found to arise in part from the DMAP and from ELV biomolecular components that are present in the vicinity of the AuNP. Biomolecular exosomal components were identified at 1123 cm^{-1} (lipids + proteins), 1172 cm^{-1} (proteins), 1307 cm^{-1} (proteins + lipids), 1366-1370 cm^{-1} (phospholipids + carbohydrates), 1445 cm^{-1} (lipids + proteins) and 1572-1576 cm^{-1} (nucleic acids). Interestingly, most of these pronounced peaks have previously been identified by others when recording Raman spectra of biological samples like erythrocytes [46] or even EVs (by classic Raman or SERS on bulk isolates) [13, 14, 27, 28, 37].

Next, we could show that the generated spectra, in combination with a PLS-DA classification model, allow us to separate between vesicles derived from B16F10 melanoma cells and RBC-derived vesicles. The fact that Raman spectroscopy is able to discriminate between vesicles from different cellular origin is in accordance with the very few reports available to date in which it was shown that classic Raman spectroscopy [13] and SERS [27, 28] on bulk or clusters of vesicles have discriminative power, even for more similar parent cells. Yet, as mentioned above, these reports are based on pure samples of one type of EV measured in bulk (i.e. millions of EVs are regarded and

analyzed as one entity). Here, instead, we tackled the pending challenge of using SERS for the identification and quantification of single cancerous ELVs that are present in a mixture with 'healthy' RBC-derived vesicles. While future research should focus on testing more complex mixtures with multiple types of vesicles, still this is a promising proof-of-concept study. We consider the subtle difference discriminated by SERS in previous work on bulk EVs as a promising indication that detecting cancerous ELVs in complex mixtures would be possible with our single vesicle SERS approach [28].

It is of note that an alternative approach with the potential of single vesicle SERS was very recently developed by Lee *et al.*. Their setup is based on Ag coated 'nanobowls' for hot-spot generation and SERS fingerprinting of EVs deposited into the nanobowls [37]. Though being a complex technological feat, our approach benefits from its simplicity and high-throughput potential. The AuNP based shell is formed by simple self-assembly and AuNP functionalized ELVs can be measured by standard Raman equipment. Furthermore, our approach can be easily combined with (standard) microfluidics and an optical trapping unit, allowing automated and fast SERS measurements. These characteristics will help to overcome the technological challenge of upscaling this technology for future clinical applications.

With the most sensitive set-up tested in this chapter, we could record clear Raman spectra at 0.5 s integration time per ELV. This means that per day it would be possible to analyze about 170 000 individual ELVs. As detectors continue to become more sensitive, and combined with the fact that a 0.5 s integration period already gave a strong and clear Raman spectrum, we expect that throughput could be increased 5-10 fold in the near future. Rapid recording of single spectra is indeed of pivotal importance for potential future diagnostic applications as 'diseased' ELVs are likely present in low abundance relative to the 'healthy' ones.

A particular challenge with our new approach is that SERS spectra of individual ELVs exhibit quite some variability, even for vesicles of the same parent cell. This originates from variability within the ELV population secreted by one cell type as discussed in **chapter 1** but potentially also from the (random) adsorption of AuNP on the vesicle surface and non-uniformity in hot spot generation [47]. In future research, therefore, it will be of interest to investigate other ways of functionalizing vesicles with AuNP with the aim to make the SERS spectra more uniform among vesicles of the same origin. This would allow to detect more subtle differences in molecular compositions and obtain more reliable molecular information from each individual vesicle. Additionally, the currently used AuNP coating component, DMAP, shields part of the region-of-interest in the obtained Raman spectra. Using an alternative molecule with a less pronounced fingerprint might enhance the obtained information, hence enlarge the discriminative power in more complex samples. In turn this will lead to even better specificity and

sensitivity. Apart from diagnostic applications, this method has the potential of being useful in an academic setting to deepen insight in molecular composition/diversity of the vesicles secreted by a certain cell type.

5. Conclusion

Our findings show that applying SERS technology on AuNP-coated ELVs in combination with PLS-DA is capable of sensing biomolecular diversity between ELVs from different origins. Although future research should focus on more complex ELV mixtures, we have clearly demonstrated the potential of single vesicle identification by SERS to obtain ratios of vesicles from different origins in a mixture.

Acknowledgements

The development and application of the dedicated multivariate statistical models (PLS-DA and MCR-ALS) was done by MM at the super resolution light microscopy and nanoscopy facility at ICFO. SS and KR are doctoral and postdoctoral fellows respectively of the Research Foundation - Flanders (FWO). The support of this institution is gratefully acknowledged. AGS gratefully acknowledges the support of BOF (Ghent University), FWO, and FP-7 EU project "DINaMIT". PB acknowledges the support of the Hercules grant AKUL2011/30. MM and PL acknowledge the Laser Lab Europe (grant agreement no.284464, EC's Seventh Framework Programme), the Photonics4Life network of excellence, the European regional Development Fund, the MINECO Severo Ochoa grant (SEV-2015-0522) and thank the support of Fundació Cellex Barcelona. We also like to thank Dr. H. Moehwald from the MPI-KG (Germany) for the use of the Raman microscopy facilities. Finally, we also thank Prof. D. Deforce for the use of the VersaDocTM imaging system.

References

[1] F. Properzi, M. Logozzi, S. Fais, Exosomes: the future of biomarkers in medicine, Biomark Med, 7 (2013) 769-778.

[2] S.A. Melo, L.B. Luecke, C. Kahlert, A.F. Fernandez, S.T. Gammon, J. Kaye, V.S. LeBleu, E.A. Mittendorf, J. Weitz, N. Rahbari, C. Reissfelder, C. Pilarsky, M.F. Fraga, D. Piwnica-Worms, R. Kalluri, Glypican-1 identifies cancer exosomes and detects early pancreatic cancer, Nature, 523 (2015) 177-182.

[3] D. Garnier, N. Jabado, J. Rak, Extracellular vesicles as prospective carriers of oncogenic protein signatures in adult and paediatric brain tumours, Proteomics, 13 (2013) 1595-1607.
[4] C. Lasser, V.S. Alikhani, K. Ekstrom, M. Eldh, P.T. Paredes, A. Bossios, M. Sjostrand, S. Gabrielsson, J. Lotvall, H. Valadi, Human saliva, plasma and breast milk exosomes contain RNA: uptake by macrophages, J. Transl. Med., 9 (2011) 9.
[5] M. Li, E. Zeringer, T. Barta, J. Schageman, A. Cheng, A.V. Vlassov, Analysis of the RNA content of the exosomes derived from blood serum and urine and its potential as biomarkers, Philos. Trans. R. Soc. Lond. B Biol. Sci., 369 (2014) 20130502.
[6] M. Szajnik, M. Derbis, M. Lach, P. Patalas, M. Michalak, H. Drzewiecka, D. Szpurek, A. Nowakowski, M. Spaczynski, W. Baranowski, T.L. Whiteside, Exosomes in Plasma of Patients with Ovarian Carcinoma: Potential Biomarkers of Tumor Progression and Response to Therapy, Gynecol Obstet (Sunnyvale), Suppl 4 (2013) 3.
[7] D.S. Choi, J. Lee, G. Go, Y.K. Kim, Y.S. Gho, Circulating extracellular vesicles in cancer diagnosis and monitoring: an appraisal of clinical potential, Mol. Diagn. Ther., 17 (2013) 265-271.
[8] H. Wang, L. Hou, A. Li, Y. Duan, H. Gao, X. Song, Expression of serum exosomal microRNA-21 in human hepatocellular carcinoma, BioMed research int., 2014 (2014) 864894.
[9] J. Skog, T. Wurdinger, S. van Rijn, D.H. Meijer, L. Gainche, M. Sena-Esteves, W.T. Curry, Jr., B.S. Carter, A.M. Krichevsky, X.O. Breakefield, Glioblastoma microvesicles transport RNA and proteins that promote tumour growth and provide diagnostic biomarkers, Nat. Cell Biol., 10 (2008) 1470-1476.
[10] M. Colombo, C. Moita, G. van Niel, J. Kowal, J. Vigneron, P. Benaroch, N. Manel, L.F. Moita, C. Thery, G. Raposo, Analysis of ESCRT functions in exosome biogenesis, composition and secretion highlights the heterogeneity of extracellular vesicles, J. Cell Sci., 126 (2013) 5553-5565.
[11] K. Laulagnier, H. Vincent-Schneider, S. Hamdi, C. Subra, D. Lankar, M. Record, Characterization of exosome subpopulations from RBL-2H3 cells using fluorescent lipids, Blood Cells Mol. Dis., 35 (2005) 116-121.
[12] J.R. Chevillet, Q. Kang, I.K. Ruf, H.A. Briggs, L.N. Vojtech, S.M. Hughes, H.H. Cheng, J.D. Arroyo, E.K. Meredith, E.N. Gallichotte, E.L. Pogosova-Agadjanyan, C. Morrissey, D.L. Stirewalt, F. Hladik, E.Y. Yu, C.S. Higano, M. Tewari, Quantitative and stoichiometric analysis of the microRNA content of exosomes, Proc. Natl. Acad. Sci. U. S. A., 111 (2014) 14888-14893.
[13] I. Tatischeff, E. Larquet, J.M. Falcon-Perez, P.Y. Turpin, S.G. Kruglik, Fast characterisation of cell-derived extracellular vesicles by nanoparticles tracking analysis, cryo-electron microscopy, and Raman tweezers microspectroscopy, J Extracell Vesicles, 1 (2012).
[14] F. Lavialle, S. Deshayes, F. Gonnet, E. Larquet, S.G. Kruglik, N. Boisset, R. Daniel, A. Alfsen, I. Tatischeff, Nanovesicles released by Dictyostelium cells: a potential carrier for drug delivery, Int. J. Pharm., 380 (2009) 206-215.
[15] D. Graham, R. Goodacre, Chemical and bioanalytical applications of surface enhanced Raman scattering spectroscopy, Chem Soc Rev, 37 (2008) 883-884.
[16] X.M. Qian, S.M. Nie, Single-molecule and single-nanoparticle SERS: from fundamental mechanisms to biomedical applications, Chem Soc Rev, 37 (2008) 912-920.
[17] G. McNay, D. Eustace, W.E. Smith, K. Faulds, D. Graham, Surface-enhanced Raman scattering (SERS) and surface-enhanced resonance Raman scattering (SERRS): a review of applications, Applied spectroscopy, 65 (2011) 825-837.

[18] B. Sharma, R.R. Frontiera, A.-I. Henry, E. Ringe, R.P. Van Duyne, SERS: Materials, applications, and the future, Materials Today, 15 (2012) 16-25.
[19] J. Langer, S.M. Novikov, L.M. Liz-Marzan, Sensing using plasmonic nanostructures and nanoparticles, Nanotechnology, 26 (2015) 322001.
[20] S.D. Hudson, G. Chumanov, Bioanalytical applications of SERS (surface-enhanced Raman spectroscopy), Anal. Bioanal. Chem., 394 (2009) 679-686.
[21] A. Yashchenok, A. Masic, D. Gorin, B.S. Shim, N.A. Kotov, P. Fratzl, H. Mohwald, A. Skirtach, Nanoengineered colloidal probes for Raman-based detection of biomolecules inside living cells, Small, 9 (2013) 351-356.
[22] S.C. Luo, K. Sivashanmugan, J.D. Liao, C.K. Yao, H.C. Peng, Nanofabricated SERS-active substrates for single-molecule to virus detection in vitro: a review, Biosens. Bioelectron., 61 (2014) 232-240.
[23] P.C. Wuytens, A.Z. Subramanian, W.H. De Vos, A.G. Skirtach, R. Baets, Gold nanodome-patterned microchips for intracellular surface-enhanced Raman spectroscopy, Analyst, 140 (2015) 8080-8087.
[24] L. Mikoliunaite, R.D. Rodriguez, E. Sheremet, V. Kolchuzhin, J. Mehner, A. Ramanavicius, D.R. Zahn, The substrate matters in the Raman spectroscopy analysis of cells, Sci. Rep., 5 (2015) 13150.
[25] T. Lemma, A. Saliniemi, V. Hynninen, V.P. Hytönen, J.J. Toppari, SERS detection of cell surface and intracellular components of microorganisms using nano-aggregated Ag substrate, VIBRAT SPEC, 83 (2016) 36-45.
[26] T. Buchner, D. Drescher, H. Traub, P. Schrade, S. Bachmann, N. Jakubowski, J. Kneipp, Relating surface-enhanced Raman scattering signals of cells to gold nanoparticle aggregation as determined by LA-ICP-MS micromapping, Anal. Bioanal. Chem., 406 (2014) 7003-7014.
[27] L. Tirinato, F. Gentile, D. Di Mascolo, M.L. Coluccio, G. Das, C. Liberale, S.A. Pullano, G. Perozziello, M. Francardi, A. Accardo, F. De Angelis, P. Candeloro, E. Di Fabrizio, SERS analysis on exosomes using super-hydrophobic surfaces, Microelectronic Eng., 97 (2012) 337-340.
[28] L.G. Laura T. Kerr, Karolina Weiner Gorzel, Shiva Sharma, Malcolm Kell, Amanda Mc Cann, Bryan M. Hennelly, Raman spectroscopy and SERS analysis of ovarian tumour derived exosomes (TEXs): a preliminary study, Biophotonics: Photonic Solutions for Better Health Care IV, 91292Q (2014).
[29] P. Vader, M.H. Fens, N. Sachini, B.A. van Oirschot, G. Andringa, A.C. Egberts, C.A. Gaillard, J.T. Rasmussen, R. van Wijk, W.W. van Solinge, R.M. Schiffelers, Taxol((R))-induced phosphatidylserine exposure and microvesicle formation in red blood cells is mediated by its vehicle Cremophor((R)) EL, Nanomedicine, 8 (2013) 1127-1135.
[30] D.I. Gittins, F. Caruso, Spontaneous phase transfer of nanoparticulate metals from organic to aqueous media, Angew. Chem. Int. Ed. Engl., 40 (2001) 3001-3004.
[31] X. Liu, M. Atwater, J. Wang, Q. Huo, Extinction coefficient of gold nanoparticles with different sizes and different capping ligands, Colloids and surfaces. B, Biointerfaces, 58 (2007) 3-7.
[32] H. Deschout, T. Martens, D. Vercauteren, K. Remaut, J. Demeester, S.C. De Smedt, K. Neyts, K. Braeckmans, Correlation of dual colour single particle trajectories for improved detection and analysis of interactions in living cells, Int J Mol Sci, 14 (2013) 16485-16514.
[33] K.G. Stamplecoskie, J.C. Scaiano, V.S. Tiwari, H. Anis, Optimal Size of Silver Nanoparticles for Surface-Enhanced Raman Spectroscopy, J. Phys. Chem. C., 115 (2011) 1403-1409.

[34] J.W. Kang, P.T. So, R.R. Dasari, D.K. Lim, High resolution live cell Raman imaging using subcellular organelle-targeting SERS-sensitive gold nanoparticles with highly narrow intra-nanogap, Nano letters, 15 (2015) 1766-1772.
[35] M. Marro, C. Nieva, R. Sanz-Pamplona, A. Sierra, Molecular monitoring of epithelial-to-mesenchymal transition in breast cancer cells by means of Raman spectroscopy, Biochim. Biophys. Acta, 1843 (2014) 1785-1795.
[36] J. Van Deun, P. Mestdagh, R. Sormunen, V. Cocquyt, K. Vermaelen, J. Vandesompele, M. Bracke, O. De Wever, A. Hendrix, The impact of disparate isolation methods for extracellular vesicles on downstream RNA profiling, J Extracell Vesicles, 3 (2014) 24858.
[37] C. Lee, R.P. Carney, S. Hazari, Z.J. Smith, A. Knudson, C.S. Robertson, K.S. Lam, S. Wachsmann-Hogiu, 3D plasmonic nanobowl platform for the study of exosomes in solution, Nanoscale, 7 (2015) 9290-9297.
[38] S. Mathivanan, C.J. Fahner, G.E. Reid, R.J. Simpson, ExoCarta 2012: database of exosomal proteins, RNA and lipids, Nucleic Acids Res., 40 (2012) D1241-1244.
[39] D.M. Pegtel, L. Peferoen, S. Amor, Extracellular vesicles as modulators of cell-to-cell communication in the healthy and diseased brain, Philos. Trans. R. Soc. Lond. B Biol. Sci., 369 (2014) 20130516.
[40] Z. Movasaghi, S. Rehman, I.U. Rehman, Raman Spectroscopy of Biological Tissues, Appl Spectroscopy Rev, 42 (2007) 493-541.
[41] D. Ballabio, V. Consonni, Classification tools in chemistry. Part 1: linear models. PLS-DA, Analytical Methods, 5 (2013) 3790-3798.
[42] D.S. Choi, D.K. Kim, Y.K. Kim, Y.S. Gho, Proteomics, transcriptomics and lipidomics of exosomes and ectosomes, Proteomics, 13 (2013) 1554-1571.
[43] A. Bonifacio, S. Dalla Marta, R. Spizzo, S. Cervo, A. Steffan, A. Colombatti, V. Sergo, Surface-enhanced Raman spectroscopy of blood plasma and serum using Ag and Au nanoparticles: a systematic study, Anal. Bioanal. Chem., 406 (2014) 2355-2365.
[44] R.A. Sperling, W.J. Parak, Surface modification, functionalization and bioconjugation of colloidal inorganic nanoparticles, Philosophical transactions. Series A, Mathematical, physical, and engineering sciences, 368 (2010) 1333-1383.
[45] C.L. Haynes, R.P. Van Duyne, Nanosphere Lithography: A Versatile Nanofabrication Tool for Studies of Size-Dependent Nanoparticle Optics, J. Phys. Chem. B., 105 (2001) 5599-5611.
[46] W.R. Premasiri, J.C. Lee, L.D. Ziegler, Surface-Enhanced Raman Scattering of Whole Human Blood, Blood Plasma, and Red Blood Cells: Cellular Processes and Bioanalytical Sensing, The J. Phys. Chem. B., 116 (2012) 9376-9386.
[47] W. Xie, P. Qiu, C. Mao, Bio-imaging, detection and analysis by using nanostructures as SERS substrates, J. Mater. Chem., 21 (2011) 5190-5202.

Supporting information

Supporting figures

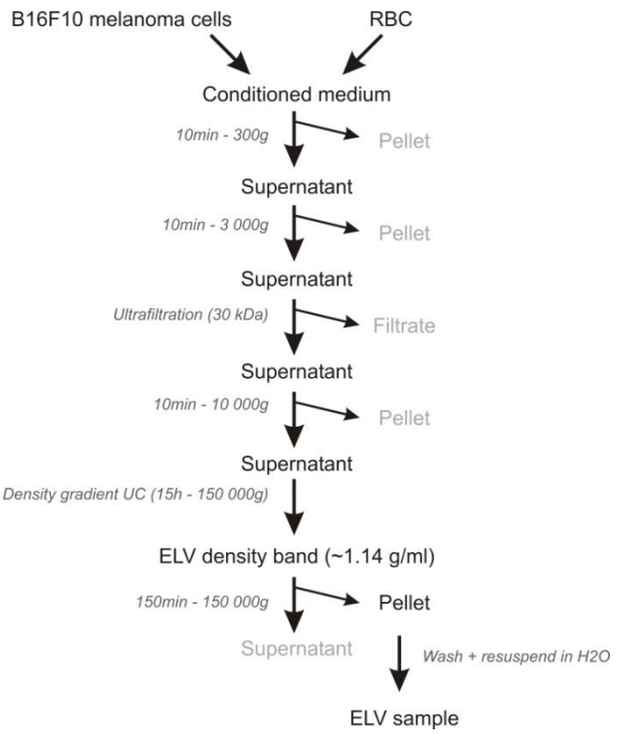

Figure S1. Schematic representation of the protocol used to purify exosome-like vesicles (ELVs) from conditioned cell medium of B16F10 melanoma cells and RBC.

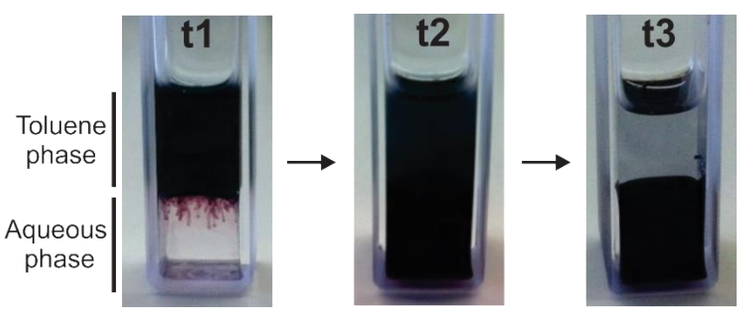

Figure S2. AuNP transfer from the toluene phase to the aqueous phase exchanging their tetraoctylammonium bromide coat for a DMAP coating at three different time points (t1 = ~5 minutes, t2 = ~20 minutes and t3 = ~60 minutes) after mixing.

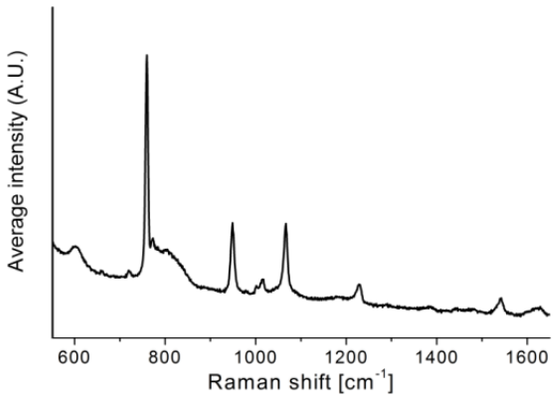

Figure S3. Raman fingerprint of 4-dimethylaminopyridine (DMAP). Average SERS spectrum of twenty normalized spectra of DMAP-coated AuNP aggregates to determine the DMAP fingerprint.

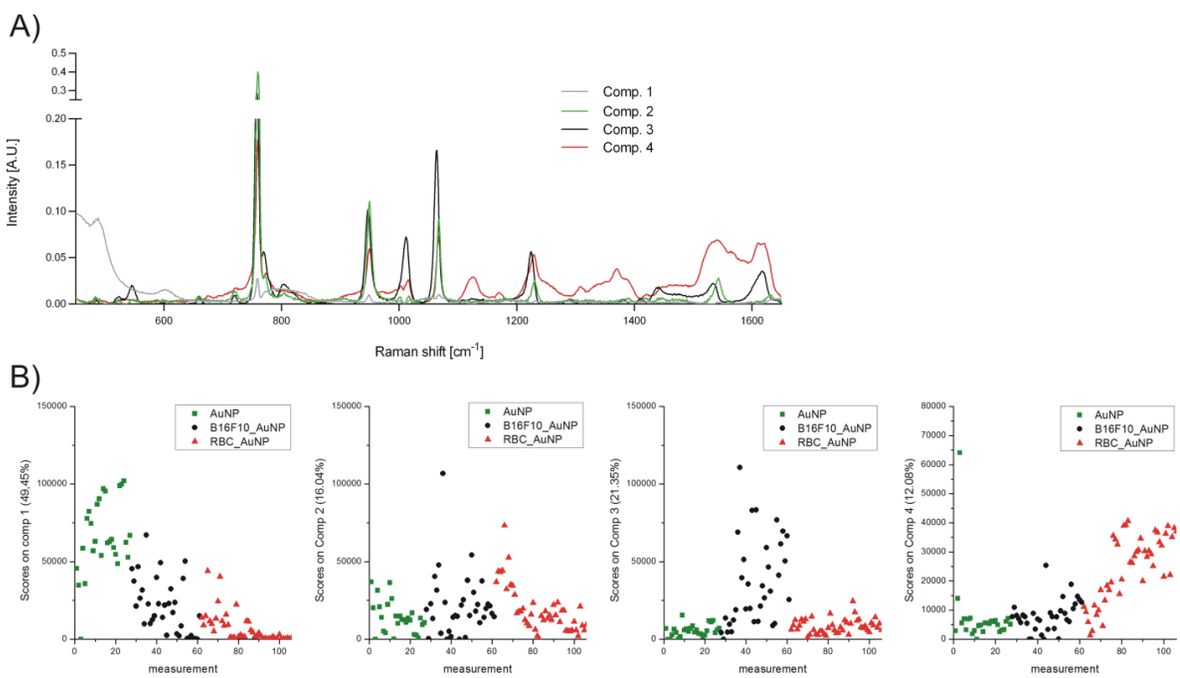

Figure S4. Output of the MCR-ALS algorithm. [A] Deconvolved Raman spectra. [B] Score for each deconvolved spectrum (y-axis) for all recorded spectra (x-axis) allowing to allocate the deconvolved spectra to a specific source (i.e. quartz, DMAP, B16F10 and RBC vesicles).

Supporting tables

Table S1. Antibodies used for immunoblotting.

Target	Dilution	Supplier	Cat.#	Reducing conditions [2]	MW (kDa)
CD 81	1:1 000	LS biosciences Inc.	LS-C108453	No	~25-30
CD 63	1:500	Tebu-bio	GTX37555	No	~40
β-actin	1:1 000	Cell Signaling Techn.	4970	Yes	~45
Hsp 70	1:1 000	LS biosciences Inc.	LS-C24142	Yes	~70
Rabbit IgG[1]	1:50 000	Millipore	AP307P	/	/

[1]The secondary antibody is linked to a HRP-enzyme; [2]Reducing conditions imply heating of the sample to 95 °C for 5 minutes in the presence of 2-mercaptoethanol.

Table S2. PLS-DA classification of the Raman spectra of unmixed samples recorded with an integration time of 500 ms.

Sample	*n* [1]	PLS-DA prediction	
		Correct identification	Wrong identification
B16F10_AuNP	53	53	0
RBC_AuNP	64	64	0

[1]*n* is the amount of spectra recorded for each sample

6

Broader international context, relevance and future perspectives

Stephan Stremersch[1], Stefaan De Smedt[1], Koen Raemdonck[1]

[1]Laboratory of General Biochemistry and Physical Pharmacy, Ghent University, Ghent, Belgium

Chapter 6: ToC

Abstract

The work presented in this thesis can be categorized in two distinct biomedical domains, namely the development of drug delivery carriers and the search for new analytical techniques with diagnostic potential. Both applications were founded on the concept of extracellular vesicles (EVs) being molecular information packages released by cells. In this final chapter these two fields of application are more broadly outlined. Moreover, the development of the EV field is reviewed from a pharmaceutical point-of-view with a discussion of the current status and future perspectives of each of the potential applications.

1. Extracellular vesicles as drug delivery vehicle

Drug delivery carriers aim to counteract intrinsic unfavorable features associated with free therapeutics. These depend on the nature of the compound and can include poor stability, poor solubility, inability to cross biological barriers and off-target effects. Ideally, a drug carrier should prevent recognition by the immune system, both the innate and adaptive immune system, to allow prolonged circulation in the bloodstream and enable repeated administration, respectively. Moreover, drug carriers should guide the therapeutic to the designated target tissue and shuttle the cargo over the relevant biological barriers. Fuelled by advances in the nanotechnology field, carriers have been developed, of which polymer- and lipid-based nano- and microparticles are most frequently investigated. The intensive research exploring this synthetic approach has only partially met the expectation with market output restricted to carriers for small molecules (e.g. Caelyx®, doxorubicin; Genoxol-PM®, paclitaxel) and extracellular active proteins/aptamers (e.g. Oncaspar®, pegaspargase; Macugen®, Pegaptanib). For the intracellular delivery of macromolecules (e.g. siRNA, DNA) many issues remain insufficiently resolved despite the many years of investigation. At the cellular level, for example, detailed analysis revealed that only ~3.5 % of the delivered (*via* lipid-based transfection agents) siRNA is able to escape the endosomes and reach the cytoplasm [1]. Moreover, only a fraction of these siRNA strands are incorporated into the RISC so that only 0.25 – 0.1 % of the total internalized siRNA is functional [2]. At the extracellular level, many inventive strategies have been developed to (1) confer stealth properties to (nano)carriers by modifying their surface with biocompatible, flexible and hydrophilic polymers (e.g. polyethylene glycol, polyvinylpyrrolidone), (2) enhance cellular internalization by equipping the carriers with antibodies/nanobodies® recognizing surface receptors of the target cell of interest [3] and (3) improve tissue targeting by reducing the carrier size to exploit the inherent augmented vascular permeability in some tissues (e.g. the EPR-effect in fast growing tumor tissue) [4]. However, despite these advances, the carrier biodistribution, targeting of other (extrahepatic) tissues of interest and the avoidance of immune recognition, remains inadequate.

Bearing in mind the above intra- and extracellular deficiencies of synthetic carriers, the drug delivery community is increasingly interested in critically examining natural carriers which have evolved over millions of years to accomplish certain tasks. Red blood cells (RBC) for example inherently have a long blood circulation time (i.e. ~120 days) making them ideal candidates for the delivery of long-acting drugs who have to function in the blood circulation (e.g. anti-coagulant agents) [5]. Another example is the exploitation of the inherent ability of cytotoxic CD8(+) T cells to cross the endothelial barrier and infiltrate tumor tissue for the delivery of hitchhiking liposome-enclosed therapeutics [6].

One of the most successful applications of bio-inspired drug delivery carriers is the use of viruses. As viruses have naturally evolved to transfer their genes into the host as an essential mechanism of self-replication, their exploitation as carrier for therapeutic nucleic acids (e.g. siRNA, mRNA and pDNA) is a rational concept which has led to the first gene-therapy based medicine approved in Europe and the USA (i.e. Glybera) [7]. In addition, also other, less known yet inventive approaches using pathogens have been explored for drug delivery, including the use of anaerobic bacteria for their potential to migrate to hypoxic areas (e.g. tumors or infarcted myocardium) [8, 9]. Unfortunately, these (modified) pathogens risk recognition by the adaptive and innate immune system limiting repeated applications and potentially provoking an overreaction of the immune system with detrimental effects (e.g. the Jesse Gelsinger case) [10]. Additionally, the possibility of insertional mutagenesis with subsequent cancer development for certain virus types (i.e. retroviruses) is reported in clinical tests, which often limits their envisioned applications for the treatment of life-threatening diseases [11].

It is within this context of bio-inspired drug delivery vehicles that EVs are considered as an endogenous, hence safe, new type of carrier for macromolecules. In this thesis, we focused on the delivery potential of EVs for oligonucleotides, more specifically siRNAs. Although a very promising study in 2011 reported on using targeted EVs for siRNA delivery to the brain in an Alzheimer mouse model [12], still many ambiguities need to be addressed before reproducible therapeutic applications of EVs become feasible.

A first step in this process is the development of strategies to obtain vesicle isolates devoid of non-EV contaminants. Different techniques have been used throughout the literature as comprehensively overviewed in **chapter 1**. Most of these techniques are derived from other fields of research (e.g. virology, biopharmacy, *etc.*) and adapted for EV purification. However, to date no consensus has been reached within the ISEV community on which methodology should be regarded as the gold standard. Recent studies [13-15], including the findings presented in **chapter 3**, have provided new insights in the purity of the isolates obtained by different strategies and highlight the impact on both loading with nucleic acids and cellular uptake of fluorescently labeled EVs.

Secondly, to translate EVs to a drug delivery vehicle, efficient methods to load EVs with a drug of interest are needed. One often used method is loading the EV producing cell with the therapeutic RNA and relies on the cell's inherent machinery to package the cargo into the EVs (i.e. pre-formation loading) [16, 17]. An alternative approach, explored throughout this thesis, is the post-formation loading of EVs isolated from conditioned cell culture medium or biological fluids. In this way, it can be anticipated that the EV loading efficiency will be independent of the RNA sequence and the cell type used. Moreover, if successful, such an approach would allow for a better control over the

loading process, enabling quantitative and homogenous loading of all EVs produced. Unfortunately, in order to load purified EVs with exogenous (small) RNA's without compromising its functionality, few methods are available. Out of the currently used nucleic acid delivery vehicles, liposomes are most analogous to EVs especially from a physicochemical point of view. Hence, reflection on almost five decades of research on liposomal drug delivery systems could provide some valuable clues on how to reach this goal [18]. Yet it is important to note that liposomal nucleic acid delivery generally involves electrostatic complexation of the negatively charged siRNA *via* cationic lipids which are notorious for their *in vitro* and *in vivo* toxicity [19]. However, EVs are known to carry a negative surface charge, hence precluding electrostatic siRNA complexation. Passive loading of siRNA into (negatively charged) liposomes requires the addition of the nucleic acids prior to liposome formation which is not feasible for isolated EVs and as a rule entails low encapsulation efficiencies. In addition, the inherent complex composition of EVs, containing proteins next to lipids, rules out the use of organic solvent based methods or repeated freeze-thaw cycles because of potential interference with protein stability and (partial) loss of functionality [20]. Pre-complexation of siRNA *via* cationic liposomes followed by fusion with isolated EVs has been evaluated for EV loading with siRNA by different groups [21, 22]. However, this approach appeared to be impractical as the EVs could not be isolated from the remaining transfection liposomes/micelles, making it impossible to determine the location of the siRNA and the associated loading efficiency [21]. Ideally, the loaded nucleic acids are encapsulated in the core of the isolated EVs as this mimics their natural localization and likely leads to the most optimal intracellular delivery. In a first effort towards such intravesicular loading, Alvarez-Erviti and colleagues used electroporation of an EV/siRNA mixture to induce transient pores in the EV membrane, allowing the siRNA to migrate through the lipid bilayer. Using this approach, these authors reported siRNA encapsulation efficiencies up to 25 % [12]. This post-loading method was followed by many others [21, 23-27]. Importantly, as thoroughly investigated in **chapter 2**, duplication of these experiments under identical experimental conditions revealed that the aforementioned siRNA encapsulation was largely due to unspecific aggregate formation, independent of the presence of EVs. The latter aggregates resulted from the interaction of multivalent cations, released from the metal electrodes in the electroporation cuvettes, with hydroxyl anions present in the electroporation buffer and were shown to co-precipitate siRNA [28]. After blocking aggregate formation, by virtue of an acidic citrate electroporation buffer or the use of polymer based electroporation cuvettes, no significant encapsulation of siRNA could be measured [29]. Our work underscores the importance of incorporating appropriate control experiments that often are not considered in the literature (i.e. electroporation of samples without EVs) and highlights the need to carefully optimize the applied electroporation buffer and EV concentration. Since the publication of our observations

[29], several groups have tried to prevent this aggregate formation through the use of chelating agents (e.g. EDTA), as used in our study, [30] or membrane stabilizers (e.g. trehalose) [24, 31]. Nonetheless, even if transient pores would be formed in the EV membrane and aggregation can be prevented, given that electroporation by definition relies on passive loading, it can only be efficient in extremely high concentrated EV isolates.

The shortcomings of electroporation and the current lack of alternatives to load hydrophilic macromolecules have prompted us to explore alternative approaches. In this respect we used cholesterol-modified siRNA (chol-siRNA) as a general, post-formation loading approach to associate siRNA to EVs (**chapter 4**). It was clearly shown that simple mixing of isolated EVs and chol-siRNA lead to insertion of the latter in the vesicular membrane. Moreover, in this chapter we postulated three complementary assays that consider the inherent complexity of EV samples, which can be readily used by other researchers to unambiguously confirm the association of a (nucleic acid) cargo with EVs. Of note, before application in a clinical setting (e.g. as IV injectable) can be contemplated, the stability of the chol-siRNA insertion in complex biological fluids (e.g. blood) needs to be verified. Nonetheless, this method has proven to be useful in less complex biological fluids and valuable for *in vitro* screenings as a fast and producer-cell independent method for loading siRNA and hence can form an interesting research tool. Despite our new loading approach being useful for our intended application (i.e. comparing EVs with synthetic nanocarriers at the cellular level), new techniques to obtain therapeutic cargo loading in the lumen of EVs are still highly desired, in particular for macromolecular drugs.

Thirdly, to truly assess the impact EVs might have on the drug delivery field it is important to compare the drug delivery efficiency of this new carrier to the state-of-the-art. Currently, the general perception in the field is that EVs are extremely efficient in macromolecular cargo delivery across cellular barriers [32]. However, the direct experimental comparison between current state-of-the-art carriers and EVs has never been made. In **chapter 4** we aimed to address this question and could show that EVs, under the indicated experimental conditions, were not efficient from a drug delivery point of view. Also other reports that describe EVs as vesicles involved in intercellular communication present data in which the functionality of EVs for macromolecular delivery is statistically significant yet the terminology 'efficient' is arguable. In the publication by Zomer *et al.,* which uses the extremely sensitive Cre-loxP system as a transfection read-out assay for mRNA delivery, a co-culture experiment shows that when culturing producer and accepter cells in a 1:1 ratio maximally 2 % of the recipient cells was functionally transfected. For a 100:1 ratio this increased to a maximum of 10 % positive cells. Intratumoral injection of purified EVs, bearing the Cre recombinase

mRNA, rendered only 0.05 % positive cells (compared to 0.02 % as negative control) [33]. The here reported efficiencies in macromolecule delivery, although tracking a different type of cargo (i.e. mRNA vs miRNA/siRNA), are in line with the lack of significant gene target knockdown obtained with EVs in our study (**Chapter 4**). Moreover, a major part of the literature reporting successful delivery of RNAi-based therapeutics with EVs, are based on EVs modified with cell penetrating peptides [12, 26] or additional aids such as Lipofectamine LTX and the fusogenic GALA peptide [34]. Indeed, an increasing number of papers focuses on modifying EVs to improve the biodistribution, cell targeting specificity and endosomal escape efficiency. For example, the RVG-targeting and delivery of siRNA using EVs, by Alvarez-Erviti and colleagues, is one of the most cited papers and supporters of the intensifying research harnessing EVs as a drug delivery carrier. However, the authors show that in the absences of RVG, no functional delivery of siRNA by EVs was observed (also not *in vitro*) [12]. Additionally, a more recent study shows that synthetic liposomes, equipped with the RVG targeting ligand, can also migrate over the blood brain barrier (BBB) [35]. In this respect it is important to discriminate between inherent features of EVs and functionalities endowed by certain modifications. The observation of the limited circulation time of IV injected EVs has prompted the PEGylation of EVs which indeed prolongs their circulation time [36]. Yet, this modification will also interfere with the EV-cell interactions, which inevitably evokes the question of how we should appraise the added value of EVs over synthetic drug delivery carriers (e.g. liposomes). Indeed, a direct comparison between EVs and state-of-the-art delivery vehicles urges itself and, given the complexity and costs associate to working with EVs, only a substantial benefit could make EVs eligible for further therapeutic development.

One of the initial characteristics attributed to EVs that evoked, among others, the interest from the drug delivery community was that EVs might have an inherent cell specificity [37-39]. This is of particular interest as targeting is one of the current hurdles in the nanomedicine research community. Such specificity could also be of value to mitigate off-target effects. In this regard, it would be of interest that next to databases as EVpedia [40], Vesiclepedia [41] and Exocarta [42], i.e. databases that collects published information on the molecular composition of EVs, a database for EV specificity would be initiated. This database could accumulate information on e.g. producer-acceptor cell pairs for which successful biomolecule/drug delivery was demonstrated. Preferably this would be accompanied by an assay, by which the efficiency of the (macro)molecular delivery was measured. This will provide valuable information from a drug delivery point-of-view as this can guide the choice of producer cell, dependent on the envisioned therapeutic application. Moreover, this will help mapping the physiological EV-mediated intercellular communication networks.

In summary, although harnessing EVs as carriers for macromolecular therapeutics is a relatively new field of research, already a substantial number of valuable achievements have been published. However, the findings in our studies revealed important issues that will have to be addressed before clinical translation becomes within reach. These new insights can guide future research towards new loading strategies and incite the drug delivery field to include comparison to state-of-the-art delivery vehicles as good scientific practice. Such an approach will provide critical information needed to truly assess the value and impact EVs will have as advanced drug delivery tools.

2. Characterization of extracellular vesicles for diagnostics

As the true complexity and heterogeneity of EVs is becoming more apparent, the search for new techniques to characterize them is increasing. Indeed, in **chapter 1** we contextualize the need for techniques that allow analysis of EVs at the single vesicle level to increase the insight in some elementary biological principles and to enhance the sensitivity of EV-based diagnostic tools. To date, only few techniques are available which are able to characterize single EVs. An overview of such techniques, with their respective information output, is provided in **table 1**. It can be appreciated that most techniques are limited to physicochemical characterization (i.e. size and surface charge) and concentration measurements. In addition, some characterization techniques provide a (quantitative) window on the presence of well-defined molecular components on single EVs. In practice this translates in techniques that allow to confirm the association between an EV and an antibody/lectin/aptamer that recognizes a specific (surface) component. This can be done by immuno-electron microscopy, high resolution flow cytometry, fluorescence correlation spectroscopy and fluorescence-based SPT, providing useful information regarding the vesicular heterogeneity [43-45]. It is important to note here that these approaches are restricted to a limited amount of well characterized (surface) markers. A broader molecular view can be obtained with Raman microspectroscopy in combination with optical trapping [46]. A Raman spectrum can be considered as a fingerprint of all molecular bonds that are present within a focal volume, albeit without defining specific molecules. Nonetheless, we (**chapter 5**) and others [47-49] have shown that based on this fingerprint it is possible to discriminate between EVs from different cellular origin. Raman spectroscopy is able to operate at single EV level in solution and provides a large amount of information. Yet, it lacks the speed of e.g. flow cytometry. Indeed, recording clear Raman spectra of individual EVs required an integration time of 5 minutes per vesicle [46]. It is in the context of this limitation that in **chapter 5** we developed a SERS-based platform for EV characterization. By decorating single EVs with self-assembling miniature SERS substrates, clear Raman spectra could be obtained within 500 ms. Based on these fingerprints it was possible to

discriminate between EVs from RBC and melanoma cells in a mixture by means of statistical models trained by reference libraries of the respective EV types.

Table 1. Techniques with the potential of EV characterization at the single vesicle level

Technique	Type of information	Background
Scattering-based SPT [50]	• Size • Surface charge • Concentration • Refractive index	Size determination *via* Rayleigh scattering-based tracking of the Brownian motion of EVs.
Tunable resistive pulse sensing [51]	• Size • Surface charge • Concentration	Monitors the change in current flow through an (adaptable) aperture.
Atomic force microscopy [52]	• Size • Mechanical stiffness	Sample information by scanning the sample using a mechanical probe.
Immuno-electron microscopy [43]	• Size • The presence of proteins *via* gold tagged antibodies	Morphological information but time consuming with low throughput.
Frequency-locked microtoroid optical resonators [53]	• The presence of surface molecules *via* antibodies	Measures the change in resonant frequency of a microtoroid upon binding of an EV to an antibody in close proximity to the microtoroid inducing a change in refractive index
Fluorescence-based SPT [45]	• Size • Surface charge • The concentration of EVs containing specific surface molecules (*via* fluorescently tagged antibodies)	Size determination *via* fluorescence-based tracking of the Brownian motion of EVs.
High resolution flow cytometry [44]	• The presence of surface molecules *via* fluorescent tagged antibodies • Concentration	A flow cell through which the sample is guided using sheath fluid with recording of Rayleigh scattering and fluorescence. For EVs smaller than 300 nm, the scattering signals are no longer able to differentiate between single events and doublets or what is called swarm analysis.
Fluorescence correlation spectroscopy [54]	• Size • The presence of surface molecules *via* fluorescently tagged antibodies • Concentration	The size distribution is obtained from fluorescence intensity fluctuations caused by particles moving by Brownian motion through a well-characterized illuminated volume. The presence of specific surface markers can be identified by fluorescently labeled antibodies.
Raman micro-spectroscopy in combination with optical trapping [46]	• A spectral fingerprint representative for the molecular bounds	Inelastic scattering of monochromatic light by vibrations of molecular bounds renders a spectrum dependent on the molecules present.

SPT single particle tracking

As EVs are regarded as easy accessible biomarkers through liquid biopsy (**chapter 1**), techniques that can provide EV-related information can be valuable in a diagnostic context. To date, most approaches use 'omics' techniques to obtain in-depth molecular information such as proteomics, transcriptomics, miRnomics, *etc*. These analysis are very valuable as they can provide a detailed view on molecular components that differ between 'healthy' and 'diseased' EVs, which can subsequently be translated in a diagnostic assay. One of the most successful clinical examples following this workflow identified EV-associated glypican-1 (i.e. a surface proteoglycan) as a biomarker for pancreatic cancer, which was subsequently developed into an antibody-based assay. Not only did it show absolute specificity and sensitivity to detect pancreatic cancer in patient samples but it was also able to detect the presence of tumor cells before they appeared on magnetic resonance imaging scans in a mouse model [55]. Despite this important achievement, only few liquid biopsy-based assays have been successfully introduced in clinical practice. One of the reasons for this is the lack of adequate analytical readout techniques. Indeed, assays often fail in achieving adequate sensitivity and specificity due to the fact that proteins or metabolites are present at an extremely low level among thousands of other comparable components. Using EVs as a biomarker source partially circumvents this needle-in-a-haystack hurdle by excluding abundant biofluid components (e.g. albumin in blood). Nonetheless, early stage diseased patients will still have a low percentage of 'diseased' EVs compared to healthy EVs [56].

Whether our SERS-based platform can provide an added value over current diagnostic methods will depend on some key technical and conceptual uncertainties that have to be addressed before the implementation in the clinic can be envisioned. A fist important question is to which extent Raman spectroscopy is specific enough to discriminate between hundreds or even thousands of EVs which are inherently present in a relevant biological fluid (e.g. urine, plasma). Moreover, we observed variability within the spectra of EVs generated by the same cell. Part of this variability will undoubtedly find its origin in the EV heterogeneity as was also previously observed (**chapter 1**) [46]. Yet, SERS is also notorious for the variability induced by the inconsistency in hotspot generation [57]. This additional factor of variability might reduce our discriminative power and hence should be taken into consideration. Secondly, it is difficult to estimate the amount of EVs that have to be screened in a diagnostic test for early disease detection. This will certainly depend on the location and the type of disease. Although difficult to predict, this factor will determine whether the current integration times are sufficiently short to enable the implementation of our SERS-based platform for clinical samples with reasonable analysis times.

If the above mentioned hurdles can be overcome, the SERS-based platform has the potential to be further developed in a clinical setting. It is however important to note

that the technology is dependent on the availability of a reference spectrum to link the measured Raman signature to a cellular origin with associated pathological condition. One possible clinical implementation of the platform would be to build a reference library of spectra of different 'diseased cell'-derived EVs (e.g. cancer cells) and screen clinical samples for the presence of these spectra. Using this approach, the technology can be positioned as a tool for early disease detection. However, this methodology might not always be befitting as it is for example known that tumor cells, and their secretome, have a high inter-patient variability, urging the implementation of personalized medicines and diagnostics. In this context, the presented platform can be exploited as a post-surgery follow-up tool in which 'tumor biopsy'-derived EVs are used to record reference spectra. Following this approach, the platform can detect tumor recurrence in an early stage after treatment/surgery *via* a simple 'liquid biopsy'.

Independent of the success of this specific diagnostic platform, it is clear that Raman spectroscopy is gaining popularity to address biomedical questions. The advantage of non-destructive label-free detection and the possibility to work in aqueous media makes this technique suitable for live cell characterization [58] and direct *in vivo* measurements with diagnostic potential [59]. The latter includes cancer detection in easy accessible organs such as the skin, cervix and the gastro-intestinal organs [60] but also as a real-time probe for surgical guidance [61]. It can be anticipated that in the field of EV characterization Raman spectroscopy in its different forms (i.e. classic Raman, SERS, TERS and CARS) will be increasingly used as is evident from different abstracts exploiting Raman spectroscopy on the latest ISEV meetings [62, 63].

3. Pharmaceutical perspectives for extracellular vesicles

The research on EVs is exponentially growing in the last decade as is evident from the increasing amount of publications on the subject appearing each year (**figure 1**) and from the growth of the ISEV community. Originally, EVs were mainly positioned as a cellular mechanism to discard waste material. This was shown in the late 1980s for certain surface proteins [64], but also more recent work reports on biomolecule removal *via* EVs as a mechanism of cellular homeostasis. With regard to miRNAs, work by Squadrito and colleagues showed that the sorting of miRNAs in EVs is dependent on the intracellular miRNA concentration. Indeed, overexpression of a miRNA target sequence results in an enrichment of the respective miRNA in processing-bodies and the cellular cytoplasm and depletion from multivesicular bodies, hence EVs. Alternatively, overexpression of the miRNA enhances its release *via* EVs [65]. Also the fact that the majority of EV-encapsulated mRNAs are fragmented [66] and the EV-mediated release of drugs by chemo-resistant malignant cells [67] strengthens this hypothesis of a waste

removal mechanism. Nevertheless, the last decade the perception on EVs has shifted to mediators of a new route of intercellular communication. Most EV-orientated research to date focuses on elucidating new EV-mediated intercellular networks [68]. However, many reports on the function of EVs should be reassessed in light of the used purification strategy. Our own observations (**chapter 3**) and other reports in the literature [13] indeed indicate that the traditional purification strategies co-isolate many non-vesicular components that might contribute to the assumed EV-induced phenotype in recipient cells. This does not imply that purification strategies categorized as less stringent (e.g. precipitation) have no place in EV research. They certainly can provide a valuable research tool but should be considered more as a preparative concentration step prior to more rigorous EV isolation and purification. When using these techniques in a research setting it is important to incorporate adequate controls that allow to reliably link an observed effect to the presence of EVs (e.g. *via* EV depletion experiments). Additionally, the nature and relevance of these EV-induced effects in an *in vivo* situation are largely unknown, which remains an important topic for future investigation.

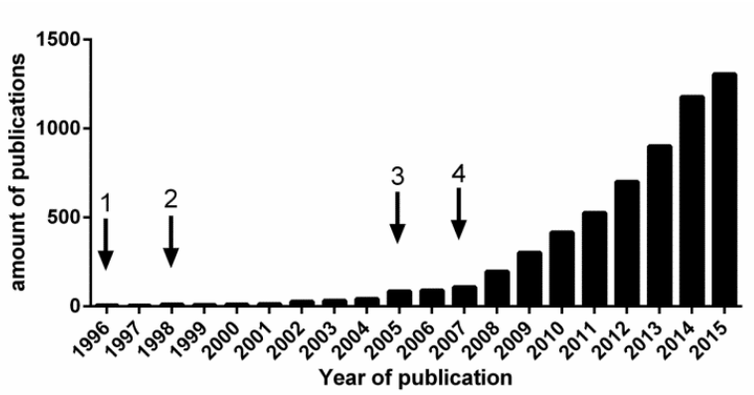

Figure 1. **The growth of EV research in the last 20 years.** The graph depicts the amount of publications that appeared each year in PubMed using: ("extracellular vesicles" OR exosomes OR ectosomes) as search keywords. Some of the key papers that were important for the development of the field are indicated in the graph: (1) EVs from B-lymphocytes are shown to be able to present antigens to T cells [69], which provides a first indication of the communication function of EVs. (2) EVs derived from dendritic cells (DC) loaded with antigens are used as an anti-cancer vaccine [70], which exploits for the first time EVs in a therapeutic context. (3) The first clinical trial using these DC-derived EVs for anti-cancer vaccination [71]. (4) Report on the presence in and functional transport of RNA by EVs [72] further confirming the communication function of EVs and attracting the attention from the drug delivery community.

This seemingly conflicting function of EVs in waste removal and intercellular communication is not necessarily incompatible. The discrepancy in observed function can be in agreement with the mounting evidence of intracellular EV heterogeneity in which it would be theoretically possible that certain EV subtypes have an important communication function while others are used for waste removal. Nonetheless, its

ambiguity again indicates the limited understanding we currently have on EV functions. In this context characterization approaches that allow single EV analysis can again provide valuable new insights.

Currently, most research still focuses on elucidating the physiological function of EVs. In addition to this fundamental research, a plethora of clinical applications are starting to develop, trying to harness EVs to benefit the patient (**chapter 1**). Here, the current status and future perspective of the EV landscape as a pharmaceutical tool is discussed by scoring the different application strategies on the 'technology readiness level' (TRL) scale (**figure 2**). It is clear that the field of vaccination, especially against prokaryotic infections, is the most developed with already a product on the market based on outer membrane vesicles (OMVs) derived from bacteria as antigen source adsorbed to $Al(OH)_3$ as adjuvant [73]. Anti-cancer vaccination is also scored high on the TRL-scale with various completed clinical trials. This should not be a surprise as this was one of the first therapeutic applications of EVs reported in the scientific literature (**figure 1**) [70]. Likely, this application will further co-develop with the anti-cancer immunotherapy field in general, fuelled by increasing knowledge regarding adjuvants and tumor microenvironment immunology [74].

Another application ranking high on the TRL-scale is the use of EVs as a biomarker source for early disease detection. Recently, the 'ExoDx Lung(ALK) test' developed by Exosome Diagnostics received FDA-approval. This test relies on qPCR-based screening of EV-derived RNA to detect five different mutations, all of them fusions between the genes encoding *echinoderm microtubule-associated protein-like 4* (EML4) and *anaplastic lymphoma kinase* (ALK), each of which giving rise to a subtype of non-small-cell lung carcinoma (NSCLC). Besides disease detection, this test can also be used as a predictive marker to evaluate treatment by ALK-inhibitors (e.g. crizotinib, ceritinib) [75], hence acting as a companion diagnostic tool. Comparable kits are currently in the pipeline of the same company for the detection of other lung cancer associated mutations and for prostate cancer. The exploitation of EVs as a biomarker source is likely the most promising application of EVs in the near future. The urgent unmet need for liquid biopsy-based tools that allow post-treatment follow-up incites the emergence of different startup companies (e.g. Codiak BioSciences, ExosomeDx, Nanosomix), attracting substantial venture capital to EV research in this context [76].

Further down the TRL scale we see the exploitation of EVs as a surrogate for cell therapy (mainly mesenchymal stem cell (MSC)-based therapy). A clinical case report on the application of MSC-derived EVs for the treatment of refractory graft-*versus*-host disease (GvHD) showed a strong reduction in symptoms with stabilization of the patient for several months, allowing a reduction in the standard corticoid treatment scheme [77]. Additionally, a Phase I clinical trial has been launched to evaluate the reduction in

inflammatory state, and hence improvement in β-cell mass, in Type I diabetes patients after IV injection of MSC-derived EVs (NCT02138331). It is envisioned that this type of application will continue to evolve in the slipstream of the development of MSC-based cell therapies for which EVs can serve as a safer alternative.

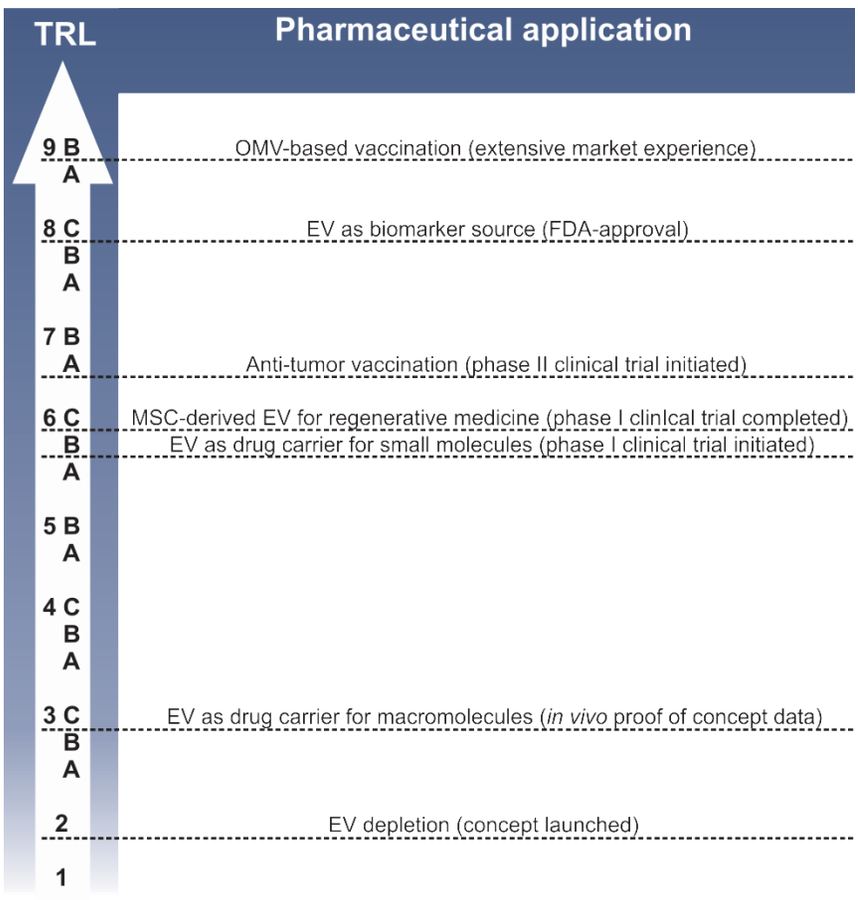

Figure 2. The different pharmaceutical applications of EVs scaled for their technology readiness level (TRL). (Status April 2016).

The exploitation of EVs as a drug carrier for macromolecules is one of the least developed applications. This should not be a surprise given the many obstacles for successful drug delivery described throughout this thesis (e.g. the loading of therapeutic macromolecules and crossing of biological barriers). Moreover, to date, a strong experimentally validated advantage over current synthetic and viral delivery vehicles is largely lacking. Many of the theoretical advantages such as long circulation time, inherent targeting and efficient cargo delivery have either been disproven or await further biological insight. In this respect, as this knowledge remains obscure to date, we cannot draw final conclusions yet on the true value of EVs as a drug delivery carrier.

Finally, a new therapeutic approach not yet discussed in this thesis, describes the depletion of cancer-derived EVs. Evidence is gathering that EVs derived from cancer

cells are important signaling factors contributing to cancer progression and metastasis. They are considered (partially) responsible for the tolerogenic microenvironment in tumor tissue [78] and appear to be a fundamental aspect in the pre-metastatic niche creation [79]. Hence, inhibition of the EV production by cancer cells would allow to disrupt a key component of the tumor cell's communication network. This concept has already been launched in the literature [80, 81] and the limited experimental data on the use of GW4869 (a neutral sphingomyelinase (nSMase) inhibitor, hence inhibitor of EV formation) shows a reduction in lung cancer multiplicities [82]. Of note, this approach not only disrupts the EV-mediated communication network of cancer cells but might also be beneficial for immunotherapy and chemotherapy as tumor-derived EVs have also been linked to drug resistance (e.g. by captivation of tumor-targeting antibodies [83] and by EV-mediated expulsion of chemotherapeutics [67, 84]). Alternatively, hemofiltration to deplete EVs from the blood circulation [81] and blocking the interaction between EVs and the target cells (e.g. integrin blocking [38]) have been suggested. However, like for the above mentioned diagnostic approaches, also the hemofiltration approach suffers from the lack of tumor EV-specific surface (glyco)proteins for which antibodies can be developed. On the other hand, tumor-derived EVs have also shown to be potent anticancer vaccines in animal models, hence making it difficult to predict the outcome of such interventions [85]. Though still in its infancy, depletion of cancer-derived EVs is likely to gain interest and its exploitation will largely depend on progress made in unraveling EV biogenesis and characterization.

Overall the EV field is attracting many new research groups offering a growing interdisciplinary toolbox to elucidate the true physiological relevance and exploitation of these vesicles in a pharmaceutical context. Despite the fact that EV biology is still an immature field, much capital is already drawn into new startup companies providing a basis to further explore EVs both in a therapeutic and diagnostic setting.

References

[1] A. Wittrup, A. Ai, X. Liu, P. Hamar, R. Trifonova, K. Charisse, M. Manoharan, T. Kirchhausen, J. Lieberman, Visualizing lipid-formulated siRNA release from endosomes and target gene knockdown, Nat. Biotechnol., 33 (2015) 870-876.

[2] L. Stalder, W. Heusermann, L. Sokol, D. Trojer, J. Wirz, J. Hean, A. Fritzsche, F. Aeschimann, V. Pfanzagl, P. Basselet, J. Weiler, M. Hintersteiner, D.V. Morrissey, N.C. Meisner-Kober, The rough endoplasmatic reticulum is a central nucleation site of siRNA-mediated RNA silencing, EMBO J., 32 (2013) 1115-1127.

[3] M.L. Immordino, F. Dosio, L. Cattel, Stealth liposomes: review of the basic science, rationale, and clinical applications, existing and potential, Int J Nanomedicine, 1 (2006) 297-315.

[4] H. Kobayashi, R. Watanabe, P.L. Choyke, Improving conventional enhanced permeability and retention (EPR) effects; what is the appropriate target?, Theranostics, 4 (2013) 81-89.
[5] J.W. Yoo, D.J. Irvine, D.E. Discher, S. Mitragotri, Bio-inspired, bioengineered and biomimetic drug delivery carriers, Nature reviews. Drug discovery, 10 (2011) 521-535.
[6] L. Wayteck, H. Dewitte, L. De Backer, K. Breckpot, J. Demeester, S.C. De Smedt, K. Raemdonck, Hitchhiking nanoparticles: Reversible coupling of lipid-based nanoparticles to cytotoxic T lymphocytes, Biomaterials, 77 (2016) 243-254.
[7] N. Moran, First gene therapy approved, Nat Biotech, 30 (2012) 1153-1153.
[8] U.N. Le, H.S. Kim, J.S. Kwon, M.Y. Kim, V.H. Nguyen, S.N. Jiang, B.I. Lee, Y. Hong, M.G. Shin, J.H. Rhee, H.S. Bom, Y. Ahn, S.S. Gambhir, H.E. Choy, J.J. Min, Engineering and visualization of bacteria for targeting infarcted myocardium, Mol. Ther., 19 (2011) 951-959.
[9] J.-J. Min, V.H. Nguyen, H.-J. Kim, Y. Hong, H.E. Choy, Quantitative bioluminescence imaging of tumor-targeting bacteria in living animals, Nat. Protocols, 3 (2008) 629-636.
[10] N. Somia, I.M. Verma, Gene therapy: trials and tribulations, Nat. Rev. Genetics, 1 (2000) 91-99.
[11] S. Hacein-Bey-Abina, A. Garrigue, G.P. Wang, J. Soulier, A. Lim, E. Morillon, E. Clappier, L. Caccavelli, E. Delabesse, K. Beldjord, V. Asnafi, E. MacIntyre, L. Dal Cortivo, I. Radford, N. Brousse, F. Sigaux, D. Moshous, J. Hauer, A. Borkhardt, B.H. Belohradsky, U. Wintergerst, M.C. Velez, L. Leiva, R. Sorensen, N. Wulffraat, S. Blanche, F.D. Bushman, A. Fischer, M. Cavazzana-Calvo, Insertional oncogenesis in 4 patients after retrovirus-mediated gene therapy of SCID-X1, J. Clin. Invest., 118 (2008) 3132-3142.
[12] L. Alvarez-Erviti, Y.Q. Seow, H.F. Yin, C. Betts, S. Lakhal, M.J.A. Wood, Delivery of siRNA to the mouse brain by systemic injection of targeted exosomes, Nat. Biotechnol., 29 (2011) 341-U179.
[13] J. Van Deun, P. Mestdagh, R. Sormunen, V. Cocquyt, K. Vermaelen, J. Vandesompele, M. Bracke, O. De Wever, A. Hendrix, The impact of disparate isolation methods for extracellular vesicles on downstream RNA profiling, J Extracell Vesicles, 3 (2014) 24858.
[14] A.N. Boing, E. van der Pol, A.E. Grootemaat, F.A. Coumans, A. Sturk, R. Nieuwland, Single-step isolation of extracellular vesicles by size-exclusion chromatography, J Extracell Vesicles, 3 (2014) 23430.
[15] R.J. Lobb, M. Becker, S.W. Wen, C.S. Wong, A.P. Wiegmans, A. Leimgruber, A. Moller, Optimized exosome isolation protocol for cell culture supernatant and human plasma, J Extracell Vesicles, 4 (2015) 27031.
[16] N. Kosaka, H. Iguchi, Y. Yoshioka, F. Takeshita, Y. Matsuki, T. Ochiya, Secretory mechanisms and intercellular transfer of microRNAs in living cells, J. Biol. Chem., 285 (2010) 17442-17452.
[17] Y. Zhang, D. Liu, X. Chen, J. Li, L. Li, Z. Bian, F. Sun, J. Lu, Y. Yin, X. Cai, Q. Sun, K. Wang, Y. Ba, Q. Wang, D. Wang, J. Yang, P. Liu, T. Xu, Q. Yan, J. Zhang, K. Zen, C.Y. Zhang, Secreted monocytic miR-150 enhances targeted endothelial cell migration, Mol. Cell, 39 (2010) 133-144.
[18] T.M. Allen, P.R. Cullis, Liposomal drug delivery systems: from concept to clinical applications, Adv Drug Deliv Rev, 65 (2013) 36-48.
[19] R. Kedmi, N. Ben-Arie, D. Peer, The systemic toxicity of positively charged lipid nanoparticles and the role of Toll-like receptor 4 in immune activation, Biomaterials, 31 (2010) 6867-6875.

[20] M.J. Haney, N.L. Klyachko, Y. Zhao, R. Gupta, E.G. Plotnikova, Z. He, T. Patel, A. Piroyan, M. Sokolsky, A.V. Kabanov, E.V. Batrakova, Exosomes as drug delivery vehicles for Parkinson's disease therapy, J. Control. Release, (2015) 18-30.
[21] J. Wahlgren, L. Karlson Tde, M. Brisslert, F. Vaziri Sani, E. Telemo, P. Sunnerhagen, H. Valadi, Plasma exosomes can deliver exogenous short interfering RNA to monocytes and lymphocytes, Nucleic Acids Res., 40 (2012) e130.
[22] T.A. Shtam, R.A. Kovalev, E.Y. Varfolomeeva, E.M. Makarov, Y.V. Kil, M.V. Filatov, Exosomes are natural carriers of exogenous siRNA to human cells in vitro, Cell Commun Signal, 11 (2013) 88.
[23] S.I. Ohno, M. Takanashi, K. Sudo, S. Ueda, A. Ishikawa, N. Matsuyama, K. Fujita, T. Mizutani, T. Ohgi, T. Ochiya, N. Gotoh, M. Kuroda, Systemically Injected Exosomes Targeted to EGFR Deliver Antitumor MicroRNA to Breast Cancer Cells, Mol. Ther., (2012) 185-191.
[24] J.L. Hood, M.J. Scott, S.A. Wickline, Maximizing exosome colloidal stability following electroporation, Anal. Biochem., 448 (2014) 41-49.
[25] Y. Tian, S. Li, J. Song, T. Ji, M. Zhu, G.J. Anderson, J. Wei, G. Nie, A doxorubicin delivery platform using engineered natural membrane vesicle exosomes for targeted tumor therapy, Biomaterials, 35 (2014) 2383-2390.
[26] J.M. Cooper, P.B. Wiklander, J.Z. Nordin, R. Al-Shawi, M.J. Wood, M. Vithlani, A.H. Schapira, J.P. Simons, S. El-Andaloussi, L. Alvarez-Erviti, Systemic exosomal siRNA delivery reduced alpha-synuclein aggregates in brains of transgenic mice, Mov. Disord., 29 (2014) 1476-1485.
[27] G. Chen, J.Y. Zhu, Z.L. Zhang, W. Zhang, J.G. Ren, M. Wu, Z.Y. Hong, C. Lv, D.W. Pang, Y.F. Zhao, Transformation of Cell-Derived Microparticles into Quantum-Dot-Labeled Nanovectors for Antitumor siRNA Delivery, Angew. Chem. Int. Ed. Engl., (2014) 1036–1040.
[28] R. Stapulionis, Electric pulse-induced precipitation of biological macromolecules in electroporation, Bioelectrochem. Bioenerg., 48 (1999) 249-254.
[29] S.A. Kooijmans, S. Stremersch, K. Braeckmans, S.C. de Smedt, A. Hendrix, M.J. Wood, R.M. Schiffelers, K. Raemdonck, P. Vader, Electroporation-induced siRNA precipitation obscures the efficiency of siRNA loading into extracellular vesicles, J. Control. Release, 172 (2013) 229-238.
[30] T.N. Lamichhane, R.S. Raiker, S.M. Jay, Exogenous DNA Loading into Extracellular Vesicles via Electroporation is Size-Dependent and Enables Limited Gene Delivery, Mol. Pharm., 12 (2015) 3650-3657.
[31] K.B. Johnsen, J.M. Gudbergsson, M.N. Skov, G. Christiansen, L. Gurevich, T. Moos, M. Duroux, Evaluation of electroporation-induced adverse effects on adipose-derived stem cell exosomes, Cytotechnol., (2016) 1-14.
[32] M. Duechler, Vehicles for Small Interfering RNA transfection: Exosomes versus Synthetic Nanocarriers, DNA and RNA Nanotechnology (2013) 16-28.
[33] A. Zomer, C. Maynard, F.J. Verweij, A. Kamermans, R. Schafer, E. Beerling, R.M. Schiffelers, E. de Wit, J. Berenguer, S.I. Ellenbroek, T. Wurdinger, D.M. Pegtel, J. van Rheenen, In Vivo imaging reveals extracellular vesicle-mediated phenocopying of metastatic behavior, Cell, 161 (2015) 1046-1057.
[34] I. Nakase, S. Futaki, Combined treatment with a pH-sensitive fusogenic peptide and cationic lipids achieves enhanced cytosolic delivery of exosomes, Sci. Rep., 5 (2015) 10112.

[35] Y. Tao, J. Han, H. Dou, Brain-targeting gene delivery using a rabies virus glycoprotein peptide modulated hollow liposome: bio-behavioral study, J. Mater. Chem., 22 (2012) 11808-11815.
[36] S.A. Kooijmans, L.A. Fliervoet, R. van der Meel, M.H. Fens, H.F. Heijnen, P.M. van Bergen En Henegouwen, P. Vader, R.M. Schiffelers, PEGylated and targeted extracellular vesicles display enhanced cell specificity and circulation time, J. Control. Release, 224 (2016) 77-85.
[37] M. Mittelbrunn, C. Gutierrez-Vazquez, C. Villarroya-Beltri, S. Gonzalez, F. Sanchez-Cabo, M.A. Gonzalez, A. Bernad, F. Sanchez-Madrid, Unidirectional transfer of microRNA-loaded exosomes from T cells to antigen-presenting cells, Nat. Commun., 2 (2011) 282.
[38] A. Hoshino, B. Costa-Silva, T.L. Shen, G. Rodrigues, A. Hashimoto, M. Tesic Mark, H. Molina, S. Kohsaka, A. Di Giannatale, S. Ceder, D. Lyden, *et al.*, Tumour exosome integrins determine organotropic metastasis, Nature, 527 (2015) 329–335.
[39] I. Hazan-Halevy, D. Rosenblum, S. Weinstein, O. Bairey, P. Raanani, D. Peer, Cell-specific uptake of mantle cell lymphoma-derived exosomes by malignant and non-malignant B-lymphocytes, Cancer Lett., 364 (2015) 59-69.
[40] D.K. Kim, J. Lee, S.R. Kim, D.S. Choi, Y.J. Yoon, J.H. Kim, G. Go, D. Nhung, K. Hong, S.C. Jang, S.H. Kim, K.S. Park, O.Y. Kim, H.T. Park, , Y.S. Gho *et al.*, EVpedia: a community web portal for extracellular vesicles research, Bioinformatics, 31 (2015) 933-939.
[41] H. Kalra, R.J. Simpson, H. Ji, E. Aikawa, P. Altevogt, P. Askenase, V.C. Bond, F.E. Borràs, X. Breakefield, V. Budnik, E. Buzas, S. Mathivanan, *et al.*, Vesiclepedia: A Compendium for Extracellular Vesicles with Continuous Community Annotation, PLoS Biol., 10 (2012) e1001450.
[42] S. Mathivanan, C.J. Fahner, G.E. Reid, R.J. Simpson, ExoCarta 2012: database of exosomal proteins, RNA and lipids, Nucleic Acids Res., 40 (2012) D1241-1244.
[43] E. Zeringer, M. Li, T. Barta, J. Schageman, K.W. Pedersen, A. Neurauter, S. Magdaleno, R. Setterquist, A.V. Vlassov, Methods for the extraction and RNA profiling of exosomes, World J Methodol., 3 (2013) 11-18.
[44] E.J. van der Vlist, E.N. Nolte-'t Hoen, W. Stoorvogel, G.J. Arkesteijn, M.H. Wauben, Fluorescent labeling of nano-sized vesicles released by cells and subsequent quantitative and qualitative analysis by high-resolution flow cytometry, Nat. Protoc., 7 (2012) 1311-1326.
[45] H. Deschout, K. Raemdonck, S. Stremersch, P. Maoddi, G. Mernier, P. Renaud, S. Jiguet, A. Hendrix, M. Bracke, R. Van den Broecke, M. Roding, M. Rudemo, J. Demeester, S.C. De Smedt, F. Strubbe, K. Neyts, K. Braeckmans, On-chip light sheet illumination enables diagnostic size and concentration measurements of membrane vesicles in biofluids, Nanoscale, 6 (2014) 1741-1747.
[46] Z.J. Smith, C. Lee, T. Rojalin, R.P. Carney, S. Hazari, A. Knudson, K. Lam, H. Saari, E.L. Ibanez, T. Viitala, T. Laaksonen, M. Yliperttula, S. Wachsmann-Hogiu, Single exosome study reveals subpopulations distributed among cell lines with variability related to membrane content, J Extracell Vesicles, 4 (2015) 28533.
[47] L.G. Laura T. Kerr, Karolina Weiner Gorzel, Shiva Sharma, Malcolm Kell, Amanda Mc Cann, Bryan M. Hennelly, Raman spectroscopy and SERS analysis of ovarian tumour derived exosomes (TEXs): a preliminary study, Biophotonics: Photonic Solutions for Better Health Care IV, 91292Q (2014).
[48] I. Tatischeff, E. Larquet, J.M. Falcon-Perez, P.Y. Turpin, S.G. Kruglik, Fast characterisation of cell-derived extracellular vesicles by nanoparticles tracking analysis, cryo-electron microscopy, and Raman tweezers microspectroscopy, J Extracell Vesicles, 1 (2012) 19179.

[49] L. Tirinato, F. Gentile, D. Di Mascolo, M.L. Coluccio, G. Das, C. Liberale, S.A. Pullano, G. Perozziello, M. Francardi, A. Accardo, F. De Angelis, P. Candeloro, E. Di Fabrizio, SERS analysis on exosomes using super-hydrophobic surfaces, Microelectronic Engineering, 97 (2012) 337-340.
[50] C. Gardiner, M. Shaw, P. Hole, J. Smith, D. Tannetta, C.W. Redman, I.L. Sargent, Measurement of refractive index by nanoparticle tracking analysis reveals heterogeneity in extracellular vesicles, J Extracell Vesicles, 3, (2014) 25361.
[51] S.L. Maas, J. De Vrij, M.L. Broekman, Quantification and size-profiling of extracellular vesicles using tunable resistive pulse sensing, JoVE, (2014) e51623.
[52] S. Sharma, H.I. Rasool, V. Palanisamy, C. Mathisen, M. Schmidt, D.T. Wong, J.K. Gimzewski, Structural-mechanical characterization of nanoparticle exosomes in human saliva, using correlative AFM, FESEM, and force spectroscopy, ACS nano, 4 (2010) 1921-1926.
[53] J. Su, Label-Free Single Exosome Detection Using Frequency-Locked Microtoroid Optical Resonators, ACS Photonics, 2 (2015) 1241-1245.
[54] E. van der Pol, A.G. Hoekstra, A. Sturk, C. Otto, T.G. van Leeuwen, R. Nieuwland, Optical and non-optical methods for detection and characterization of microparticles and exosomes, J. Thromb. Haemost., 8 (2010) 2596-2607.
[55] S.A. Melo, L.B. Luecke, C. Kahlert, A.F. Fernandez, S.T. Gammon, J. Kaye, V.S. LeBleu, E.A. Mittendorf, J. Weitz, N. Rahbari, C. Reissfelder, C. Pilarsky, M.F. Fraga, D. Piwnica-Worms, R. Kalluri, Glypican-1 identifies cancer exosomes and detects early pancreatic cancer, Nature, 523 (2015) 177-182.
[56] E. Drucker, K. Krapfenbauer, Pitfalls and limitations in translation from biomarker discovery to clinical utility in predictive and personalised medicine, The EPMA journal, 4 (2013) 7.
[57] A. Shiohara, Y. Wang, L.M. Liz-Marzán, Recent approaches toward creation of hot spots for SERS detection, J. Photochem. Photobiol., 21 (2014) 2-25.
[58] K. Klein, A.M. Gigler, T. Aschenbrenner, R. Monetti, W. Bunk, F. Jamitzky, G. Morfill, R.W. Stark, J. Schlegel, Label-free live-cell imaging with confocal Raman microscopy, Biophys. J., 102 (2012) 360-368.
[59] E.M. Kanter, E. Vargis, S. Majumder, M.D. Keller, E. Woeste, G.G. Rao, A. Mahadevan-Jansen, Application of Raman spectroscopy for cervical dysplasia diagnosis, J biophotonics, 2 (2009) 81-90.
[60] I. Pence, A. Mahadevan-Jansen, Clinical instrumentation and applications of Raman spectroscopy, Chem Soc Rev, 45 (2016) 1958-1979.
[61] J.D. Horsnell, J.A. Smith, M. Sattlecker, A. Sammon, J. Christie-Brown, C. Kendall, N. Stone, Raman spectroscopy--a potential new method for the intra-operative assessment of axillary lymph nodes, Surgeon, 10 (2012) 123-127.
[62] C. Supplement, Abstracts from the Fourth International Meeting of ISEV, ISEV2015, Washington, D.C., USA, 23-26 April 2015, (2015).
[63] C. Supplement, The Fifth International Meeting of ISEV ISEV2016, Rotterdam, The Netherlands, 4 – 7 May 2016, (2016).
[64] R.M. Johnstone, M. Adam, J.R. Hammond, L. Orr, C. Turbide, Vesicle formation during reticulocyte maturation. Association of plasma membrane activities with released vesicles (exosomes), J. Biol. Chem., 262 (1987) 9412-9420.

[65] Mario L. Squadrito, C. Baer, F. Burdet, C. Maderna, Gregor D. Gilfillan, R. Lyle, M. Ibberson, M. De Palma, Endogenous RNAs Modulate MicroRNA Sorting to Exosomes and Transfer to Acceptor Cells, Cell Reports, 8 (2014) 1432-1446.
[66] A.O. Batagov, I.V. Kurochkin, Exosomes secreted by human cells transport largely mRNA fragments that are enriched in the 3'-untranslated regions, Biol. Direct, 8 (2013) 12.
[67] R. Safaei, B.J. Larson, T.C. Cheng, M.A. Gibson, S. Otani, W. Naerdemann, S.B. Howell, Abnormal lysosomal trafficking and enhanced exosomal export of cisplatin in drug-resistant human ovarian carcinoma cells, Mol. Cancer Ther., 4 (2005) 1595-1604.
[68] M. Yanez-Mo, P.R. Siljander, Z. Andreu, A.B. Zavec, F.E. Borras, E.I. Buzas, K. Buzas, E. Casal, F. Cappello, J. Carvalho, O. De Wever, *et al.*, Biological properties of extracellular vesicles and their physiological functions, Journal of extracellular vesicles, 4 (2015) 27066.
[69] G. Raposo, H.W. Nijman, W. Stoorvogel, R. Liejendekker, C.V. Harding, C.J. Melief, H.J. Geuze, B lymphocytes secrete antigen-presenting vesicles, J. Exp. Med., 183 (1996) 1161-1172.
[70] L. Zitvogel, A. Regnault, A. Lozier, J. Wolfers, C. Flament, D. Tenza, P. Ricciardi-Castagnoli, G. Raposo, S. Amigorena, Eradication of established murine tumors using a novel cell-free vaccine: dendritic cell-derived exosomes, Nat. Med., 4 (1998) 594-600.
[71] B. Escudier, T. Dorval, N. Chaput, F. Andre, M.P. Caby, S. Novault, C. Flament, C. Leboulaire, C. Borg, S. Amigorena, C. Boccaccio, C. Bonnerot, O. Dhellin, M. Movassagh, S. Piperno, C. Robert, V. Serra, N. Valente, J.B. Le Pecq, A. Spatz, O. Lantz, T. Tursz, E. Angevin, L. Zitvogel, Vaccination of metastatic melanoma patients with autologous dendritic cell (DC) derived-exosomes: results of thefirst phase I clinical trial, J. Transl. Med., 3 (2005) 10.
[72] H. Valadi, K. Ekstrom, A. Bossios, M. Sjostrand, J.J. Lee, J.O. Lotvall, Exosome-mediated transfer of mRNAs and microRNAs is a novel mechanism of genetic exchange between cells, Nat. Cell Biol., 9 (2007) 654-U672.
[73] D. Panatto, D. Amicizia, P.L. Lai, M.L. Cristina, A. Domnich, R. Gasparini, New versus old meningococcal group B vaccines: how the new ones may benefit infants & toddlers, Indian J. Med. Res., 138 (2013) 835-846.
[74] K. Kono, Current status of cancer immunotherapy, J. Stem Cells Regen. Med., 10 (2014) 8-13.
[75] FDA, FDA expands use of Xalkori to treat rare form of advanced non-small cell lung cancer, URL: http://www.fda.gov/NewsEvents/Newsroom/PressAnnouncements/ucm490329.htm (2016).
[76] B. Fidler, Big Bucks, Tiny Bubbles: Ex-Biogen Exec's Exosome Startup Nabs $80M, xconomy, URL: http://www.xconomy.com (2015).
[77] L. Kordelas, V. Rebmann, A.K. Ludwig, S. Radtke, J. Ruesing, T.R. Doeppner, M. Epple, P.A. Horn, D.W. Beelen, B. Giebel, MSC-derived exosomes: a novel tool to treat therapy-refractory graft-versus-host disease, Leukemia, 28 (2014) 970-973.
[78] P. Altevogt, N.P. Bretz, J. Ridinger, J. Utikal, V. Umansky, Novel insights into exosome-induced, tumor-associated inflammation and immunomodulation, Semin. Cancer Biol., 28 (2014) 51-57.
[79] B. Costa-Silva, N.M. Aiello, A.J. Ocean, S. Singh, H. Zhang, B.K. Thakur, A. Becker, A. Hoshino, M.T. Mark, H. Molina, J. Xiang, T. Zhang, T.-M. Theilen, G. Garcia-Santos, C. Williams, Y. Ararso, Y. Huang, G. Rodrigues, T.-L. Shen, K.J. Labori, I.M.B. Lothe, E.H. Kure, J. Hernandez, A. Doussot, S.H. Ebbesen, P.M. Grandgenett, M.A. Hollingsworth, M. Jain, K. Mallya, S.K. Batra, W.R. Jarnagin, R.E. Schwartz, I. Matei, H. Peinado, B.Z. Stanger, J. Bromberg, D. Lyden, Pancreatic

cancer exosomes initiate pre-metastatic niche formation in the liver, Nat. Cell Biol., 17 (2015) 816-826.
[80] P. Vader, X.O. Breakefield, M.J. Wood, Extracellular vesicles: emerging targets for cancer therapy, Trends Mol. Med., 20 (2014) 385-393.
[81] A.M. Marleau, C.S. Chen, J.A. Joyce, R.H. Tullis, Exosome removal as a therapeutic adjuvant in cancer, J. Transl. Med., 10 (2012) 134.
[82] M. Fabbri, A. Paone, F. Calore, R. Galli, E. Gaudio, R. Santhanam, F. Lovat, P. Fadda, C. Mao, G.J. Nuovo, N. Zanesi, M. Crawford, G.H. Ozer, D. Wernicke, H. Alder, M.A. Caligiuri, P. Nana-Sinkam, D. Perrotti, C.M. Croce, MicroRNAs bind to Toll-like receptors to induce prometastatic inflammatory response, Proc. Natl. Acad. Sci. U. S. A., 109 (2012) E2110-2116.
[83] V. Ciravolo, V. Huber, G.C. Ghedini, E. Venturelli, F. Bianchi, M. Campiglio, D. Morelli, A. Villa, P. Della Mina, S. Menard, P. Filipazzi, L. Rivoltini, E. Tagliabue, S.M. Pupa, Potential role of HER2-overexpressing exosomes in countering trastuzumab-based therapy, J. Cell. Physiol., 227 (2012) 658-667.
[84] C. Federici, F. Petrucci, S. Caimi, A. Cesolini, M. Logozzi, M. Borghi, S. D'Ilio, L. Lugini, N. Violante, T. Azzarito, C. Majorani, D. Brambilla, S. Fais, Exosome release and low pH belong to a framework of resistance of human melanoma cells to cisplatin, PLoS One, 9 (2014) e88193.
[85] K.E. Kunigelis, M.W. Graner, The Dichotomy of Tumor Exosomes (TEX) in Cancer Immunity: Is It All in the ConTEXt?, Vaccines, 3 (2015) 1019-1051.

SUMMARY AND CONCLUSIONS

Extracellular vesicles (EVs) are membranous structures that are released by cells in the surrounding biofluid. EVs consist of a lipid and protein shell that encapsulates an aqueous core containing, among others, proteins and nucleic acids. It is believed that the molecular composition of EVs is in part actively regulated by the producing cell and, once released, it has been demonstrated that EVs are able to interact with other cells. As they are composed of numerous, potentially bioactive molecules, this interaction can induce phenotypic alternations in the recipient cell. In this respect, EVs are increasingly considered as important mediators of intercellular communication, enabling the functional transfer of (macro)molecules from one cell to another. Their inherent physiological effects can be exploited in a therapeutic context for which numerous examples are provided and discussed in **chapter 1** (e.g. cell free vaccination, MSC surrogate therapy, *etc.*). Interestingly, it is believed that part of the induced alterations are due to the EV's ability to fuse with the cell and/or endosomal membrane, thus allowing subsequent delivery of their nucleic acid cargo (e.g. miRNAs and mRNAs) to the receptive cell's cytoplasm. This is a very interesting feature that attracted the attention of the drug delivery community, given that efficient cytoplasmic delivery of macromolecular biotherapeutics (including nucleic acids and proteins) is currently one of the major hurdles hampering clinical translation of biologics with an intracellular target.

In this thesis the ability of EVs to functionally deliver small interfering RNA (siRNA) was explored. Despite some interesting earlier reports in the literature on the value of EVs as bio-inspired drug carriers, many fundamental biological questions, pertaining to the EV biodistribution, cell uptake specificity and cargo release, remain largely unanswered to date. Additionally, technical hurdles such as inadequate purification strategies and the lack of an efficient loading strategy for macromolecular therapeutics should be overcome to reliably assess the true advantage EVs might have over current state-of-the-art delivery strategies (e.g. liposomes and viral vectors).

A first step in pursuit of harnessing EVs for siRNA delivery is the development of a method to obtain purified vesicles. It is important to realize that EVs represent only a fraction of the cell's secretome. Different methods to isolate and purify EVs out of conditioned cell medium and biological fluids have been suggested. These approaches rely on the EV's typical size, density, solubility, surface components or a combination of the above. Currently, no consensus on a gold standard protocol exists, which hampers unambiguous comparison of different studies and increases the risk of misconceptions due to residual impurities when using insufficiently stringent purification protocols. In **chapter 3** a number of commonly used techniques to purify EVs from endogenous (e.g.

protein complexes) and exogenous (e.g. fluorescent dyes) components were compared. Protocols based on a density gradient and size-exclusion chromatography outperformed differential centrifugation- and precipitation-based approaches. In combination with a better understanding of the influence of the respective isolation procedures on the EV functionality, these observations can contribute to the implementation of a more standardized purification protocol.

A second technical hurdle that was addressed in this thesis, is the loading of isolated EVs with exogenous siRNA. One of the strategies suggested in the literature is the electroporation of EVs in the presence of the siRNA of interest. Despite the fact that this technique has already been adopted by different groups, the underlying biophysical loading mechanism was never thoroughly investigated. In **chapter 2** an in-depth study on this process revealed that electric pulses in electroporation buffers result in extensive precipitation of siRNA into salt aggregates. This phenomenon was a consequence of metal ions, released from the cuvette electrodes, forming insoluble aggregates with the hydroxide ions present in pH neutral buffers. During this aggregate formation process, siRNAs (and EVs) are co-precipitated. As a result, the encapsulation efficiency for siRNA is easily overestimated when commonly used electroporation conditions and quantification techniques are employed. When preventing aggregation, e.g. by using chelating acidic buffers or polymer-based cuvettes, the measured encapsulation of siRNA into EVs decreased to negligible amounts.

The shortcomings of electroporation and the current lack of alternatives to load hydrophilic macromolecules into EVs prompted us to explore new approaches. In **chapter 4** we developed a generally applicable method to attach siRNA to the surface of isolated EVs by means of a cholesterol anchor. Moreover, given the complexity and heterogeneity of EV isolates and the previously described loading artifacts with electroporation, here we used a combination of three complementary assays to confirm and quantify siRNA loading (i.e. a gel retention assay, an antibody capture assay and a density gradient co-localization assay). As this approach was also able to load pre-formed liposomes with siRNA with comparable efficiency, a direct comparison between EVs and synthetic liposomes with regard to siRNA delivery could be made. To this end, we selected negatively charged, fusogenic liposomes with a size distribution comparable to EVs. Unfortunately, under the tested *in vitro* conditions, EVs underperformed compared to the liposomes for their ability to functionally deliver the siRNA therapeutic, which could be attributed to the lack of an intrinsic mechanism to induce endosomal escape prior to trafficking to lysosomes for degradation. Likewise, the endogenously present miRNAs were not functionally delivered to recipient cells. These observations question the efficiency and universal applicability of EVs as a gene therapy nanocarrier.

Besides therapeutic applications, EVs have also been the subject of investigation in a diagnostic context. The EV architecture and part of the molecular composition are common among EVs isolated from different cells. However, some EV-associated components are unique for the producing cell type and even cellular status. Moreover, upon *in vivo* release, part of the EVs end up in neighboring biological fluids making them available for liquid biopsies. In this respect, EVs can be considered as easy accessible windows on otherwise difficult to reach (diseased) cells. These features make them ideal biomarker candidates for early disease detection and treatment monitoring.

Yet, as contextualized in **chapter 1**, to optimally exploit EVs in a diagnostic setting, there is a need for new characterization techniques which can attain high sensitivity on a single vesicle level. In an attempt to address this need, in **chapter 5** a nanotechnological platform relying on enhanced Raman spectroscopy for individual EV characterization, was developed. The signal enhancement was evoked by decorating the surface of each individual vesicle with a gold nanoparticle-based plasmonic substrate, which allowed to obtain a Raman spectrum with acceptable acquisition speed. Subsequently, the acquired spectra could be subjected to downstream analysis using dedicated multivariate statistical models allowing to discriminate between EVs derived from red blood cells and EVs derived from melanoma cells. Furthermore, due to the single vesicle approach, this technique was able to quantify the relative abundance of each EV type in a mixture.

Conclusions

In conclusion, in a first part of this dissertation the potential of EVs as a drug delivery carrier for siRNA was assessed. We could obtain pure EVs by means of a density gradient purification protocol and load them by exploiting the hydrophobic interaction between the EV membrane and a cholesterol tag covalently attached to one of the siRNA strands. However, under the experimental conditions EVs were unable to bypass the endolysosomal degradation pathway and hence were unable to functionally deliver siRNA upon cellular internalization. To a certain extent, our observations temper the high expectations linked to exploiting EVs as a drug delivery carrier and call for a more in-depth biological understanding of the EV's cellular delivery mechanism and related cell type specificity. Nonetheless, other therapeutic applications of EVs, as discussed in **chapter 6**, are very promising and are already developed up to market level (e.g. EV-based immunotherapy). In the second part of this dissertation, we developed a new nanotechnological platform that allows the fast characterization of individual EVs *via* surface enhanced Raman spectroscopy. As EVs are very promising biomarkers, the high sensitivity inherent to the developed technology makes this an attractive platform to explore further in a diagnostic setting.

SAMENVATTING EN CONCLUSIES

Extracellulaire vesikels (EVs) zijn membranaire structuren die door cellen vrijgesteld worden in het omliggende medium. Ze zijn opgebouwd uit een schil van lipiden en proteïnen die een waterige kern omhult. Deze laatste bevat onder meer proteïnen en nucleïnezuren. De moleculaire samenstelling is actief gereguleerd door de producerende cel en, eens vrijgesteld, zijn EVs in staat te interageren met andere cellen. Aangezien ze samengesteld zijn uit potentieel bioactieve moleculen, hoeft het niet te verbazen deze interactie fenotypische veranderingen induceren in de ontvangende cel. Door deze mogelijkheid om (macro)moleculen functioneel te transfereren van de ene naar de andere cel, worden EVs steeds meer aanzien als een nieuw type mediator van intercellulaire communicatie. Deze intrinsieke fysiologische effecten benut worden in een therapeutische context waarvan enkele voorbeelden worden besproken in **hoofdstuk 1** (vb. EVs afkomstig van tumorcellen in immunotherapie en EVs afkomstig van MSC in regeneratieve geneeskunde). Er wordt aangenomen dat een deel van deze geïnduceerde veranderingen een gevolg is van de mogelijkheid van EVs om te fuseren met het cel- en/of endosomale membraan. Op deze manier kunnen ze hun nucleïnezuurlading (o.a. miRNA en mRNA) functioneel afleveren in het cytoplasma van de ontvangende cel. Deze eigenschap heeft de aandacht getrokken van verschillende onderzoeksgroepen in het veld van de gentherapie aangezien efficiënte afgifte van macromoleculaire biotherapeutica in het cytoplasma nog steeds één van de grote struikelblokken vormt die de klinische vertaling van biofarmaceutica met een intracellulair target bemoeilijkt.

In deze thesis wordt de capaciteit van EVs om siRNA functioneel af te leveren onderzocht. Ondanks enkele interessante bevindingen die eerder werden gepubliceerd over deze nieuwe carriers, blijven vele fundamentele biologische vragen rond de EV distributie, cel opname specificiteit en interactiemechanismen grotendeels onbeantwoord. Daarenboven zijn er nog enkele technische obstakels zoals een gebrek aan adequate opzuiverings- en opladingsmethoden voor macromoleculaire therapeutica. Verder onderzoek is daarom noodzakelijk om de ware voordelen van EVs ten opzichte van de huidige afleveringsmethoden (vb. liposomen en virale vectoren) te kunnen inschatten.

Een eerste stap om gebruik te kunnen maken van EVs voor het afleveren van siRNA, is de ontwikkeling van een opzuiveringsmethode. Dit is noodzakelijk aangezien EVs slechts een klein deel vormen van wat de cel vrijstelt. Verschillende werkwijzen om ze te isoleren uit geconditioneerd cel medium of uit biologische vloeistoffen zijn reeds ontwikkeld. Ze zijn voornamelijk gebaseerd op de typerende EV grootte, densiteit, oplosbaarheid, oppervlakte merkers of een combinatie hiervan. Momenteel is er nog

geen consensus over een 'gouden' standaard protocol. Dit bemoeilijkt een directe vergelijking tussen verschillende studies en vergroot bovendien de kans op misinterpretaties als gevolg van achtergebleven onzuiverheden. In **hoofdstuk 3** werden een aantal courant gebruikte technieken om EVs te isoleren van endogene (vb. proteïne complexen) en exogene (vb. fluorescente labels) componenten met elkaar vergeleken. Strategieën gebaseerd op een densiteit gradiënt en SEC blijken superieur aan methoden gebaseerd op differentiële centrifugatie en precipitatie. Deze observaties kunnen, samen met inzichten over de invloed van de isolatieprocedures op de functionaliteit van EVs, verder bijdragen aan de realisatie van een meer gestandaardiseerd opzuiveringsprotocol.

Een tweede technisch struikelblok dat werd aangepakt in deze thesis, is het opladen van geïsoleerde EVs met exogeen siRNA. Eén van de technieken voorgesteld in de literatuur maakt gebruik van elektroporatie van EVs in aanwezigheid van het gewenst siRNA. Ondanks het feit dat deze techniek reeds is overgenomen door verschillende onderzoeksgroepen, zijn de onderliggende biofysische ladingsmechanismen nooit grondig onderzocht. In **hoofdstuk 2** brengt een diepgaande studie aan het licht dat elektrische pulsen in standaard buffers resulteren in extensieve precipitatie van siRNA in zout aggregaten. Dit fenomeen blijkt een gevolg te zijn van metaalionen (die loskomen van de cuvetelektrodes) en hydroxide ionen (aanwezig in pH neutrale buffers), die samen onoplosbare complexen vormen. Tijdens dit proces van aggregaat vorming worden siRNAs en EVs samen neergeslaan. Dit leidt ertoe dat bij vaak gebruikte elektroporatie condities en daaropvolgende kwantificatietechnieken, de incorporatie-efficiëntie van siRNA overschat wordt. Wanneer aggregatie werd voorkomen door bijvoorbeeld gebruik te maken van chelatoren of geleidende polymeer cuvetten, daalde de gemeten incorporatie van siRNA in EVs tot verwaarloosbare hoeveelheden.

De tekortkomingen van elektroporatie en het gebrek aan alternatieven om hydrofiele macromoleculen te laden in EVs, heeft ons ertoe aangezet om nieuwe strategieën te verkennen. In **hoofdstuk 4** hebben we een breed toepasbare methode ontwikkeld om siRNA te koppelen aan het oppervlak van geïsoleerde EVs via een cholesterol anker. Gestuurd door de complexiteit en heterogeniteit van EV isolaten en de voordien beschreven oplaadmoeilijkheden met elektroporatie, hebben we een combinatie van drie complementaire assays gebruikt om de siRNA oplading te bevestigen en te kwantificeren (gebaseerd op gel retentie, antilichaam captatie en dichtheidsgradiënt co-lokalisatie). Bovendien liet deze benadering ook toe om liposomen met vergelijkbare efficiëntie te laden met siRNA, zodat een directe vergelijking van siRNA aflevering mogelijk is tussen EVs en synthetische liposomen. Hiervoor gebruikten we negatief geladen, fusogene liposomen met een grootte vergelijkbaar aan die van EVs. Helaas blijken deze laatste, onder de geëvalueerde omstandigheden, veel minder efficiënt voor siRNA aflevering dan

de synthetische liposomen. De oorzaak hiervan was het ontbreken van een intrinsiek mechanisme dat de vrijstelling uit het endosoom induceert voordat de EVs worden afgevoerd naar de lysosomen voor afbraak. Het endogeen aanwezige miRNA wordt om dezelfde reden niet functioneel afgeleverd aan de ontvangende cel. Deze observaties plaatsen een vraagteken bij de efficiëntie en de universele toepasbaarheid van EVs als gentherapie nanocarrier.

Naast therapeutische applicaties, worden EVs ook geëvalueerd voor diagnostische toepassingen. De structuur en een deel van de moleculaire samenstelling zijn dezelfde voor EVs afkomstig van verschillende celtypes. Doch, sommige EV-geassocieerde moleculen zijn uniek voor (de toestand van) het producerende celtype. Wanneer de EVs *in vivo* worden vrijgesteld, komt een deel in de nabijgelegen biologische vloeistoffen terecht, wat hen toegankelijk maakt voor laag invasieve, vloeibare biopsieën. In dit opzicht kunnen EVs beschouwd worden als een gemakkelijk bereikbare representatie van (zieke) cellen. Deze eigenschappen maken van hen ideale biomerker kandidaten voor vroege diagnostiek en opvolging van behandelingen.

Zoals uiteengezet in **hoofdstuk 1**, is er vraag naar nieuwe technieken om optimaal gebruik te maken van deze EVs in een diagnostische context. Voornamelijk methoden die een hoge gevoeligheid genereren door te functioneren op het enkelvoudige vesikel niveau, zijn gegeerd. In een poging om hieraan tegemoet te komen, werd in **hoofdstuk 5** een nanotechnologisch platform ontwikkeld, gebaseerd op versterkte Raman spectroscopie voor individuele EV karakterisatie. Deze signaalversterking werd bekomen door het oppervlak van elk vesikel afzonderlijk te omhullen met een plasmonisch substraat bestaande uit goud nanopartikels. Op deze wijze werden Raman spectra bekomen binnen een aanvaardbare tijdspanne. De verworven spectra werden vervolgens onderworpen aan specifieke statistische modellen waardoor objectief een onderscheid kan gemaakt worden tussen EVs afkomstig van erytrocyten en EVs afkomstig van melanoom cellen. Doordat op individueel EV niveau gemeten wordt, is deze techniek daarenboven in staat de relatieve samenstelling van beide EV types in een mengsel te kwantificeren.

Conclusies

In het eerste deel van deze thesis werd het potentieel van EVs als drager van siRNA geëvalueerd. Zuivere EVs werden bekomen d.m.v. een densiteitsgradiënt en oplading met siRNA gebeurt d.m.v. hydrofobe interactie tussen het EV membraan en een cholesterol anker dat covalent gebonden werd aan één van de siRNA strengen. Onder de geëvalueerde experimentele omstandigheden ontbrak het de EVs echter aan de mogelijkheid om de endolysosomale degradatie te omzeilen en bleken dus ook niet in staat om hun siRNA lading functioneel af te leveren. Onze bevindingen temperen in

zekere zin de hoge verwachtingen rond het gebruik van EVs als geneesmiddel afleveringsmethode en vragen een meer diepgaand biologisch inzicht van de cellulaire afleveringsmechanismen en daaraan gelinkte celtype specificiteit. Niettegenstaande zijn andere therapeutische toepassingen van EVs, zoals besproken in **hoofdstuk 6**, beloftevol en sommige zijn reeds ontwikkeld tot een geregulariseerd commercieel product (vb. EVs voor immunotherapie). In het tweede deel van deze thesis hebben we een nieuw nanotechnologisch platform ontwikkeld. Dit maakt een snelle karakterisatie van enkelvoudige EVs via versterkte Raman spectroscopie mogelijk. Aangezien EVs aanzien worden als veelbelovende biomerkers, zorgt de hoge gevoeligheid, inherent aan de ontwikkelde methode, ervoor dat dit platform aantrekkelijk is om verder te ontwikkelen in een diagnostisch kader.

CURRICULUM VITAE

Personalia

Last name	Stremersch
First name	Stephan
Nationality	Belgian
Date of birth	April 3, 1989
Place of birth	Beveren
Private address	Zwijnaardsesteenweg 774, 9000 Ghent, Belgium
Private telephone	+32 498 39 18 43
Professional address	Laboratory for General Biochemistry and Physical Pharmacy, Faculty of Pharmaceutical Sciences, Ghent University, Ottergemsesteenweg 460, 9000 Ghent, Belgium
Professional telephone	+32 9 264 80 49
E-mail	Stephan.stremersch@ugent.be Stephan.stremersch@gmail.com
Websites	https://www.researchgate.net/profile/Stephan_Stremersch

Education

2010-2012 Master of Science in Drug Development
(with greatest distinction)
Faculty of Pharmaceutical sciences, Ghent University, Gent, Belgium

Master thesis: *Ultrasound as a key component to selective antitumor therapy: 'liposome coated microbubbles' and 'sonodynamic therapy'.*
Promoter: Prof. N. Sanders of the laboratory of gene therapy, Faculty of veterinary medicine, Ghent University, Merelbeke, Belgium
This thesis was awarded with the 'prize of pharmacy 2011'.

2007-2010 Bachelor of Science in Pharmaceutical Sciences
(with great distinction)
Faculty of Pharmaceutical sciences, Ghent University, Ghent, Belgium

2001-2007 Sciences & Mathematics
Sint-Jozef-Klein-Seminarie, 9100 Sint-Niklaas, Belgium

International peer-reviewed publications

S. Balusu, E. Van Wonterghem, R. De Rycke, K. Raemdonck, **S. Stremersch**, K. Gevaert, M. Brkic, D. Demeestere, V. Vanhooren, A. Hendrix, C. Libert, R.E. Vandenbroucke, Identification of a novel mechanism of blood-brain communication during peripheral inflammation via choroid plexus-derived extracellular vesicles, EMBO Mol. Med., *in press* (2016).

S. Stremersch, S.C. De Smedt, K. Raemdonck, Therapeutic and diagnostic applications of extracellular vesicles, J. Control. Release, *in press* (2016).

S. Stremersch, M. Marro, B.-E. Pinchasik, P. Baatsen, A. Hendrix, S.C. De Smedt, P. Loza-Alvarez, A.G. Skirtach, K. Raemdonck, K. Braeckmans, Identification of Individual Exosome-Like Vesicles by Surface Enhanced Raman Spectroscopy, Small, 12 (2016) 3292-301.

S. Stremersch, R.E. Vandenbroucke, E. Van Wonterghem, A. Hendrix, S.C. De Smedt, K. Raemdonck, Comparing exosome-like vesicles with liposomes for the functional cellular delivery of small RNAs, J. Control. Release, 232 (2016) 51-61.

S. Devos, **S. Stremersch**, K. Raemdonck, K. Braeckmans, B. Devreese, Intra- and Interspecies Effects of Outer Membrane Vesicles from Stenotrophomonas maltophilia on beta-Lactam Resistance, Antimicrob. Agents Chemother., 60 (2016) 2516-2518.

R.S. Santos, G.R. Dakwar, R. Xiong, K. Forier, K. Remaut, **S. Stremersch**, N. Guimaraes, S. Fontenete, J. Wengel, M. Leite, C. Figueiredo, S.C. De Smedt, K. Braeckmans, N.F. Azevedo, Effect of Native Gastric Mucus on in vivo Hybridization Therapies Directed at Helicobacter pylori, Molecular therapy. Nucleic acids, 4 (2015) e269.

S. Devos, L. Van Oudenhove, **S. Stremersch**, W. Van Putte, R. De Rycke, G. Van Driessche, J. Vitse, K. Raemdonck, B. Devreese, The effect of imipenem and diffusible signaling factors on the secretion of outer membrane vesicles and associated Ax21 proteins in Stenotrophomonas maltophilia, Frontiers in microbiology, 6 (2015) 298.

H. Deschout, K. Raemdonck, **S. Stremersch**, P. Maoddi, G. Mernier, P. Renaud, S. Jiguet, A. Hendrix, M. Bracke, R. Van den Broecke, M. Roding, M. Rudemo, J. Demeester, S.C. De Smedt, F. Strubbe, K. Neyts, K. Braeckmans, On-chip light sheet illumination enables diagnostic size and concentration measurements of membrane vesicles in biofluids, Nanoscale, 6 (2014) 1741-1747.

P. Vader, S.A. Kooijmans, **S. Stremersch**, K. Raemdonck, New considerations in the preparation of nucleic acid-loaded extracellular vesicles, Ther. Deliv., 5 (2014) 105-107.

S.A. Kooijmans *, **S. Stremersch ***, K. Braeckmans, S.C. de Smedt, A. Hendrix, M.J. Wood, R.M. Schiffelers, K. Raemdonck, P. Vader, Electroporation-induced siRNA precipitation obscures the efficiency of siRNA loading into extracellular vesicles, J. Control. Release, 172 (2013) 229-238. *** Equal contribution**

S.K. Cool, B. Geers, S. Roels, **S. Stremersch**, K. Vanderperren, J.H. Saunders, S.C. De Smedt, J. Demeester, N.N. Sanders, Coupling of drug containing liposomes to microbubbles improves ultrasound triggered drug delivery in mice, J. Control. Release, 172 (2013) 885-893.

Conference proceedings

K. Raemdonck, L. De Backer, L. Wayteck, **S. Stremersch**, K. Braeckmans, J. Demeester, S. De Smedt, Bio-inspired approaches for siRNA delivery, Hum. Gene Ther., 25 (2014) A75-A75.

H. Deschout, K. Raemdonck, **S. Stremersch**, P. Maoddi, G. Mernier, P. Renaud, S. Jiguet, A. Hendrix, M. Bracke, R. Van den Broecke, Disposable microfluidic chip with integrated light sheet illumination enables diagnostics based on membrane vesicles, 17th International Conference on Miniaturized Systems for Chemistry and Life Sciences, MicroTAS 2013 (2014) pp. 2010-2012.

Patent applications

S. Stremersch, K. Braeckmans, A. Skirtach, K. Raemdonck, J. Demeester, S.C. De Smedt. Method and system for characterizing extracellular vesicles. *Patent application No. EP15201241.5* (2015).

National and international conferences with oral presentation

Stremersch S., Marro M., Pinchasik B., Baatsen P., Hendrix A., De Smedt S., Loza-Alvarez P., Skirtach A., Raemdonck K., Braeckmans K. Identification of individual extracellular vesicles by surface enhanced Raman spectroscopy. ISEV2016, Rotterdam, The Netherlands, May 4th - 7th 2016.

Stremersch S., Braeckmans K., Vandenbroucke R., De Smedt S., Raemdonck K. A comparative analysis between extracellular vesicles and synthetic nanocarriers as delivery vehicle for small interfering RNAs. ISEV research seminar 2015: EV associated RNA, Utrecht, The Netherlands, September 24th - 25th 2015.

Stremersch S., Braeckmans K., Vandenbroucke R., De Smedt S., Raemdonck K. A comparative analysis between extracellular vesicles and liposomes as delivery vehicle for small interfering RNAs. ISEV2015, Washington DC, USA, April 22th - 27th 2015.

Stremersch S., Braeckmans K., Vandenbroucke R., De Smedt S., Raemdonck K. Evaluation of the potential of extracellular vesicles as a delivery vehicle for small

interfering RNA. Biopharmacy meeting, Vlaardingen, The Netherlands, December 12th 2014.

Stremersch S., Braeckmans K., Vandenbroucke R., De Smedt S., Raemdonck K. Hijacking nature's own communication system: Evaluation of extracellular vesicles as a siRNA delivery vehicle. NanoBio&Med2014, Barcelona, Spain, November 18th – 21th 2014.

Stremersch S., Braeckmans K., Vandenbroucke R., De Smedt S., Raemdonck K. Aggregate formation severely overestimates the loading efficacy of siRNA in extracellular vesicles by electroporation. 17the forum of pharmaceutical sciences, Spa, Belgium, September 17th – 18th 2013.

National and international conferences with poster presentation

Stremersch S., Marro M., Pinchasik B., Baatsen P., Hendrix A., De Smedt S., Loza-Alvarez P., Skirtach A., Raemdonck K., Braeckmans K. Identification of individual extracellular vesicles by surface enhanced Raman spectroscopy. 12th Edition of Knowledge for growth, Ghent, Belgium, May 26th 2016. **Abstract was selected for an oral pitch and awarded with the poster and pitch prize KFG2016.**

Stremersch S., Braeckmans K., De Smedt S., Raemdonck K. Exosomes underperform compared to liposomes for functional, in vitro siRNA delivery. Controlled release society annual meeting, Edinburgh, Scotland, July 26th – 29th 2015.

Stremersch S., Braeckmans K., De Smedt S., Raemdonck K. The evaluation of a hybrid extracellular vesicle-polymer nanocomposite for RNAi therapy. ISEV2014, Rotterdam, The Netherlands, April 30th – May 3th 2014.

Stremersch S., Braeckmans K., De Smedt S., Raemdonck K. Extracellular vesicles as a siRNA deliver vehicle: Evaluation of electroporation as a loading method. 13th European Symposium on Controlled Drug Delivery, Egmond-aan-zee, the Netherlands, April 16th - 18th 2014.

Stremersch S., Braeckmans K., De Smedt S., Raemdonck K. Extracellular vesicles as a siRNA deliver vehicle: Evaluation of electroporation as a loading method. Biopharmacy meeting, Ghent, Belgium, December 18th 2013.

Stremersch S., Braeckmans K., De Smedt S., Raemdonck K. Encapsulation of siRNA into extracellular vesicles by electroporation is biased by siRNA precipitation. Molecular

medicine congress: Biomarkers and applications of Exosomes, Frankfurt, Germany, September 3th – 4th 2013.

Stremersch S., Braeckmans K., De Smedt S., Raemdonck K. Loading of siRNA into exosomes by electroporation is biased by siRNA precipitation. 9th edition of Knowledge for growth, Ghent, Belgium, May 24th 2013.

International research experience

The Institute of Photonic Sciences (ICFO), Castelldefels (Barcelona), Spain

Subject: Surface enhanced Raman spectroscopy of exosomes under supervision of Prof. P. Loza-Alvarez, March 2nd – March 5th 2015.

Max Planck institute für Kolloid- und Grenzflächenforschung, Potsdam, Germany

Subject: Surface enhanced Raman spectroscopy of exosomes under supervision of Prof. A. Skirtach, October 11th – October 13th 2015 and March 28th – April 4th 2014.

Teaching activities

Lecture on bio-inspired drug delivery vehicles (course 'Biopharmacy' - Prof. S.C. De Smedt). (2015)

Seminars on genetics (course 'General biochemistry' - 2nd bachelor Pharmaceutical sciences - Prof. J. Demeester). (2013-2015)

Tutor and lab instructor for the Pharmaceutical Bachelor Proof (FaBaP). (2014 – 2015)

Supervisor of: Niels Daelman, Bachelor dissertation (medical laboratory techniques, Odisee). Characterizing extracellular vesicles as nano-sized delivery vehicles for small interfering RNA. (2015)

Wannes Deckers, Master dissertation (Industrial pharmacy – Ghent University). Development of extracellular vesicle-coated nanogels for advanced cancer vaccination. (2014)

Awards

Laureate poster and pitch prize knowledge for growth 2016

Laureate 'prize of pharmacy 2011' for the master thesis *Ultrasound as a key component to selective antitumor therapy: 'liposome coated microbubbles' and 'sonodynamic therapy'.* An annual national, inter-university competition to reward the best pharmaceutical (drug development) master thesis.

Scholarships

ISEV scholarship to attend the ISEV2015 conference (Washington DC; USA)

FWO travel grant to attend the ISEV2015 conference (Washington DC; USA)

FCWO travel grant to attend the ISEV2014 conference (Rotterdam; The Nederlands)

BSPS travel grant to attend the Nanobio&Med2014 conference (Barcelona; Spain)

FWO-aspiranten scholarship (October 2012 – September 2016) for the project: Exosome-inspired nanocarriers for the delivery of small interfering RNA

Courses

Tech transfer course organized by the TT-office of Ghent University, Ghent 2015 (5 days)

qPCR course organized by Biogazelle, Vlerick Business School - Ghent Campus 2015 (2 days)

Multicolor flow cytometry course organized by BD Biosciences, 2014

Applied Flow Cytometry organized by Doctoral Schools, Ghent, 2013 (3 days)

Particle Characterization course organized by BePCIS, Ghent, 2013 (2 days)

ACKNOWLEDGEMENTS / DANKWOORD

In de afgelopen 4 jaar heb ik het geluk gehad nauw te kunnen samenwerken met een groot aantal mensen die elk op hun eigen manier een stuk(je) hebben bijgedragen aan deze thesis. Een woordje van dank is dan ook meer dan op zijn plaats.

Allereerst **Koen**, mijn wetenschappelijke mentor. Bedankt voor het vertrouwen en de ondersteuning die je mij de afgelopen jaren hebt gegeven. Als de experimenten niet liepen zoals gepland stond je steeds klaar met een nieuw idee of had je weer iets interessants gelezen. Ook je oog voor detail heeft de nodige indruk nagelaten en deze thesis tot een hoger niveau getild. Je benoeming is dan ook meer dan verdiend! Op persoonlijk vlak klikte het gelukkig ook want we hebben de nodige uren samen doorgebracht op congressen. De steun en tips die je mij gaf rond het nakende vaderschap heb ik uitermate weten te appreciëren en zal ik niet snel vergeten. **Stefaan**, je begeesterende manier van lesgeven heeft ervoor gezorgd dat ik mijn doctoraat absoluut in het fameuze labo biochemie wou afleggen. Ondanks je drukke schema stond je deur steeds open voor vragen en (filosofische) raadgevingen. Wat mij echter het meest is bijgebleven is het immense vertrouwen dat je in mij stelde, ook op momenten dat ik zelf twijfelde. **Kevin**, ergens onderweg heb je mij geadopteerd en werd je één van mijn promoteren. Je 'to-the-point' aanpak maakte de samenwerking zeer efficiënt, maar tegelijkertijd was je ook steeds te vinden voor wat grappen bij één van onze bezoeken aan TT. Bedankt voor de kans die je mij geeft om nog wat langer te blijven en ik hoop een drijvende kracht te zijn om die mooie technologie ook buiten de labomuren te brengen.

Ook de andere PI's **Katrien**, **Ine L** en **Jo** wil ik bedanken voor de steun en het creëren van deze mooie onderzoeksgroep. Ik besef maar al te goed dat het een voorrecht is geweest om onder deze omstandigheden onderzoek te kunnen verrichten. Als we spreken over het creëren van optimale omstandigheden om efficiënt te werken kom ik uiteraard terecht bij **Bart**. De man die ALLES regelt en dit altijd met de glimlach. Je komt in elk dankwoord naar voor als draaischijf van het labo en dat is dan ook meer dan terecht. Echt bedankt voor al je hulp! Bovendien ben je tijdens de events buiten de labomuren ook altijd van de partij (het kleurenpallet van u been na een nachtje charlatan zal ik toch niet snel vergeten). Gelukkig heb je nu ook de steun van **Hilde** om de werkdruk wat te verdelen, zeker een meerwaarde voor het labo. Daarnaast ook **Katharine en Ilse**, jullie vormen dan weer de draaischijven van het papierwerk. Bedankt om ons steeds opnieuw te helpen zodat wij onze weg niet zelf hoeven te zoeken in de jungle van formulieren, boekingen, congresregistraties,… echte *timesavers*!

Binnen labo biochemie is naast het harde labeur gelukkig ook plaats voor veel plezier. Ik heb de eer gehad om de voorbije 4 jaar te vertoeven in het gezelschap van prachtige collega's (ondertussen vrienden) die zorgden voor een heerlijke sfeer met ontelbare events (afterworks, labweekends, traktaties, bbq's, labparties, Running Team ExCELLerate, congressen, …) en evenveel onvergetelijke momenten (*#bestlabever*). **Thomas**, hoewel ik begonnen ben in het pre-meter/peter tijdperk, heb je die taak op eigen initiatief opgenomen. Toen ik 4 jaar geleden de bureau binnen kwam heb je me meteen onder je vleugels genomen en mij de *'tips and tricks'* aangereikt om mijn PhD vlot door te komen. Je bent onderweg dan ook een echte vriend geworden met de nodige vuistjes en politiek niet correcte opmerkingen zodat mijn eerste jaren doctoraat een waar plezier waren. Daar zitten echter ook mijn andere *officemates* voor veel tussen. **Karen**, we zijn samen begonnen aan dit avontuur en gaandeweg hebben we elkaar van de nodige steun en luisterend oor voorzien. Je staat altijd klaar om mensen te helpen en bent tegelijkertijd ook één van de drijvende kracht achter de geweldige sfeer in dit labo! De manier waarop jij je drukke leven managet is bewonderenswaardig. Ik ben er dan ook rotsvast van overtuigd dat je alles in huis hebt om een prachtige (academische) carrière uit te bouwen. **Rita (the machine) Santos**, it was a true pleasure to have you in our office. Your perseverance, both for work and sports, is incredible and your compassion and empathy created a familial atmosphere in our office (kaarsje branden voor sollicitaties, medeleven met het vaderschap, enz.). **Eline**, the junior of the office, de woordenschat die ik de afgelopen 2 jaar van u heb opgepikt, zal ervoor zorgen dat ik de komende 20 jaar mijn eigen kinderen ga kunnen overklassen wat *Slang* betreft. Maar je was vooral ook gewoon altijd je aangename en hard werkende zelve! Ik hoop dat we met z'n allen nog regelmatig a *little terrace* kunnen doen! **Katrien F**, bedankt voor al die heerlijke photoshop Fridays (ze worden echte hard gemist) en mij te behoeden voor het gebruiken van LaTeX ☺.

Koen Ro (CPO/CPV), nooit gedacht dat ik nog iemand ging vinden in een labo die dezelfde verregaande interesse heeft in de complete nonsens die te vinden is op MTV en de commentarensectie van de HLN-website('op de kap van de kleine man'). Het lopen en fitnessen over de middag zorgden voor de nodige energie om die middagdip op te vangen (wel gepaard met het nodige nazweten, maar dat nemen we er met plezier bij ☺). Zelfs voor discussies over de koers, voetbal, de juiste voedingssupplementen (ik moet u trouwens nog een pot recovery) en het verstrekken van gratis pintjes op de feestjes kon ik altijd bij u terecht. **Rein**, Ryan voor de vrienden, één van die ideeën moeten we omzetten in een business en het gaat ons rijk maken, *mark my words*. U bourgondische manier van naar de wereld kijken zorgde altijd voor de nodige gezelligheid zowel tijdens de middagpauzes als naast de BBQ met een biertje. Tijdens de middag wat voorzetjes trappen met **Pieterjan** en **Jelter** hebben we spijtig genoeg pas deze zomer ontdekt ☺. **PJ**, de man van de surprises en medevoorvechter van het naar

waarde schatten en te pas en onpas citeren van "Willy's en Marjetten". Ik ben blij te zien dat het college in Sint-Niklaas inderdaad toppers blijft aanleveren aan dit labo ;-). **George** we started together and will finish together (in Dutch we say: samen uit, samen thuis). Your networking skills are inimitable and simply the fact that I could have written this just as well in Dutch evokes incredible respect. **Toon,** als je het mij vraagt een echte aanwinst, zowel binnen als buiten het labo. Steeds klaar voor een gezellige babbel, beantwoorden van al mijn microscopievragen of snel even een matlab gui schrijven, bedankt voor alle hulp! **Sangram**, always very positive, supportive and friendly. Best of luck with your new research group in India. **Hua**, my deepest respect for your high impact work!

Freya, nog zo een maatje van het eerste uur. We zaten vaak in hetzelfde stadium van ons doctoraat waarbij het deugd deed om het hart eens te kunnen luchten. Nog even en jij kan een ongetwijfeld prachtig doctoraat afleggen. Bedankt voor alle steun de afgelopen 4 jaar, carrément (ik gebruik het waarschijnlijk fout ☺). **Heleen**, hoewel onze kijk op de wereld nog wel eens durft te verschillen, heb ik toch een zeer grote bewondering voor jou. Alles waar je u schouders onder zet lijkt een succes te worden. Samenwerken met u was ook altijd een waar plezier, zowel voor DC-experimenten als een partijtje kicker (zolang we maar winnen ☺). **Joke(r)**, naast Koen Ro en mezelf waarschijnlijk de enige persoon binnen de UGent die programma's als "are you the one", "Ex on the beach" en "geordie shore" voor de ware mesterwerken in televisieland aanziet die ze toch ontegensprekelijk zijn. Maar naast het bediscussiëren van deze complete nonsense rond de lunchtafel was je er ook steeds voor een goede babbel, feestjes en hart onder de riem als dat nodig was! **Lotte**, ik bewonder u ongekend relativeringsvermogen na al die 'swept field' miserie. Ik was ook steeds een grote fan van u *ad rem* opmerkingen. **Lynn**, dikke merci voor u steun tijdens die laatste weekjes en al u goede raad om "den boek" af te krijgen. **Laura**, je empathisch vermogen is ongekend, super veel succes met je toekomstige carrière. **Silke**, nog een lid van team Waasland, met u ongeremdheid zorg je steeds voor een aangename sfeer en ik wens je dan ook alle succes met je ultrasound setup en met je doctoraat in het algemeen. **Ine DC** echt knap dat je de kans grijpt om een jaar naar de States te gaan voor een post-doc, een voorbeeld voor iedereen. **Elisa**, thanks for your ever happy presence and best of luck with your thesis! **Jing, heyang, molood** you all are still at the beginning of your PhD so I wish you all the best!

I would also like to thank all external collaborators with who I have worked for their help with experiments, interesting discussions, scientific input and nice moments at conferences. **Sander, Pieter en Raymond** bedankt voor de zeer aangename en toch wel succesvolle samenwerking rond de 'electroporatiepaper'. **Roos** mijn grote bewondering voor u gedrevenheid en doorzettingsvermogen en uiteraard mijn dank voor

de hulp rond PCR en miRNA profiling. **An** bedankt om mij te leren werken met de Nanosight, onmisbaar in mijn onderzoek. Vooral het feit dat ik altijd welkom was, is voor mij zeer belangrijk geweest om efficiënt te kunnen werken. Veel succes met het verder uitbouwen van een exosoomgroep hier in Gent. **Bat-El** and **Monica**, thanks for introducing me to Raman spectroscopy and your hospitality both in Potsdam and Barcelona. **An en Davy**, het was altijd een plezier om naar TT af te zakken. Zeer knap hoe snel jullie alles oppikken en implementeren in een patent context. Een waar voorbeeld voor mezelf. Uiteraard wil ik ook het FWO-Vlaanderen bedanken om mij elke maand van de nodige botterhammen te voorzien ☺.

Gelukkig was er ook naast het labo de nodige afleiding met de **maten van 't Waasland (Trappers)**. Bedankt voor de fietstochtjes (ja ik meestal in het wiel ☺), criteriums, RVV BBQ's, Champions league kijken met een biertje in de hand,…. Nu ik terug naar de roots kom, hoop ik geen events meer te moeten missen!

En dan tot slot de belangrijkste mensen: **Mama, Papa, Cédric**, ontzettend bedankt voor jullie onvoorwaardelijke steun. Altijd geïnteresseerd in waar ik mee bezig ben en meelevend als het wat minder gaat. Ook de hulp die we nu weer krijg bij de bouw is voor ons van onschatbare waarde. Echt waar ik kan jullie niet genoeg bedanken!!! **Annelies**, al bijna 9 jaar delen wij lief en leed. Jij hebt mij in de afgelopen 4 jaar regelmatig moeten missen door de vele uurtjes in het labo en moeten samenleven met de minder gezellige mij als het weer eens allemaal tegenzat. Maar je hebt mij altijd gesteund en op de juiste momenten gekalmeerd en zelfvertrouwen gegeven. De afgelopen maanden zijn ongelofelijk hectisch geweest met het afleggen van dit doctoraat, de bouw van ons nieuw nestje en met de komst van **Emiel**, maar je was steeds begripvol en nam een groot deel van de zorgen op jou zodat ik mij kon focussen op mijn verdedigingen. Sinds kort zijn we dus met ons drietjes en als ik zie hoe een prachtige mama en sterke vrouw je bent, groeit mijn bewondering en liefde voor jou enkel nog meer. Ik beloof plechtig dat ik meer tijd voor ons gezinnetje zal vrijmaken (voilà het staat op papier)! **Emiel**, het is zwaar geweest die laatste weekjes, maar één blik naar jou en al mijn zorgen verdwenen als sneeuw voor de zon. Ik kan je nu al niet meer missen!

As comfort is the enemy of achievement, it is time to start a new adventure. First another year in the lab with a set of completely new challenges, afterwards somewhere else …. Yet, looking back at the last 4 years I can genially say: **The pleasure was all mine!**

Cheers,

- Stephan -